US010725124B2

(12) **United States Patent**
Boesch et al.

(10) **Patent No.: US 10,725,124 B2**
(45) **Date of Patent: Jul. 28, 2020**

(54) **DNV MAGNETIC FIELD DETECTOR**

(71) Applicant: **LOCKHEED MARTIN CORPORATION**, Besthesda, MD (US)

(72) Inventors: **Brian P. Boesch**, Reston, VA (US); **Gregory Scott Bruce**, Abington, PA (US); **Jeff D. Cammerata**, Medford Lakes, NJ (US); **David Nelson Coar**, Cherry Hill, NJ (US); **Laird Nicholas Egan**, Philadelphia, PA (US); **Bryan Neal Fisk**, Madison, AL (US); **Wilbur Lew**, Mount Laurel, NJ (US); **Arul Manickam**, Mount Laurel, NJ (US); **Stephen Michael Sekelsky**, Princeton, NJ (US); **John B. Stetson, Jr.**, New Hope, NJ (US); **Peter G. Kaup**, Marlton, NJ (US); **Julie Lynne Miller**, Auberry, CA (US); **Jon C. Russo**, Cherry Hill, NJ (US); **Emanuel Solomon Stockman**, Philadelphia, PA (US); **Thomas J. Meyer**, Corfu, NY (US); **James Michael Krause**, Saint Michael, MN (US); **James P. Mabry**, McLean, VA (US); **Elton Pepa**, Dumfries, VA (US)

(73) Assignee: **LOCKHEED MARTIN CORPORATION**, Bethesda, MD (US)

(*) Notice: Subject to any disclaimer, the term of this patent is extended or adjusted under 35 U.S.C. 154(b) by 312 days.

(21) Appl. No.: **15/912,461**

(22) Filed: **Mar. 5, 2018**

(65) **Prior Publication Data**

US 2018/0196111 A1 Jul. 12, 2018

Related U.S. Application Data

(63) Continuation of application No. 15/179,957, filed on Jun. 10, 2016, now Pat. No. 9,910,105, which is a
(Continued)

(51) **Int. Cl.**
G01R 33/032 (2006.01)
G05D 1/00 (2006.01)
(Continued)

(52) **U.S. Cl.**
CPC ***G01R 33/032*** (2013.01); ***G01C 21/00*** (2013.01); ***G05D 1/0088*** (2013.01); ***G05D 1/101*** (2013.01); *B64C 2201/141* (2013.01)

(58) **Field of Classification Search**
CPC G01R 33/032; G01R 33/26; G01R 33/35; G01R 33/44; G01R 33/48; G01R 33/02;
(Continued)

(56) **References Cited**

U.S. PATENT DOCUMENTS

2,746,027 A 5/1956 Murray
3,359,812 A 12/1967 Everitt
(Continued)

FOREIGN PATENT DOCUMENTS

CN 105738845 A 7/2016
CN 106257602 12/2016
(Continued)

OTHER PUBLICATIONS

International Search Report and Written Opinion for PCT Appl. Ser. No. PCT/US2018/041411 dated Feb. 8, 2019, 13 pages.
(Continued)

Primary Examiner — Jermele M Hollington
Assistant Examiner — Taqi R Nasir
(74) *Attorney, Agent, or Firm* — Foley & Lardner LLP

(57) **ABSTRACT**

A system for magnetic detection includes a nitrogen vacancy (NV) diamond material comprising a plurality of NV centers, a radio frequency (RF) excitation source configured to provide RF excitation to the NV diamond material, an optical excitation source configured to provide optical excitation to the NV diamond material, an optical detector
(Continued)

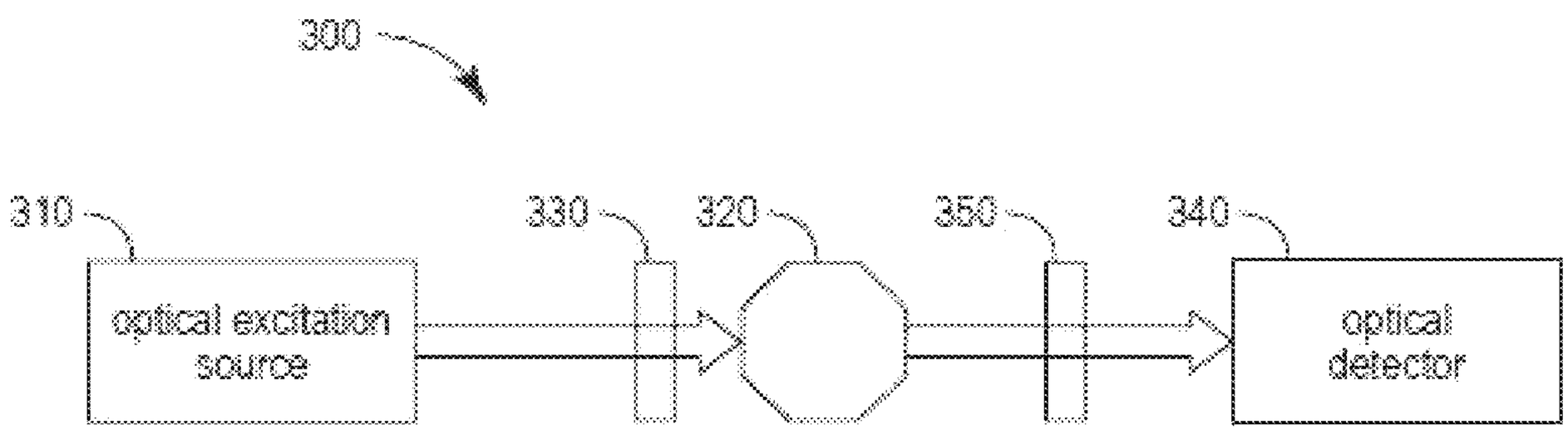

configured to receive an optical signal emitted by the NV diamond material, and a controller. The optical signal is based on hyperfine states of the NV diamond material. The controller is configured to detect a gradient of the optical signal based on the hyperfine states emitted by the NV diamond material.

20 Claims, 57 Drawing Sheets

Related U.S. Application Data

continuation-in-part of application No. 15/003,336, filed on Jan. 21, 2016, now abandoned, and a continuation-in-part of application No. 15/003,667, filed on Jan. 21, 2016, now Pat. No. 9,614,589, and a continuation-in-part of application No. 15/003,292, filed on Jan. 21, 2016, now Pat. No. 10,006,973, and a continuation-in-part of application No. 15/003,062, filed on Jan. 21, 2016, now abandoned, and a continuation-in-part of application No. 15/003,309, filed on Jan. 21, 2016, now Pat. No. 10,520,558, and a continuation-in-part of application No. 15/003,088, filed on Jan. 21, 2016, now Pat. No. 9,845,153, and a continuation-in-part of application No. 15/003,209, filed on Jan. 21, 2016, now Pat. No. 10,088,336, and a continuation-in-part of application No. 15/003,281, filed on Jan. 21, 2016, now Pat. No. 9,817,081, and a continuation-in-part of application No. 15/003,634, filed on Jan. 21, 2016, now Pat. No. 9,823,313, and a continuation-in-part of application No. 15/003,718, filed on Jan. 21, 2016, now Pat. No. 9,541,610, and a continuation-in-part of application No. 15/003,177, filed on Jan. 21, 2016, now abandoned, and a continuation-in-part of application No. 15/003,590, filed on Jan. 21, 2016, now Pat. No. 9,557,391, and a continuation-in-part of application No. 15/003,256, filed on Jan. 21, 2016, now Pat. No. 9,835,693, and a continuation-in-part of application No. 15/003,558, filed on Jan. 21, 2016, now Pat. No. 9,829,545, and a continuation-in-part of application No. 15/003,797, filed on Jan. 21, 2016, now Pat. No. 9,910,104, and a continuation-in-part of application No. 15/003,193, filed on Jan. 21, 2016, now abandoned, and a continuation-in-part of application No. 15/003,145, filed on Jan. 21, 2016, now Pat. No. 10,088,452, and a continuation-in-part of application No. 15/003,206, filed on Jan. 21, 2016, now Pat. No. 9,824,597, and a continuation-in-part of application No. 15/003,298, filed on Jan. 21, 2016, now Pat. No. 9,551,763, and a continuation-in-part of application No. 15/003,396, filed on Jan. 21, 2016, now abandoned, and a continuation-in-part of application No. 15/003,617, filed on Jan. 21, 2016, now abandoned, and a continuation-in-part of application No. 15/003,577, filed on Jan. 21, 2016, now abandoned, and a continuation-in-part of application No. 15/003,519, filed on Jan. 21, 2016, now Pat. No. 10,120,039, and a continuation-in-part of application No. 15/003,670, filed on Jan. 21, 2016, now Pat. No. 10,338,162, and a continuation-in-part of application No. 15/003,678, filed on Jan. 21, 2016, now abandoned, and a continuation-in-part of application No. 15/003,652, filed on Jan. 21, 2016, and a continuation-in-part of application No. 15/003,704, filed on Jan. 21, 2016, now Pat. No. 10,241,158, and a continuation-in-part of application No. 15/003,176, filed on Jan. 21, 2016, now Pat. No. 10,012,704, and a continuation-in-part of application No. 14/866,730, filed on Sep. 25, 2015, now Pat. No. 10,168,393, and a continuation-in-part of application No. 14/680,877, filed on Apr. 7, 2015, now Pat. No. 9,590,601, and a continuation-in-part of application No. 14/676,740, filed on Apr. 1, 2015, now Pat. No. 9,853,837, and a continuation-in-part of application No. 14/659,498, filed on Mar. 16, 2015, now Pat. No. 9,638,821.

(60) Provisional application No. 62/277,657, filed on Jan. 12, 2016, provisional application No. 62/261,643, filed on Dec. 1, 2015, provisional application No. 62/258,003, filed on Nov. 20, 2015, provisional application No. 62/257,988, filed on Nov. 20, 2015, provisional application No. 62/250,874, filed on Nov. 4, 2015, provisional application No. 62/214,792, filed on Sep. 4, 2015, provisional application No. 62/196,288, filed on Jul. 23, 2015, provisional application No. 62/190,209, filed on Jul. 8, 2015, provisional application No. 62/190,218, filed on Jul. 8, 2015, provisional application No. 62/112,709, filed on Feb. 4, 2015, provisional application No. 62/112,071, filed on Feb. 4, 2015, provisional application No. 62/109,551, filed on Jan. 29, 2015, provisional application No. 62/109,006, filed on Jan. 28, 2015, provisional application No. 62/107,289, filed on Jan. 23, 2015, provisional application No. 62/055,607, filed on Sep. 25, 2014, provisional application No. 61/975,997, filed on Apr. 7, 2014, provisional application No. 61/976,009, filed on Apr. 7, 2014, provisional application No. 61/955,918, filed on Mar. 20, 2014.

(51) **Int. Cl.**
G05D 1/10 (2006.01)
G01C 21/00 (2006.01)

(58) **Field of Classification Search**
CPC B82Y 25/00; B82Y 30/00; B82Y 35/00; G01C 21/00; G05D 1/0088; G05D 1/101; B64C 2201/141
USPC ... 324/66–67, 160–180, 71.1–157, 425–470, 324/200–263, 750.01–764.01; 702/1–199; 73/37–65.09
See application file for complete search history.

(56) **References Cited**

U.S. PATENT DOCUMENTS

3,389,333	A	6/1968	Wolff et al.
3,490,032	A	1/1970	Zurflueh
3,514,723	A	5/1970	Cutler
3,518,531	A	6/1970	Huggett
3,621,380	A	11/1971	Barlow, Jr.
3,745,452	A	7/1973	Osburn et al.
3,899,758	A	8/1975	Maier et al.
4,025,873	A	5/1977	Chilluffo
4,047,805	A	9/1977	Sekimura
4,078,247	A	3/1978	Albrecht
4,084,215	A	4/1978	Willenbrock
4,322,769	A	3/1982	Cooper
4,329,173	A	5/1982	Culling
4,359,673	A	11/1982	Bross et al.
4,368,430	A	1/1983	Dale et al.
4,410,926	A	10/1983	Hafner et al.
4,437,533	A	3/1984	Bierkarre et al.
4,514,083	A	4/1985	Fukuoka
4,588,993	A	5/1986	Babij et al.

(56) **References Cited**

U.S. PATENT DOCUMENTS

4,636,612	A	1/1987	Cullen	
4,638,324	A	1/1987	Hannan	
4,675,522	A	6/1987	Arunkumar	
4,768,962	A	9/1988	Kupfer et al.	
4,818,990	A	4/1989	Fernandes	
4,820,986	A	4/1989	Mansfield et al.	
4,945,305	A	7/1990	Blood	
4,958,328	A	9/1990	Stubblefield	
4,982,158	A	1/1991	Nakata et al.	
5,019,721	A	5/1991	Martens et al.	
5,038,103	A	8/1991	Scarzello et al.	
5,113,136	A	5/1992	Hayashi et al.	
5,134,369	A	7/1992	Lo et al.	
5,189,368	A	2/1993	Chase	
5,200,855	A	4/1993	Meredith et al.	
5,210,650	A	5/1993	O'Brien et al.	
5,245,347	A	9/1993	Bonta et al.	
5,252,912	A	10/1993	Merritt et al.	
5,301,096	A	4/1994	Klontz et al.	
5,384,109	A	1/1995	Klaveness et al.	
5,396,802	A	3/1995	Moss	
5,420,549	A	5/1995	Prestage	
5,425,179	A	6/1995	Nickel et al.	
5,427,915	A	6/1995	Ribi et al.	
5,548,279	A	8/1996	Gaines	
5,568,516	A	10/1996	Strohallen et al.	
5,586,069	A	12/1996	Dockser	
5,597,762	A	1/1997	Popovici et al.	
5,638,472	A	6/1997	Van Delden	
5,694,375	A	12/1997	Woodall	
5,719,497	A	2/1998	Veeser et al.	
5,731,996	A	3/1998	Gilbert	
5,764,061	A	6/1998	Asakawa et al.	
5,818,352	A	10/1998	McClure	
5,846,708	A	12/1998	Hollis et al.	
5,888,925	A	3/1999	Smith et al.	
5,894,220	A	4/1999	Wellstood et al.	
5,907,420	A	5/1999	Chraplyvy et al.	
5,907,907	A	6/1999	Ohtomo et al.	
5,915,061	A	6/1999	Vanoli	
5,995,696	A	11/1999	Miyagi et al.	
6,042,249	A	3/2000	Spangenberg	
6,057,684	A	5/2000	Murakami et al.	
6,064,210	A	5/2000	Sinclair	
6,121,053	A	9/2000	Kolber et al.	
6,124,862	A	9/2000	Boyken et al.	
6,130,753	A	10/2000	Hopkins et al.	
6,144,204	A	11/2000	Sementchenko	
6,195,231	B1	2/2001	Sedlmayr et al.	
6,215,303	B1	4/2001	Weinstock et al.	
6,262,574	B1	7/2001	Cho et al.	
6,360,173	B1	3/2002	Fullerton	
6,398,155	B1	6/2002	Hepner et al.	
6,433,944	B1	8/2002	Nagao et al.	
6,437,563	B1	8/2002	Simmonds et al.	
6,472,651	B1	10/2002	Ukai	
6,472,869	B1	10/2002	Upschulte et al.	
6,504,365	B2	1/2003	Kitamura	
6,518,747	B2	2/2003	Sager et al.	
6,542,242	B1	4/2003	Yost et al.	
6,621,377	B2	9/2003	Osadchy et al.	
6,621,578	B1	9/2003	Mizoguchi	
6,636,146	B1	10/2003	Wehoski	
6,686,696	B2	2/2004	Mearini et al.	
6,690,162	B1	2/2004	Schopohl et al.	
6,765,487	B1	7/2004	Holmes et al.	
6,788,722	B1	9/2004	Kennedy et al.	
6,809,829	B1	10/2004	Takata et al.	
7,118,657	B2	10/2006	Golovchenko et al.	
7,221,164	B1	5/2007	Barringer	
7,277,161	B2	10/2007	Claus	
7,305,869	B1	12/2007	Berman et al.	
7,307,416	B2	12/2007	Islam et al.	
7,342,399	B1	3/2008	Wiegert	
RE40,343	E	5/2008	Anderson	
7,400,142	B2	7/2008	Greelish	
7,413,011	B1	8/2008	Chee et al.	
7,427,525	B2	9/2008	Santori et al.	
7,448,548	B1	11/2008	Compton	
7,471,805	B2	12/2008	Goldberg	
7,474,090	B2	1/2009	Islam et al.	
7,543,780	B1	6/2009	Marshall et al.	
7,546,000	B2	6/2009	Spillane et al.	
7,570,050	B2 *	8/2009	Sugiura	G01R 33/56375 324/307
7,608,820	B1	10/2009	Berman et al.	
7,705,599	B2	4/2010	Strack et al.	
7,741,936	B1	6/2010	Weller et al.	
7,805,030	B2	9/2010	Bratkovski et al.	
7,868,702	B2	1/2011	Ohnishi	
7,889,484	B2	2/2011	Choi	
7,916,489	B2	3/2011	Okuya	
7,932,718	B1	4/2011	Wiegert	
7,983,812	B2	7/2011	Potter	
8,022,693	B2	9/2011	Meyersweissflog	
8,120,351	B2	2/2012	Rettig et al.	
8,120,355	B1	2/2012	Stetson	
8,124,296	B1	2/2012	Fischel	
8,138,756	B2	3/2012	Barclay et al.	
8,193,808	B2	6/2012	Fu et al.	
8,294,306	B2	10/2012	Kumar et al.	
8,310,251	B2	11/2012	Orazem	
8,311,767	B1	11/2012	Stetson	
8,334,690	B2	12/2012	Kitching et al.	
8,415,640	B2	4/2013	Babinec et al.	
8,471,137	B2	6/2013	Adair et al.	
8,480,653	B2	7/2013	Birchard et al.	
8,525,516	B2	9/2013	Le Prado et al.	
8,547,090	B2	10/2013	Lukin et al.	
8,574,536	B2	11/2013	Boudou et al.	
8,575,929	B1	11/2013	Wiegert	
8,686,377	B2	4/2014	Twitchen et al.	
8,704,546	B2	4/2014	Konstantinov	
8,758,509	B2	6/2014	Twitchen et al.	
8,803,513	B2	8/2014	Hosek et al.	
8,854,839	B2	10/2014	Cheng et al.	
8,885,301	B1	11/2014	Heidmann	
8,913,900	B2	12/2014	Lukin et al.	
8,933,594	B2	1/2015	Kurs	
8,947,080	B2	2/2015	Lukin et al.	
8,963,488	B2	2/2015	Campanella et al.	
9,103,873	B1	8/2015	Martens et al.	
9,157,859	B2	10/2015	Walsworth et al.	
9,245,551	B2	1/2016	El Hallak et al.	
9,249,526	B2	2/2016	Twitchen et al.	
9,270,387	B2	2/2016	Wolfe et al.	
9,291,508	B1	3/2016	Biedermann et al.	
9,317,811	B2	4/2016	Scarsbrook	
9,369,182	B2	6/2016	Kurs et al.	
9,442,205	B2	9/2016	Geiser et al.	
9,541,610	B2	1/2017	Kaup et al.	
9,551,763	B1	1/2017	Hahn et al.	
9,557,391	B2	1/2017	Egan et al.	
9,570,793	B2	2/2017	Borodulin	
9,590,601	B2	3/2017	Krause et al.	
9,614,589	B1	4/2017	Russo et al.	
9,632,045	B2	4/2017	Englund et al.	
9,645,223	B2	5/2017	Megdal et al.	
9,680,338	B2	6/2017	Malpas et al.	
9,689,679	B2	6/2017	Budker et al.	
9,720,055	B1	8/2017	Hahn et al.	
9,778,329	B2	10/2017	Heidmann	
9,779,769	B2	10/2017	Heidmann	
9,891,297	B2	2/2018	Sushkov et al.	
2002/0144093	A1	10/2002	Inoue et al.	
2002/0167306	A1	11/2002	Zalunardo et al.	
2003/0058346	A1	3/2003	Bechtel et al.	
2003/0076229	A1	4/2003	Blanpain et al.	
2003/0094942	A1	5/2003	Friend et al.	
2003/0098455	A1	5/2003	Amin et al.	
2003/0235136	A1	12/2003	Akselrod et al.	
2004/0013180	A1	1/2004	Giannakis et al.	
2004/0022179	A1	2/2004	Giannakis et al.	
2004/0042150	A1	3/2004	Swinbanks et al.	

(56) **References Cited**

U.S. PATENT DOCUMENTS

2004/0081033	A1	4/2004	Arieli et al.	
2004/0095133	A1	5/2004	Nikitin et al.	
2004/0109328	A1	6/2004	Dahl et al.	
2004/0247145	A1	12/2004	Luo et al.	
2005/0031840	A1	2/2005	Swift et al.	
2005/0068249	A1	3/2005	Du Toit et al.	
2005/0099177	A1	5/2005	Greelish	
2005/0112594	A1	5/2005	Grossman	
2005/0126905	A1	6/2005	Golovchenko et al.	
2005/0130601	A1	6/2005	Palermo et al.	
2005/0134257	A1	6/2005	Etherington et al.	
2005/0138330	A1	6/2005	Owens et al.	
2005/0146327	A1	7/2005	Jaka	
2006/0012385	A1	1/2006	Tsao et al.	
2006/0054789	A1	3/2006	Miyamoto et al.	
2006/0055584	A1	3/2006	Waite et al.	
2006/0062084	A1*	3/2006	Drew	G01V 1/008 367/68
2006/0071709	A1	4/2006	Maloberti et al.	
2006/0245078	A1	11/2006	Kawamura	
2006/0247847	A1	11/2006	Carter et al.	
2006/0255801	A1*	11/2006	Ikeda	G01R 33/54 324/307
2006/0291771	A1	12/2006	Braunisch et al.	
2007/0004371	A1	1/2007	Okanobu	
2007/0120563	A1	5/2007	Kawabata et al.	
2007/0247147	A1	10/2007	Xiang et al.	
2007/0273877	A1	11/2007	Kawano et al.	
2008/0016677	A1	1/2008	Creighton, IV	
2008/0048640	A1	2/2008	Hull et al.	
2008/0078233	A1	4/2008	Larson et al.	
2008/0089367	A1	4/2008	Srinivasan et al.	
2008/0204004	A1	8/2008	Anderson	
2008/0217516	A1	9/2008	Suzuki et al.	
2008/0239265	A1	10/2008	Den Boef	
2008/0253264	A1	10/2008	Nagatomi et al.	
2008/0265895	A1	10/2008	Strack et al.	
2008/0266050	A1	10/2008	Crouse et al.	
2008/0279047	A1	11/2008	An et al.	
2008/0299904	A1	12/2008	Yi et al.	
2009/0001979	A1	1/2009	Kawabata	
2009/0015262	A1	1/2009	Strack et al.	
2009/0042592	A1	2/2009	Cho et al.	
2009/0058697	A1	3/2009	Aas et al.	
2009/0060790	A1	3/2009	Okaguchi et al.	
2009/0079417	A1	3/2009	Mort et al.	
2009/0079426	A1	3/2009	Anderson	
2009/0132100	A1	5/2009	Shibata	
2009/0157331	A1	6/2009	Van Netten	
2009/0161264	A1	6/2009	Meyersweissflog	
2009/0195244	A1*	8/2009	Mouget	G01V 3/28 324/221
2009/0222208	A1	9/2009	Speck	
2009/0243616	A1	10/2009	Loehken et al.	
2009/0244857	A1	10/2009	Tanaka	
2009/0277702	A1	11/2009	Kanada et al.	
2009/0310650	A1	12/2009	Chester et al.	
2010/0004802	A1	1/2010	Bodin et al.	
2010/0015438	A1	1/2010	Williams et al.	
2010/0015918	A1	1/2010	Liu et al.	
2010/0045269	A1	2/2010	Lafranchise et al.	
2010/0071904	A1	3/2010	Burns et al.	
2010/0102809	A1	4/2010	May	
2010/0102820	A1	4/2010	Martinez et al.	
2010/0134922	A1	6/2010	Yamada et al.	
2010/0157305	A1	6/2010	Henderson	
2010/0188081	A1	7/2010	Lammegger	
2010/0237149	A1	9/2010	Olmstead	
2010/0271016	A1	10/2010	Barclay et al.	
2010/0271032	A1	10/2010	Helwig	
2010/0277121	A1	11/2010	Hall et al.	
2010/0308813	A1	12/2010	Lukin et al.	
2010/0315079	A1	12/2010	Lukin et al.	
2010/0321117	A1	12/2010	Gan	
2010/0326042	A1	12/2010	McLean et al.	
2011/0031969	A1	2/2011	Kitching et al.	
2011/0034393	A1	2/2011	Justen et al.	
2011/0059704	A1	3/2011	Norimatsu et al.	
2011/0062957	A1	3/2011	Fu et al.	
2011/0062967	A1	3/2011	Mohaupt	
2011/0066379	A1	3/2011	Mes	
2011/0120890	A1	5/2011	MacPherson et al.	
2011/0127999	A1	6/2011	Lott et al.	
2011/0165862	A1	7/2011	Yu et al.	
2011/0175604	A1	7/2011	Polzer et al.	
2011/0176563	A1	7/2011	Friel et al.	
2011/0243267	A1	10/2011	Won et al.	
2011/0270078	A1	11/2011	Wagenaar et al.	
2011/0279120	A1	11/2011	Sudow et al.	
2011/0315988	A1	12/2011	Yu et al.	
2012/0016538	A1	1/2012	Waite et al.	
2012/0019242	A1	1/2012	Hollenberg et al.	
2012/0037803	A1	2/2012	Strickland	
2012/0044014	A1	2/2012	Stratakos et al.	
2012/0051996	A1	3/2012	Scarsbrook et al.	
2012/0063505	A1	3/2012	Okamura et al.	
2012/0087449	A1	4/2012	Ling et al.	
2012/0089299	A1	4/2012	Breed	
2012/0140219	A1	6/2012	Cleary	
2012/0181020	A1*	7/2012	Barron	B01J 13/02 166/250.1
2012/0194068	A1	8/2012	Cheng et al.	
2012/0203086	A1	8/2012	Rorabaugh et al.	
2012/0232838	A1	9/2012	Kemppi et al.	
2012/0235633	A1	9/2012	Kesler et al.	
2012/0235634	A1	9/2012	Hall et al.	
2012/0245885	A1	9/2012	Kimishima	
2012/0257683	A1	10/2012	Schwager et al.	
2012/0281843	A1	11/2012	Christensen et al.	
2012/0326793	A1	12/2012	Gan	
2013/0043863	A1	2/2013	Ausserlechner et al.	
2013/0070252	A1	3/2013	Feth	
2013/0093424	A1	4/2013	Blank et al.	
2013/0107253	A1	5/2013	Santori	
2013/0127518	A1	5/2013	Nakao	
2013/0179074	A1	7/2013	Haverinen	
2013/0215712	A1	8/2013	Geiser et al.	
2013/0223805	A1	8/2013	Ouyang et al.	
2013/0265042	A1	10/2013	Kawabata et al.	
2013/0265782	A1	10/2013	Barrena et al.	
2013/0270991	A1	10/2013	Twitchen et al.	
2013/0279319	A1	10/2013	Matozaki et al.	
2013/0292472	A1	11/2013	Guha	
2014/0012505	A1	1/2014	Smith et al.	
2014/0015522	A1	1/2014	Widmer et al.	
2014/0037932	A1	2/2014	Twitchen et al.	
2014/0044208	A1	2/2014	Woodsum	
2014/0061510	A1	3/2014	Twitchen et al.	
2014/0070622	A1	3/2014	Keeling et al.	
2014/0072008	A1	3/2014	Faraon et al.	
2014/0077231	A1	3/2014	Twitchen et al.	
2014/0081592	A1	3/2014	Bellusci et al.	
2014/0104008	A1	4/2014	Gan	
2014/0126334	A1	5/2014	Megdal et al.	
2014/0139322	A1	5/2014	Wang et al.	
2014/0153363	A1	6/2014	Juhasz et al.	
2014/0154792	A1	6/2014	Moynihan et al.	
2014/0159652	A1	6/2014	Hall et al.	
2014/0166904	A1	6/2014	Walsworth et al.	
2014/0167759	A1*	6/2014	Pines	G01N 24/081 324/322
2014/0168174	A1	6/2014	Idzik et al.	
2014/0180627	A1	6/2014	Naguib et al.	
2014/0191139	A1	7/2014	Englund	
2014/0191752	A1	7/2014	Walsworth et al.	
2014/0197831	A1	7/2014	Walsworth	
2014/0198463	A1	7/2014	Klein	
2014/0210473	A1	7/2014	Campbell et al.	
2014/0215985	A1	8/2014	Pollklas	
2014/0225606	A1	8/2014	Endo et al.	
2014/0247094	A1	9/2014	Englund et al.	
2014/0264723	A1	9/2014	Liang et al.	
2014/0265555	A1	9/2014	Hall et al.	
2014/0272119	A1	9/2014	Kushalappa et al.	

(56) **References Cited**

U.S. PATENT DOCUMENTS

2014/0273826	A1	9/2014	Want et al.
2014/0291490	A1	10/2014	Hanson et al.
2014/0297067	A1	10/2014	Malay
2014/0306707	A1	10/2014	Walsworth et al.
2014/0327439	A1	11/2014	Cappellaro et al.
2014/0335339	A1	11/2014	Dhillon et al.
2014/0340085	A1	11/2014	Cappellaro et al.
2014/0368191	A1	12/2014	Goroshevskiy et al.
2015/0001422	A1	1/2015	Englund et al.
2015/0009746	A1	1/2015	Kucsko et al.
2015/0015247	A1	1/2015	Goodwill et al.
2015/0018018	A1	1/2015	Shen et al.
2015/0022404	A1	1/2015	Chen et al.
2015/0048822	A1	2/2015	Walsworth et al.
2015/0054355	A1	2/2015	Ben-Shalom et al.
2015/0061590	A1	3/2015	Widmer et al.
2015/0061670	A1	3/2015	Fordham et al.
2015/0090033	A1	4/2015	Budker et al.
2015/0128431	A1	5/2015	Kuo
2015/0137793	A1	5/2015	Englund et al.
2015/0153151	A1	6/2015	Kochanski
2015/0192532	A1	7/2015	Clevenson et al.
2015/0192596	A1	7/2015	Englund et al.
2015/0225052	A1	8/2015	Cordell
2015/0235661	A1	8/2015	Heidmann
2015/0253355	A1	9/2015	Grinolds et al.
2015/0268373	A1	9/2015	Meyer
2015/0269957	A1	9/2015	El Hallak et al.
2015/0276897	A1	10/2015	Leussler et al.
2015/0288352	A1	10/2015	Krause et al.
2015/0299894	A1	10/2015	Markham et al.
2015/0303333	A1	10/2015	Yu et al.
2015/0314870	A1	11/2015	Davies
2015/0326030	A1	11/2015	Malpas et al.
2015/0326410	A1	11/2015	Krause et al.
2015/0354985	A1	12/2015	Judkins et al.
2015/0358026	A1	12/2015	Gan
2015/0374250	A1	12/2015	Hatano et al.
2015/0377865	A1	12/2015	Acosta et al.
2015/0377987	A1	12/2015	Menon et al.
2016/0018269	A1	1/2016	Maurer et al.
2016/0031339	A1	2/2016	Geo
2016/0036529	A1	2/2016	Griffith et al.
2016/0052789	A1	2/2016	Gaathon et al.
2016/0054402	A1	2/2016	Meriles
2016/0061914	A1	3/2016	Jelezko
2016/0071532	A9	3/2016	Heidmann
2016/0077167	A1	3/2016	Heidmann
2016/0097702	A1	4/2016	Zhao et al.
2016/0113507	A1	4/2016	Reza et al.
2016/0131723	A1	5/2016	Nagasaka
2016/0139048	A1	5/2016	Heidmann
2016/0146904	A1	5/2016	Stetson, Jr. et al.
2016/0161429	A1	6/2016	Englund et al.
2016/0161583	A1	6/2016	Meriles et al.
2016/0174867	A1	6/2016	Hatano
2016/0214714	A1	7/2016	Sekelsky
2016/0216304	A1	7/2016	Sekelsky
2016/0216340	A1	7/2016	Egan et al.
2016/0216341	A1	7/2016	Boesch et al.
2016/0221441	A1	8/2016	Hall et al.
2016/0223621	A1	8/2016	Kaup et al.
2016/0231394	A1	8/2016	Manickam et al.
2016/0266220	A1	9/2016	Sushkov et al.
2016/0282427	A1	9/2016	Heidmann
2016/0291191	A1	10/2016	Fukushima et al.
2016/0313408	A1	10/2016	Hatano et al.
2016/0348277	A1	12/2016	Markham et al.
2016/0356863	A1	12/2016	Boesch et al.
2017/0010214	A1	1/2017	Osawa et al.
2017/0010334	A1	1/2017	Krause et al.
2017/0010338	A1	1/2017	Bayat et al.
2017/0010594	A1	1/2017	Kottapalli et al.
2017/0023487	A1	1/2017	Boesch
2017/0030982	A1	2/2017	Jeske et al.
2017/0038314	A1	2/2017	Suyama et al.
2017/0038411	A1	2/2017	Yacobi et al.
2017/0068012	A1	3/2017	Fisk
2017/0074660	A1	3/2017	Gann et al.
2017/0075020	A1	3/2017	Gann et al.
2017/0075205	A1	3/2017	Kriman et al.
2017/0077665	A1	3/2017	Liu et al.
2017/0104426	A1	4/2017	Mills
2017/0138735	A1	5/2017	Cappellaro et al.
2017/0139017	A1	5/2017	Egan et al.
2017/0146615	A1	5/2017	Wolf et al.
2017/0199156	A1	7/2017	Villani et al.
2017/0205526	A1	7/2017	Meyer
2017/0207823	A1	7/2017	Russo et al.
2017/0211947	A1	7/2017	Fisk
2017/0212046	A1	7/2017	Cammerata
2017/0212177	A1	7/2017	Coar et al.
2017/0212178	A1	7/2017	Hahn et al.
2017/0212179	A1	7/2017	Hahn et al.
2017/0212180	A1	7/2017	Hahn et al.
2017/0212181	A1	7/2017	Coar et al.
2017/0212182	A1	7/2017	Hahn et al.
2017/0212183	A1	7/2017	Egan et al.
2017/0212184	A1	7/2017	Coar et al.
2017/0212185	A1	7/2017	Hahn et al.
2017/0212186	A1	7/2017	Hahn et al.
2017/0212187	A1	7/2017	Hahn et al.
2017/0212190	A1	7/2017	Reynolds et al.
2017/0212258	A1	7/2017	Fisk
2017/0261629	A1	9/2017	Gunnarsson et al.
2017/0343617	A1	11/2017	Manickam et al.
2017/0343619	A1	11/2017	Manickam et al.
2017/0343620	A1	11/2017	Hahn et al.
2017/0343621	A1	11/2017	Hahn et al.
2017/0343695	A1	11/2017	Stetson et al.
2018/0136291	A1	5/2018	Pham et al.
2018/0275209	A1	9/2018	Mandeville et al.
2018/0275212	A1	9/2018	Hahn et al.
2018/0275224	A1	9/2018	Manickam et al.
2018/0275225	A1	9/2018	Hahn
2018/0348393	A1	12/2018	Hansen et al.
2019/0018085	A1	1/2019	Wu et al.

FOREIGN PATENT DOCUMENTS

DE	69608006	T2	2/2001
DE	19600241	C2	8/2002
DE	10228536	A1	1/2003
EP	0 161 940	B1	12/1990
EP	0 718 642		6/1996
EP	0 726 458		8/1996
EP	1 505 627		2/2005
EP	1 685 597		8/2006
EP	1 990 313		11/2008
EP	2 163 392		3/2010
EP	2 495 166	A1	9/2012
EP	2 587 232	A1	5/2013
EP	2 705 179		3/2014
EP	2 707 523		3/2014
EP	2 745 360		6/2014
EP	2 769 417		8/2014
EP	2 790 031		10/2014
EP	2 837 930	A1	2/2015
EP	2 907 792		8/2015
GB	2 423 366	A	8/2006
GB	2 433 737		7/2007
GB	2 482 596		2/2012
GB	2 483 767		3/2012
GB	2 486 794		6/2012
GB	2 490 589		11/2012
GB	2 491 936		12/2012
GB	2 493 236		1/2013
GB	2 495 632	A	4/2013
GB	2 497 660		6/2013
GB	2 510 053	A	7/2014
GB	2 515 226		12/2014
GB	2 522 309		7/2015
GB	2 526 639		12/2015
JP	3782147	B2	6/2006

(56) **References Cited**

FOREIGN PATENT DOCUMENTS

JP	4800896	B2	10/2011
JP	2012-103171		5/2012
JP	2012-110489		6/2012
JP	2012-121748		6/2012
JP	2013-028497		2/2013
JP	5476206	B2	4/2014
JP	5522606	B2	6/2014
JP	5536056	B2	7/2014
JP	5601183	B2	10/2014
JP	2014-215985		11/2014
JP	2014-216596		11/2014
JP	2015-518562	A	7/2015
JP	5764059	B2	8/2015
JP	2015-167176		9/2015
JP	2015-529328		10/2015
JP	5828036	B2	12/2015
JP	5831947	B2	12/2015
WO	WO-87/04028	A1	7/1987
WO	WO-88/04032	A1	6/1988
WO	WO-95/33972	A1	12/1995
WO	WO-2009/073736		6/2009
WO	WO-2011/046403	A2	4/2011
WO	WO-2011/153339	A1	12/2011
WO	WO-2012/016977	A2	2/2012
WO	WO-2012/084750		6/2012
WO	WO-2013/027074		2/2013
WO	WO-2013/059404	A1	4/2013
WO	WO-2013/066446	A1	5/2013
WO	WO-2013/066448		5/2013
WO	WO-2013/093136	A1	6/2013
WO	WO-2013/188732	A1	12/2013
WO	WO-2013/190329	A1	12/2013
WO	WO-2014/011286	A2	1/2014
WO	WO-2014/099110	A2	6/2014
WO	WO-2014/135544	A1	9/2014
WO	WO-2014/135547	A1	9/2014
WO	WO-2014/166883	A1	10/2014
WO	WO-2014/210486	A1	12/2014
WO	WO-2015/015172	A1	2/2015
WO	WO-2015/142945		9/2015
WO	WO-2015/157110	A1	10/2015
WO	WO-2015/157290	A1	10/2015
WO	WO-2015/158383	A1	10/2015
WO	WO-2015/193156	A1	12/2015
WO	WO-2016/075226	A1	5/2016
WO	WO-2016/118756	A1	7/2016
WO	WO-2016/118791	A1	7/2016
WO	WO-2016/122965	A1	8/2016
WO	WO-2016/122966	A1	8/2016
WO	WO-2016/126435	A1	8/2016
WO	WO-2016/126436	A1	8/2016
WO	WO-2016/190909	A2	12/2016
WO	WO-2017/007513	A1	1/2017
WO	WO-2017/007514	A1	1/2017
WO	WO-2017/014807	A1	1/2017
WO	WO-2017/039747	A1	3/2017
WO	WO-2017/095454	A1	6/2017
WO	WO-2017/127079	A1	7/2017
WO	WO-2017/127080	A1	7/2017
WO	WO-2017/127081	A1	7/2017
WO	WO-2017/127085	A1	7/2017
WO	WO-2017/127090	A1	7/2017
WO	WO-2017/127091	A1	7/2017
WO	WO-2017/127093	A1	7/2017
WO	WO-2017/127094	A1	7/2017
WO	WO-2017/127095	A1	7/2017
WO	WO-2017/127096	A1	7/2017
WO	WO-2017/127097	A1	7/2017
WO	WO-2017/127098	A1	7/2017

OTHER PUBLICATIONS

Rosskopf, "Advanced quantum sensing using nitrogen vacancy centers in diamond", Dissertation, p. 91 (12 pages), XP055500261, DOI: 10.3929/ethz-b-000168296 Retrieved from the Internet: URL: https://epo.summon.serialssolutions.com/2.0.0/Link/0/elvHCXMwY2BQsUxJMUsOMJTWNQWwlomqZYWuoIJ5qa6qaagq5BSjEzMLUG7kSOdTULczYPcTXwQHUXQqkrUWXXQ_a21WpJRpZukC26gWBhZmjEzsAJbAuaWkH1HrEqAZSIojWVyZkkqUoXhJsjA44106S3EwJSaJ8Lg5AidcFcoLAV6qDRXoRiOfDwvXaEUTAJzV1E-MEIVyIIKTQYWeAmJIJLB5ppCZpwCMRmCCSRFIMHVzDXH201X (retr.

Schonfeld, "Optical readout of single spins for quantum computing and magnetic sensing", Dissertation, Fachbereich Physlk der Freien Universitat Berlin, May 1, 2011, 21 Pages (relevant pages only), XP055143403. Retrieved from the Internet: URL: http://www.diss.fu-berlin.de/diss/servlets/MCRFileNodeServIeUFU Diss derivate_000000012199/DIssertatIon_Slmon-choenfela PublIcVersion-2.pdfJsessionid-89A943688E59.

U.S. Final Office Action for U.S. Appl. No. 15/003,396 dated Mar. 22, 2019, 13 pages.

U.S. Final Office Action for U.S. Appl. No. 15/382,045 dated Apr. 26, 2019, 16 pages.

U.S. Final Office Action for U.S. Appl. No. 15/443,422 dated Mar. 7, 2019, 17 pages.

U.S. Non-Final Office Action for U.S. Appl. No. 15/003,193 dated Apr. 11, 2019, 7 pages.

U.S. Non-Final Office Action for U.S. Appl. No. 15/003,309 dated Feb. 13, 2019, 16 pages.

U.S. Non-Final Office Action for U.S. Appl. No. 15/003,617 dated Feb. 26, 2019, 10 pages.

U.S. Non-Final Office Action for U.S. Appl. No. 15/372,201 dated Apr. 2, 2019, 10 pages.

U.S. Non-Final Office Action for U.S. Appl. No. 15/419,832 dated Feb. 8, 2019, 12 pages.

U.S. Non-Final Office Action for U.S. Appl. No. 15/440,194 dated Feb. 15, 2019, 21 pages.

U.S. Non-Final Office Action for U.S. Appl. No. 15/446,373 dated Apr. 19, 2019, 8 pages.

U.S. Non-Final Office Action for U.S. Appl. No. 15/468,314 dated Mar. 28, 2019, 17 pages.

U.S. Non-Final Office Action for U.S. Appl. No. 15/468,410 dated Apr. 11, 2019, 15 pages.

U.S. Non-Final Office Action for U.S. Appl. No. 15/468,559 dated Apr. 11, 2019, 12 pages.

U.S. Non-Final Office Action for U.S. Appl. No. 15/469,374 dated Feb. 28, 2019, 14 pages.

U.S. Notice of Allowance for U.S. Appl. No. 15/003,617 dated Apr. 30, 2019, 9 pages.

U.S. Notice of Allowance for U.S. Appl. No. 15/207,457 dated Mar. 6, 2019, 16 pages.

U.S. Notice of Allowance for U.S. Appl. No. 15/376,244 dated Feb. 21, 2019, 7 pages.

U.S. Notice of Allowance for U.S. Appl. No. 15/380,419 dated Feb. 26, 2019, 5 pages.

U.S. Notice of Allowance for U.S. Appl. No. 15/400,794 dated Apr. 25, 2019, 5 pages.

U.S. Notice of Allowance for U.S. Appl. No. 15/437,038 dated Mar. 21, 2019, 13 pages.

U.S. Notice of Allowance for U.S. Appl. No. 15/437,222 dated Mar. 25, 2019, 11 pages.

U.S. Notice of Allowance for U.S. Appl. No. 15/468,282 dated Feb. 19, 2019, 8 pages.

U.S. Notice of Allowance for U.S. Appl. No. 15/468,56 dated Apr. 22, 2019, 8 pages.

U.S. Notice of Allowance for U.S. Appl. No. 15/468,582 dated Mar. 21, 2019, 13 pages.

U.S. Notice of Allowance for U.S. Appl. No. 15/468,951 dated Mar. 28, 2019, 8 pages.

European Extended Search Report for Appl. Ser. No. 16740794.9 dated Nov. 12, 2018, 12 pages.

Halbach et al., "Design of Permanent Multipole Magnets with Oriented Rare Earth Cobalt Material", Nuclear Instruments and

(56) **References Cited**

OTHER PUBLICATIONS

Methods, North Holland Publishing Co., Amsterdam, NL., vol. 169, Jan. 1, 1980, pp. 1-5, XP001032085, DOI: 10.1016/0029-554X(80)90094-4.
Hodges et al., "Time-keeping with electron spin states in diamond", Dept. of Electrical Engineering and Dept. of Applied Physics and Applied Mathematics, Columbia University, New York, New York 10027, Aug. 30, 2011, 13 pages.
Hodges et al., Appendix, "Time-keeping with electron spin states in diamond", Dept. of Electrical Engineering and Dept. of Applied Physics and Applied Mathematics, Columbia University, New York, New York 10027, Aug. 27, 2012, 46 pages.
International Search Report and Written Opinion for PCT Appl. Ser. No. PCT/US2018/041527 dated Feb. 4, 2019, 22 pages.
U.S. Ex Parte Quayle Action for U.S. Appl. No. 15/468,641 dated Nov. 28, 2018, 11 pages.
U.S. Non-Final Office Action for U.S. Appl. No. 15/003,177 dated Jan. 14, 2019, 15 pages.
U.S. Non-Final Office Action for U.S. Appl. No. 15/003,670 dated Nov. 27, 2018, 14 pages.
U.S. Non-Final Office Action for U.S. Appl. No. 15/382,045 dated Dec. 31, 2018, 16 pages.
U.S. Non-Final Office Action for U.S. Appl. No. 15/400,794 dated Jan. 10, 2019, 6 pages.
U.S. Non-Final Office Action for U.S. Appl. No. 15/468,356 dated Jan. 2, 2019, 10 pages.
U.S. Non-Final Office Action for U.S. Appl. No. 15/468,951 dated Dec. 13, 2018, 9 pages.
U.S. Notice of Allowance for U.S. Appl. No. 15/003,670 dated Feb. 1, 2019, 7 pages.
U.S. Notice of Allowance for U.S. Appl. No. 15/350,303 dated Dec. 26, 2018, 10 pages.
U.S. Notice of Allowance for U.S. Appl. No. 15/450,504 dated Dec. 13, 2018, 7 pages.
U.S. Notice of Allowance for U.S. Appl. No. 15/454,162 dated Jan. 17, 2019, 8 pages.
U.S. Notice of Allowance for U.S. Appl. No. 15/468,397 dated Dec. 12, 2018, 5 pages.
U.S. Notice of Allowance for U.S. Appl. No. 15/468,641 dated Feb. 7, 2019, 10 pages.
U.S. Notice of Allowance for U.S. Appl. No. 15/479,256 dated Feb. 4, 2019, 7 pages.
Teeling-Smith et al., "Electron Paramagnetic Resonance of a Single NV Nanodiamond Attached to an Individual Biomolecule", Biophysical Journal 110, May 10, 2016, pp. 2044-2052.
UK Office Action dated Jun. 8, 2018, from related application No. GB1617438.5, 3 pages.
U.S. Final Office Action dated Jul. 26, 2018 from related U.S. Appl. No. 15/003,177, 14 pages.
U.S. Non-Final Office Action dated Aug. 6, 2018 from related U.S. Appl. No. 15/376,244, 28 pages.
U.S. Non-Final Office Action dated Aug. 9, 2018 from related U.S. Appl. No. 15/003,309, 22 pages.
U.S. Non-Final Office Action dated Jul. 20, 2018 from related U.S. Appl. No. 15/350,303, 13 pages.
U.S. Non-Final Office Action dated Jul. 26, 2018 from related U.S. Appl. No. 15/380,419, 11 pages.
U.S. Non-Final Office Action dated Jul. 3, 2018 from related U.S. Appl. No. 15/003,396, 19 pages.
U.S. Notice of Allowance dated Jul. 18, 2018 from related U.S. Appl. No. 15/468,386, 12 pages.
U.S. Notice of Allowance dated Jul. 6, 2018 from related U.S. Appl. No. 15/672,953, 11 pages.
U.S. Notice of Allowance dated Jun. 27, 2018 from related U.S. Appl. No. 15/003,519, 21 pages.
U.S. Notice of Allowance dated May 15, 2018, from related U.S. Appl. No. 15/003,209, 7 pages.
U.S. Notice of Allowance dated May 16, 2018, from related U.S. Appl. No. 15/003,145, 8 pages.
U.S. Office Action dated Jun. 19, 2018, from related U.S. Appl. No. 15/450,504, 12 pages.
European Extended Search Report for Appl. Ser. No. 16743879.5 dated Sep. 11, 2018, 11 pages.
European Extended Search Report for Appl. Ser. No. 16800410.9 dated Oct. 12, 2018, 11 pages.
Fenglian Niu, "Crack Detection of Power Line Based on Metal Magnetic Memory Non-destructive", Telkomnika Indonesian Journal of Electrical Engineering, vol. 12, No. 11, Nov. 1, 2014, pp. 7764-7771.
U.S. Final Office Action for U.S. Appl. No. 15/380,691 dated Sep. 21, 2018, 12 pages.
U.S. Final Office Action for U.S. Appl. No. 15/479,256 dated Sep. 10, 2018, 20 pages.
U.S. Non-Final Office Action for U.S. Appl. No. 15/443,422 dated Oct. 2, 2018, 16 pages.
U.S. Non-Final Office Action for U.S. Appl. No. 15/446,373 dated Oct. 1, 2018, 13 pages.
U.S. Non-Final Office Action for U.S. Appl. No. 15/454,162 dated Sep. 10, 2018, 13 pages.
U.S. Non-Final Office Action for U.S. Appl. No. 15/468,282 dated Oct. 10, 2018, 12 pages.
U.S. Non-Final Office Action for U.S. Appl. No. 15/372,201 dated Oct. 15, 2018, 12 pages.
U.S. Non-Final Office Action for U.S. Appl. No. 15/468,274 dated Oct. 26, 2018, 11 pages.
U.S. Notice of Allowance U.S. Appl. No. 14/866,730 dated Aug. 15, 2018, 9 pages.
U.S. Notice of Allowance for U.S. Appl. No. 15/468,289 dated Oct. 17, 2018, 12 pages.
U.S. Notice of Allowance for U.S. Appl. No. 15/003,704 dated Nov. 2, 2018, 19 pages.
U.S. Office Action for U.S. Appl. No. 15/468,397 dated Sep. 13, 2018, 7 pages.
International Search Report and Written Opinion for PCT Appl. Ser. No. PCT/US2019/022097 dated May 15, 2019, 13 pages.
U.S. Final Office Action for U.S. Appl. No. 15/003,309 dated May 23, 2019, 8 pages.
U.S. Non-Final Office Action for U.S. Appl. No. 15/468,274 dated May 14, 2019, 15 pages.
U.S. Non-Final Office Action for U.S. Appl. No. 15/468,303 dated Jun. 25, 2019, 14 pages.
U.S. Notice of Allowance for U.S. Appl. No. 15/419,832 dated Jun. 24, 2019, 5 pages.
U.S. Notice of Allowance for U.S. Appl. No. 15/443,422 dated Jul. 23, 2019, 10 pages.
U.S. Notice of Allowance for U.S. Appl. No. 15/469,374 dated Jun. 20, 2019, 5 pages.
"Diamond Sensors, Detectors, and Quantum Devices' in Patent Application Approval Process," Chemicals & Chemistry, pp. 1-6, (Feb. 28, 2014), 6 pages.
"Findings from University of Stuttgart in physics reported," Science Letter, (Jul. 7, 2009), 2 pages.
"New Findings on Nitrogen from Ecole Normale Superieure Summarized (Magnetic imaging with an ensemble of nitrogen vacancy-centers in diamond)," Physics Week, pp. 1-2, (Jul. 21, 2015), 2 pages.
"Patent Issued for Diamond Sensors, Detectors, and Quantum Devices (USPTO 9249526)," Journal of Engineering, pp. 1-5 (Feb. 15, 2016), 5 pages.
"Researchers Submit Patent Application, 'Diamond Sensors, Detectors, and Quantum Devices', for Approval," Chemicals & Chemistry, pp. 1-7, (Apr. 11, 2014), 7 pages.
Acosta et al., "Broadband magnetometry by infrared-absorption detection of nitrogen-vacancy ensembles in diamond," Appl. Phys. Letters 97: 174104 (Oct. 29, 2010), 4 pages.
Acosta et al., "Diamonds with a high density of nitrogen-vacancy centers for magnetometry applications," Physical Review B 80(115202): 1-15 (Sep. 9, 2009), 15 pages.
Acosta et al., "Nitrogen-vacancy centers: physics and applications," MRS Bulletin 38(2): 127-130 (Feb. 2013), 4 pages.

(56) **References Cited**

OTHER PUBLICATIONS

Acosta, "Optical Magnetometry with Nitrogen-Vacancy Centers in Diamond," University of California Berkeley, (Spring 2011), 118 pages.
Aiello et al., "Composite-pulse magnetometry with a solid-state quantum sensor," Nature Communications 4(1419): 1-6 (Jan. 29, 2013), 6 pages.
Alam, "Solid-state 13C magic angle spinning NMR spectroscopy characterization of particle size structural variations in synthetic nanodiamonds," Materials Chemistry and Physics 85(2-3): 310-315 (Jun. 15, 2004), 6 pages.
Albrecht et al., "Coupling of nitrogen vacancy centres in nanodiamonds by means of phonons," New Journal of Physics 15(083014): 1-26 (Aug. 6, 2013), 27 pages.
Appel et al., "Nanoscale microwave imaging with a single electron spin in diamond," New Journal of Physics 17(112001): 1-6 (Nov. 3, 2015), 7 pages.
Arai et al., "Fourier magnetic imaging with nanoscale resolution and compressed sensing speed-up using electronic spins in diamond," Nature Nanotechnology 10: 859-864 (Aug. 10, 2015), 7 pages.
Aslam et al., "Single spin optically detected magnetic resonance with 60-90 GHz (E-band) microwave resonators," Review of Scientific Instruments 86(064704): 1-8 (Jun. 22, 2015), 9 pages.
Awschalom et al., "Diamond age of spintronics," Scientific American 297: 84-91 (Oct. 2007), 8 pages.
Babamoradi et al., "Correlation between entanglement and spin density in nitrogen-vacancy center of diamond," European Physical Journal D 65: 597-603 (Dec. 1, 2011), 7 pages.
Babunts et al., "Diagnostics of NV defect structure orientation in diamond using optically detected magnetic resonance with a modulated magnetic field," Technical Physics Letters 41(6): 583-586 (Jun. 2015; first published online Jul. 14, 2015), 4 pages.
Babunts et al., "Temperature-scanned magnetic resonance and the evidence of two-way transfer of a nitrogen nuclear spin hyperfine interaction in coupled NV-N pairs in diamond," JETP Letters 95(8): 429432 (Jun. 27, 2012), 4 pages.
Bagguley et al., "Zeeman effect of acceptor states in semiconducting diamond," Journal of the Physical Society of Japan 21(Supplement): 244-248 (1966), 7 pages.
Balasubramanian et al., "Nanoscale imaging magnetometry with diamond spins under ambient conditions," Nature 455: 648-651 (Oct. 2, 2008), 5 pages.
Balmer et al., "Chemical Vapour deposition synthetic diamond: materials technology and applications," J. of Physics: Condensed Matter 21(36): 1-51 (Aug. 19, 2009), 51 pages.
Baranov et al., "Enormously High Concentrations of Fluorescent Nitrogen-Vacancy Centers Fabricated by Sintering of Detonation Nanodiamonds," Small 7(11): 1533-1537 (Jun. 6, 2011; first published online Apr. 26, 2011), 5 pages.
Barfuss et al., "Strong mechanical driving of a single electron spin," Nature Physics 11: 820-824 (Aug. 3, 2015), 6 pages.
Barry et al., "Optical magnetic detection of single-neuron action potentials using quantum defects in diamond," as submitted to Quantum Physics on Feb. 2, 2016, 23 pages.
Bennett et al., "CVD Diamond for High Power Laser Applications," SPIE 8603, High-Power Laser Materials Processing: Lasers, Beam Delivery, Diagnostics, and Applications II, 860307 (Feb. 22, 2013), 10 pages.
Berman & Chernobrod, "Single-spin microscope with sub-nanoscale resolution based on optically detected magnetic resonance," SPIE 7608, Quantum Sensing and Nanophotonic Devices VII, 76080Y (Jan. 23, 2010), 4 pages.
Berman et al. "Measurement of single electron and nuclear spin states based on optically detected magnetic resonance," J. Physics: Conf. Series 38: 167-170 (2006), 5 pages.
Blakley et al., "Room-temperature magnetic gradiometry with fiber-coupled nitrogen-vacancy centers in diamond," Optics Letters 40(16): 3727-3730 (Aug. 5, 2015), 4 pages.
Bourgeois, et al., "Photoelectric detection of electron spin resonance of nitrogen-vacancy centres in diamond," Nature Communications 6(8577): 1-8 (Oct. 21, 2015), 8 pages.
Brenneis, et al. "Ultrafast electronic readout of diamond nitrogen-vacancy centres coupled to graphene." Nature nanotechnology 10.2 (2015): 135-139.
Bucher et al, "High Resolution Magnetic Resonance Spectroscopy Using Solid-State Spins", May 25, 2017, downloaded from https://arxiv.org/ (arXiv.org > quant-ph > arXiv:1705.08887) on May 25, 2017, pp. 1-24.
Budker & Kimball, "Optical Magnetometry," Cambridge Press, (2013), 11 pages.
Budker & Romalis, "Optical Magnetometry," Nature Physics 3: 227-243 (Apr. 2007), 8 pages.
Bui et al., "Noninvasive Fault Monitoring of Electrical Machines by Solving the Steady-State Magnetic Inverse Problem," in IEEE Transactions on Magnetics, vol. 44, No. 6, pp. 1050-1053, Jun. 24, 2008.
Casanova, et al., "Effect of magnetic field on phosphorus centre in diamond," Physica Status Solidi A 186(2): 291-295 (Jul. 30, 2001), 6 pages.
Castelletto, et al., "Frontiers in diffraction unlimited optical methods for spin manipulation, magnetic field sensing and imaging using diamond nitrogen vacancy defects," Nanophotonics 1(2): 139-153 (Nov. 2012), 15 pages.
Chadebec et al., "Rotor fault detection of electrical machines by low frequency magnetic stray field analysis," 2005 5th IEEE International Symposium on Diagnostics for Electric Machines, Power Electronics and Drives, Vienna, 2005, submitted Mar. 22, 2006, pp. 1-6.
Chapman, et al., "Anomalous saturation effects due to optical spin depolarization in nitrogen-vacancy centers in diamond nanocrystals," Physical Review B 86(045204): 1-8 (Jul. 10, 2012), 8 pages.
Chavez, et al. "Detecting Arctic oil spills with NMR: a feasibility study." Near Surface Geophysics 13.4 (Feb. 2015): 409-416.
Chen et al., "Vector magnetic field sensing by a single nitrogen vacancy center in diamond," EPL 101(67003): 1-5 (Mar. 2013), 6 pages.
Chernobrod et al., "Improving the sensitivity of frequency modulation spectroscopy using nanomechanical cantilevers," Applied Physics Letters 85(17): 3896-3898 (Oct. 25, 2004), 3 pages.
Chernobrod et al., "Spin Microscope Based on Optically Detected Magnetic Resoncance," Journal of Applied Physics 97(014903): 1-3, (2005; first published online Dec. 10, 2004), 4 pages.
Childress et al., "Coherent dynamics of coupled electron and nuclear spin qubits in diamond," Science 314(5797): 281-285 (Oct. 13, 2006), 6 pages.
Chipaux et al., "Magnetic imaging with an ensemble of nitrogen vacancy-centers in diamond," European Physical Journal D 69(166): 1-10 (Jul. 2, 2015), 10 pages.
Chipaux et al., "Nitrogen vacancies (NV) centers in diamond for magnetic sensors and quantum sensing," SPIE 9370, Quantum Sensing and Nanophotonic Devices XII, 93701V (Feb. 8, 2015), 6 pages.
Chipaux, et al., "Wide bandwidth instantaneous radio frequency spectrum analyzer based on nitrogen vacancy centers in diamond," Applied Physics Letters 107(233502): 1-5 (2015), 6 pages.
Clevenson et al., "Broadband magnetometry and temperature sensing with a light-trapping diamond waveguide," Nature Physics 11: 393-397 (May 2015; first published online Apr. 6, 2015), 6 pages.
Constable, "Geomagnetic Spectrum, Temporal." In Encyclopedia of Geomagnetism and Paleomagnetism, pp. 353-355, Springer: Dordrecht, Netherlands (2007), 3 pages.
Cooper et al., "Time-resolved magnetic sensing with electronic spins in diamond," Nature Communications 5:3141: 1-7 (Jan. 24, 2014), 7 pages.
Creedon et al., "Strong coupling between P1 diamond impurity centers and a three-dimensional lumped photonic microwave cavity," Physical Review B 91(140408R): 1-5 (Apr. 24, 2015), 5 pages.
Dale, et al. "Medical applications of diamond magnetometry: commercial viability." arXiv preprint arXiv:1705.01994 (May 8, 2017), pp. 1-7.

(56) **References Cited**

OTHER PUBLICATIONS

Davies, "Current problems in diamond: towards a quantitative understanding," Physica B 273-274: 1513 (Dec. 15, 1999), 9 pages.
De Lange et al., "Single-Spin Magnetometry with Multipulse Sensing Sequences," Physical Review Letters 106(080802): 1-4 (Feb. 24, 2011), 4 pages.
Degen, "Scanning magnetic field microscope with a diamond single-spin sensor," Applied Physics Letters 92(243111): 1-3 (Jun. 17, 2008), 3 pages.
Delacroix et al., "Design, manufacturing, and performance analysis of mid-infrared achromatic half-wave plates with diamond subwavelength gratings," Applied Optics 51(24): 5897-5902 (Aug. 16, 2012), 6 pages.
Denatale et al., "Fabrication and characterization of diamond moth eye antireflective surfaces on Ge," J. of Applied Physics 71: 1388-1393 (Mar. 1992), 8 pages.
Dobrovitski et al., "Quantum Control over Single Spins in Diamond," Annual Review of Condensed Matter Physics 4: 23-50 (Apr. 2013), 30 pages.
Doherty et al., "The nitrogen-vacancy colour centre in diamond," Physics Reports 528: 1-45 (Jul. 1, 2013), 45 pages.
Doherty et al., "Theory of the ground-state spin of the NV- center in diamond," Physical Review B 85(205203): 1-21 (May 3, 2012), 21 pages.
Doi et al., "Pure negatively charged state of the NV center in n-type diamond," Physical Review B 93(081203): 1-6 (Feb. 3, 2016), 6 pages.
Drake et al., "Influence of magnetic field alignment and defect concentration on nitrogen-vacancy polarization in diamond," New Journal of Physics 18(013011): 1-8 (Jan. 2016; first published on Dec. 24, 2015), 9 pages.
Dreau et al., "Avoiding power broadening in optically detected magnetic resonance of single NV defects for enhanced dc magnetic field sensitivity," Physical Review B 84(195204): 1-8 (Nov. 23, 2011), 8 pages.
Dreau et al., "High-resolution spectroscopy of single NV defects coupled with nearby 13C nuclear spins in diamond," Physical Review B 85(134107): 1-7 (Apr. 20, 2012), 7 pages.
Dumeige et al., "Magnetometry with nitrogen-vacancy ensembles in diamond based on infrared absorption in a doubly resonant optical cavity," Physical Review B 87(155202): 1-9 (Apr. 8, 2013), 9 pages.
Epstein et al., "Anisotropic interactions of a single spin and dark-spin spectroscopy in diamond," Nature Physics 1:94-98 (Nov. 2005), 5 pages.
Fallah et al., "Multi-sensor approach in vessel magnetic wake imaging," Wave Motion 51(1): 60-76 (Jan. 2014), retrieved from http://www.sciencedirect.com/science/article/pii/S0165212513001133 (Aug. 21, 2016).
Fedotov et al., "High-resolution magnetic field imaging with a nitrogen-vacancy diamond sensor integrated with a photonic-crystal fiber," Optics Letters 41(3): 472-475 (Feb. 1, 2016; published Jan. 25, 2016), 4 pages.
Fedotov et al., "Photonic-crystal-fiber-coupled photoluminescence interrogation of nitrogen vacancies in diamond nanoparticles," Laser Physics Letters 9(2): 151-154 (Feb. 2012; first published online Dec. 2, 2011), 5 pages.
Feng & Wei, "A steady-state spectral method to fit microwave absorptions of NV centers in diamonds: application to sensitive magnetic field sensing," Measurement Science & Technology 25(105102): 1-6 (Oct. 2014; first published online Aug. 29, 2014), 7 pages.
Fologea, et al. "Detecting single stranded DNA with a solid state nanopore." Nano Letters 5.10 (Aug. 15, 2005): 1905-1909.
Freitas, et al., "Solid-State Nuclear Magnetic Resonance (NMR) Methods Applied to the Study of Carbon Materials," Chemistry and Physics of Carbon, vol. 31 (2012), 45 pages.
Froidurot et al., "Magnetic discretion of naval propulsion machines," in IEEE Transactions on Magnetics, vol. 38, No. 2, pp. 1185-1188, Mar. 2002.
Gaebel, et al. "Room-temperature coherent coupling of single spins in diamond." Nature Physics 2.6 (May 28, 2006): 408-413.
GB Examination Report from United Kingdom application No. GB 1618202.4 dated Jan. 10, 2017.
Geiselmann et al., "Fast optical modulation of the fluorescence from a single nitrogen-vacancy centre," Nature Physics 9: 785-789 (Dec. 2013; first published online Oct. 13, 2013), 5 pages.
Gombert & Blasi, "The Moth-Eye Effect-From Fundamentals to Commercial Exploitation," Functional Properties of Bio-Inspired Surfaces: 79-102, (Nov. 2009), 26 pages.
Gong et al., "Generation of Nitrogen-Vacancy Center Pairs in Bulk Diamond by Molecular Nitrogen Implantation," Chinese Physics Letters 33(2)(026105): 1-4 (Feb. 2016), 5 pages.
Gould et al., "An imaging magnetometer for bio-sensing based on nitrogen-vacancy centers in diamond," SPIE 8933, Frontiers in Biological Detection: From Nanosensors to Systems VI, 89330L (Mar. 18, 2014), 8 pages.
Gould et al., "Room-temperature detection of a single 19 nm superparamagnetic nanoparticle with an imaging magnetometer," Applied Physics Letters 105(072406): 1-4 (Aug. 19, 2014), 5 pages.
Gruber et al., "Scanning confocal optical microscopy and magnetic resonance on single defect centers," Science 276(5321): 2012-2014 (Jun. 27, 1997), 4 pages.
Haeberle et al., "Nanoscale nuclear magnetic imaging with chemical contrast," Nature Nanotechnology 10: 125-128 (Feb. 2015; first published online Jan. 5, 2015), 4 pages.
Haihua et al., "Design of wideband anti-reflective sub wavelength nanostructures," Infrared and Laser Engineering 40(2): 267-270 (Feb. 2011), 4 pages.
Hall et al., "Sensing of Fluctuating Nanoscale Magnetic Fields Using Nitrogen-Vacancy Centers in Diamond," Physical Review Letters 103(220802): 1-4 (Nov. 25, 2009), 4 pages.
Hanson et al., "Coherent Dynamics of a Single Spin Interacting with an Adjustable Spin Bath," Science 320(5874): 352-355 (Apr. 18, 2008), 5 pages.
Hanson et al., "Polarization and Readout of Coupled Single Spins in Diamond," Physical Review Letters 97(087601): 1-4 (Aug. 23, 2006), 4 pages.
Hanson et al., "Room-temperature manipulation and decoherence of a single spin in diamond," Physical Review 74(161203): 1-4 (Oct. 26, 2006), 4 pages.
Hanzawa et al., "Zeeman effect on the zero-phonon line of the NV center in synthetic diamond," Physica B 184(1-4): 137-140 (Feb. 1993), 4 pages.
Heerema, et al. "Graphene nanodevices for DNA sequencing." Nature nanotechnology 11.2 (Feb. 3, 2016): 127-136.
Hegyi & Yablonovitch, "Molecular imaging by optically detected electron spin resonance of nitrogen-vacancies in nanodiamonds," Nano Letters 13(3): 1173-1178 (Mar. 2013; first published online Feb. 6, 2013), 6 pages.
Hegyi & Yablonovitch, "Nanodiamond molecular imaging with enhanced contrast and expanded field of view," Journal of Biomedical Optics 19(1)(011015): 1-8 (Jan. 2014), 9 pages.
Hilser et al., "All-optical control of the spin state in the NV-center in diamond," Physical Review B 86(125204): 1-8 (Sep. 14, 2012), 8 pages.
Hobbs, "Study of the Environmental and Optical Durability of AR Microstructures in Sapphire, ALON, and Diamond," SPIE 7302, Window and Dome Technologies and Materials XI, 73020J (Apr. 27, 2009), 14 pages.
Huebener et al., "ODMR of NV centers in nano-diamonds covered with N©C60," Physica Status Solidi B 245(10): 2013-2017 (Oct. 2008; first published online Sep. 8, 2008), 5 page.
Huxter et al., "Vibrational and electronic dynamics of nitrogen-vacancy centres in diamond revealed by two-dimensional ultrafast spectroscopy," Nature Physics 9: 744-749 (Sep. 29, 2013), 6 pages.
IEEE Standards Association, "Part 11: Wireless LAN Medium Access Control (MAC) and Physical Layer (PHY) Specifications", IEEE Std 802.11 TM-2012, Mar. 29, 2012, pp. 1605, 16811686, 1694-1710 (27 total pages, including cover and publication pages).
International Search Report and Written Opinion from related PCT application PCT/US2017/035315 dated Aug. 24, 2017, 7 pages.

(56) **References Cited**

OTHER PUBLICATIONS

International Search Report and Written Opinion of the International Searching Authority dated Apr. 1, 2016 from related PCT application PCT/US2016/014384, 12 pages.
International Search Report and Written Opinion of the International Searching Authority dated Apr. 11, 2016 from related PCT application PCT/US2016/014376, 12 pages.
International Search Report and Written Opinion of the International Searching Authority dated Apr. 11, 2016 from related PCT application PCT/US2016/014388, 14 pages.
International Search Report and Written Opinion of the International Searching Authority dated Apr. 11, 2016 from related PCT application PCT/US2016/014395, 15 pages.
International Search Report and Written Opinion of the International Searching Authority dated Apr. 4, 2017 from related PCT application PCT/US16/68366, 9 pages.
International Search Report and Written Opinion of the International Searching Authority dated Feb. 15, 2017 from related PCT application PCT/US2016/014390, 20 pages.
International Search Report and Written opinion of the International Searching Authority dated Jul. 12, 2016, from related PCT application PCT/US2016/014287, 14 pages.
International Search Report and Written Opinion of the International Searching Authority dated Jul. 16, 2015, from related PCT application PCT/US2015/24723, 8 pages.
International Search Report and Written Opinion of the International Searching Authority dated Jul. 6, 2015, from related PCT application PCT/US2015/021093, 9 pages.
International Search Report and Written Opinion of the International Searching Authority dated Jul. 8, 2015, from related PCT application PCT/US2015/024265, 11 pages.
International Search Report and Written Opinion of the International Searching Authority dated Jun. 1, 2017, from related PCT application PCT/US17/21811, 9 pages.
International Search Report and Written Opinion of the International Searching Authority dated Jun. 1, 2017, in related PCT application PCT/US17/22279, 20 pages.
International Search Report and Written Opinion of the International Searching Authority dated Jun. 10, 2016 from related PCT application PCT/US2016/014290, 11 pages.
International Search Report and Written Opinion of the International Searching Authority dated Jun. 15, 2017, from related PCT application PCT/US2017/024175, 10 pages.
International Search Report and Written Opinion of the International Searching Authority dated Jun. 2, 2016, from related PCT application PCT/US2016/014386, 14 pages.
International Search Report and Written Opinion of the International Searching Authority dated Jun. 2, 2016, from related PCT application PCT/US2016/014387, 13 pages.
International Search Report and Written Opinion of the International Searching Authority dated Jun. 6, 2016, from related PCT application PCT/US2016/014291, 13 pages.
International Search Report and Written Opinion of the International Searching Authority dated Jun. 9, 2016 from related PCT application PCT/US2016/014333, 16 pages.
International Search Report and Written Opinion of the International Searching Authority dated Jun. 9, 2017, from related patent application PCT/US2017/024181, 13 pages.
International Search Report and Written Opinion of the International Searching Authority dated Jun. 9, 2017, from related PCT application PCT/US2017/024179, 9 pages.
International Search Report and Written Opinion of the International Searching Authority dated Mar. 13, 2017 from related PCT application PCT/US2016/68320, 10 pages.
International Search Report and Written Opinion of the International Searching Authority dated Mar. 24, 2016 from related PCT application PCT/US2016/014336, 17 pages.
International Search Report and Written Opinion of the International Searching Authority dated Mar. 24, 2016 from related PCT application PCT/US2016/014297, 15 pages.
International Search Report and Written Opinion of the International Searching Authority dated Mar. 24, 2016 from related PCT application PCT/US2016/014392, 8 pages.
International Search Report and Written Opinion of the International Searching Authority dated Mar. 2016 from related PCT application PCT/US2016/014403, 10 pages.
International Search Report and Written Opinion of the International Searching Authority dated Mar. 2016, from related PCT application PCT/US2016/014363, 8 pages.
International Search Report and Written Opinion of the International Searching Authority dated Mar. 25, 2016, from related PCT application PCT/US2016/014389, 19 pages.
International Search Report and Written Opinion of the International Searching Authority dated Mar. 27, 2017 from related PCT application PCT/US16/68344, 16 pages.
International Search Report and Written Opinion of the International Searching Authority dated Mar. 28, 2016, from related PCT application PCT/US2016/014380, 9 pages.
International Search Report and Written Opinion of the International Searching Authority dated Mar. 28, 2016, from related PCT application PCT/US2016/014394, 17 pages.
International Search Report and Written Opinion of the International Searching Authority dated Mar. 29, 2016 from related PCT application PCT/US2016/014325, 11 pages.
International Search Report and Written Opinion of the International Searching Authority dated Mar. 29, 2016 from related PCT application PCT/US2016/014330, 8 pages.
International Search Report and Written Opinion of the International Searching Authority dated Mar. 29, 2016, from related PCT application PCT/US2016/014328, 7 pages.
International Search Report and Written Opinion of the International Searching Authority dated Mar. 29, 2016, from related PCT application PCT/US2016/014385, 11 pages.
International Search Report and Written Opinion of the International Searching Authority dated Mar. 30, 2016 from related PCT application PCT/US2016/014298, 14 pages.
International Search Report and Written Opinion of the International Searching Authority dated Mar. 31, 2016 from related PCT application PCT/US2016/014375, 11 pages.
International Search Report and Written Opinion of the International Searching Authority dated Mar. 31, 2016 from related PCT application PCT/US2016/014396, 11 pages.
International Search Report and Written Opinion of the International Searching Authority dated Mar. 31, 2017 from related PCT application PCT/US2016/066566, 11 pages.
International Search Report and Written Opinion of the International Searching Authority dated May 10, 2017 from related PCT application PCT/US17/19411, 8 pages.
International Search Report and Written Opinion of the International Searching Authority dated May 18, 2017, from related PCT application PCT/US2017/021593, 10 pages.
International Search Report and Written Opinion of the International Searching Authority dated May 19, 2017, from related PCT application PCT/US17/18099, 16 pages.
International Search Report and Written Opinion of the International Searching Authority dated May 26, 2016, from related PCT application PCT/US2016/014331, 15 pages.
International Search Report and Written Opinion of the International Searching Authority dated May 3, 2017 from related PCT application PCT/US2017/018701, 8 pages.
International Search Report and Written Opinion of the International Searching Authority dated May 4, 2017 from related PCT application PCT/US2017/018709, 8 pages.
International Search Report and Written Opinion of the International Searching Authority dated May 8, 2017 from related PCT application PCT/US2017/17321, 17 pages.
International Search Report and Written Opinion of the International Searching Authority dated Sep. 13, 2016, from related PCT application PCT/US16/14377, 11 pages.
International Search Report and Written Opinion of the International Searching Authority dated Jul. 14, 2017, from related PCT application PCT/US2017/022118, 13 pages.

(56) **References Cited**

OTHER PUBLICATIONS

International Search Report and Written Opinion of the International Searching Authority dated Jul. 17, 2017, from related PCT application PCT/US2017/024177, 11 pages.
International Search Report and Written Opinion of the International Searching Authority dated Jul. 18, 2017, from related PCT application PCT/US2017/024167, 11 pages.
International Search Report and Written Opinion of the International Searching Authority dated Jul. 18, 2017, from related PCT application PCT/US2017/024173, 13 pages.
International Search Report and Written Opinion of the International Searching Authority dated Jul. 19, 2017, from related PCT application PCT/US2017/024171, 12 pages.
International Search Report and Written Opinion of the International Searching Authority dated Jun. 15, 2017, from related PCT application PCT/US2017/024182, 21 pages.
International Search Report and Written Opinion of the International Searching Authority dated Jun. 22, 2017, in related PCT application PCT/US2017/024180, 10 pages.
International Search Report and Written Opinion of the International Searching Authority dated Jun. 5, 2017, from related PCT application PCT/US2017/024169, 11 pages.
International Search Report and Written Opinion of the International Searching Authority dated Jun. 5, 2017, from related PCT application PCT/US2017/024174, 8 pages.
International Search Report and Written Opinion of the International Searching Authority dated Jun. 5, 2017, in related PCT application PCT/US2017/024168, 7 pages.
International Search Report and Written Opinion of the International Searching Authority dated Jun. 6, 2017, from related PCT application PCT/2017/024165, 9 pages.
International Search Report and Written Opinion of the International Searching Authority dated Jun. 6, 2017, from related PCT application PCT/US2017/024172, 9 pages.
Ivady et al., "Pressure and temperature dependence of the zero-field splitting in the ground state of NV centers in diamond: A first-principles study," Physical Review B 90(235205): 1-8 (Dec. 2014), 8 pages.
Jarmola et al., "Temperature- and Magnetic-Field-Dependent Longitudinal Spin Relaxation in Nitrogen-Vacancy Ensembles in Diamond," Physical Review Letters 108 (197601): 1-5 (May 2012), 5 pages.
Jensen et al., "Light narrowing of magnetic resonances in ensembles of nitrogen-vacancy centers in diamond," Physical Review B 87(014115): 1-10 (Jan. 2013), 10 pages.
Kailath, "Linear Systems," Prentice Hall, (1979), 6 pages.
Karlsson et al., "Diamond micro-optics: microlenses and antireflection structures surfaces for the infrared spectral region," Optics Express 11(5): 502-507 (Mar. 10, 2003), 6 pages.
Keyser "Enhancing nanopore sensing with DNA nanotechnology." Nature nanotechnology 11.2 (Feb. 2016): 106-108.
Khan & Hemmer, "Noise limitation in nano-scale imaging," Proceedings of SPIE vol. 5842: 302-305, (Dec. 2005), 7 pages.
Kim et al., "Electron spin resonance shift and linewidth broadening of nitrogen-vacancy centers in diamond as a function of electron irradiation dose," Applied Physics Letters 101(082410): 1-5 (Aug. 2012), 6 pages.
Kim et al., "Jahn-Teller Splitting and Zeeman Effect of Acceptors in Diamond," Physica B 273-274: 647-627 (Jul. 1999), 4 pages.
Kim et al., "Magnetospectroscopy of acceptors in 'blue' diamonds," Physica B 302-301: 88-100 (Aug. 2001), 13 pages.
Kim et al., "Zeeman effect of electronic Raman lines of accepters in elemental semiconductors: Boron in blue diamond," Physical Review B 62(12): 8038-8052 (Sep. 2000), 15 pages.
King et al., "Optical polarization of 13C nuclei in diamond through nitrogen vacancy centers," Physical Review B 81(073201): 1-4 (Feb. 2010), 4 pages.
Kok et al., "Materials Science: Qubits in the pink," Nature 444(2): 49 (Nov. 2006), 1 page.
Konenko et al., "Formation of antireflective surface structures on diamond films by laser patterning," Applied Physics A 68:99-102 (Jan. 1999), 4 pages.
Kraus et al., "Magnetic field and temperature sensing with atomic-scale spin defects in silicon carbide," Scientific Reports 4(5303): 1-8 (Jul. 2014), 8 pages.
Kwon et al., "Analysis of the far field of permanent-magnet motors and effects of geometric asymmetries and unbalance in magnet design," in IEEE Transactions on Magnetics, vol. 40, No. 2, pp. 435-442, Mar. 2004.
Lai et al., "Influence of a static magnetic field on the photoluminescence of an ensemble of nitrogen vacancy color centers in a diamond single-crystal," Applied Physics Letters 95, (Sep. 2009), 4 pages.
Lai et al., "Optically detected magnetic resonance of a single Nitrogen-Vacancy electronic spin in diamond nanocrystals," CLEO/EQEC, (Jun. 14-19, 2009), 1 page.
Laraoui et al., "Nitrogen-vacancy assisted magnetometry of paramagnetic centers in an individual diamond nanocrystal," Nano Letters 12: 3477-3482 (Jul. 2012), 6 pages.
Lazariev et al., "A nitrogen-vacancy spin based molecular structure microscope using multiplexed projection reconstruction," Scientific Reports 5(14130): 1-8 (Sep. 2015), 8 pages.
Le Sage et al., "Efficient photon detection from color centers in a diamond optical waveguide," Phys. Rev. B 85: 121202(R), pp. 121202-1-121202-4, (Mar. 23, 2012), 4 pages.
Lee et al., "Vector magnetometry based on S=3/2 electronic spins," Physical Review B 92 (115201): 1-7 (Sep. 2015), 7 pages.
Lesik et al., "Preferential orientation of NV defects in CVD diamond films grown on (113)-oriented substrates," Diamond and Related Materials 56: 47-53 (Jun. 2015), 7 pages.
Levchenko et al., "Inhomogeneous broadening of optically detected magnetic resonance of the ensembles of nitrogen-vacancy centers in diamond by interstitial carbon atoms," Applied Physics Letters 106, (Mar. 2015; published online Mar. 9, 2015), 6 pages.
Lindsay "The promises and challenges of solid-state sequencing." Nature nanotechnology 11.2 (Feb. 2016): 109-111.
Liu et al., "Electron spin studies of nitrogen vacancy centers in nanodiamonds," Acta Physica Sinica 62(16) 164208: 1-5 (Aug. 2013), 5 pages.
Liu et al., "Fiber-integrated diamond-based magnetometer," Applied Physics Letters 103(143105): 1-4 (Sep. 2013), 5 pages.
MacLaurin et al., "Nanoscale magnetometry through quantum control of nitrogen-vacancy centres in rotationally diffusing nanodiamonds," New Journal of Physics 15, (Jan. 2013), 16 pages.
MacQuarie et al., "Mechanical spin control of nitrogen-vacancy centers in diamond," Retrieved from http://www.arxiv.org/pdf/1306.6356.pdf, pp. 1-8, (Jun. 2013), 8 pages.
Macs et al., "Diamond as a magnetic field calibration probe," Journal of Physics D: Applied Physics 37, (Apr. 2004; published Mar. 17, 2004), 6 pages.
Maertz et al., "Vector magnetic field microscopy using nitrogen vacancy centers in diamond", Applied Physics Letters 96, No. 9, Mar. 1, 2010, pp. 092504-1-092504-3.
Maletinsky et al., "A robust scanning diamond sensor for nanoscale imaging with single nitrogen-vacancy centres," Nature Nanotechnology 7: 320-324, (May 2012; published Apr. 15, 2012), 5 pages.
Mamin et al., "Multipulse Double-Quantum Magnetometry with Near-Surface Nitrogen-Vacancy Centers," Physical Review Letters 13(030803): 1-5 (Jul. 2014), 5 pages.
Mamin et al., "Nanoscale Nuclear Magnetic Resonance with a Nitrogen-Vacancy Spin Sensor," Science 339, (Feb. 2013), 5 pages.
Manson et al., "GR transitions in diamond: magnetic field measurements," Journal of Physics C Solid St. Phys 13: L1005-L1009, (Nov. 1980), 6 pages.
Massachusetts Institute of Technology, "Wide-Field Imaging Using Nitrogen Vacancies," in Patent Application Approval Process, Physics Week: 1-5, (Jan. 20, 2015), 5 pages.
Matlashov, et al. "SQUIDs for magnetic resonance imaging at ultra-low magnetic field." PIERS online 5.5 (2009): 466-470.
Matlashov, et al. "SQUIDs vs. induction coils for ultra-low field nuclear magnetic resonance: experimental and simulation comparison." IEEE Transactions on Applied Superconductivity 21.3 (Jan. 1, 2012): 465-468.

(56) **References Cited**

OTHER PUBLICATIONS

Matsuda et al., "Development of a plastic diamond anvil cell for high pressure magneto-photoluminescence in pulsed high magnetic fields," International Journal of Modern Physics B 18(2729), (Nov. 2004), 7 pages.
Maze et al., "Nanoscale magnetic sensing using spin qubits in diamond," Proc. SPIE 7225, Advanced Optical Concepts in Quantum Computing, Memory, and Communication II, 722509 (Feb. 2, 2009) 8 pages.
Maze et al., "Nanoscale magnetic sensing with an individual electronic spin in diamond," Nature Physics 455: 644-647 (Oct. 2, 2008), 5 pages.
Meijer et al., "Generation of single color centers by focused nitrogen implantation," Applied Physics Letters 87(261909): 1-3 (Dec. 2005), 4 pages.
Michaelovich et al., "Polarization Dependencies of the Nitrogen-Vacancy Center." Undergraduate Project Report, Ben-Gurion University, Aug. 2015, pp. 1-9.
Millot et al., "High-field Zeeman and Paschen-Back effects at high pressure in oriented ruby," Physical Review B 78 (155125): 1-7 (Oct. 2008), 7 pages.
Moessle, et al. "SQUID-detected magnetic resonance imaging in microtesla fields." Annu. Rev. Biomed. Eng. 9 (May 23, 2008): 389-413.
Moriyama et al., "Importance of electron-electron interactions and Zeeman splitting in single-wall carbon nanotube quantum dots," Physica E 26: 473-476 (Feb. 2005), 4 pages.
Mrozek et al., "Circularly polarized microwaves for magnetic resonance study in the GHz range: Application to nitrogen-vacancy in diamonds," Applied Physics Letters, pp. 1-4 (Jul. 2015), 4 pages.
Nagl et al., "Improving surface and defect center chemistry of fluorescent nanodiamonds for imaging purposes-a review," Analytical and Bioanalaytical Chemistry 407: 7521-7536 (Oct. 2015; published online Jul. 29, 2015), 16 pages.
Neumann et al., "Excited-state spectroscopy of single NV defects in diamond using optically detected magnetic resonance," New Journal of Physics 11(013017): 1-10, (Jan. 2009), 11 pages.
Nizovtsev & Kilin, "Optically Detected Magnetic Resonance Spectra of the 14NV-13C Spin Systems in Diamond: Analytical Theory and Experiment," Doklady of the National Academy of Sciences of Belarus, (2013), 27 pages with English machine translation.
Nizovtsev et al., "Modeling fluorescence of single nitrogen-vacancy defect centers in diamond," Physica B—Condensed Matter, 608-611 (Dec. 2001), 4 pages.
Nizovtsev et al., "Theoretical study of hyperfine interactions and optically detected magnetic resonance spectra by simulation of the C-291(NV)H-(172) diamond cluster hosting nitrogen-vacancy center," New Journal of Physics 16(083014): 1-21 (Aug. 2014), 22 pages.
Nobauer et al., "Smooth optimal quantum control for robust solid state spin magnetometry," Retrieved from http://www.arxiv.org/abs/1412.5051, pp. 1-12, (Dec. 2014), 12 pages.
Nowodzinski et al., "Nitrogen-Vacancy centers in diamond for current imaging at the redistributive layer level of Integrated Circuits," Microelectronics Reliability 55: 1549-1553 (Aug. 2015), 5 pages.
Nusran et al., "Optimizing phase-estimation algorithms for diamond spin magnetometry," Physical Review B 90(024422): 1-12 (Jul. 2014), 12 pages.
Ohashi et al., "Negatively Charged Nitrogen-Vacancy Centers in a 5 nm Thin 12C Diamond Film," Nano Letters 13: 4733-4738 (Oct. 2013), 6 pages.
Pelliccione, et al., Two-dimensional nanoscale imaging of gadolinium spins via scanning probe relaxometry with a single spin in diamond, Phys. Rev. Applied 2.5, (Sep. 8, 2014): 054014 pp. 1-17.
Plakhotnik et al., "Super-Paramagnetic Particles Chemically Bound to Luminescent Diamond : Single Nanocrystals Probed with Optically Detected Magnetic Resonance," Journal of Physical Chemistry C 119: 20119-20124 (Aug. 2015), 6 pages.
Polatomic. "AN/ASQ-233A Digital Magnetic Anomaly Detective Set." Retrieved May 9, 2016, from http://polatomic.com/images/DMAD_Data_Sheet_09-2009.pdf (2009), 1 page.
Poole, "What is GMSK Modulation—Gaussian Minimum Shift Keying." Radio-Electronics, retrieved from https://web.archive.org/web/20150403045840/http://www.radio-electronics.com/info/rf-technology-design/pm-phase-modulation/what-is-gmsk-gaussian-minimum-shift-keyingtutorial.php (Apr. 3, 2015), 4 pages.
Qiu et al., "Low-field NMR Measurement Procedure when Squid Detection is Used," IEEE/CSC & ESAS European Superconductivity News Forum, No. 5, Jul. 2008.
Qiu, et al. "SQUID-detected NMR in Earth's magnetic field." Journal of Physics: Conference Series. vol. 97. No. 1. IOP Publishing, Mar. 2008, pp. 1-7.
Rabeau et al., "Implantation of labelled single nitrogen vacancy centers in diamond using 15N," Applied Physics Letters 88, (Jan. 2006), 4 pages.
Ramsey, et al., "Phase Shifts in the Molecular Beam Method of Separated Oscillating Fields", Physical Review, vol. 84, No. 3, Nov. 1, 1951, pp. 506-507.
Ranjbar et al., "Many-electron states of nitrogen-vacancy centers in diamond and spin density calculations," Physical Review B 84(165212): 1-6 (Oct. 2011), 6 pages.
Reynhardt, "Spin-lattice relaxation of spin-1/2 nuclei in solids containing diluted paramagnetic impurity centers. I. Zeeman polarization of nuclear spin system," Concepts in Magnetic Resonance Part A, pp. 20-35, (Sep. 2003), 16 pages.
Rogers et al., "Singlet levels of the NV(−) centre in diamond," New Journal of Physics 17, (Jan. 2015), 13 pages.
Rondin et al., "Magnetometry with nitrogen-vacancy defects in diamond," Reports on Progress in Physics 77(056503) 1-26 (May 2014), 27 pages.
Rondin et al., "Nanoscale magnetic field mapping with a single spin scanning probe magnetometer," Applied Physics Letters 100, (Apr. 2012), 5 pages.
Sarkar et al., "Magnetic properties of graphite oxide and reduced graphene oxide," Physica E 64: 7882 (Nov. 2014), 5 pages.
Scheuer et al., "Accelerated 2D magnetic resonance spectroscopy of single spins using matrix completion," Scientific Reports 5(17728): 1-8 (Dec. 2015), 8 pages.
Schirhagl et al., "Nitrogen-vacancy centers in diamond: Nanoscale sensors for physics and biology," Annual Review of Physical Chemistry 65: 83-105 (Jan. 2014), 26 pages.
Schoenfeld & Harneit, "Real time magnetic field sensing and imaging using a single spin in diamond," Physical Review Letters 106(030802): 1-4 (Jan. 2011), 4 pages.
Sedov et al., "Si-doped nano- and microcrystalline diamond films with controlled bright photoluminescence of silicon-vacancy color centers," Diamond and Related Materials 56: 23-28 (Jun. 2015; available online Apr. 18, 2015), 6 pages.
Shames et al., "Magnetic resonance tracking of fluorescent nanodiamond fabrication," Journal of Physics D: Applied Physics 48(155302): 1-13 (Apr. 2015; published Mar. 20, 2015), 14 pages.
Shao et al., "Diamond Color Center Based Fm Microwave Demodulator," in Conference on Lasers and Electro-Optics, OSA Technical Digest (online) (Optical Society of America), paper JTh2A.136, (Jun. 5- 10, 2016), 2 pages.
Sheinker et al., "Localization in 3-D Using Beacons of Low Frequency Magnetic Field." IEEE Transactions on Instrumentation and Measurement 62(12): 3194-3201 (Dec. 2013), 8 pages.
Simanovskaia et al., "Sidebands in optically detected magnetic resonance signals of nitrogen vacancy centers in diamond," Physical Review B 87(224106): 1-11 (Jun. 2013), 11 pages.
Sotoma et al., "Effective production of fluorescent nanodiamonds containing negatively-charged nitrogen-vacancy centers by ion irradiation," Diamond and Related Materials 49: 33-38 (Oct. 2014), 6 pages.
Soykal et al., "Quantum metrology with a single spin-3/2 defect in silicon carbide," Mesoscale and Nanoscale Physics (May 24, 2016), retrieved from https://arxiv.org/abs/1605.07628 (Sep. 22, 2016), 9 pages.

(56) **References Cited**

OTHER PUBLICATIONS

Steiner et al., "Universal enhancement of the optical readout fidelity of single electron spins at nitrogen-vacancy centers in diamond," Physical Review B 81(035205): 1-6 (Jan. 2010), 6 pages.
Steinert et al., "High-sensitivity magnetic imaging using an array of spins in diamond," Rev. Sci. Inst. 81(043705): 1-5 (Apr. 23, 2010), 5 pages.
Steinert et al., "Magnetic spin imaging under ambient conditions with sub-cellular resolution." Nature Comms 4:1607 (Mar. 19, 2013).
Stepanov et al., "High-frequency and high-field optically detected magnetic resonance of nitrogen-vacancy centers in diamond," Applied Physics Letters 106, (Feb. 2015), 5 pages.
Sternschulte et al., "Uniaxial stress and Zeeman splitting of the 1.681 eV optical center in a homoepitaxial CVD diamond film," Diamond and Related Materials 4: 1189-1192 (Sep. 1995), 4 pages.
Storteboom et al., "Lifetime investigation of single nitrogen vacancy centres in nanodiamonds," Optics Express 23(9): 11327-11333 (May 4, 2015; published Apr. 22, 2015), 7 pages.
Sushkov, et al. "All-optical sensing of a single-molecule electron spin." Nano letters 14.11 (Nov. 7, 2013): 6443-6448.
Tahara et al., "Quantifying selective alignment of ensemble nitrogen-vacancy centers in (111) diamond," Applied Physics Letters 107:193110 (Nov. 2015; published online Nov. 13, 2015), 5 pages.
Taylor et al., "High-sensitivity diamond magnetometer with nanoscale resolution," Nature Physics 4: 810-816 (Oct. 2008), 7 pages.
Teale, "Magnetometry with Ensembles of Nitrogen Vacancy Centers in Bulk Diamond," Master's Thesis, Massachusetts Institute of Technology Department of Electrical Engineering and Computer Science (Sep. 2015), 57 pages.
Terblanche et al., "13C spin-lattice relaxation in natural diamond: Zeeman relaxation at 4.7 T and 300 K due to fixed paramagnetic nitrogen defects," Solid State Nuclear Magnetic Resonance 20: 1-22 (Aug. 2001), 22 pages.
Terblanche et al., "13C spin-lattice relaxation in natural diamond: Zeeman relaxation in fields of 500 to 5000 G at 300 K due to fixed paramagnetic nitrogen defects," Solid State Nuclear Magnetic Resonance 19: 107-129 (May 2001), 23 pages.
Tetienne et al., "Magnetic-field-dependent photodynamics of single NV defects in diamond: an application to qualitative all-optical magnetic imaging," New Journal of Physics 14(103033): 1-5 (Oct. 2012), 16 pages.
Tetienne, et al. "Spin relaxometry of single nitrogen-vacancy defects in diamond nanocrystals for magnetic noise sensing." Physical Review B 87.23 (Apr. 3, 2013): 235436-1-235436-5.
Tong et al., "A hybrid-system approach for W state and cluster state generation," Optics Communication 310: 166-172, (Jan. 2014; available online Aug. 12, 2013), 7 pages.
Uhlen et al., "New diamond nanofabrication process for hard x-ray zone plates," J. of Vacuum Science & Tech. B 29(6) (06FG03): 1-4 (Nov./Dec. 2011), 4 pages.
UK Office Action dated Oct. 12, 2017 from related application 1618202.4, 4 pages.
U.S. Notice of Allowance dated Apr. 20, 2016, from related U.S. Appl. No. 15/003,718, 9 pages.
U.S. Notice of Allowance dated Aug. 11, 2017 from related U.S. Appl. No. 15/003,558, 5 pages.
U.S. Notice of Allowance dated Aug. 17, 2016, from related U.S. Appl. No. 15/003,718, 8 pages.
U.S. Notice of Allowance dated Dec. 13, 2016, from related U.S. Appl. No. 14/680,877, 8 pages.
U.S. Notice of Allowance dated Dec. 22, 2016, from related U.S. Appl. No. 14/659,498, 10 pages.
U.S. Notice of Allowance dated Feb. 14, 2017, from related U.S. Appl. No. 15/003,677, 8 pages.
U.S. Notice of Allowance dated Feb. 2, 2018, from U.S. Appl. No. 15/003,292, 8 pages.
U.S. Notice of Allowance dated Feb. 21, 2018, from related U.S. Appl. No. 15/003,176, 9 pages.
U.S. Notice of Allowance dated Jul. 18, 2017 from related U.S. Appl. No. 15/003,634, 6 pages.
U.S. Notice of Allowance dated Jul. 24, 2017 from related U.S. Appl. No. 15/003,088, 12 pages.
U.S. Notice of Allowance dated Jun. 20, 2017, from related U.S. Appl. No. 15/204,675, 9 pages.
U.S. Notice of Allowance dated Jun. 28, 2017 from related U.S. Appl. No. 15/003,256, 10 pages.
U.S. Notice of Allowance dated Jun. 8, 2017, from related U.S. Appl. No. 15/351,862, 7 pages.
U.S. Notice of Allowance dated Mar. 15, 2017, from related U.S. Appl. No. 15/351,862, 6 pages.
U.S. Notice of Allowance dated Mar. 29, 2016, from related U.S. Appl. No. 15/003,590, 11 pages.
U.S. Notice of Allowance dated May 26, 2017 from related U.S. Appl. No. 15/218,821, 7 pages.
U.S. Notice of Allowance dated Oct. 19, 2017, from related U.S. Appl. No. 15/179,957, 5 pages.
U.S. Notice of Allowance dated Oct. 23, 2017, from related U.S. Appl. No. 15/003,797, 6 pages.
U.S. Notice of Allowance dated Sep. 1, 2017, from related U.S. Appl. No. 14/676,740, 7 pages.
U.S. Notice of Allowance dated Sep. 14, 2017, from related U.S. Appl. No. 15/476,636, 10 pages.
U.S. Notice of Allowance dated Sep. 18, 2017, from related U.S. Appl. No. 15/003,206, 11 pages.
U.S. Notice of Allowance dated Sep. 26, 2017, from related U.S. Appl. No. 15/003,281, 7 pages.
U.S. Notice of Allowance dated Sep. 8, 2016, from related patent U.S. Appl. No. 15/003,298, 10 pages.
U.S. Office Action dated Apr. 17, 2017, from related U.S. Appl. No. 15/003,558, 12 pages.
U.S. Office Action dated Aug. 15, 2017 from related U.S. Appl. No. 15/003,281, 12 pages.
U.S. Office Action dated Aug. 24, 2016 from related U.S. Appl. No. 14/676,740, 19 pages.
U.S. Office Action dated Feb. 1, 2018, from related U.S. Appl. No. 15/003,577, 16 pages.
U.S. Office Action dated Feb. 10, 2017, from related U.S. Appl. No. 14/676,740, 20 pages.
U.S. Office Action dated Feb. 10, 2017, from related U.S. Appl. No. 15/003,088, 11 pages.
U.S. Office Action dated Feb. 16, 2017, from related U.S. Appl. No. 15/204,675, 7 pages.
U.S. Office Action dated Feb. 5, 2018, from related U.S. Appl. No. 15/450,504, 12 pages.
U.S. Office Action dated Jan. 25, 2018, from related U.S. Appl. No. 15/672,953, 28 pages.
U.S. Office Action dated Jan. 26, 2018, from related U.S. Appl. No. 15/003,678, 14 pages.
U.S. Office Action dated Jul. 27, 2017 from related U.S. Appl. No. 15/003,577, 15 pages.
U.S. Office Action dated Jul. 29, 2016 from related U.S. Appl. No. 14/680,877, 8 pages.
U.S. Office Action dated Jun. 1, 2017, from related U.S. Appl. No. 15/003,797, 29 pages.
U.S. Office Action dated Jun. 1, 2017, from related U.S. Appl. No. 15/179,957, 29 pages.
U.S. Office Action dated Jun. 12, 2017, from related U.S. Appl. No. 15/003,256, 9 pages.
U.S. Office Action dated Jun. 12, 2017, from related U.S. Appl. No. 15/003,336, 14 pages.
U.S. Office Action dated Jun. 16, 2017, from related U.S. Appl. No. 15/003,678, 15 pages.
U.S. Office Action dated Jun. 2, 2017, from related U.S. Appl. No. 15/476,636, 10 pages.
U.S. Office Action dated Mar. 1, 2017, from related U.S. Appl. No. 15/003,634, 7 pages.
U.S. Office Action dated Mar. 16, 2017, from related U.S. Appl. No. 15/218,821, 7 pages.
U.S. Office Action dated Mar. 27, 2018, from related U.S. Appl. No. 15/468,386, 21 pages.

(56) **References Cited**

OTHER PUBLICATIONS

U.S. Office Action dated Mar. 28, 2018, from related U.S. Appl. No. 15/003,177, 12 pages.
U.S. Office Action dated Mar. 5, 2018, from related U.S. Appl. No. 14/866,730, 14 pages.
U.S. Office Action dated Mar. 8, 2018, from related U.S. Appl. No. 15/380,691, 12 pages.
U.S. Office Action dated Mar. 8, 2018, from related U.S. Appl. No. 15/479,256, 30 pages.
U.S. Office Action dated May 13, 2016, from related U.S. Appl. No. 14/676,740, 15 pages.
U.S. Office Action dated May 22, 2017, from related U.S. Appl. No. 15/003,206, 12 pages.
U.S. Office Action dated May 6, 2016, from related U.S. Appl. No. 14/659,498.
U.S. Office Action dated Nov. 2, 2016, from related U.S. Appl. No. 15/003,256, 19 pages.
U.S. Office Action dated Nov. 24, 2017, from related U.S. Appl. No. 15/003,145, 14 pages.
U.S. Office Action dated Nov. 27, 2017, from U.S. Appl. No. 15/468,386, 28 pages.
U.S. Office Action dated Nov. 3, 2016, from related U.S. Appl. No. 15/204,675, 9 pages.
U.S. Office Action dated Oct. 14, 2016 from related U.S. Appl. No. 15/003,677, 13 pages.
U.S. Office Action dated Oct. 19, 2016, from related U.S. Appl. No. 15/218,821, 6 pages.
U.S. Office Action dated Sep. 27, 2017, from related U.S. Appl. No. 15/003,176, 8 pages.
U.S. Office Action dated Sep. 8, 2017, from related U.S. Appl. No. 15/003,292, 8 pages.
Vershovskii & Dmitriev, "Combined excitation of an optically detected magnetic resonance in nitrogen-vacancy centers in diamond for precision measurement of the components of a magnetic field vector," Technical Physics Letters 41(11): 1026-1029 (Nov. 2015), 4 pages.
Vershovskii & Dmitriev, "Micro-scale three-component quantum magnetometer based on nitrogen-vacancy color centers in diamond crystal," Technical Physics Letters 41(4): 393-396 (Apr. 2015), 4 pages.
Wahlstrom et al., "Modeling Magnetic Fields Using Gaussian Processes," 2013 IEEE International Conference on Acoustics, Speech, and Signal Processing, pp. 3522-3526 (May 26-31, 2013), 5 pages.
Wang et al., "Optimizing ultrasensitive single electron magnetometer based on nitrogen-vacancy center in diamond," Chinese Science Bulletin, 58(24): 2920-2923, (Aug. 2013), 4 pages.
Webber et al., "Ab initio thermodynamics calculation of the relative concentration of NV- and NV0 defects in diamond," Physical Review B 85,(014102): 1-7 (Jan. 2012), 7 pages.
Wegerich, "Similarity based modeling of time synchronous averaged vibration signals for machinery health monitoring," 2004 IEEE Aerospace Conference Proceedings (IEEE Cat. No. 04TH8720), 2004, pp. 3654-3662 vol. 6.
Wells, et al. "Assessing graphene nanopores for sequencing DNA." Nano letters 12.8 (Jul. 10, 2012): 4117-4123.
Widmann et al., "Coherent control of single spins in silicon carbide at room temperature," Nature Materials, 14: 164-168 (2015) (available online Dec. 1, 2014), 5 pages.
Wikipedia, "Continuous phase modulation", downloaded from https://web.archive.org/web/20151017015236/https://en.wikipedia.org/wiki/Continuous_phase_modulation on May 10, 2017, 3 pages.
Wikipedia, "Minimum-shift keying", downloaded from https://web.archive.org/web/20151017175828/https://en.wikipedia.org/wiki/Minimum-shift_keying on May 10, 2017, 2 pages.
Wolf et al., "Subpicotesla Diamond Magnetometry," Physical Review X 5(041001): 1-10 (Oct. 2015), 10 pages.
Wolfe et al., "Off-resonant manipulation of spins in diamond via precessing magnetization of a proximal ferromagnet," Physical Review B 89(180406): 1-5 (May 2014), 5 pages.
Wroble, "Performance Analysis of Magnetic Indoor Local Positioning System." Western Michigan University Master's Theses, Paper 609 (Jun. 2015), 42 pages.
Wysocki et al., "Modified Walsh-Hadamard sequences for DS CDMA wireless systems." Int. J. Adaptive Control and Signal Processing 16(8): 589-602 (Oct. 2002; first published online Sep. 23, 2002), 25 pages.
Xue & Liu, "Producing GHZ state of nitrogen-vacancy centers in cavity QED," Journal of Modern Optics 60(6-7), (Mar. 2013), 8 pages.
Yang & Gu, "Novel calibration techniques for high pulsed-magnetic fields using luminescence caused by photo," (with English machine translation), Journal of Huazhong University of Science and Technology, (Jun. 2007), 11 pages.
Yavkin et al., "Defects in Nanodiamonds: Application of High-Frequency cw and Pulse EPR, ODMR," Applied Magnetic Resonance, 45: 1035-1049 (Oct. 2014; published online Sep. 10, 2014), 15 pages.
Yu et al., "Bright fluorescent nanodiamonds: no photobleaching and low cytotoxicity," J. Am. Chem. Soc., 127: 17604-17605 (Nov. 25, 2005), 2 pages.
Zhang et al., "Laser-polarization-dependent and magnetically controlled optical bistability in diamond nitrogen-vacancy centers," Physics Letters A 377: 2621-2627 (Nov. 2013), 7 pages.
Zhang et al., "Laser-polarization-dependent spontaneous emission of the zero phonon line from single nitrogen-vacancy center in diamond," Chinese Physics B 24(3), (Apr. 2014), 13 pages.
Zhang et al., "Scalable quantum information transfer between nitrogen-vacancy-center ensembles," Annals of Physics, 355: 170-181 (Apr. 2015; available online Feb. 14, 2013), 12 pages.
Zhao et al., "Atomic-scale magnetometry of distant nuclear spin clusters via nitrogen-vacancy spin in diamond," Nature Nanotechnology, 5: 242-246 (Apr. 2011), 5 pages.

* cited by examiner

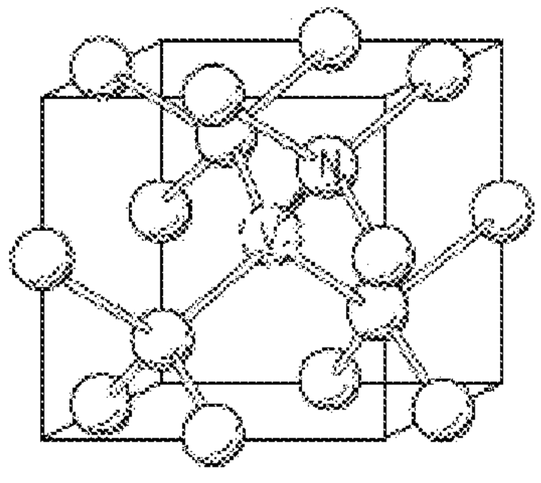

FIG. 1

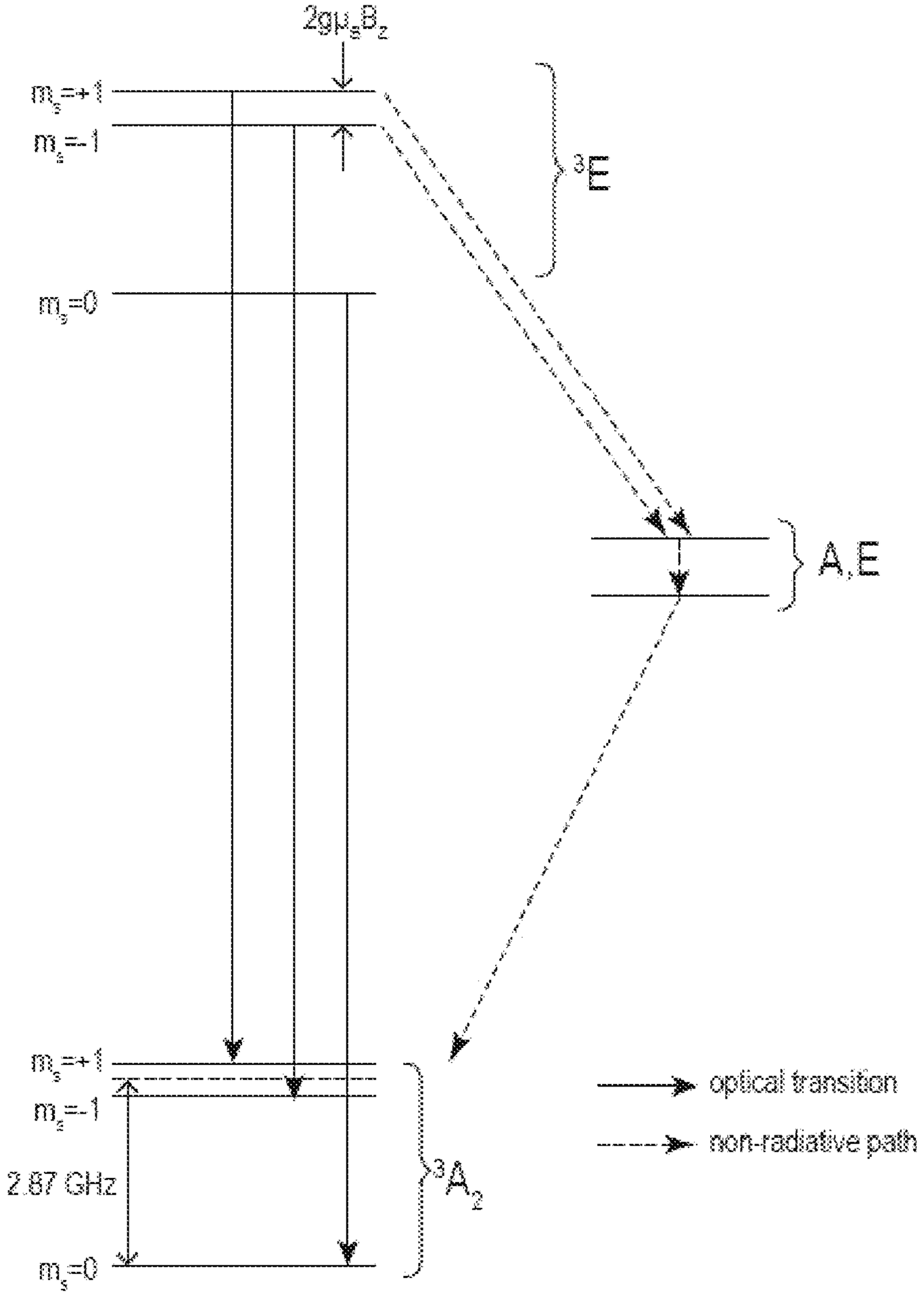
$2g\mu_s B_z$
$m_s=+1$
$m_s=-1$
$m_s=0$
^3E
A_1E
$m_s=+1$
$m_s=-1$
2.87 GHz
$m_s=0$
$^3A_2$
optical transition
non-radiative path

FIG. 2

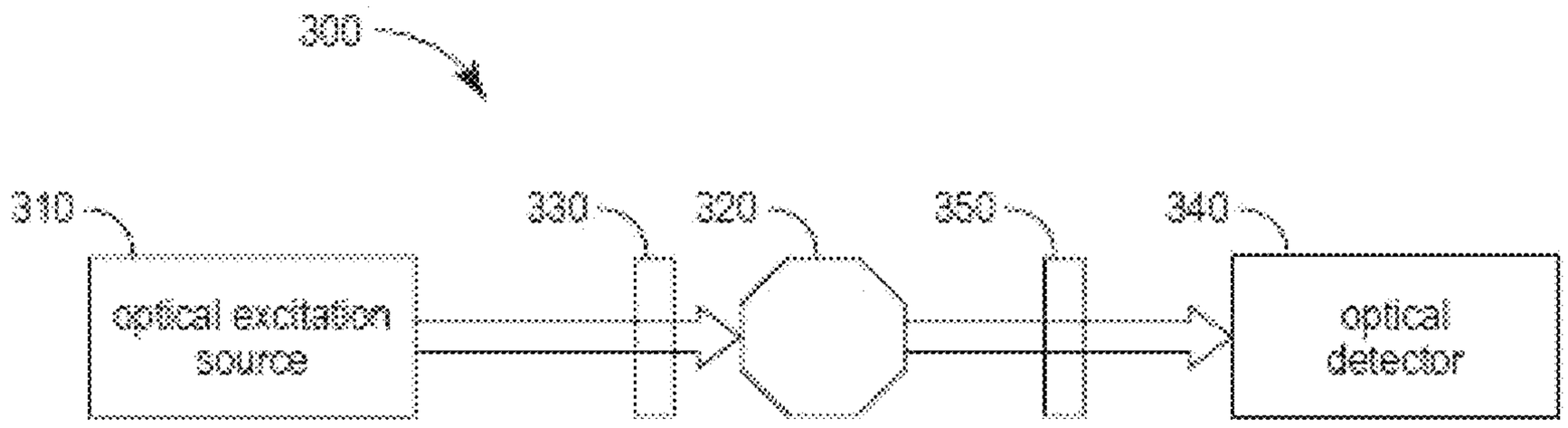

FIG. 3

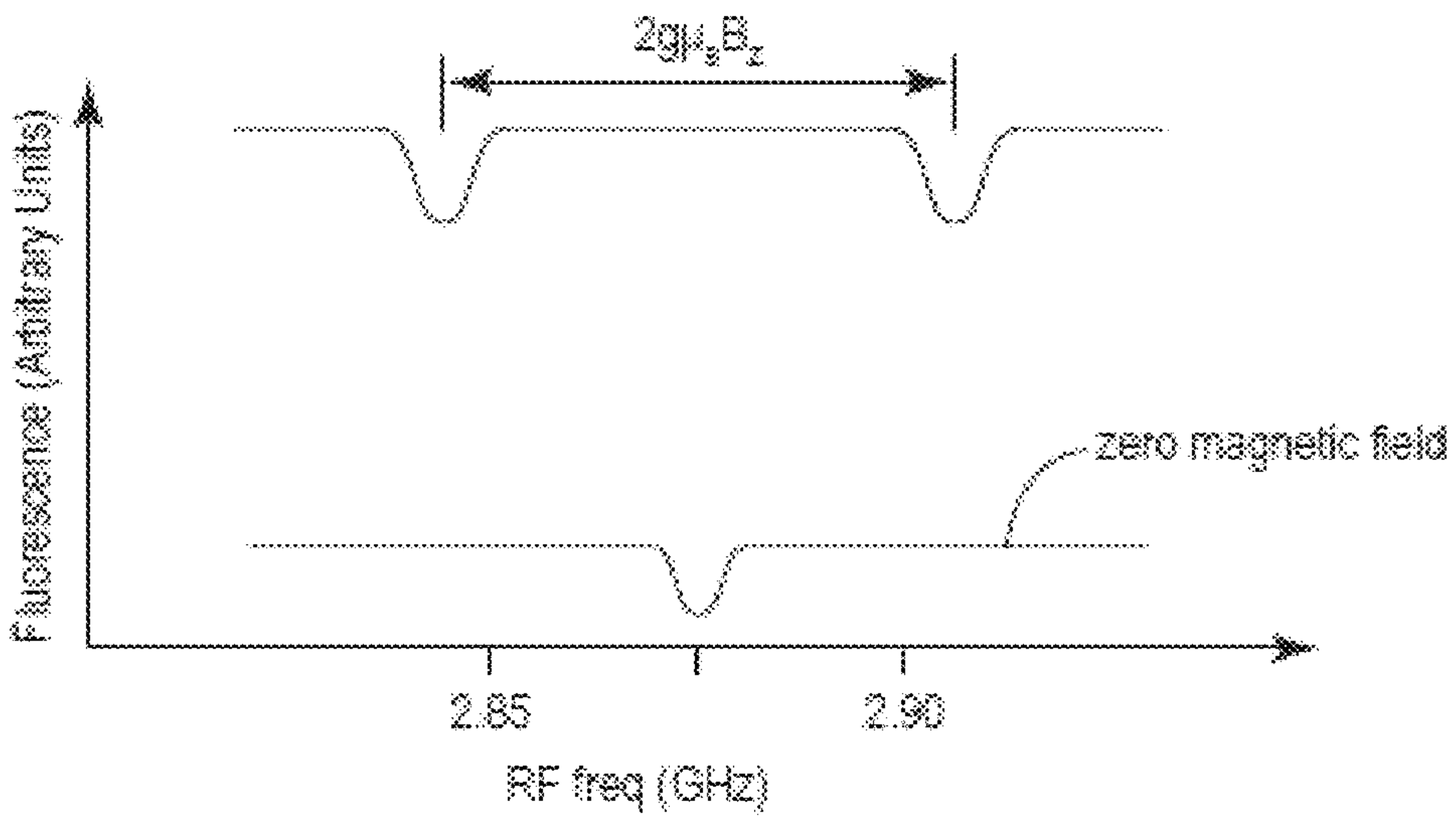

FIG. 4

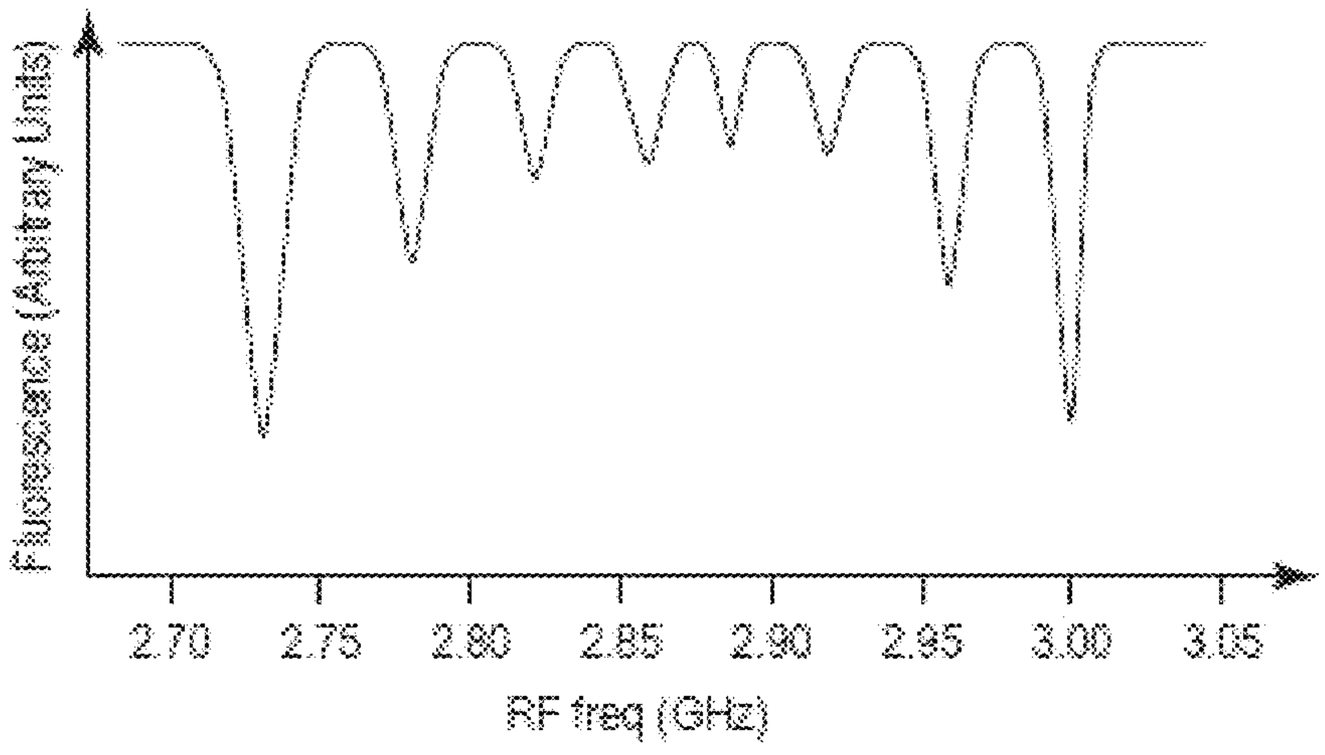

FIG. 5

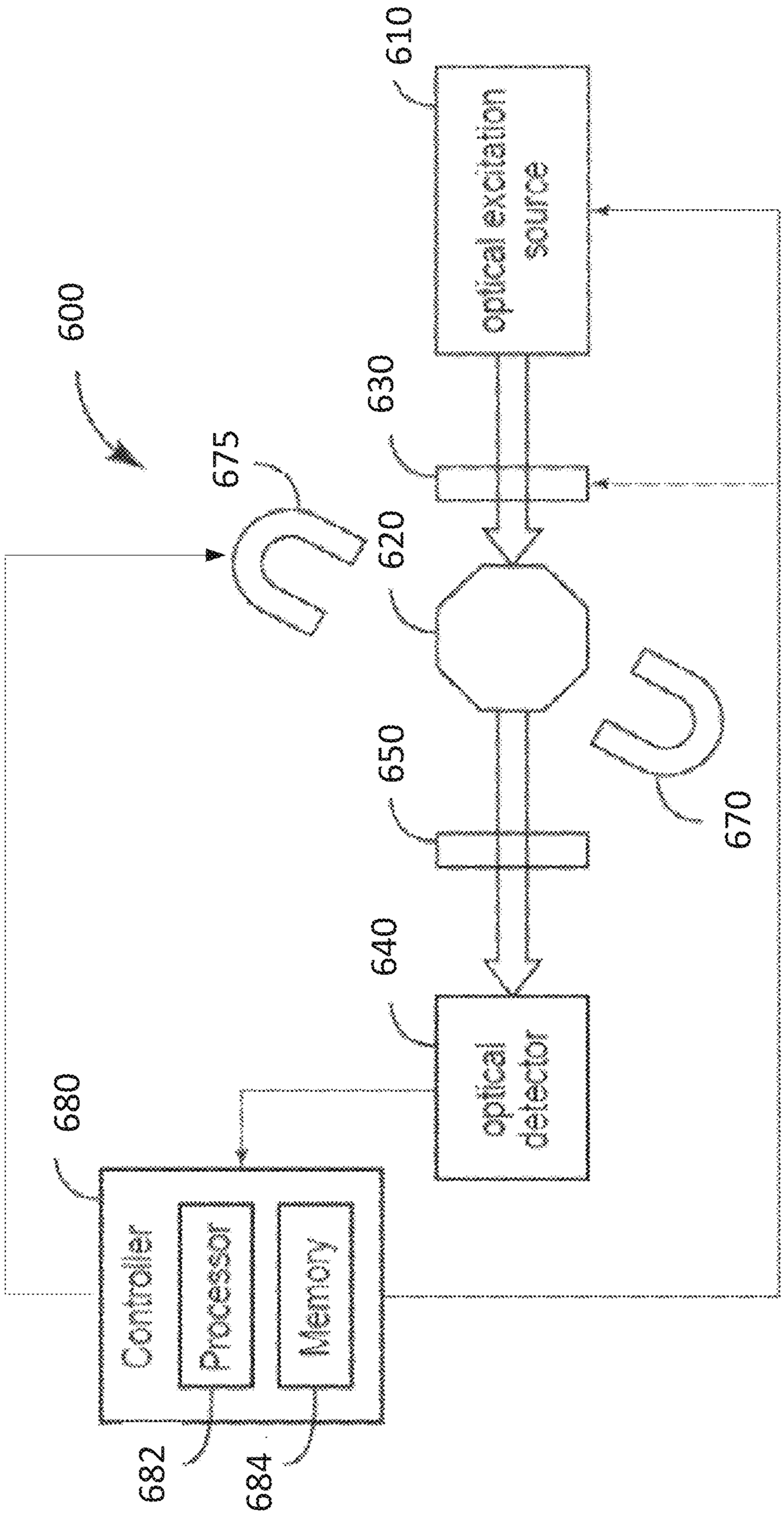
600
610
optical excitation source
630
675
620
650
670
640
optical detector
680
Controller
Processor
Memory
682
684

FIG. 6

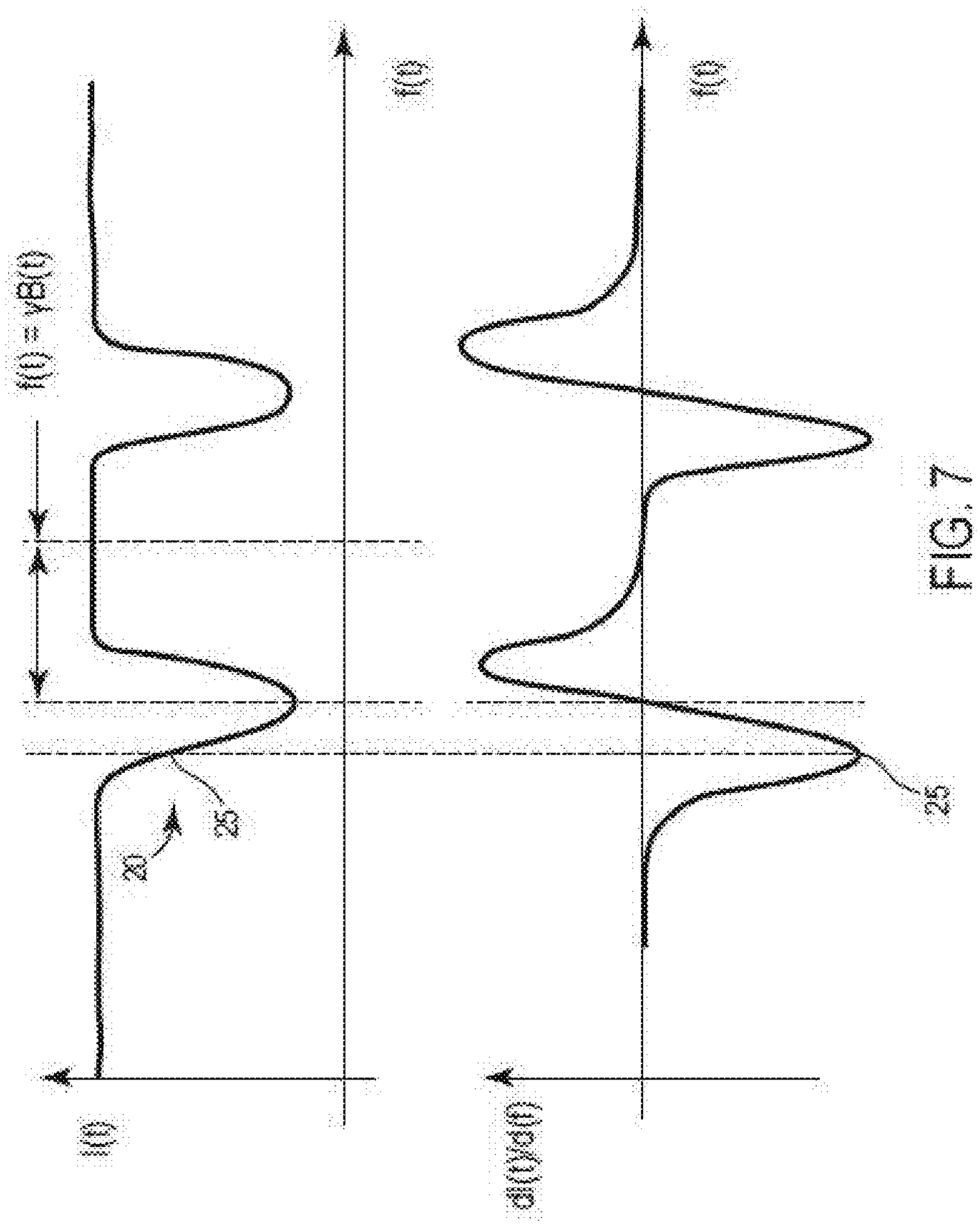

FIG. 7

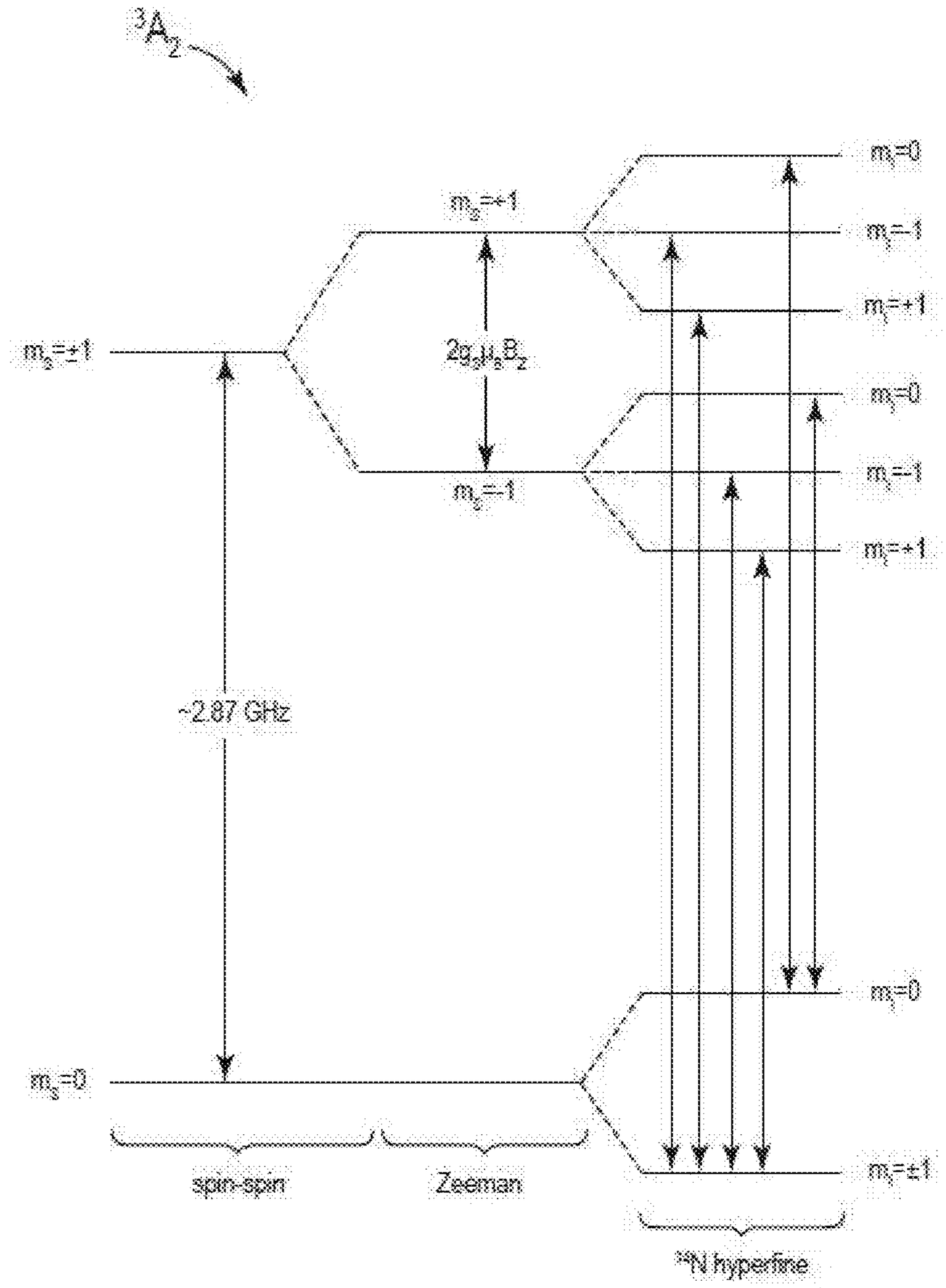
$^3A_2$
m_s=+1
m_s=±1
$2g_s\mu_sB_z$
m_s=−1
~2.87 GHz
m_s=0
spin-spin
Zeeman
m_s=0
m_s=−1
m_s=+1
m_s=0
m_s=−1
m_s=+1
m_s=0
m_s=±1
^{14}N hyperfine

FIG. 8

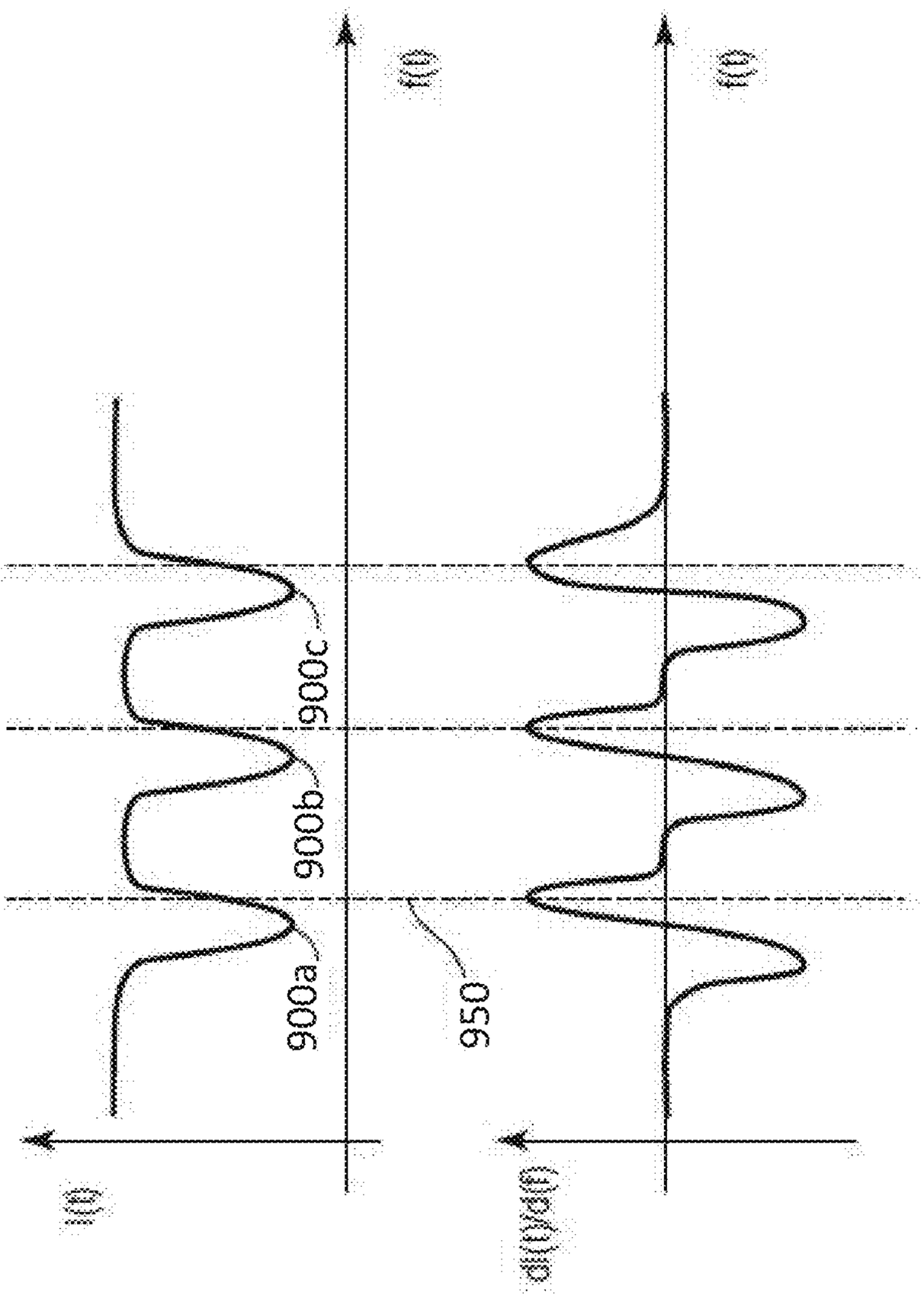

FIG. 9

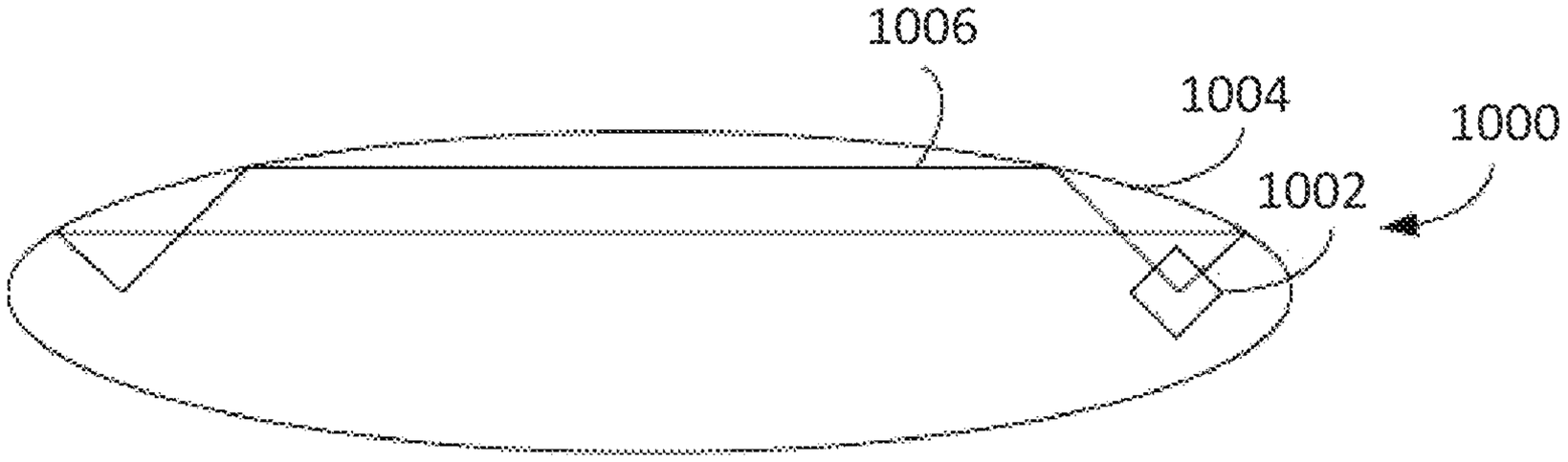

FIG. 10

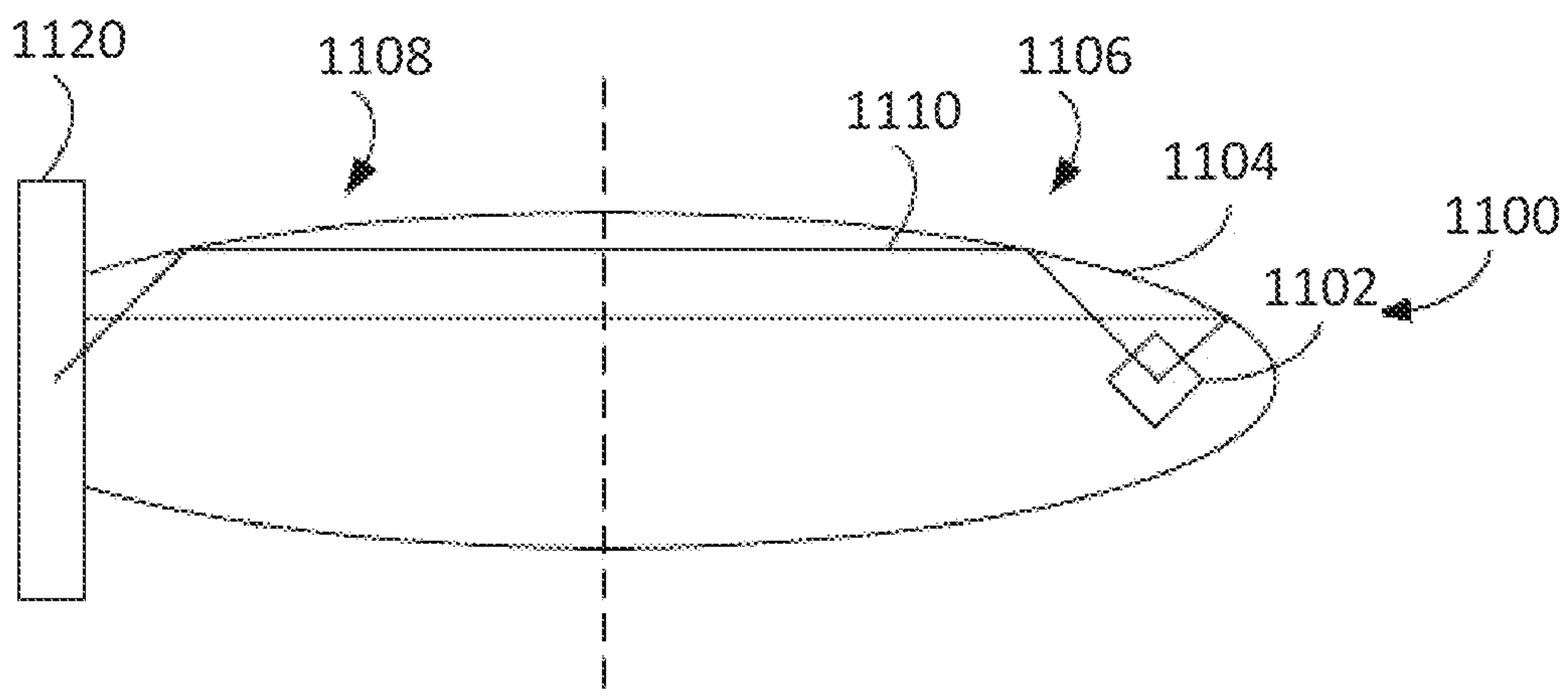

FIG. 11

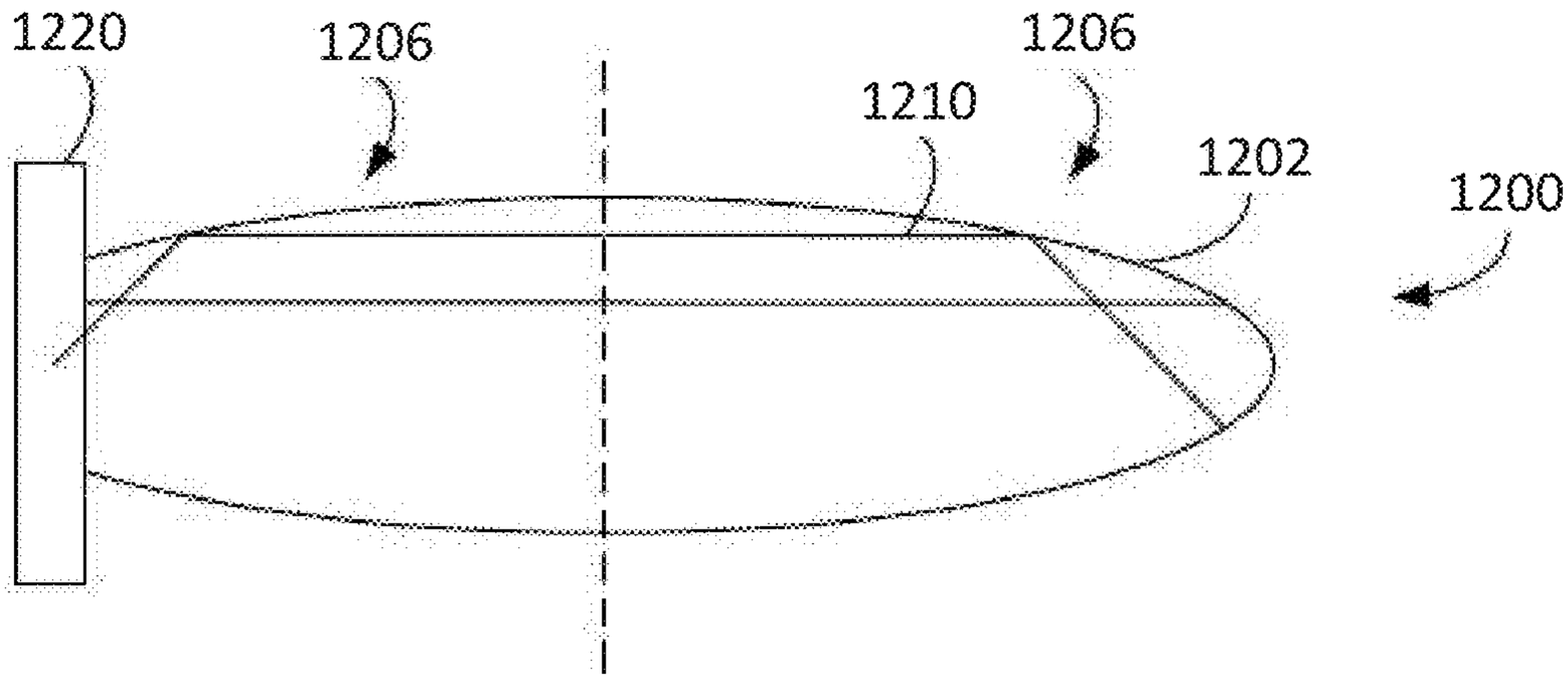

FIG. 12

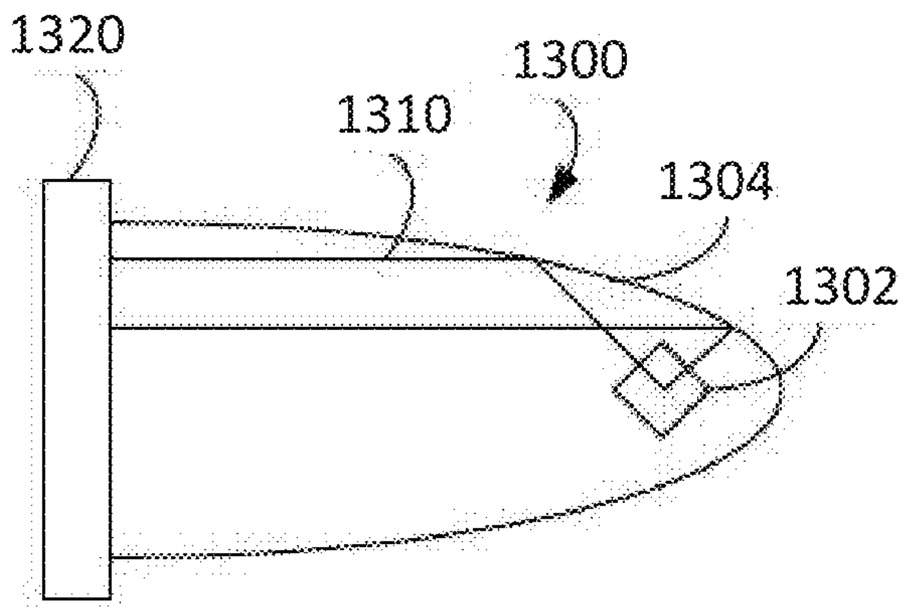

FIG. 13

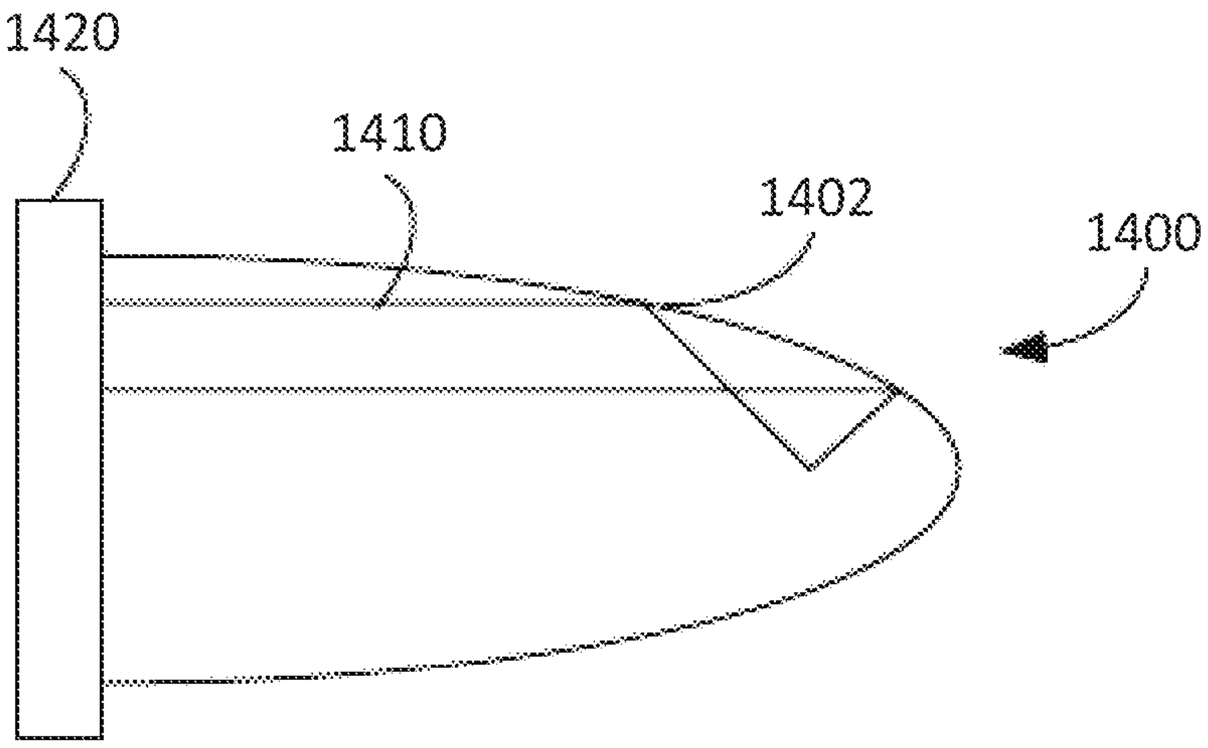

FIG. 14

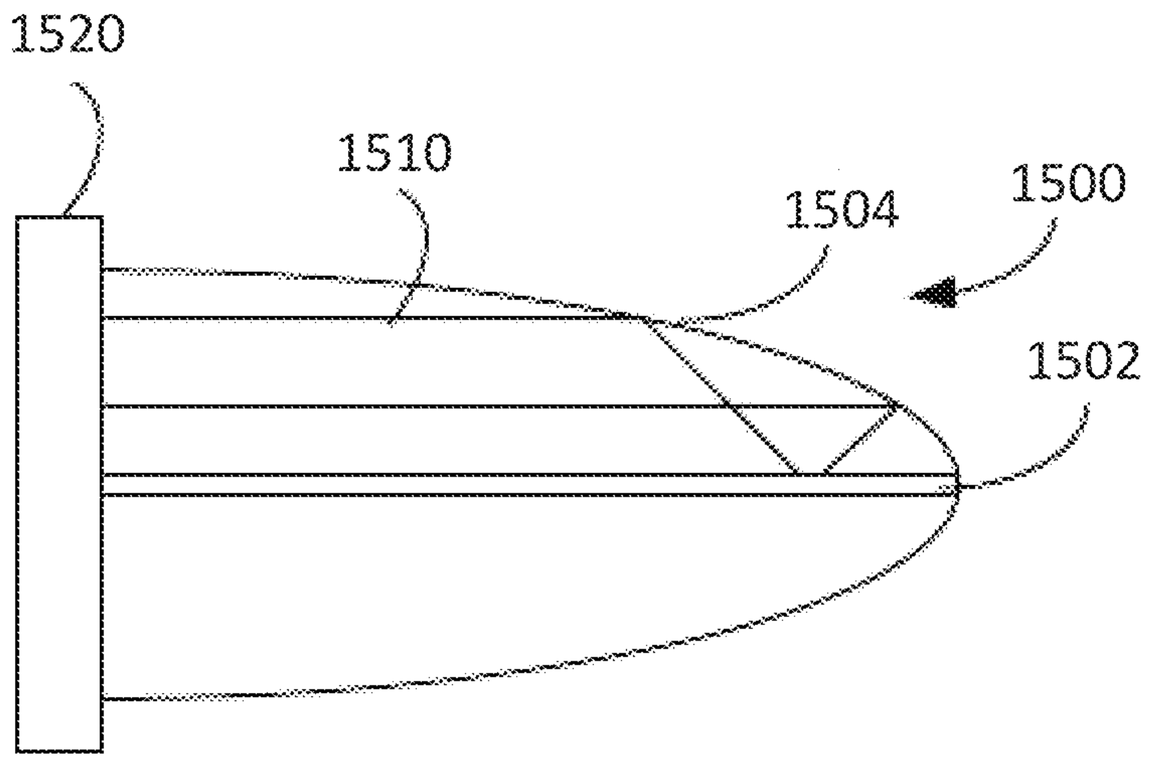

FIG. 15

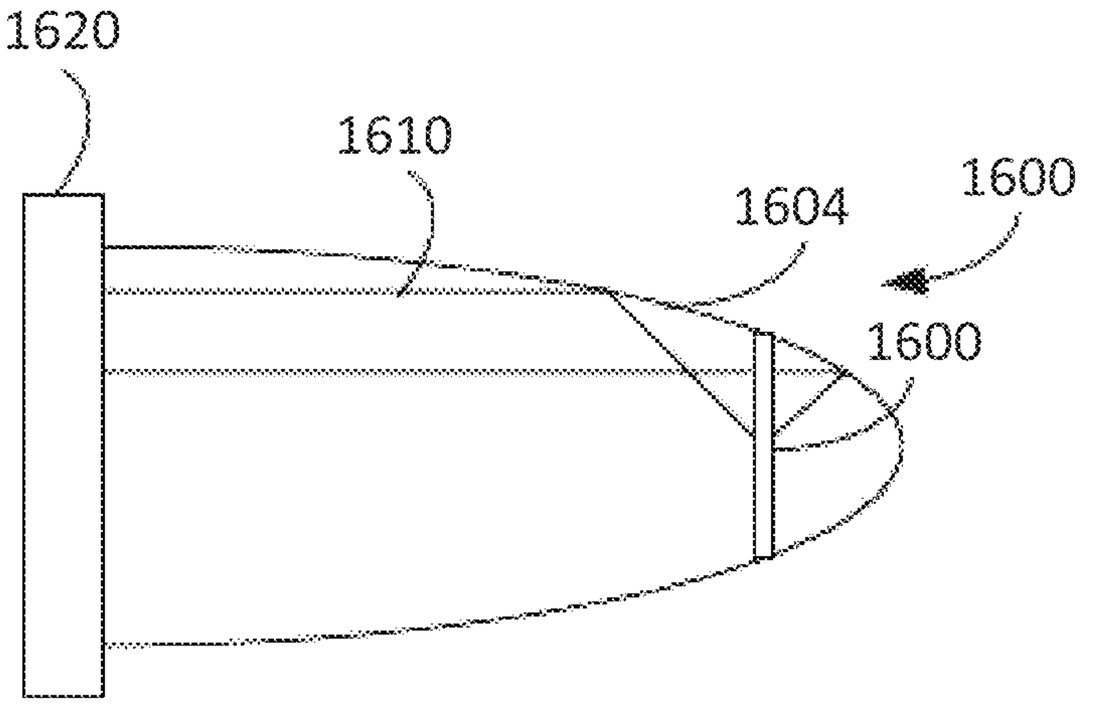

FIG. 16

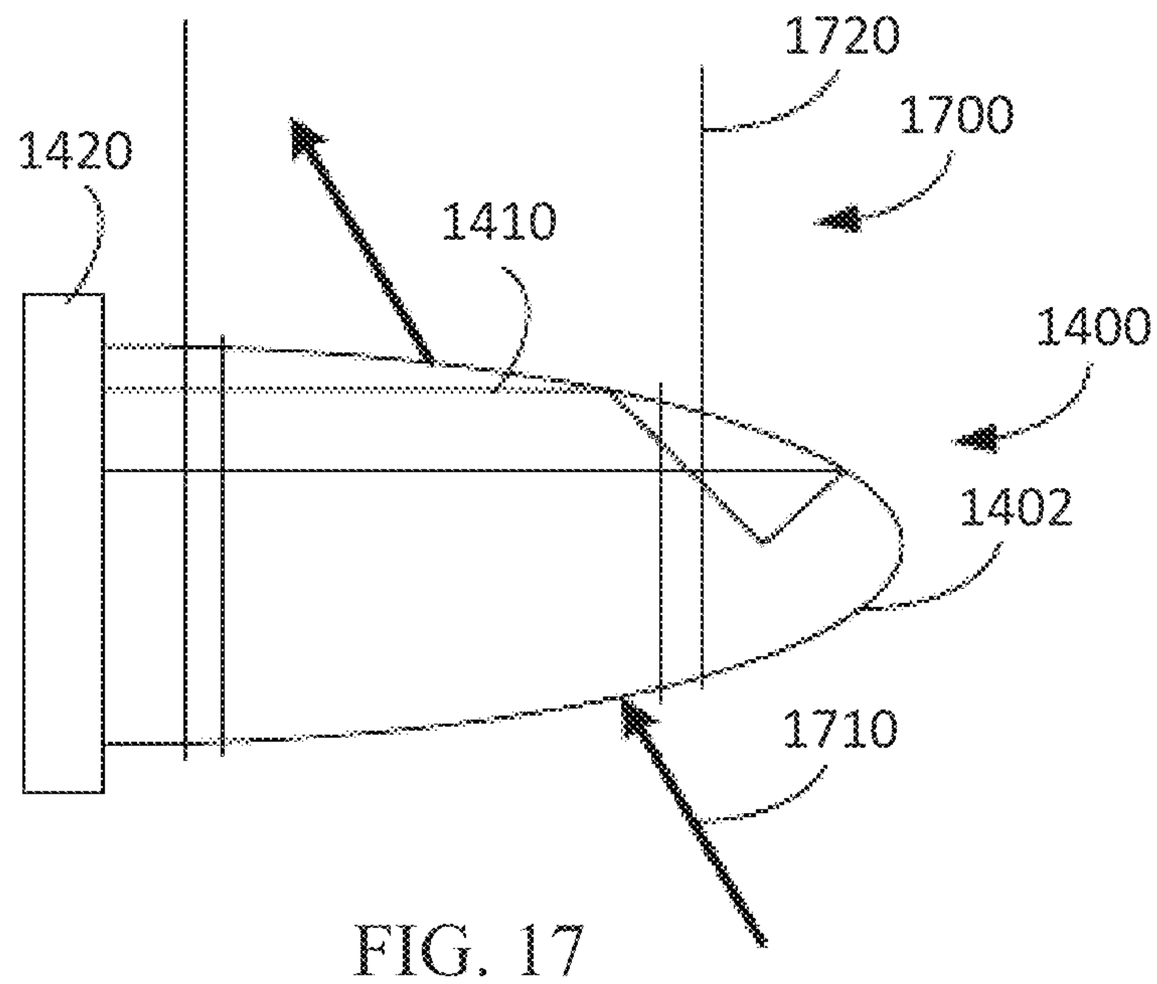

FIG. 17

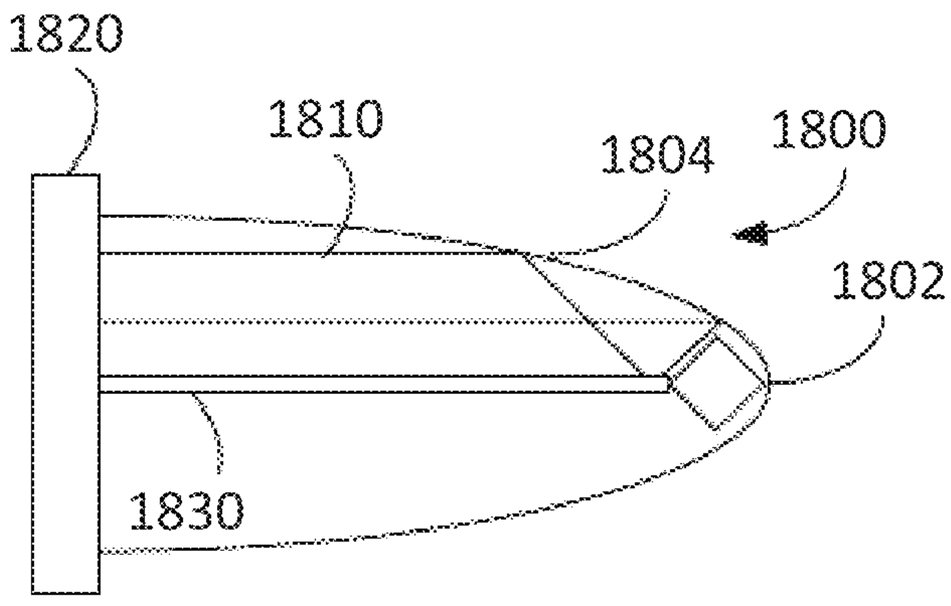

FIG. 18

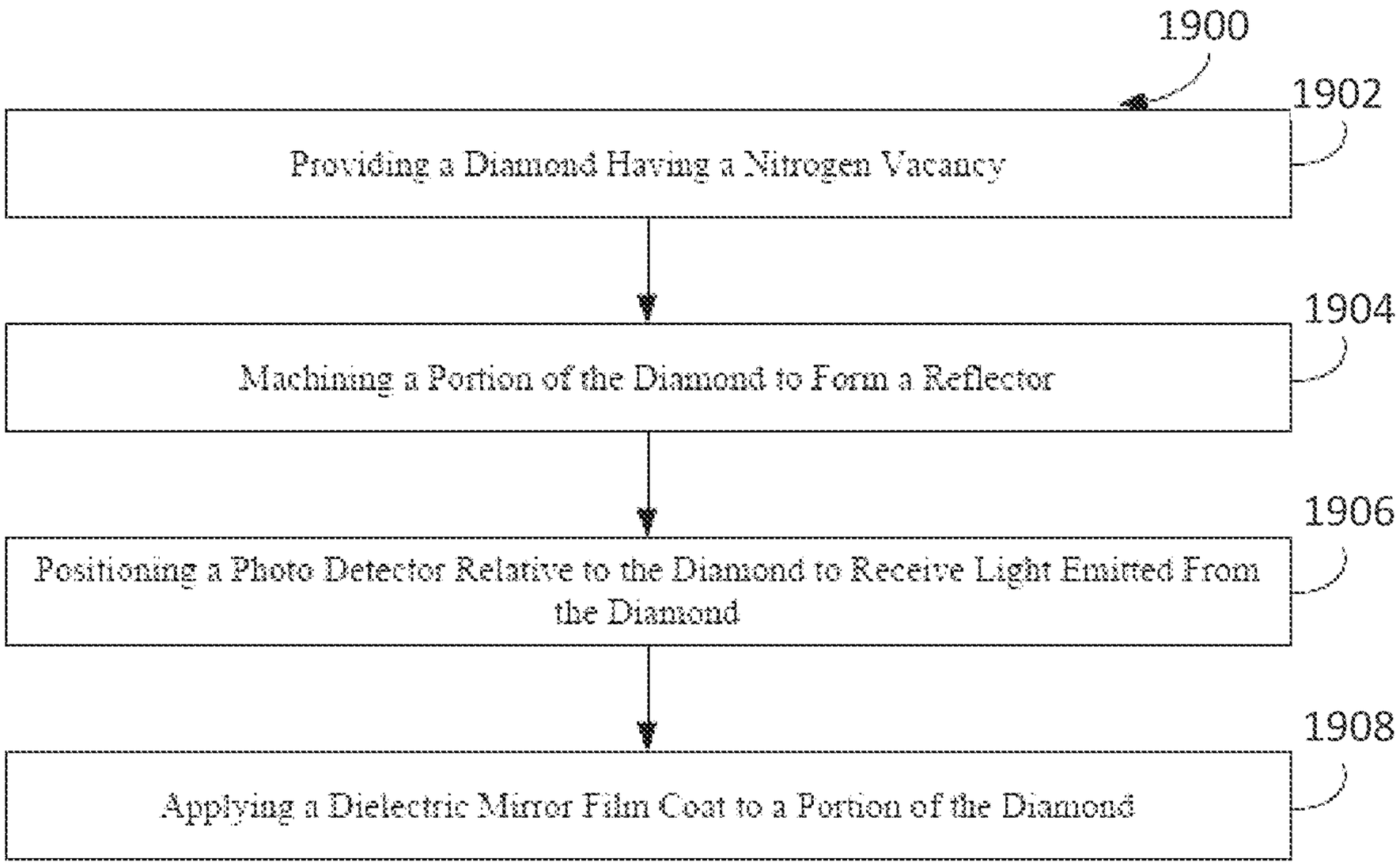
1900
1902
Providing a Diamond Having a Nitrogen Vacancy
1904
Machining a Portion of the Diamond to Form a Reflector
1906
Positioning a Photo Detector Relative to the Diamond to Receive Light Emitted From the Diamond
1908
Applying a Dielectric Mirror Film Coat to a Portion of the Diamond

FIG. 19

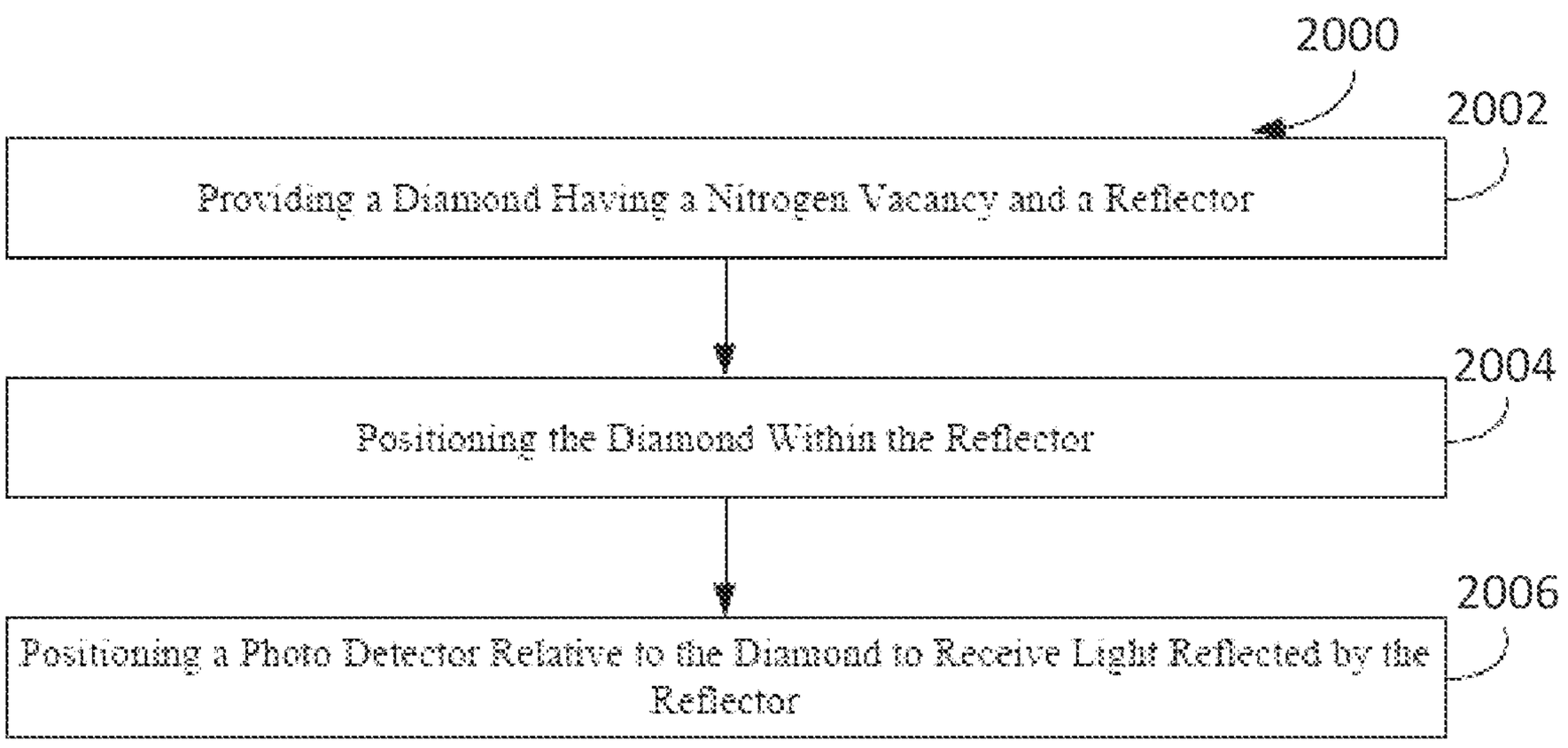
2000
2002
Providing a Diamond Having a Nitrogen Vacancy and a Reflector
2004
Positioning the Diamond Within the Reflector
2006
Positioning a Photo Detector Relative to the Diamond to Receive Light Reflected by the Reflector

FIG. 20

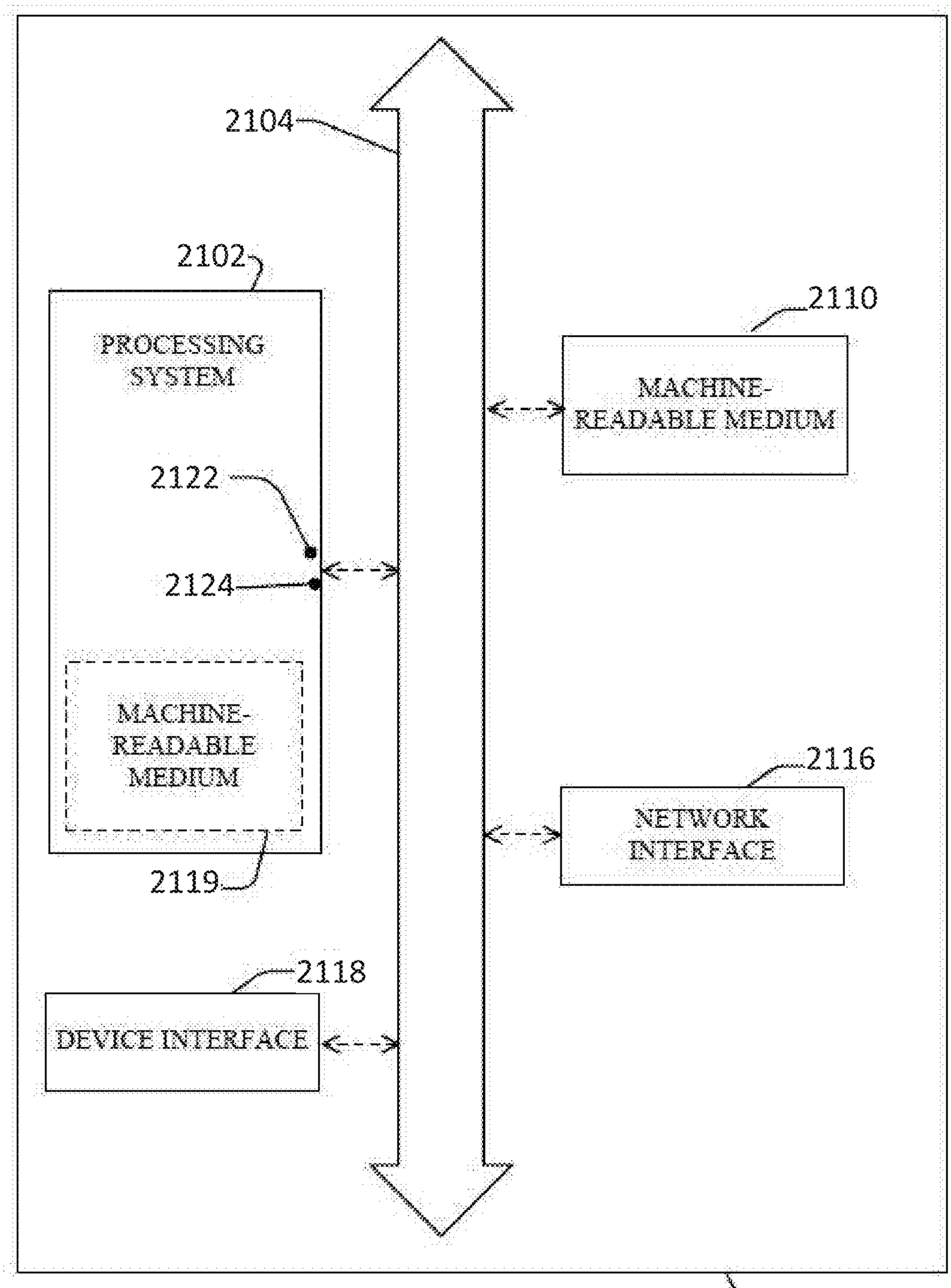
2104
2102
PROCESSING SYSTEM
2122
2124
MACHINE-READABLE MEDIUM
2119
2118
DEVICE INTERFACE
2110
MACHINE-READABLE MEDIUM
2116
NETWORK INTERFACE
2100

FIG. 21

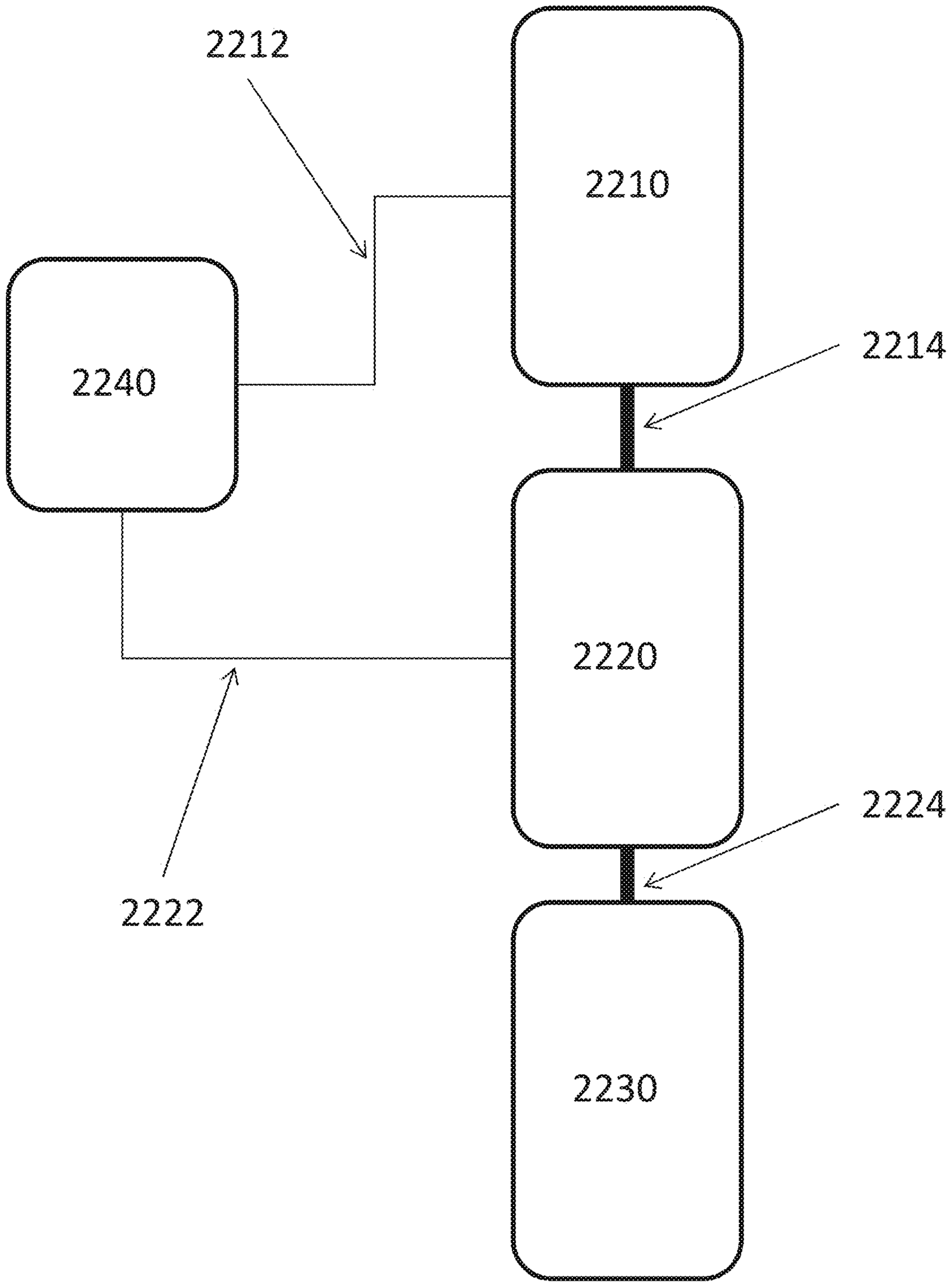

FIG. 22

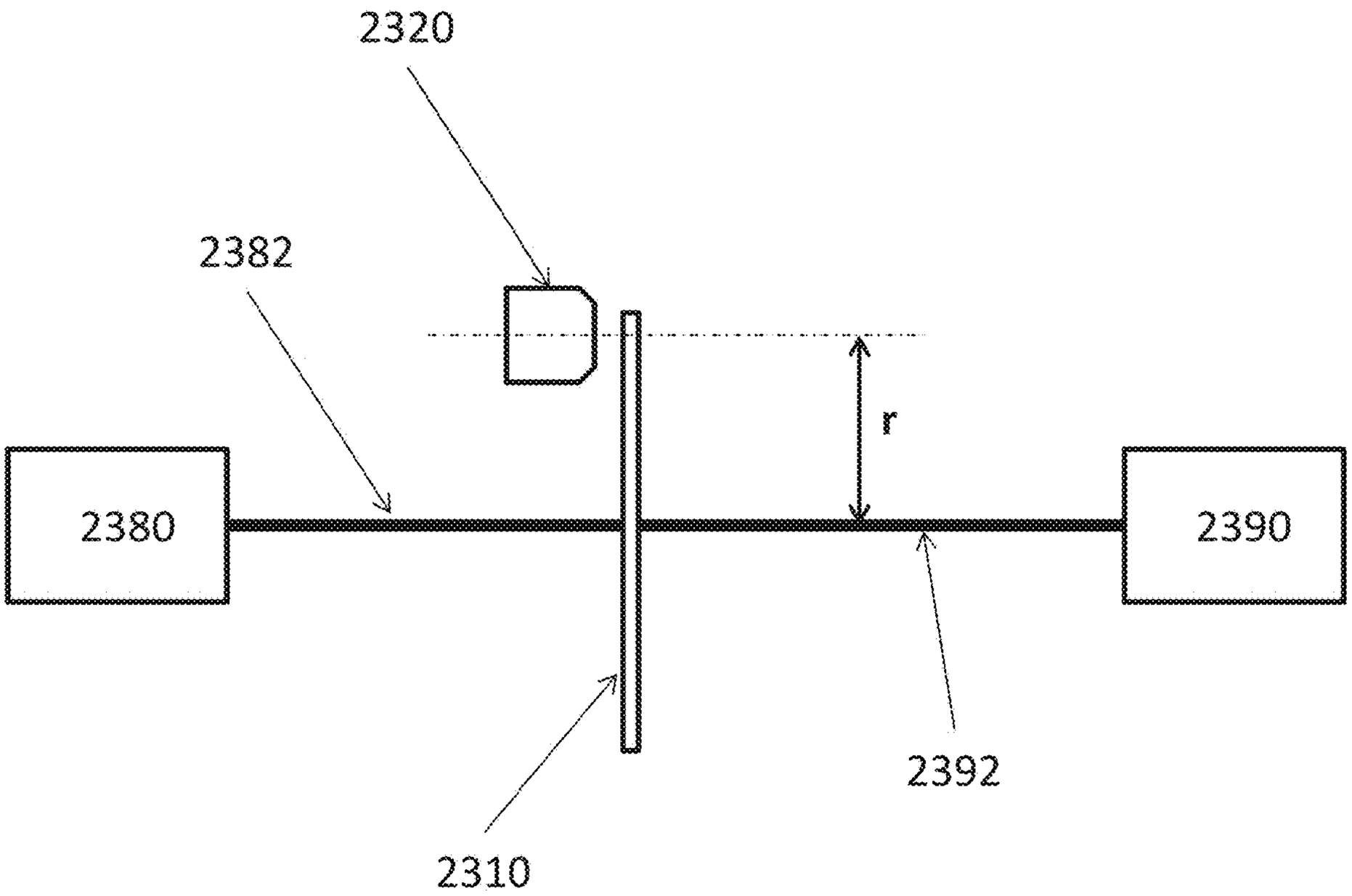

FIG. 23

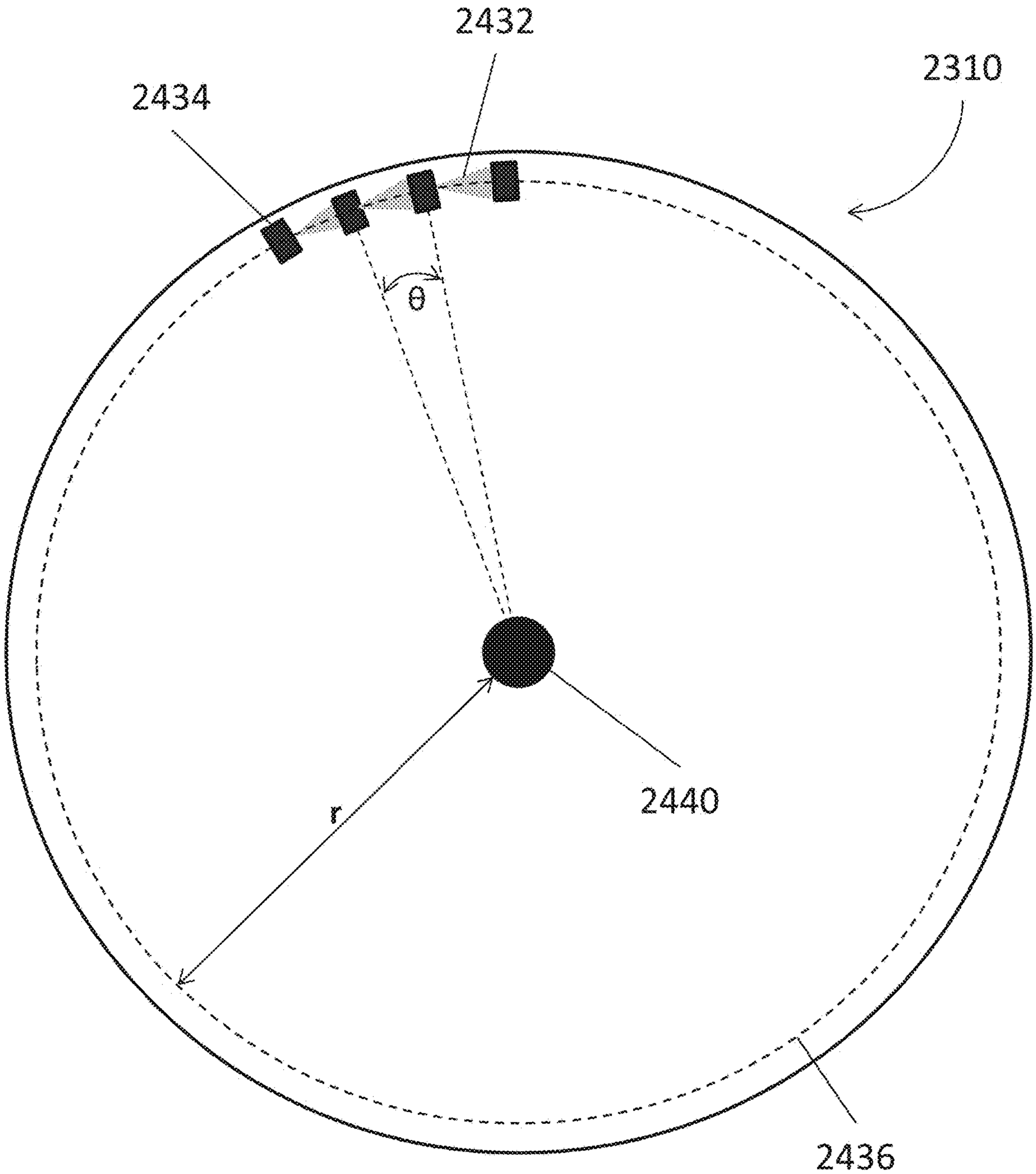

FIG. 24

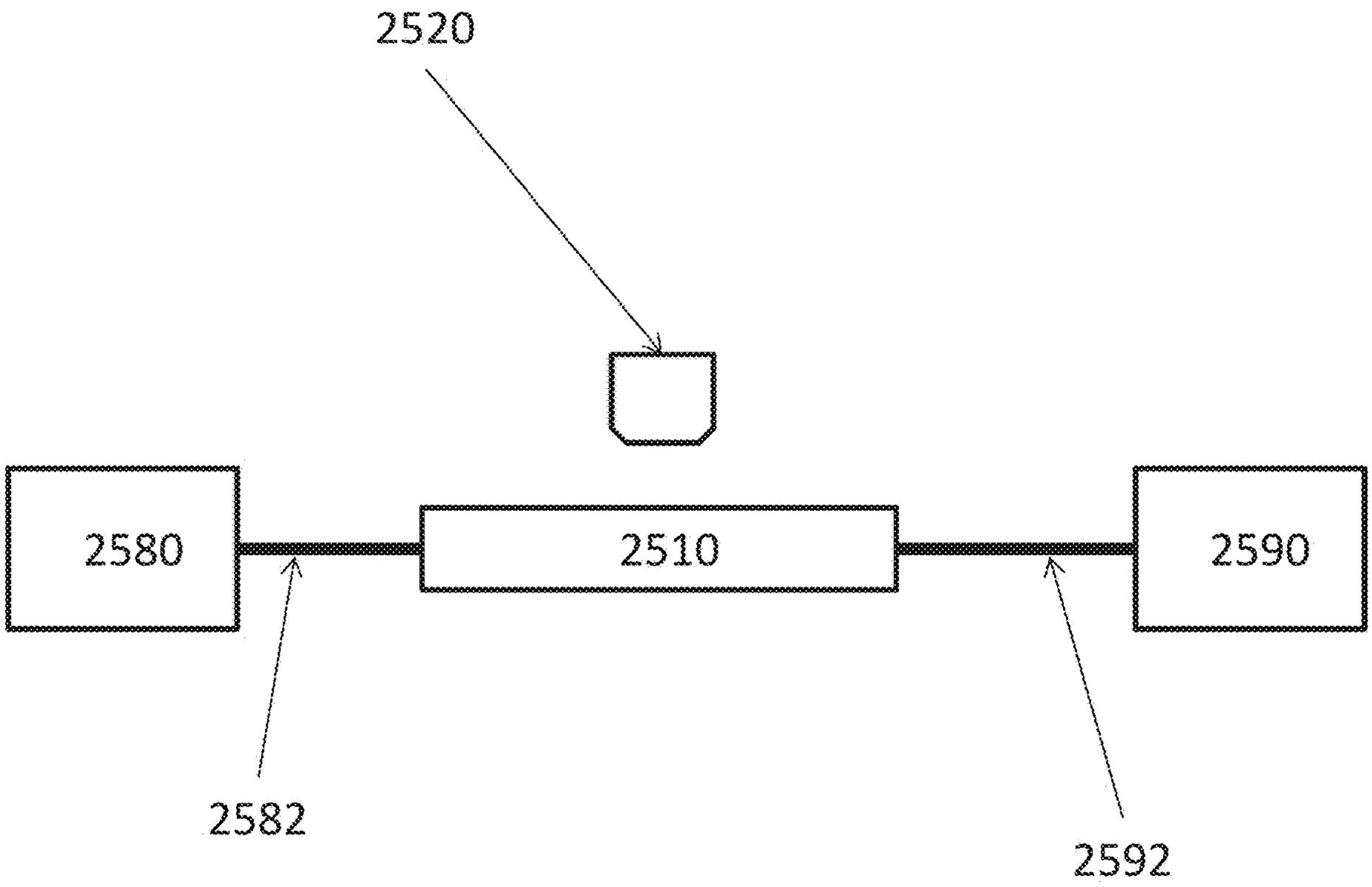

FIG. 25

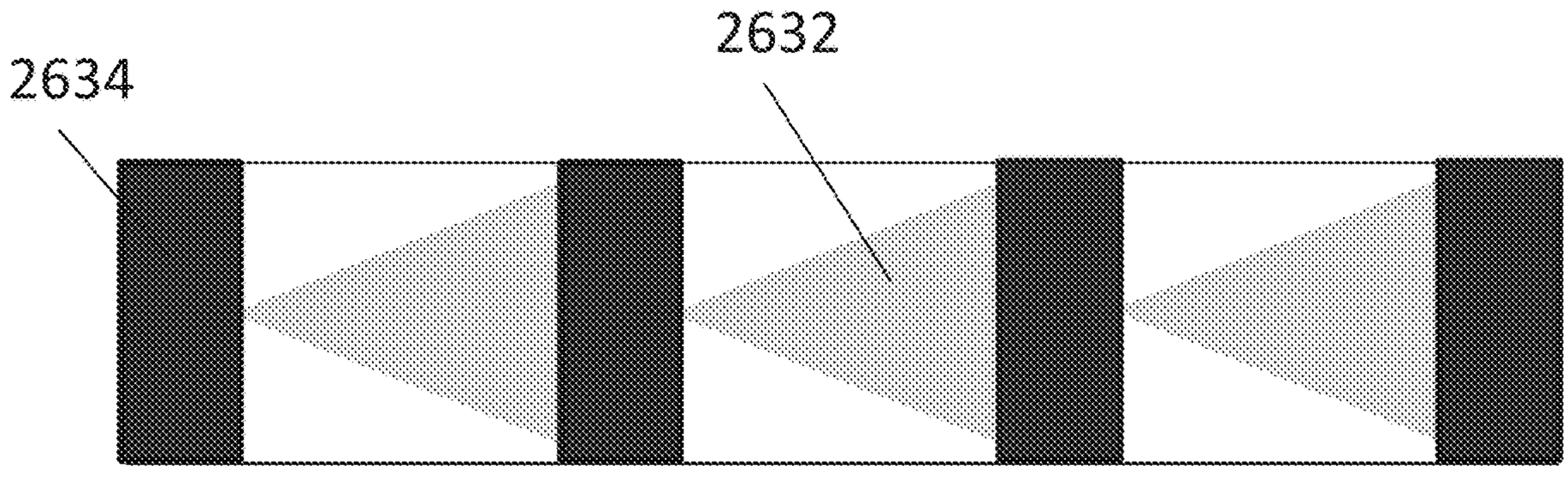

FIG. 26

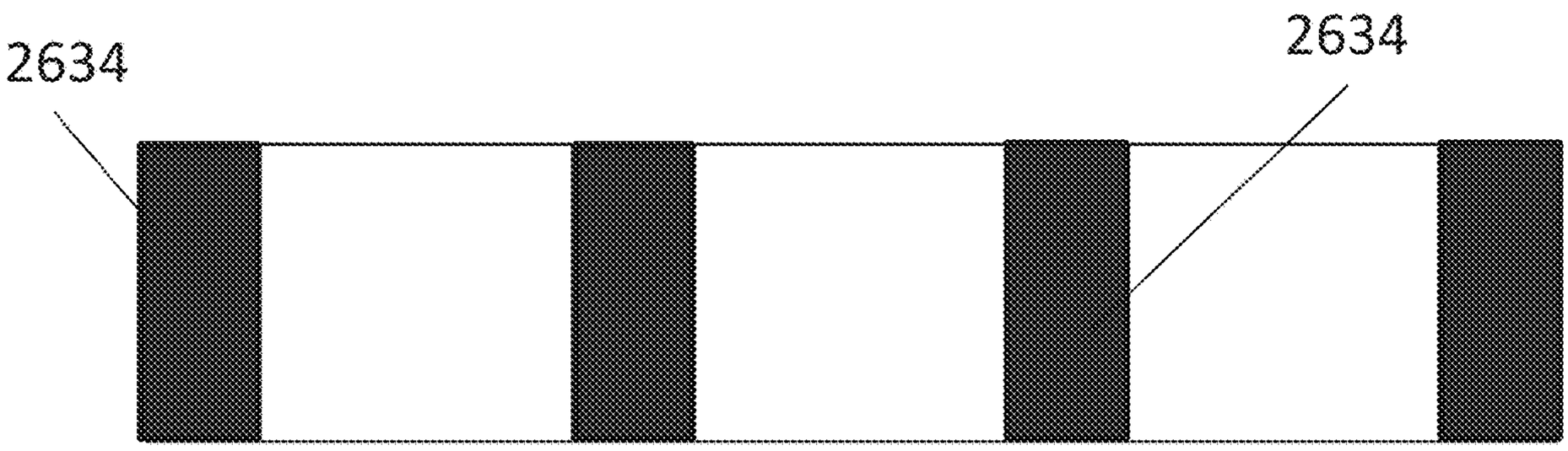

FIG. 27

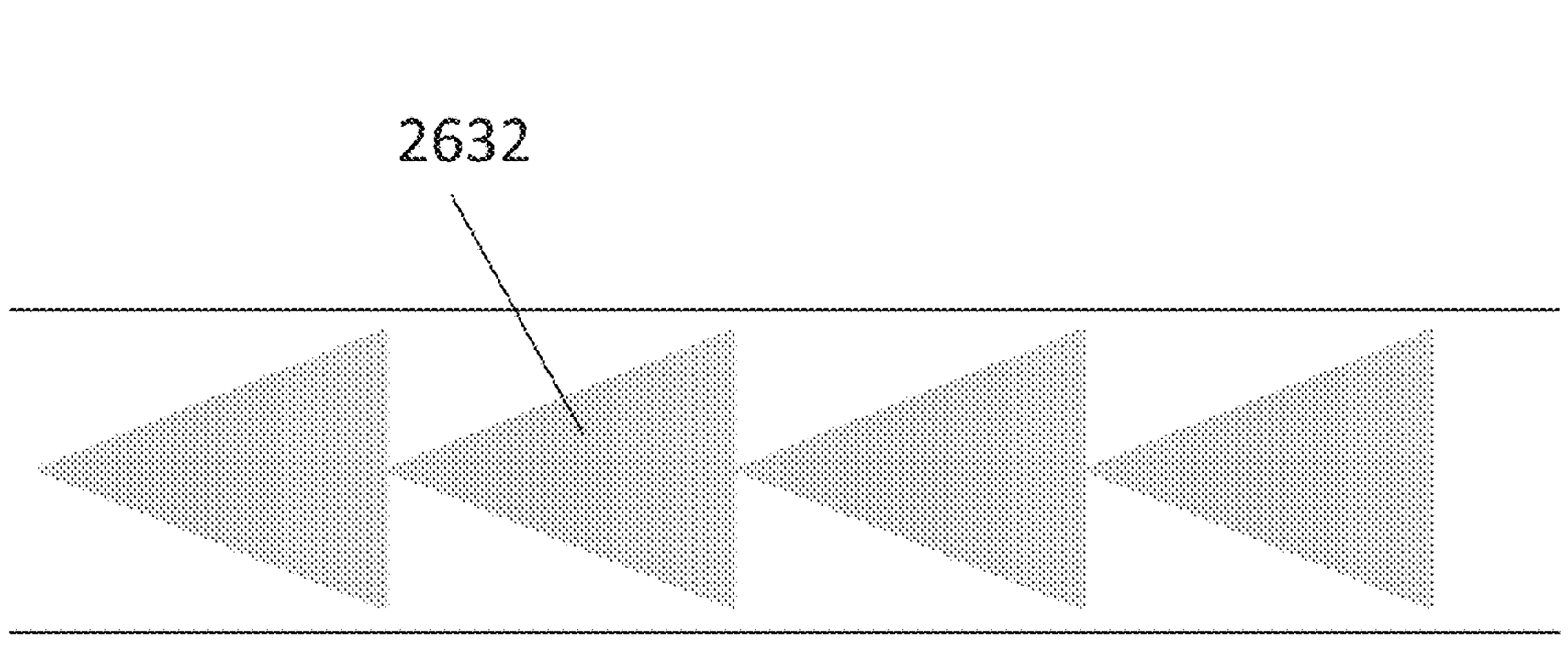

FIG. 28

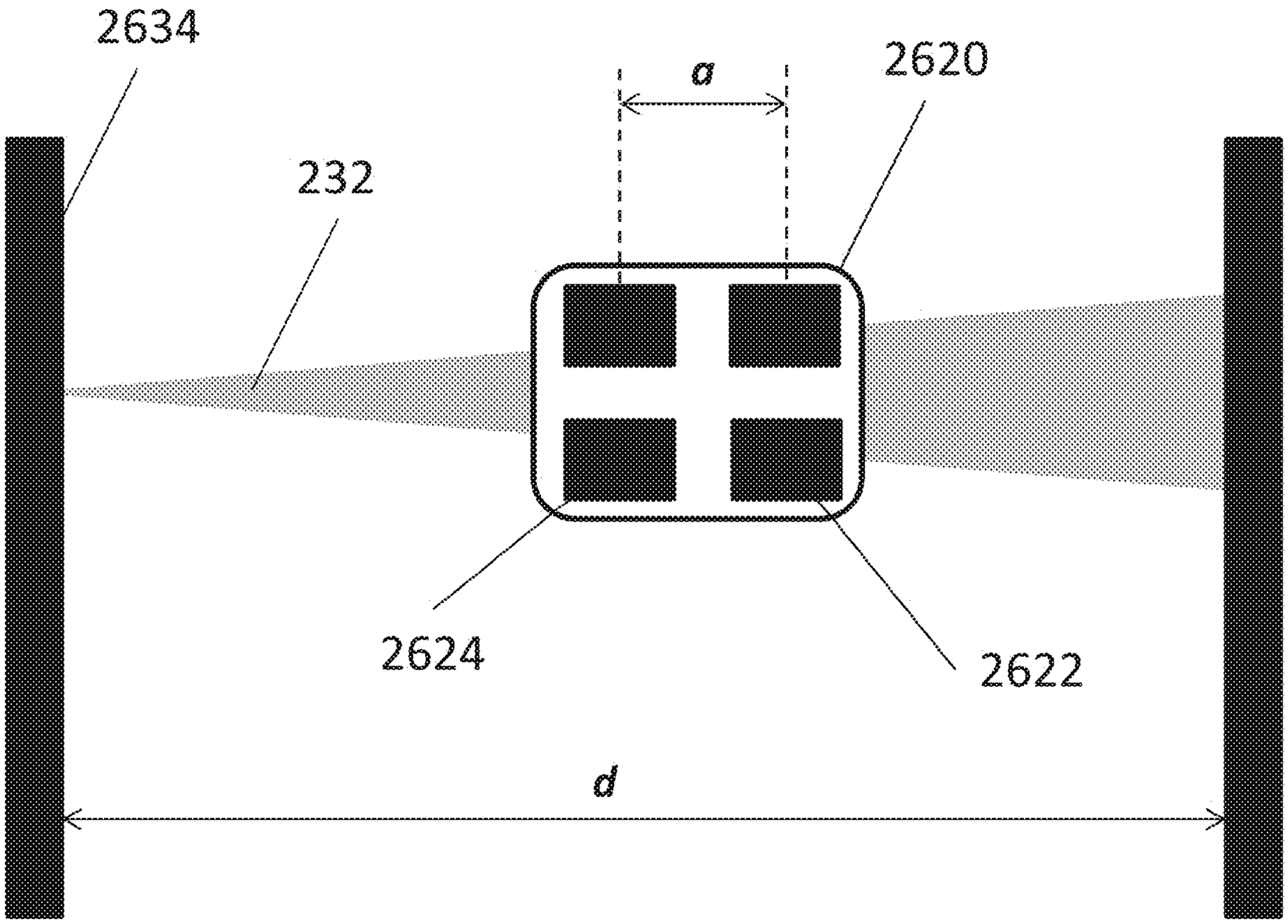

FIG. 29

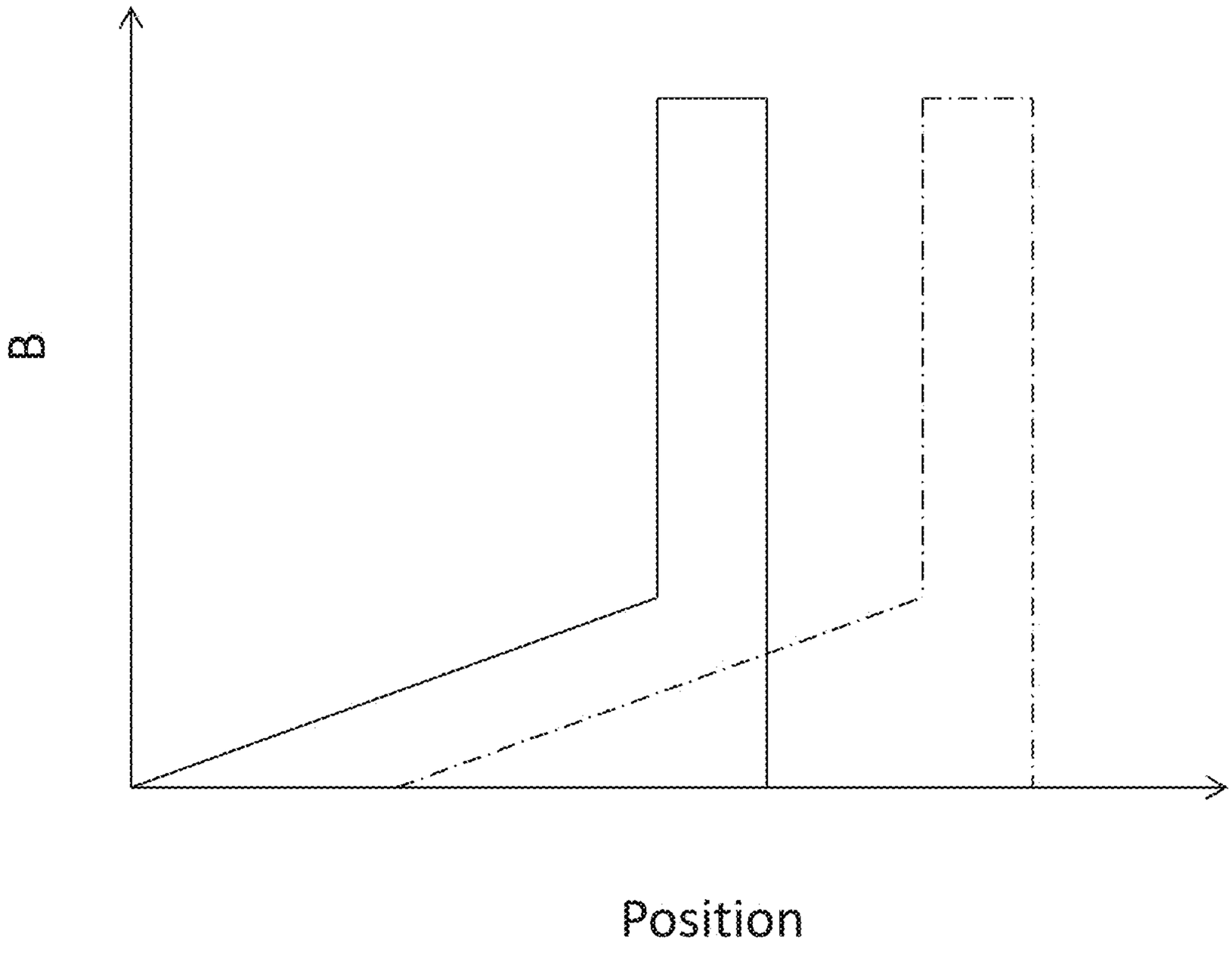

FIG. 30

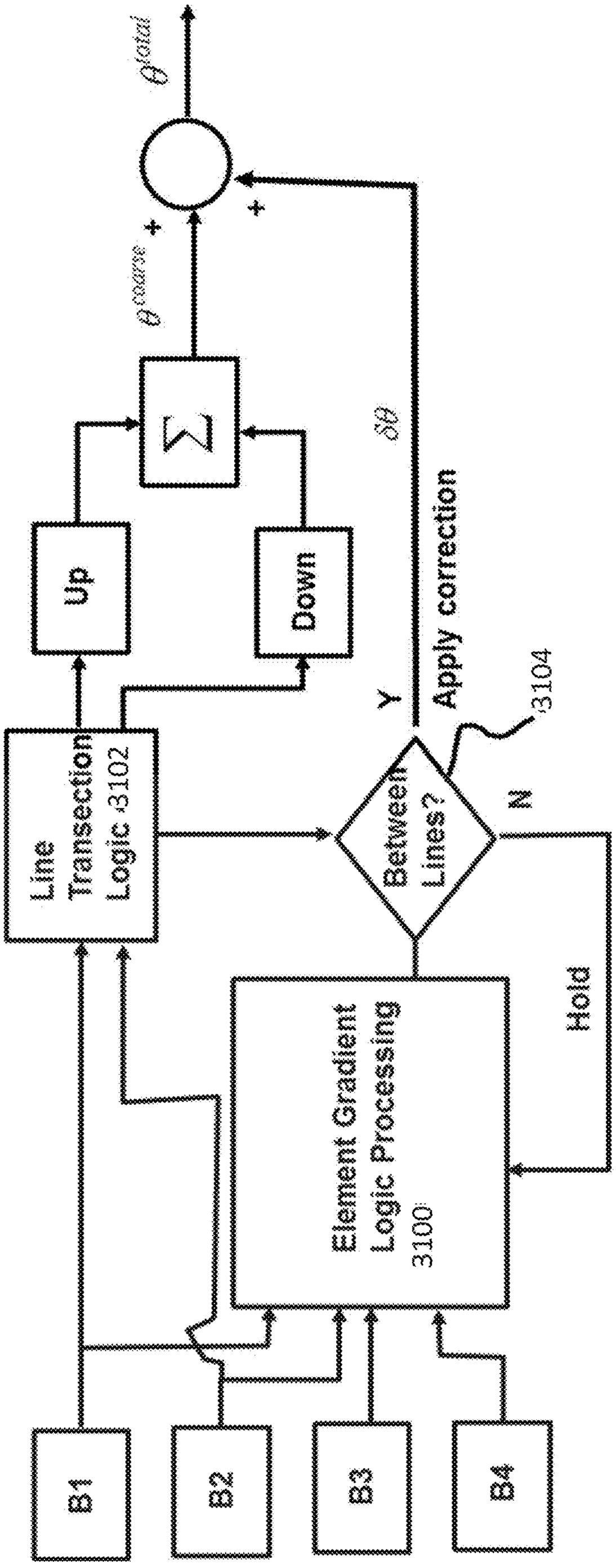
B1
B2
B3
B4
Element Gradient Logic Processing 3100
Line Transection Logic 3102
Up
Down
Σ
Between Lines?
3104
Y
N
Apply correction
Hold
δθ
θ coarse
θ total
+
+
+

FIG. 31

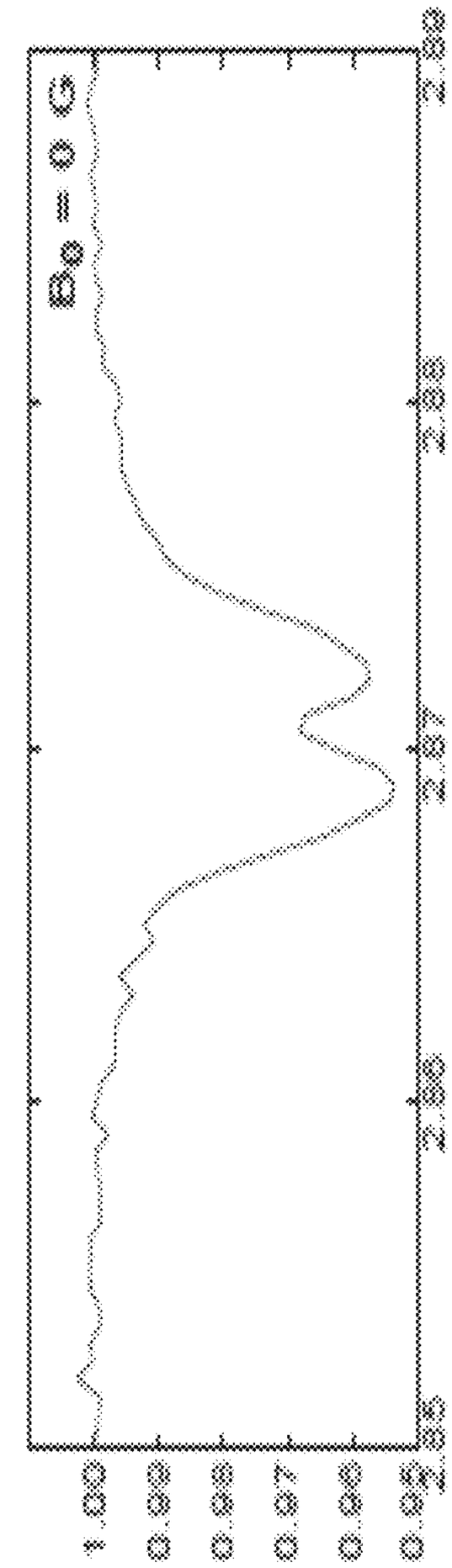

Fig. 32A

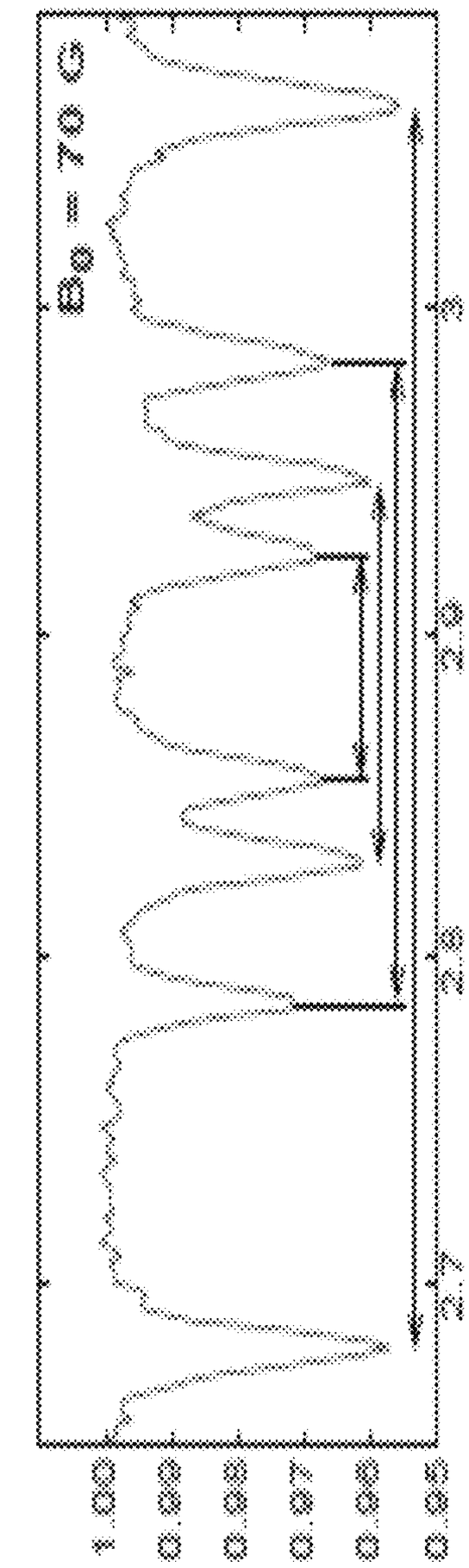

Fig. 32B

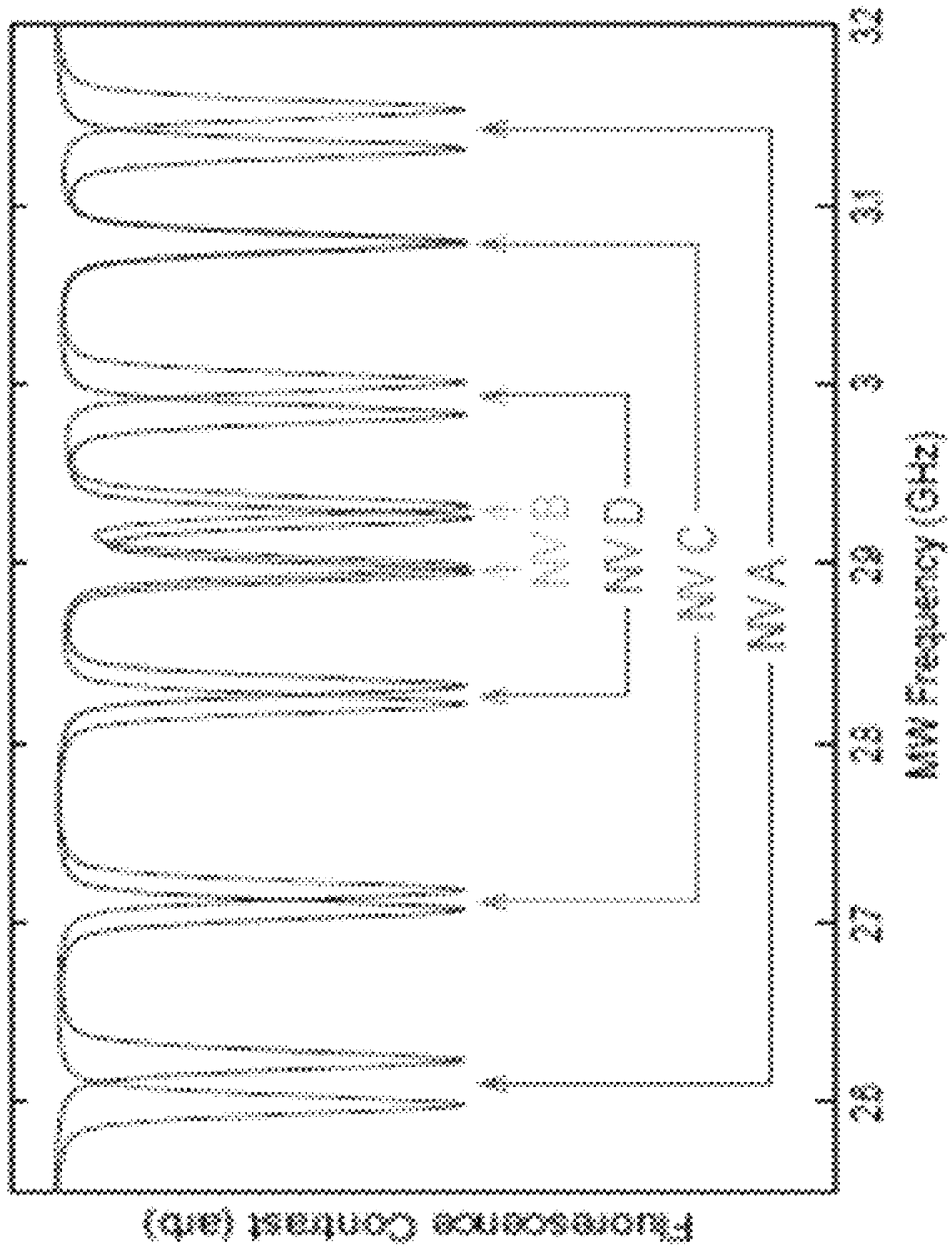

Fig. 33B

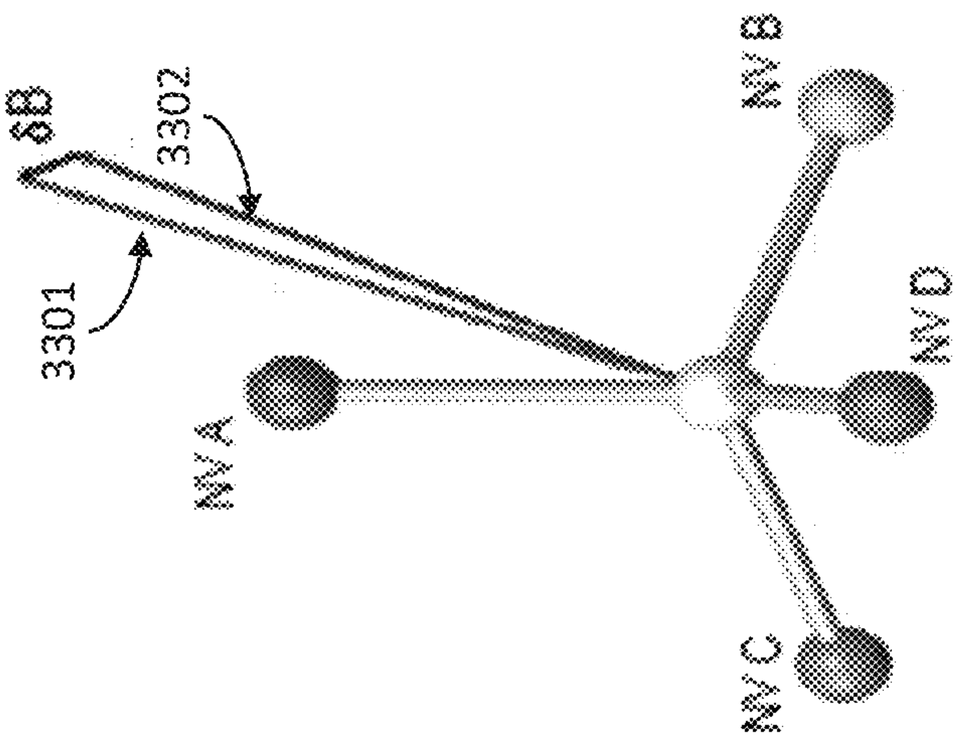

Fig. 33A

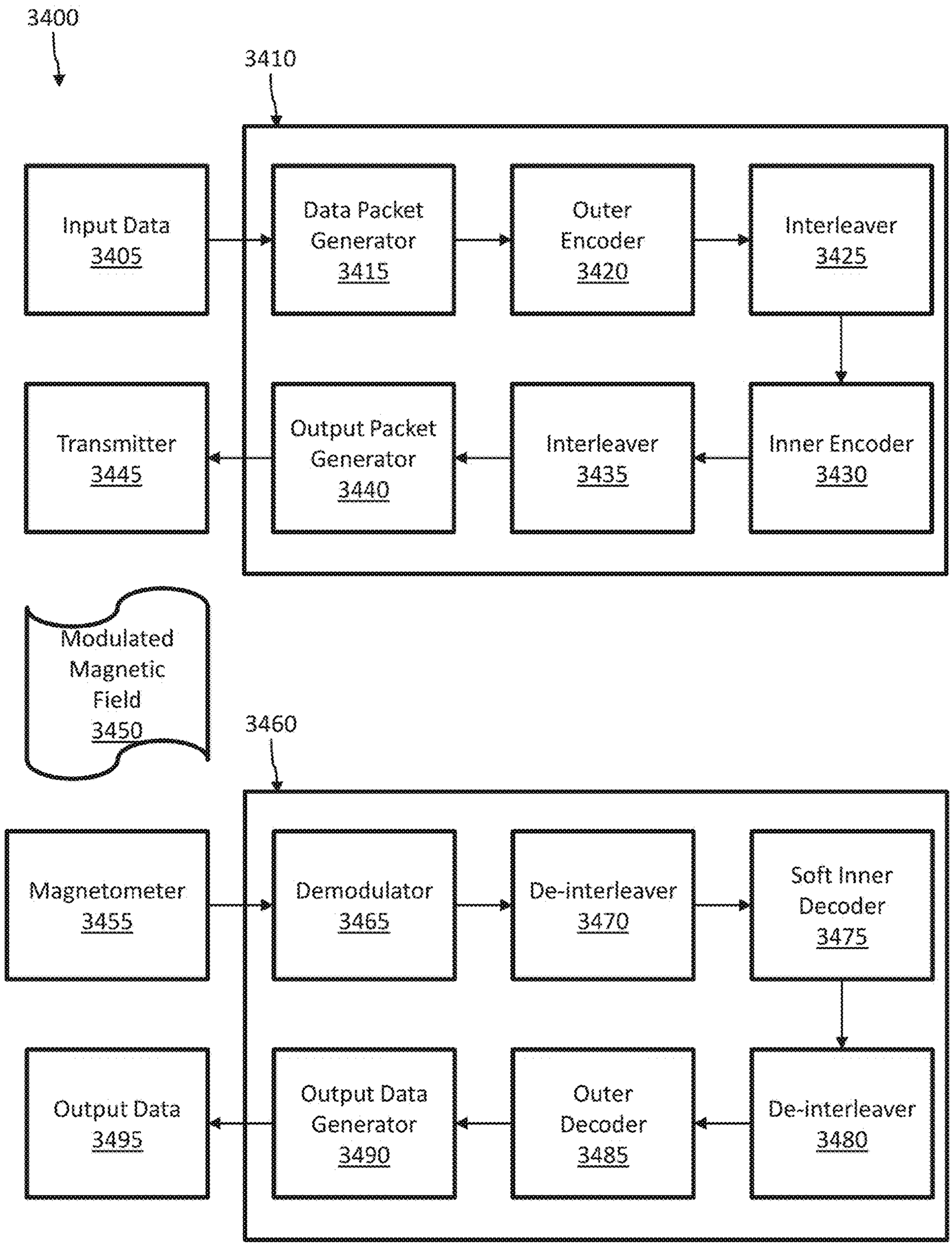
3400
3410
Input Data
3405
Data Packet
Generator
3415
Outer
Encoder
3420
Interleaver
3425
Transmitter
3445
Output Packet
Generator
3440
Interleaver
3435
Inner Encoder
3430
Modulated
Magnetic
Field
3450
3460
Magnetometer
3455
Demodulator
3465
De-interleaver
3470
Soft Inner
Decoder
3475
Output Data
3495
Output Data
Generator
3490
Outer
Decoder
3485
De-interleaver
3480

Fig. 34

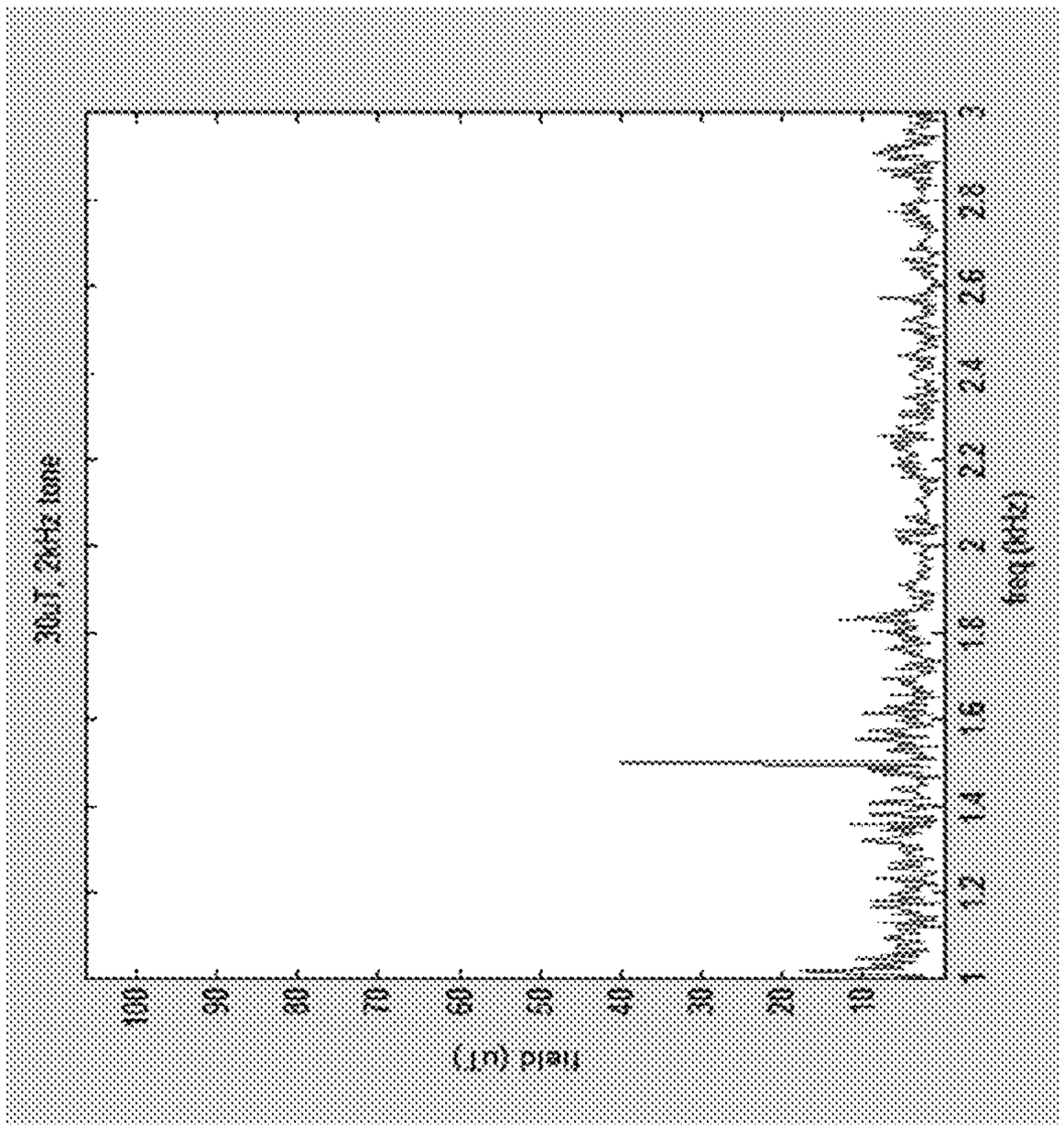

Fig. 35A

Fig. 35B

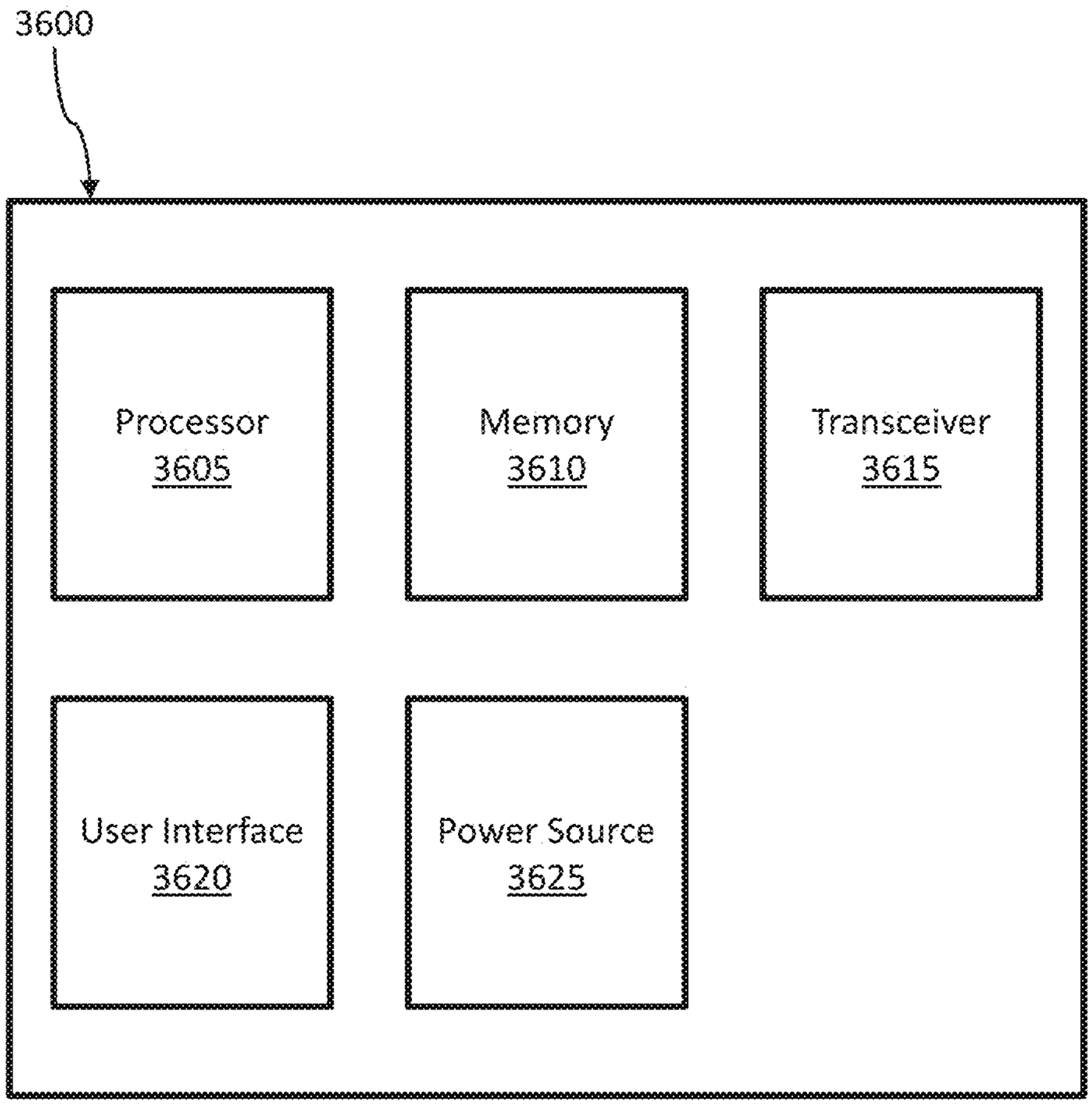
3600
Processor
3605
Memory
3610
Transceiver
3615
User Interface
3620
Power Source
3625

Fig. 36

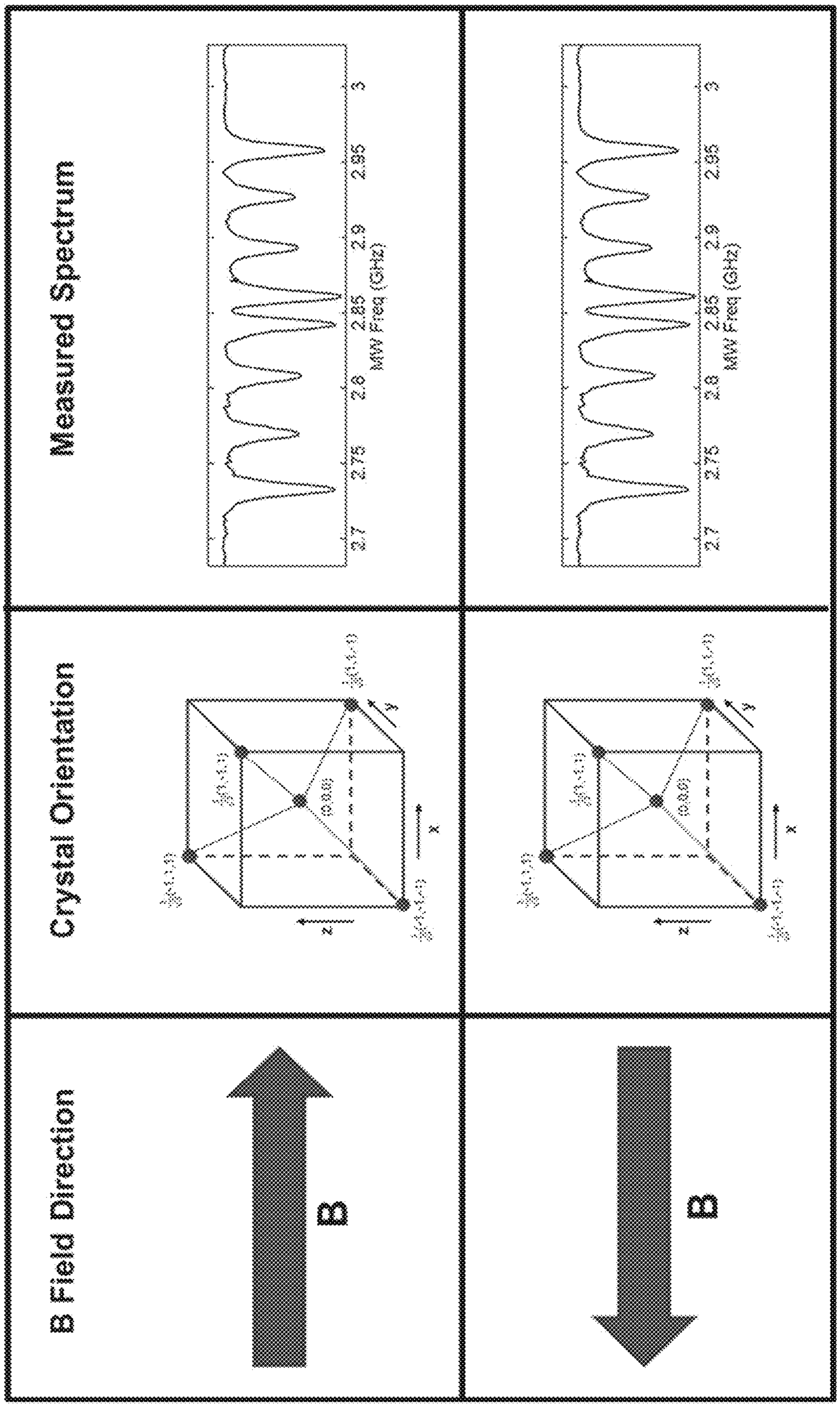
Measured Spectrum
MW Freq (GHz)
2.7
2.75
2.8
2.85
2.9
2.95
3
Crystal Orientation
B Field Direction
B

FIG. 37

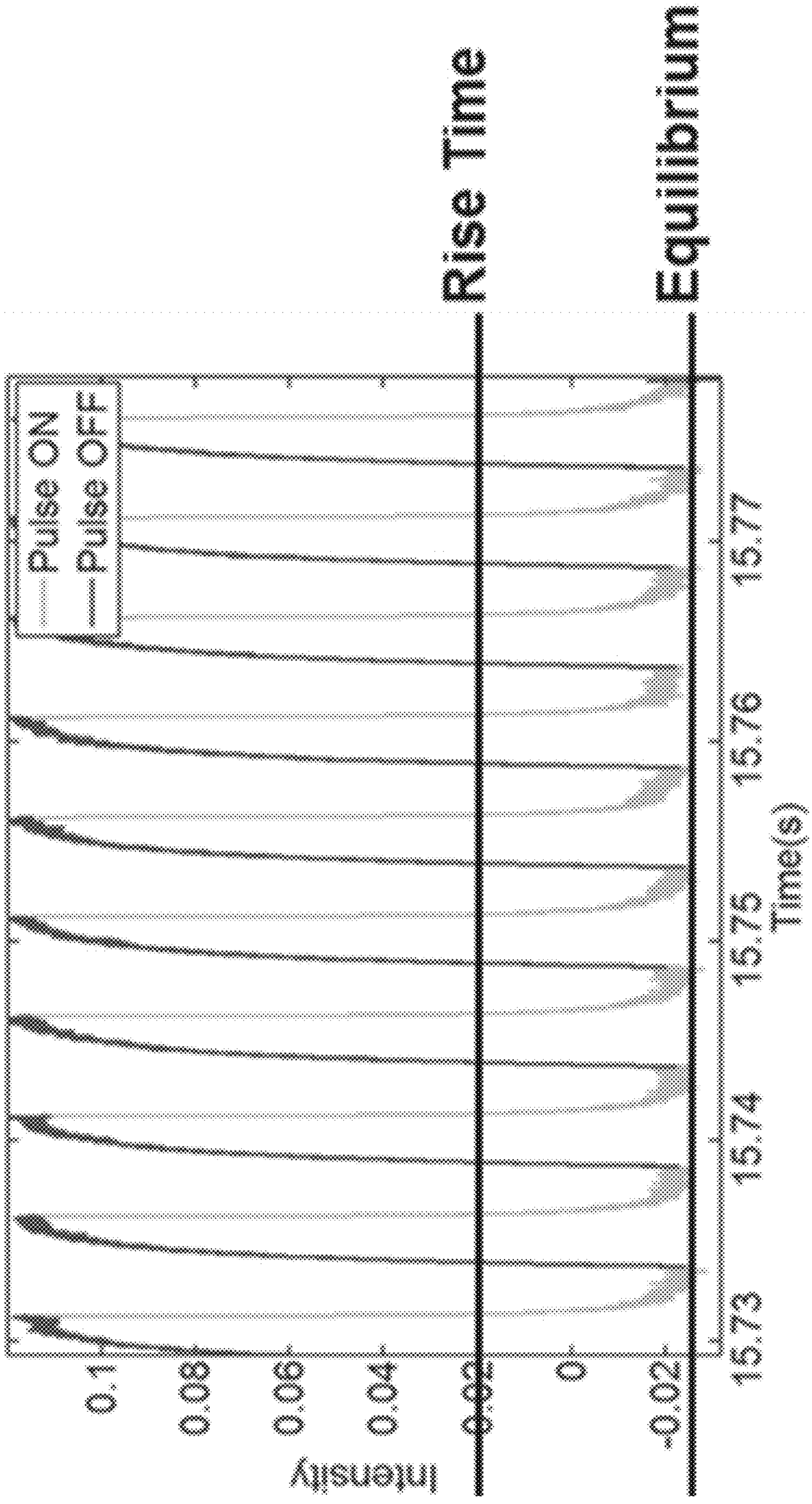
Rise Time
Equilibrium
Pulse ON
Pulse OFF
Intensity
0.1
0.08
0.06
0.04
0.02
0
-0.02
15.73
15.74
15.75
15.76
15.77
Time(s)

FIG. 38

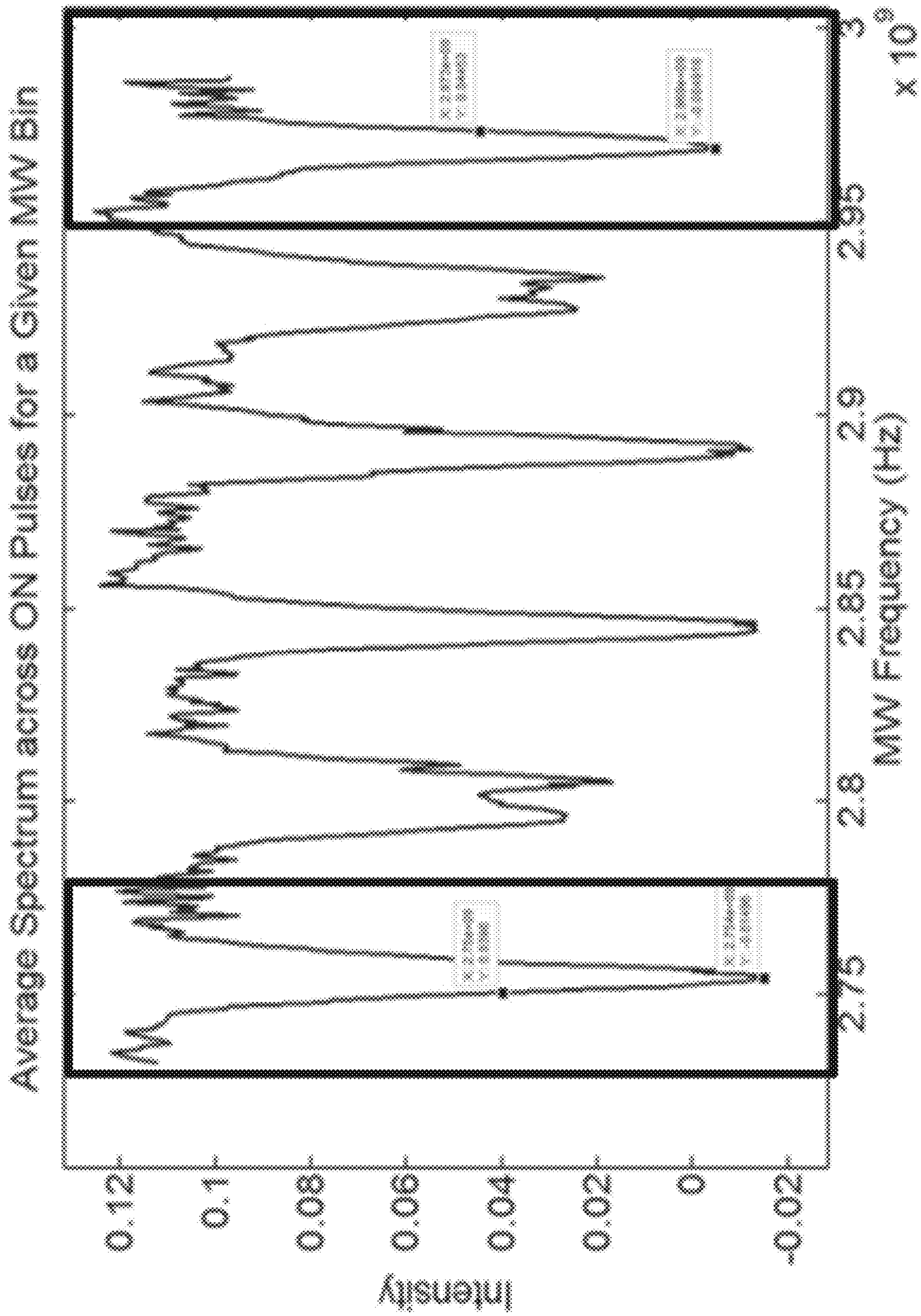
Average Spectrum across ON Pulses for a Given MW Bin
Intensity
0.12
0.1
0.08
0.06
0.04
0.02
0
-0.02
2.8
2.85
2.9
MW Frequency (Hz)
2.875
2.825
2.775

FIG. 39

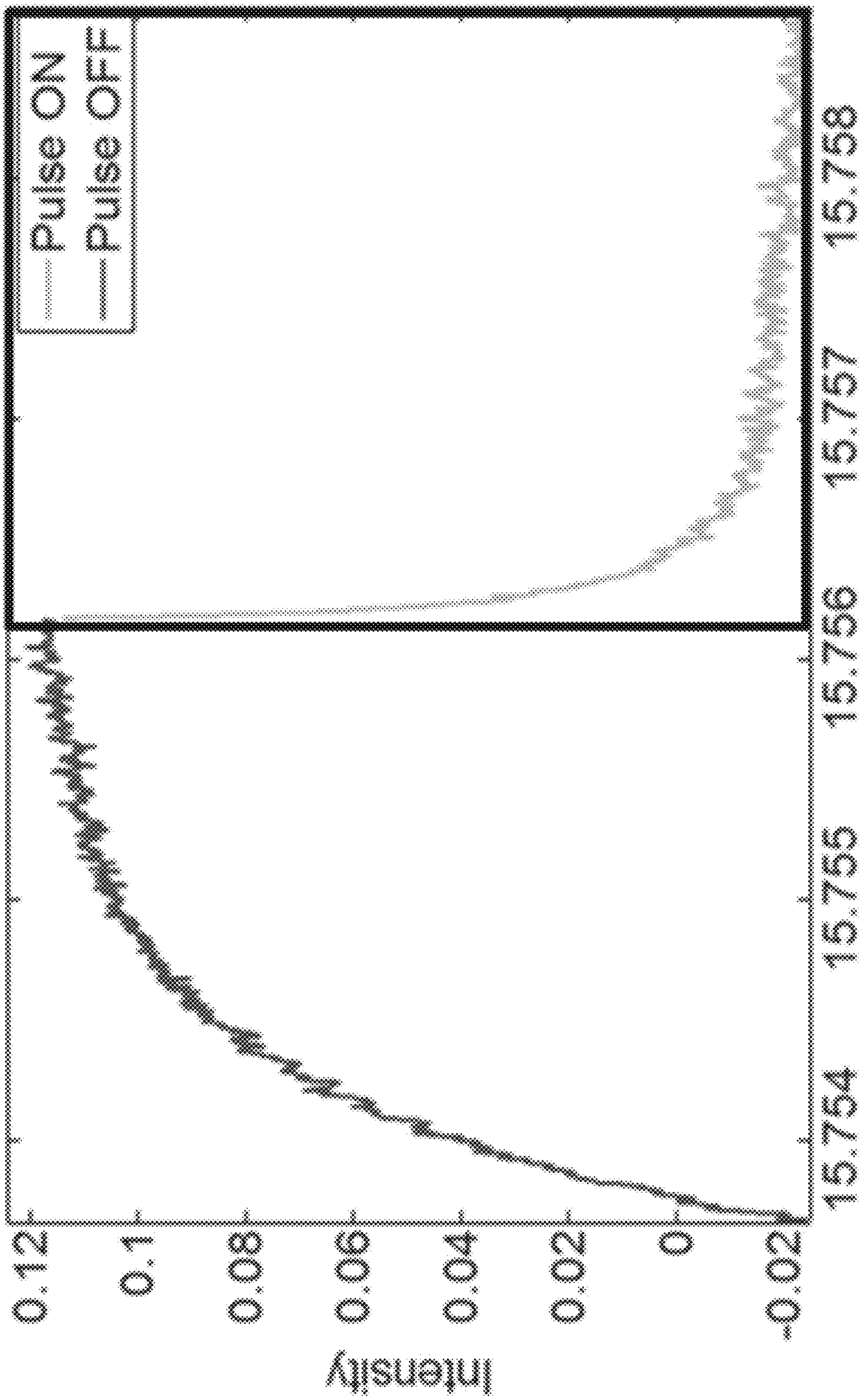
Pulse ON
Pulse OFF
Intensity
0.12
0.1
0.08
0.06
0.04
0.02
0
-0.02
15.754
15.755
15.756
15.757
15.758
Time(s)

FIG. 40

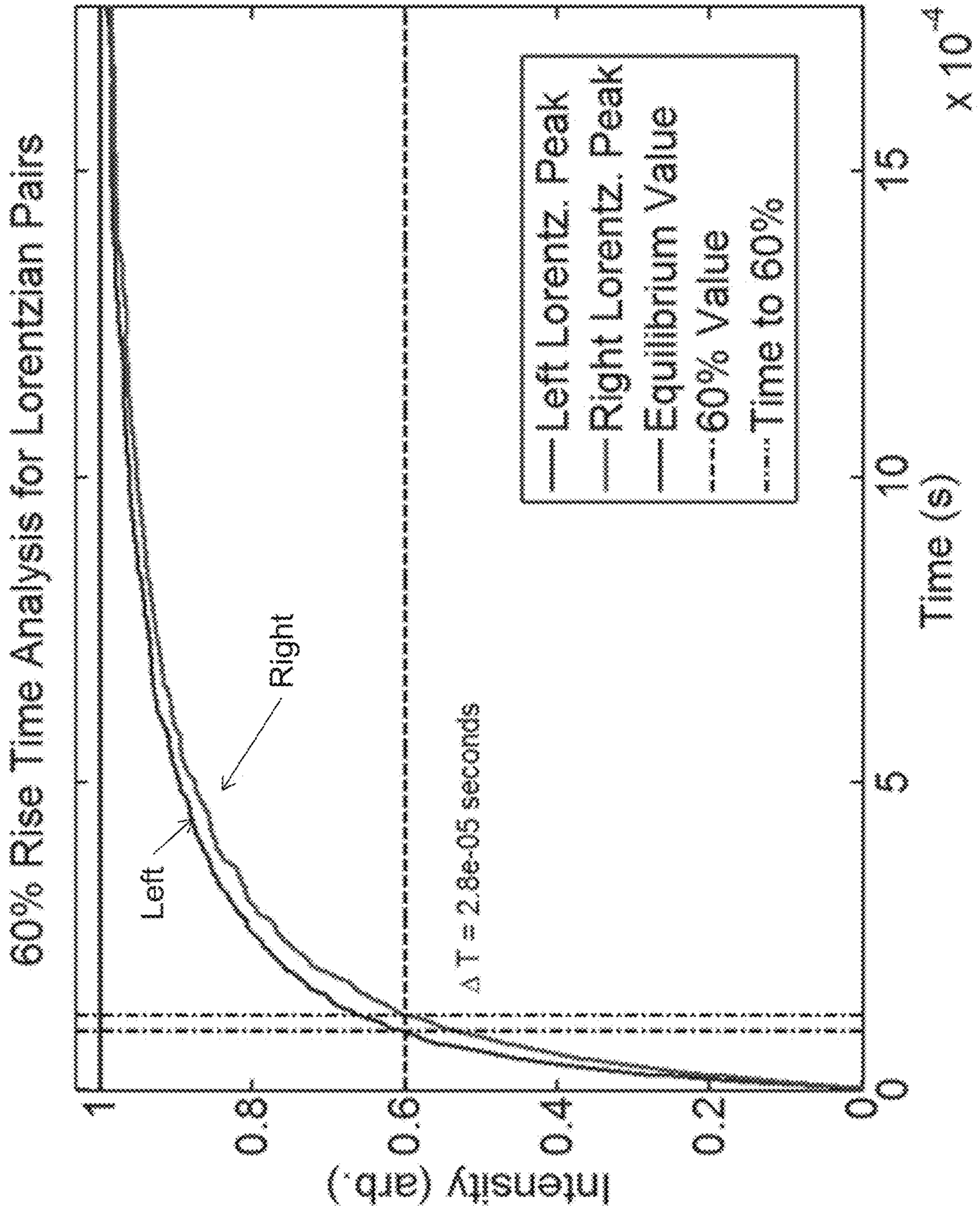
60% Rise Time Analysis for Lorentzian Pairs
Left
Right
Δτ = 2.8e-05 seconds
Left Lorentz. Peak
Right Lorentz. Peak
Equilibrium Value
60% Value
Time to 60%
Intensity (arb.)
Time (s)
0
0.2
0.4
0.6
0.8
1
5
10
15
x 10^-4

FIG. 41

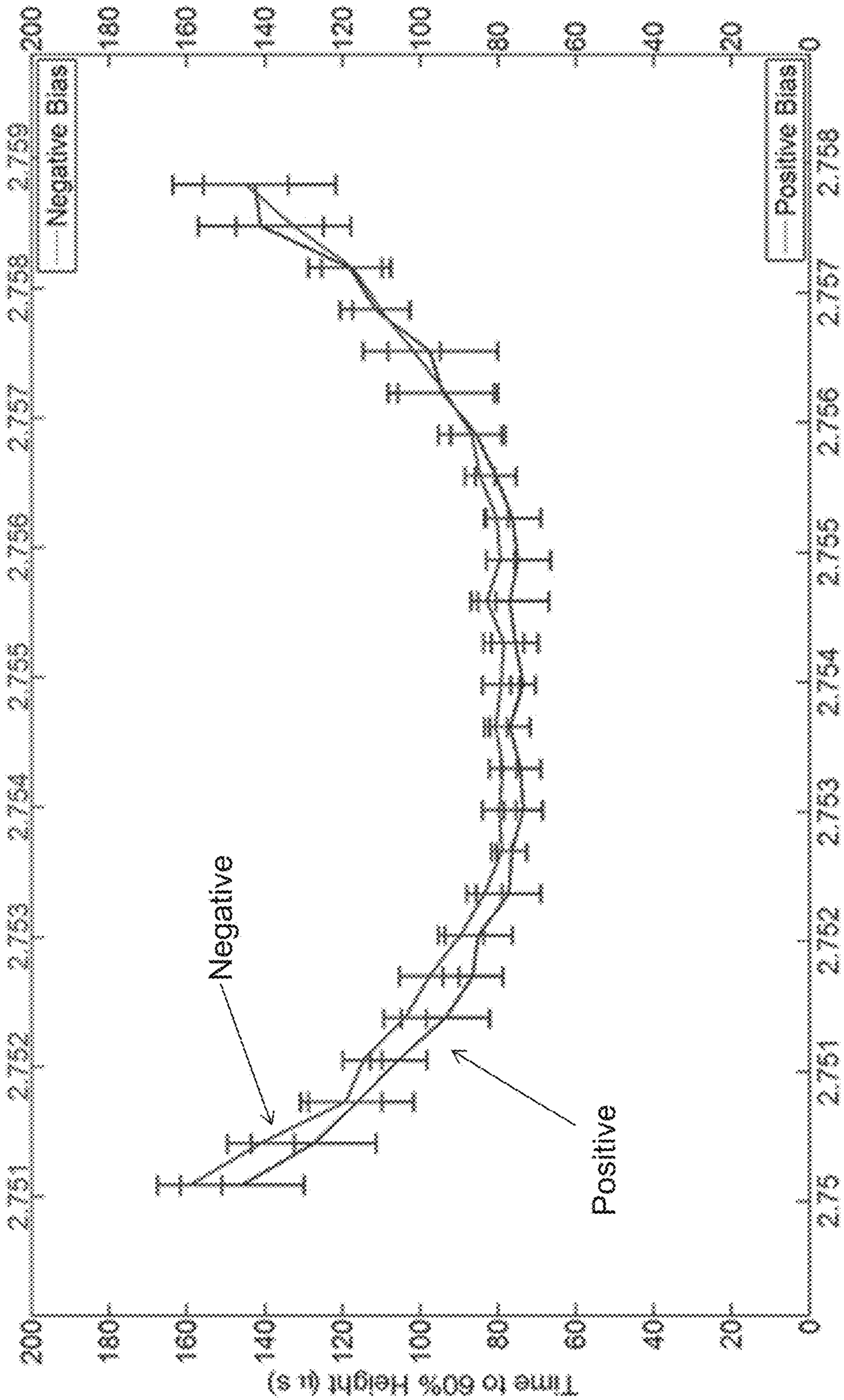
Lorentzian Pair Peaks rise time to 60% equil.
Negative Bias
Positive Bias
Negative
Positive
MW Freq(GHz)
Time to 60% Height (x s)
2.759
2.758
2.757
2.756
2.755
2.754
2.753
2.752
2.751
2.75
200
180
160
140
120
100
80
60
40
20
0

FIG. 42

Fig. 43A

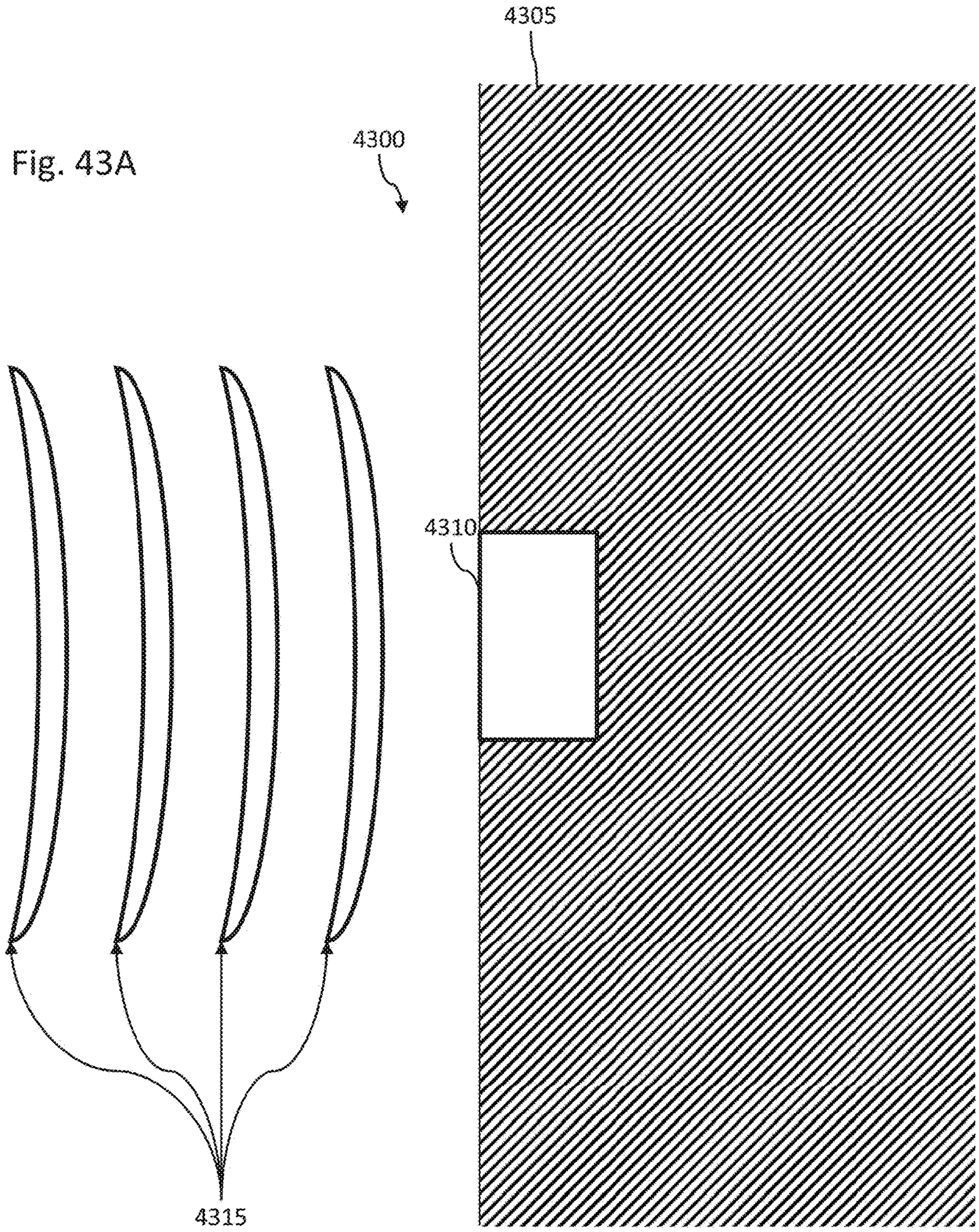

Fig. 43B

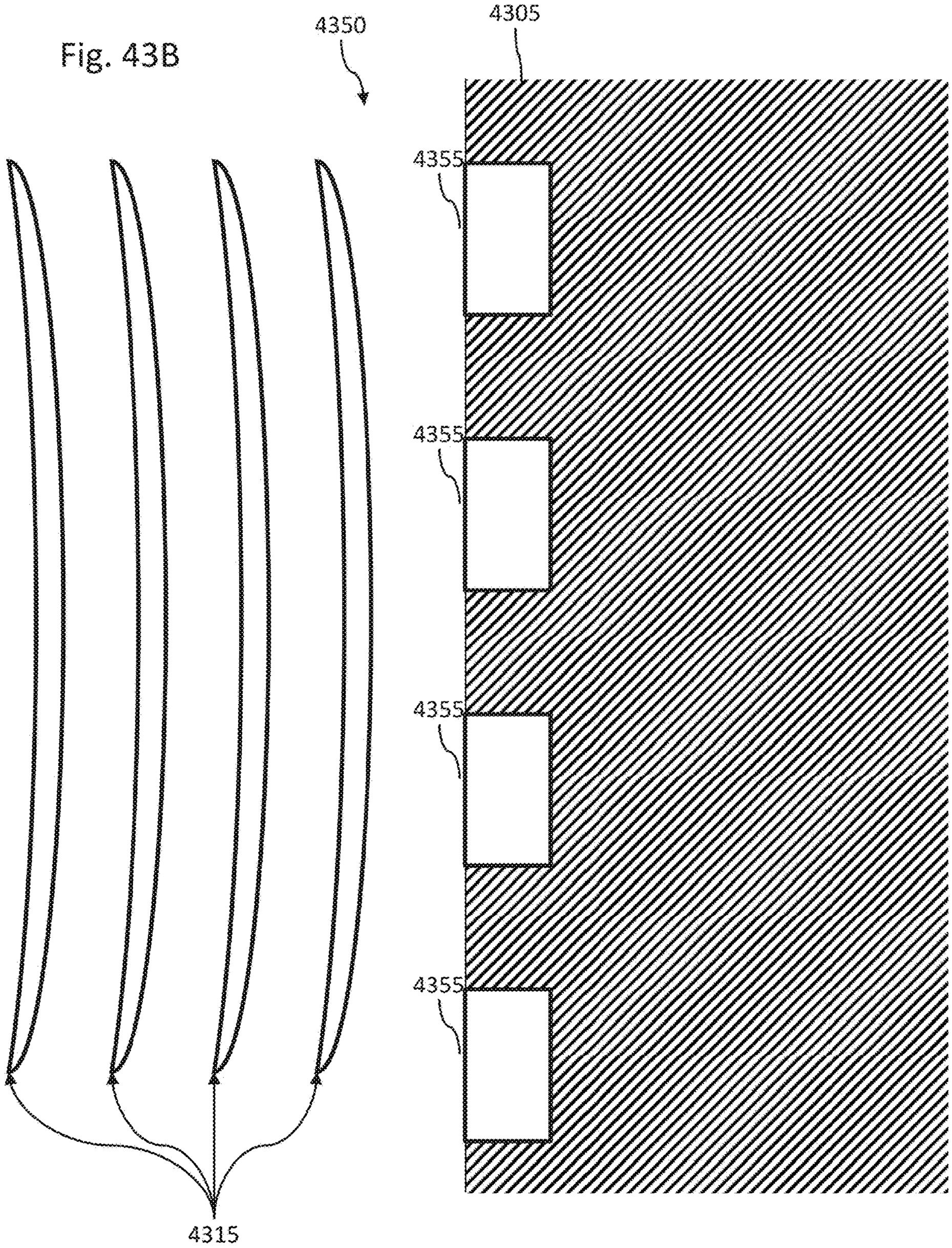

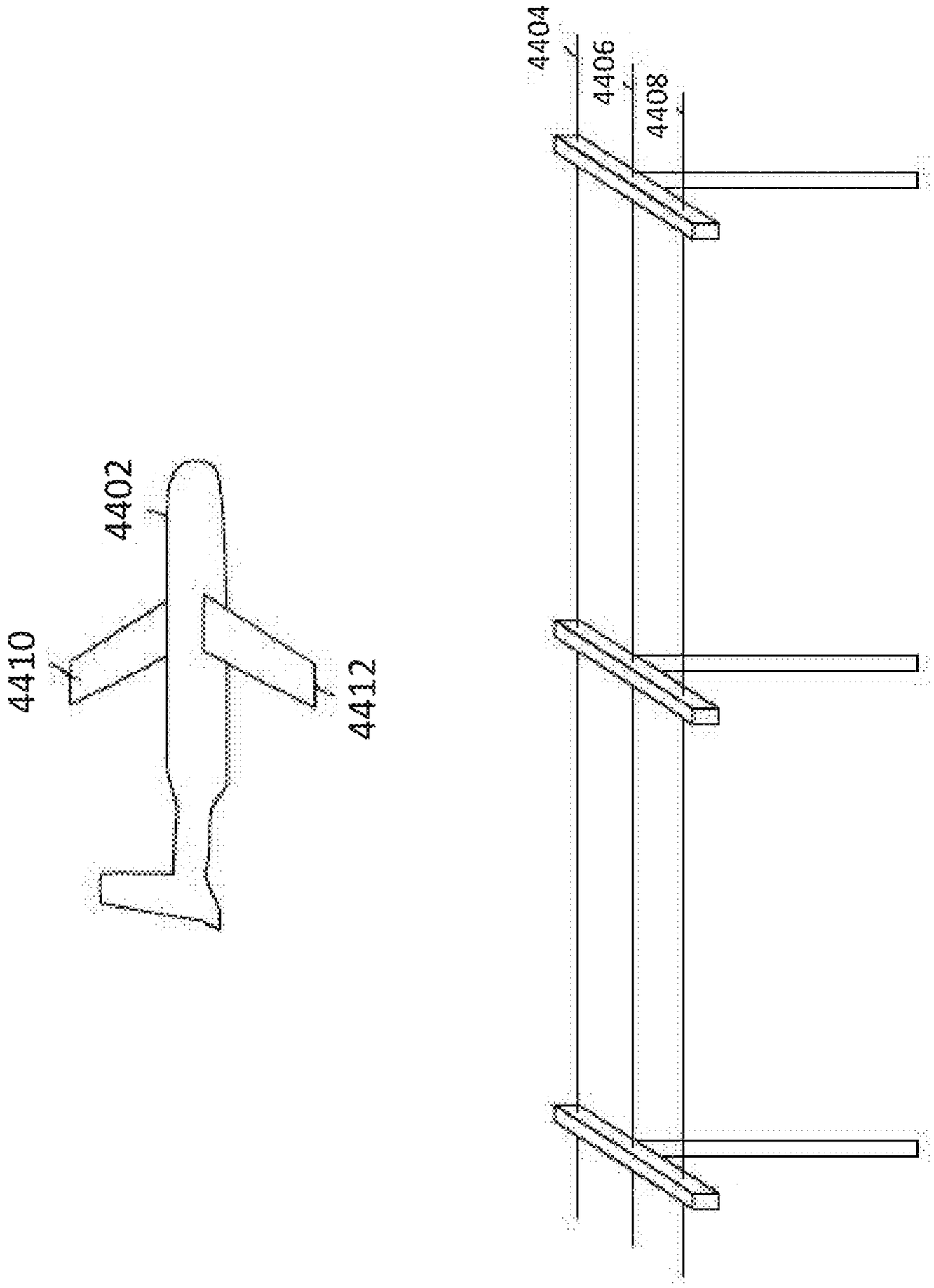

FIG. 44

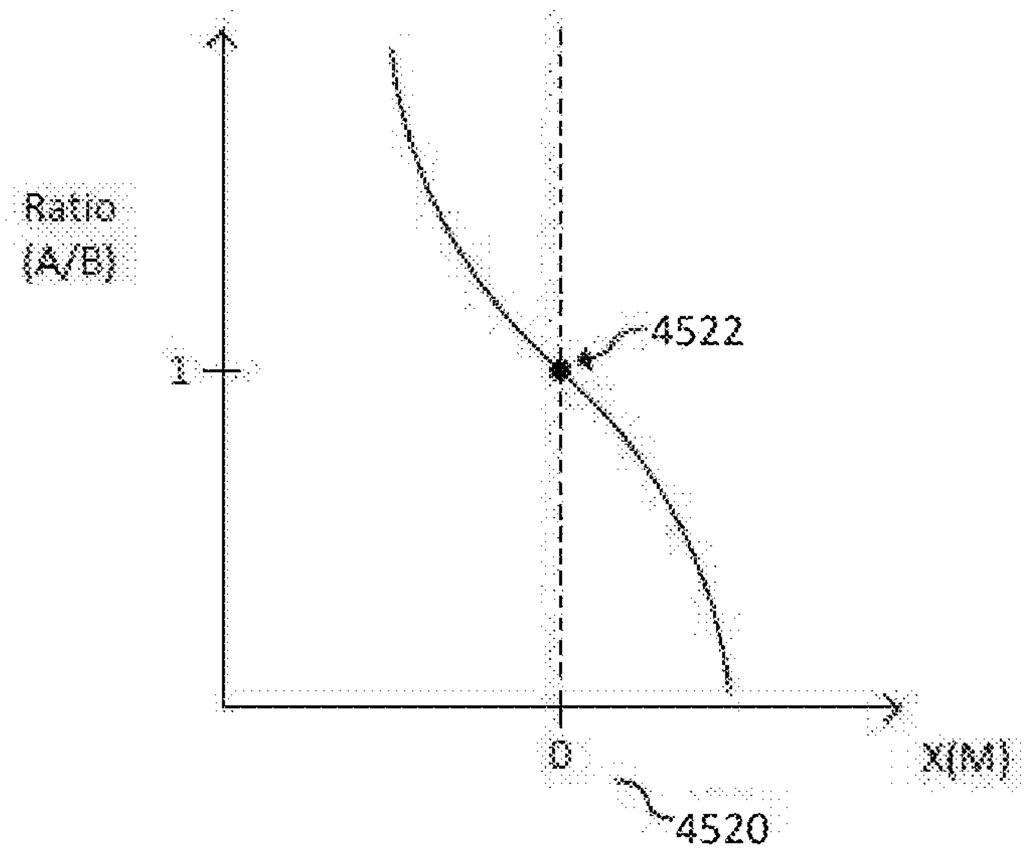

FIG. 45A

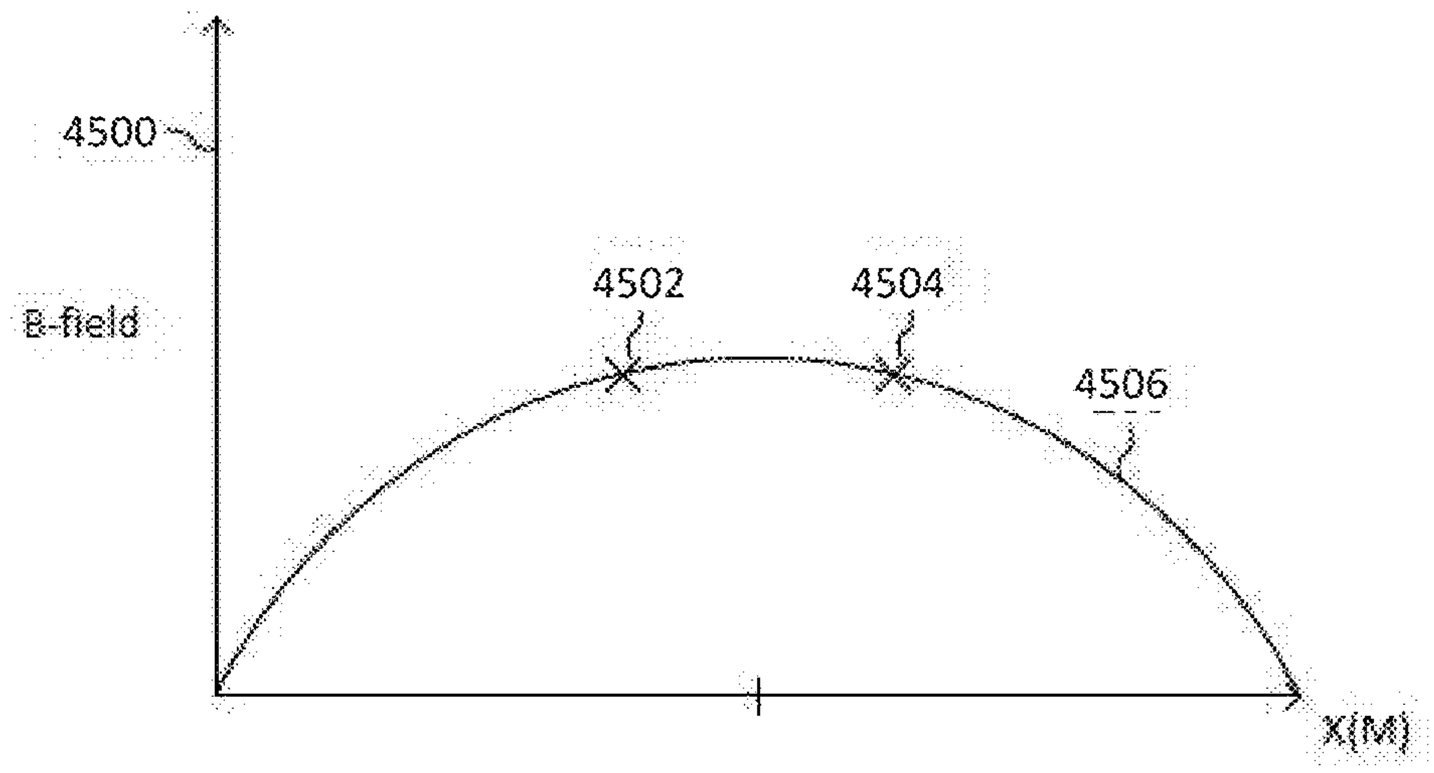

FIG. 45B

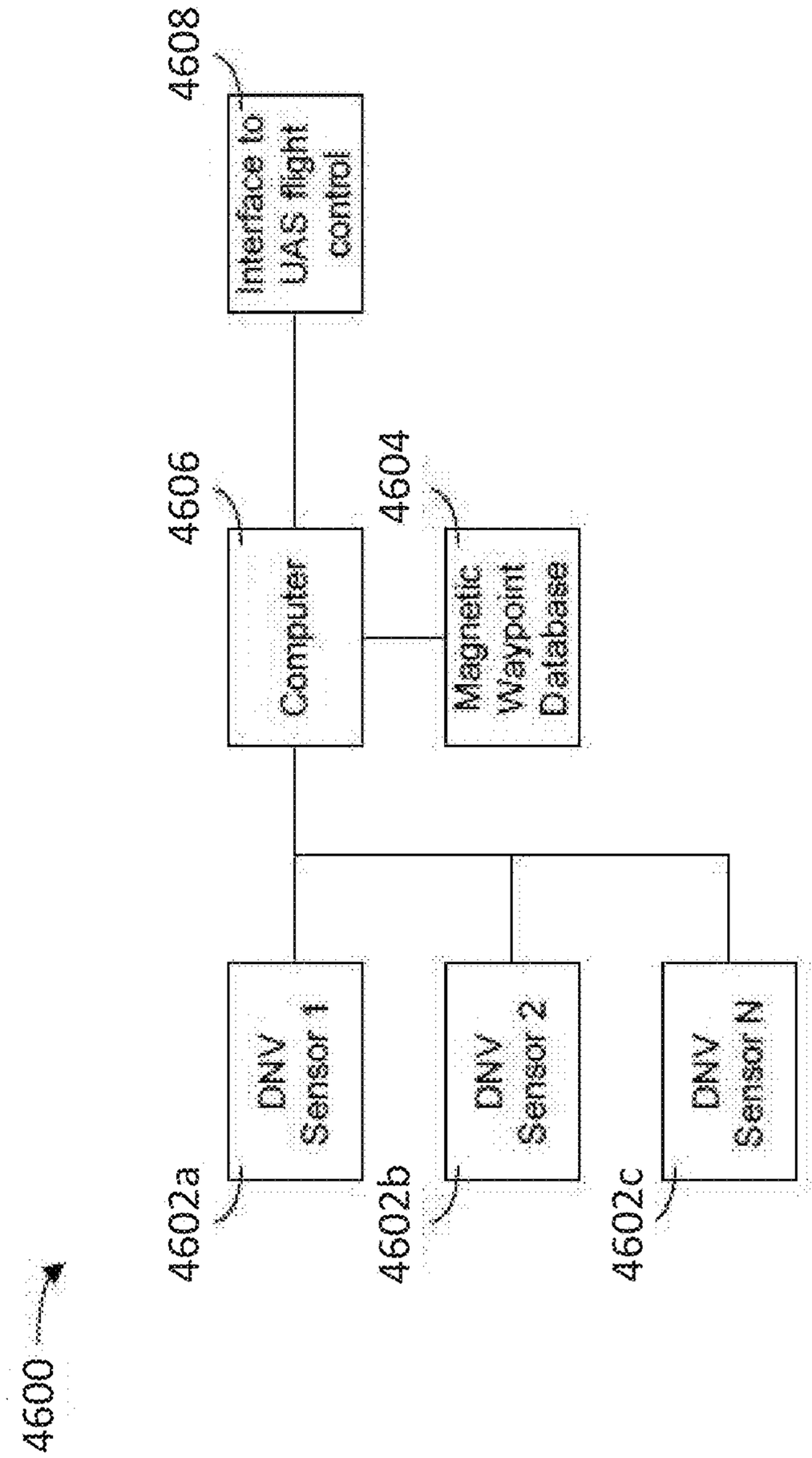
4600
4602a
DNV Sensor 1
4602b
DNV Sensor 2
4602c
DNV Sensor N
4606
Computer
4604
Magnetic Waypoint Database
4608
Interface to UAS flight control

FIG. 46

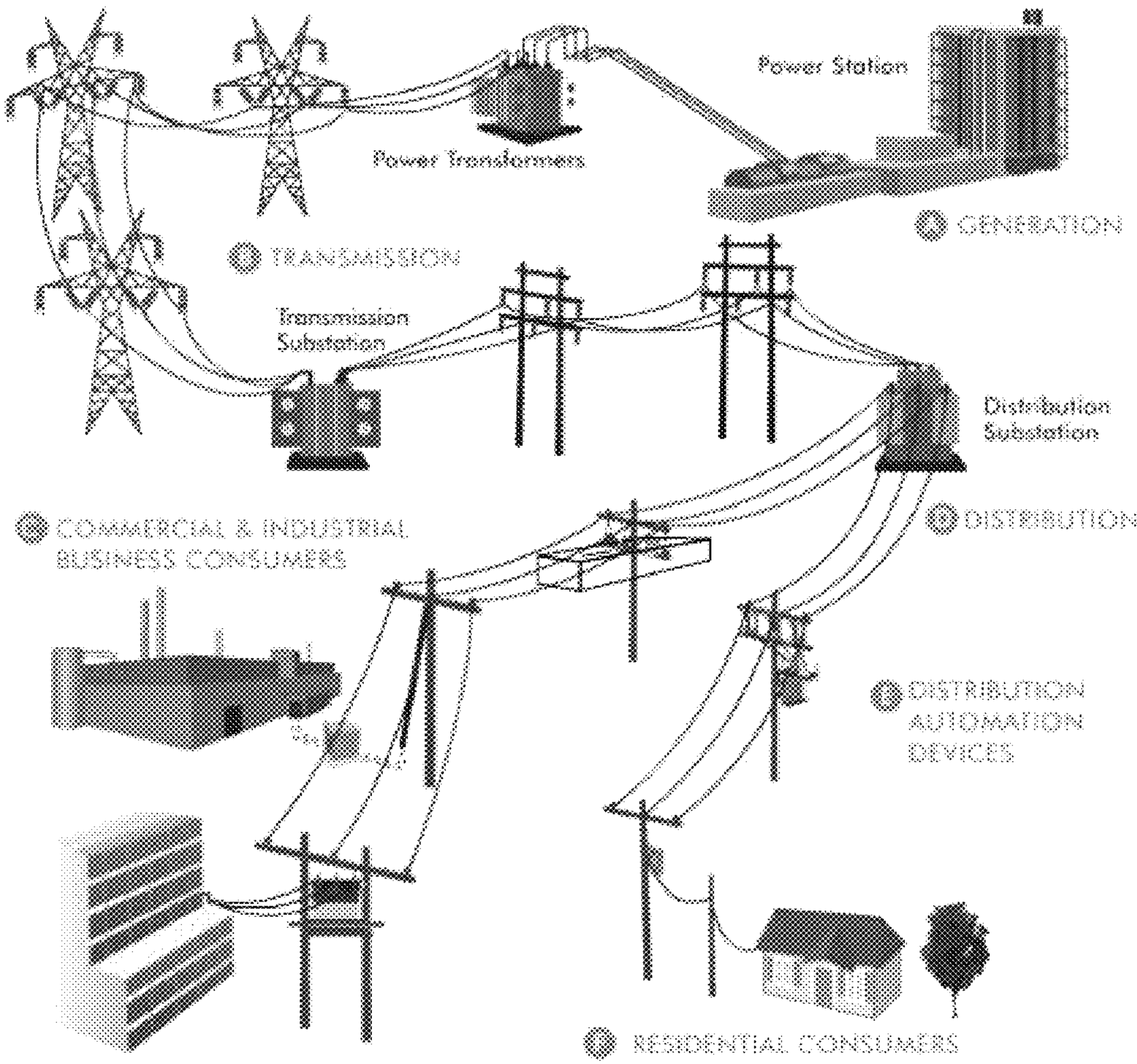
Power Station
Power Transformers
GENERATION
TRANSMISSION
Transmission Substation
Distribution Substation
DISTRIBUTION
COMMERCIAL & INDUSTRIAL BUSINESS CONSUMERS
DISTRIBUTION AUTOMATION DEVICES
RESIDENTIAL CONSUMERS

FIG. 47

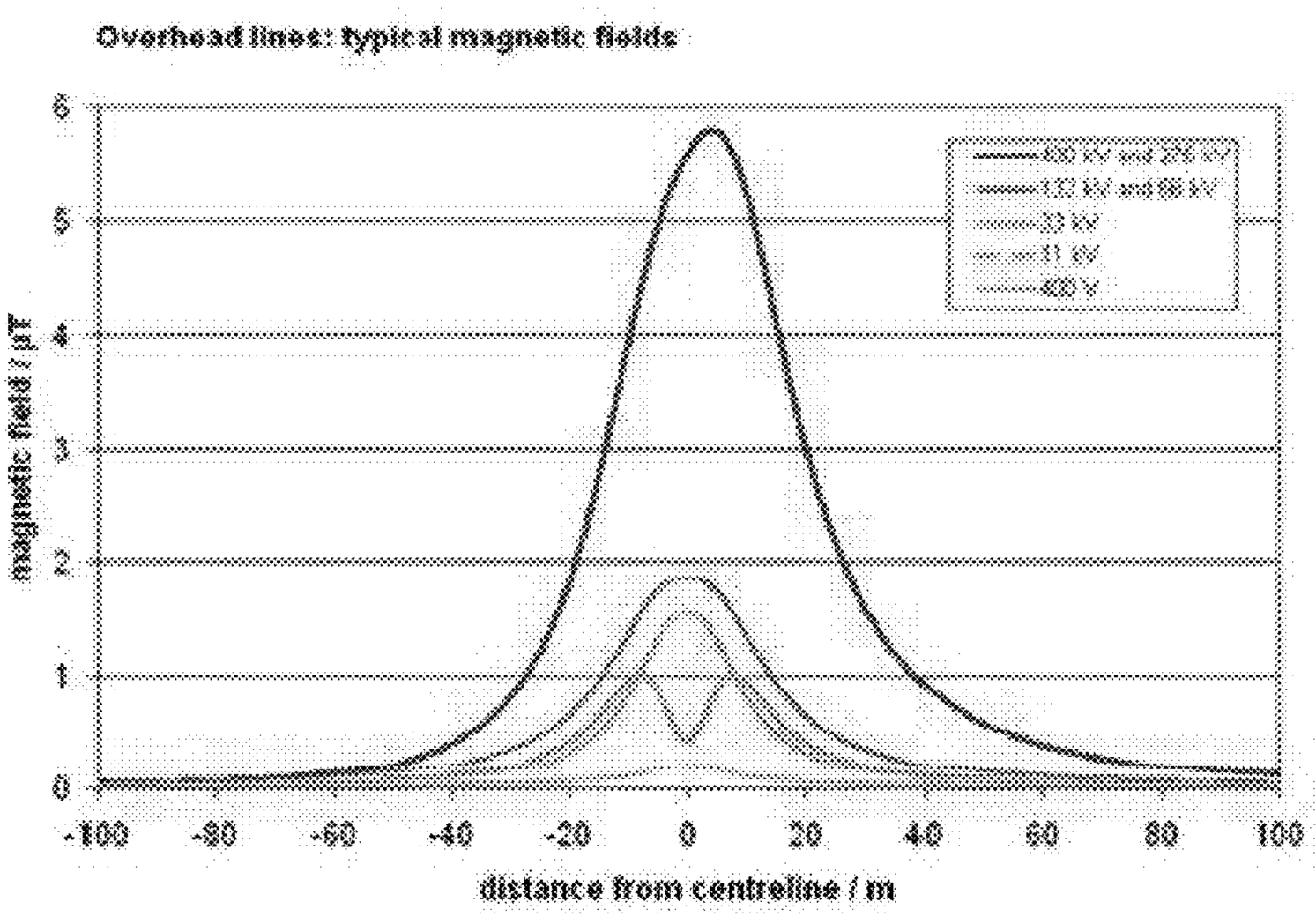

FIG. 48A

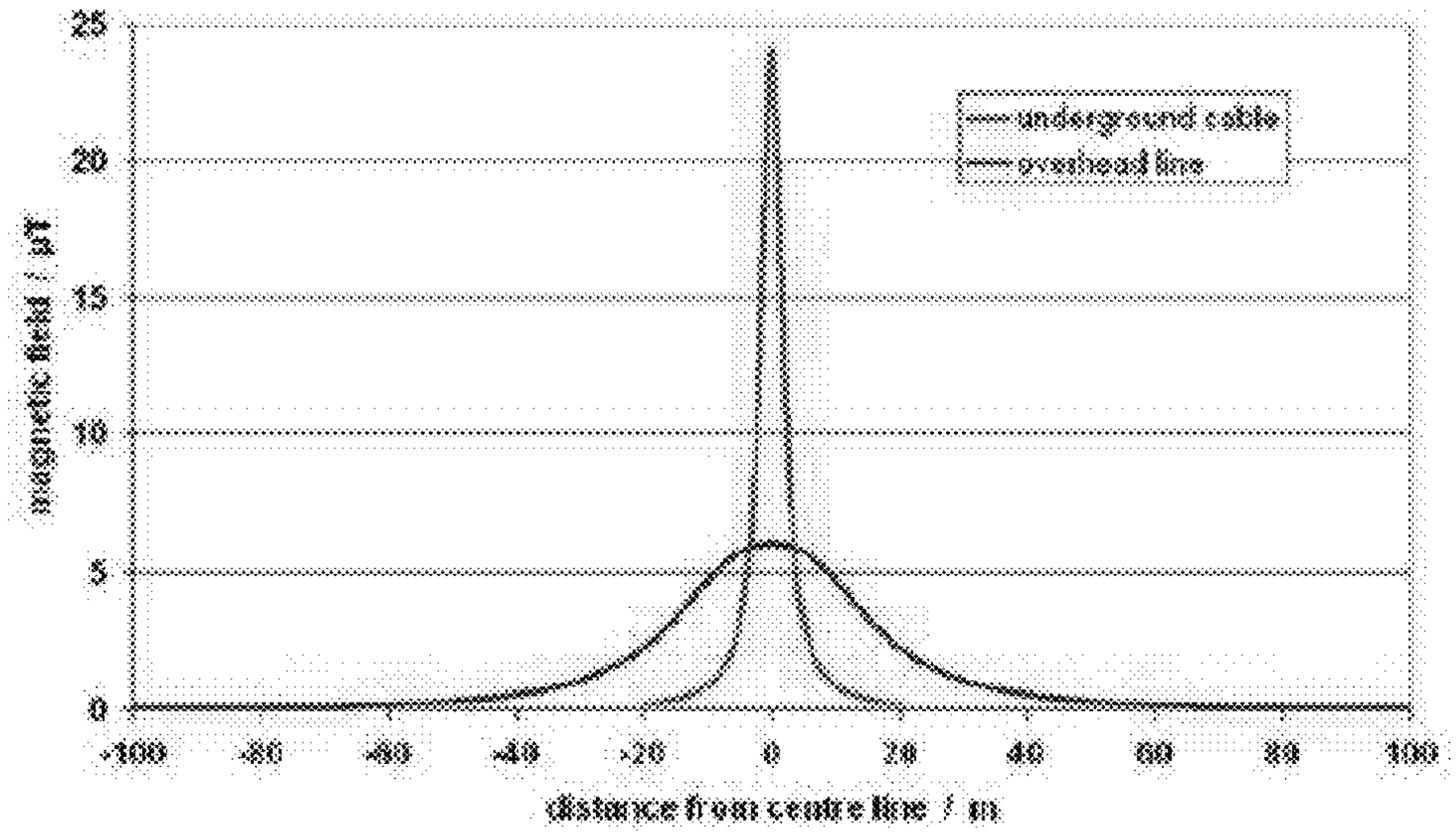

FIG. 48B

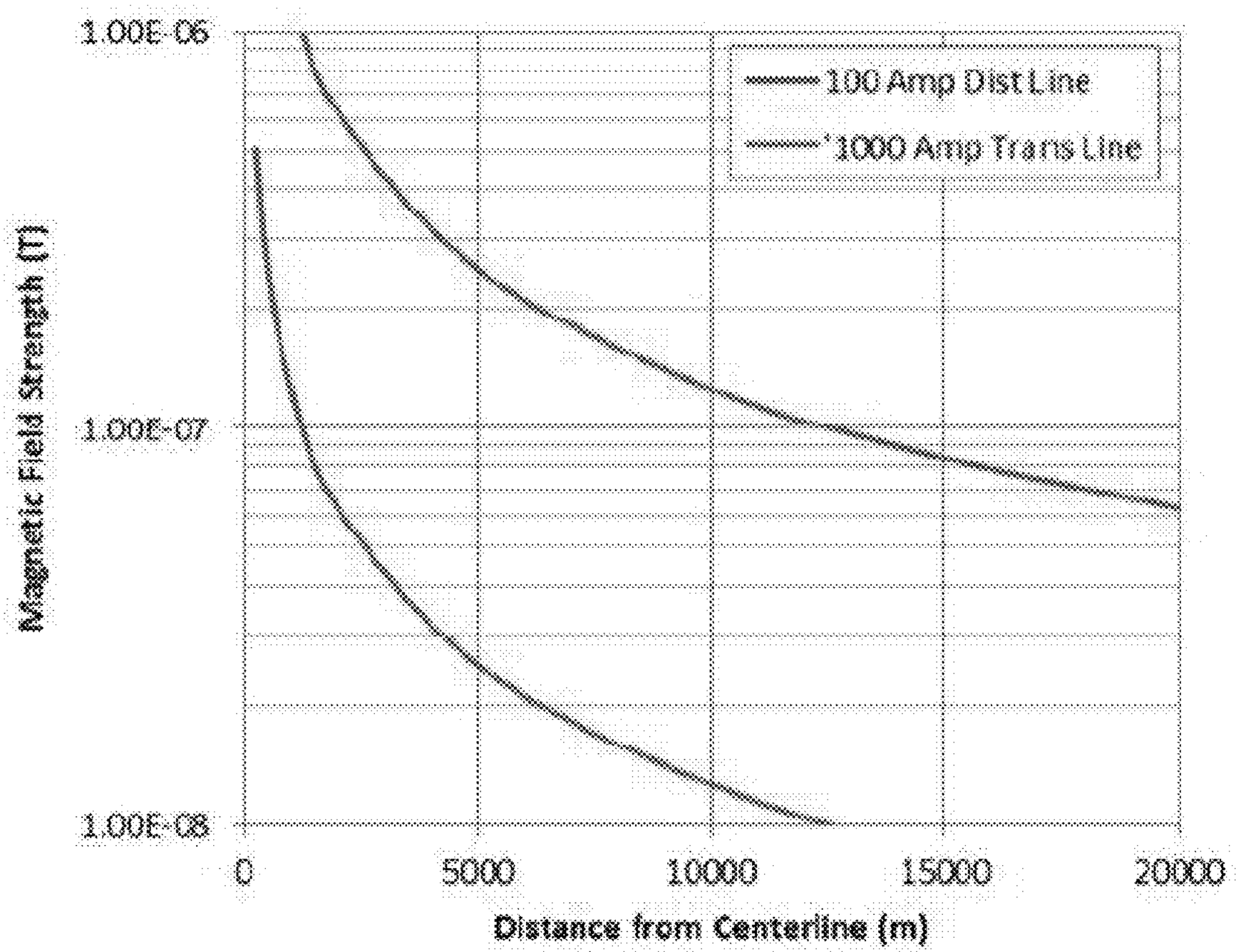
1.00E-06
1.00E-07
1.00E-08
Magnetic Field Strength (T)
0
5000
10000
15000
20000
Distance from Centerline (m)
100 Amp Dist Line
1000 Amp Trans Line

FIG. 49

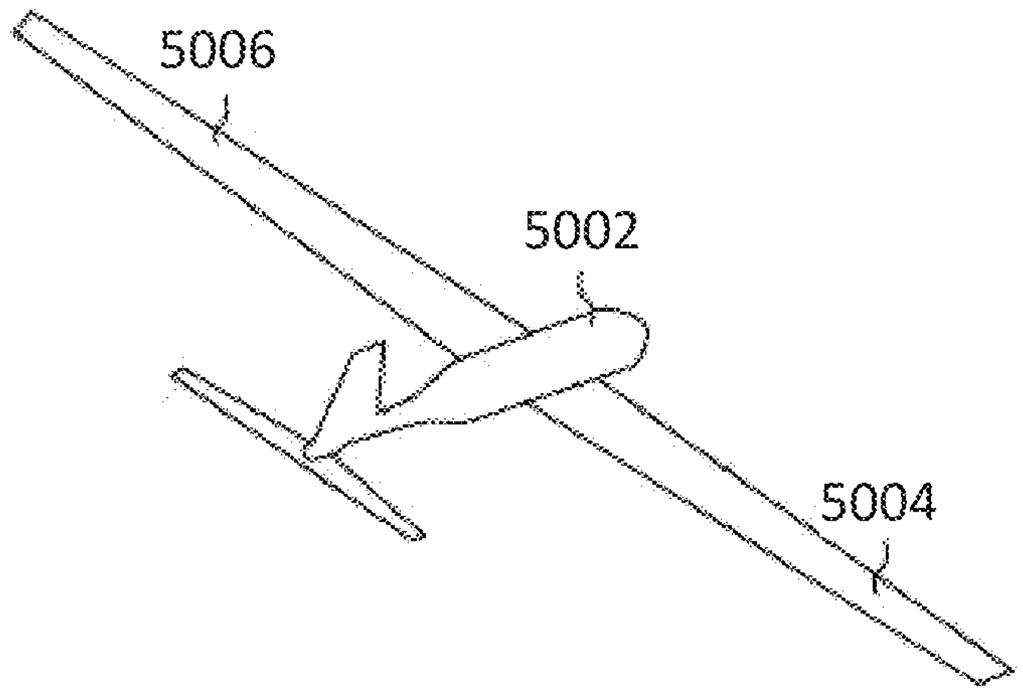
5006
5002
5004

FIG. 50

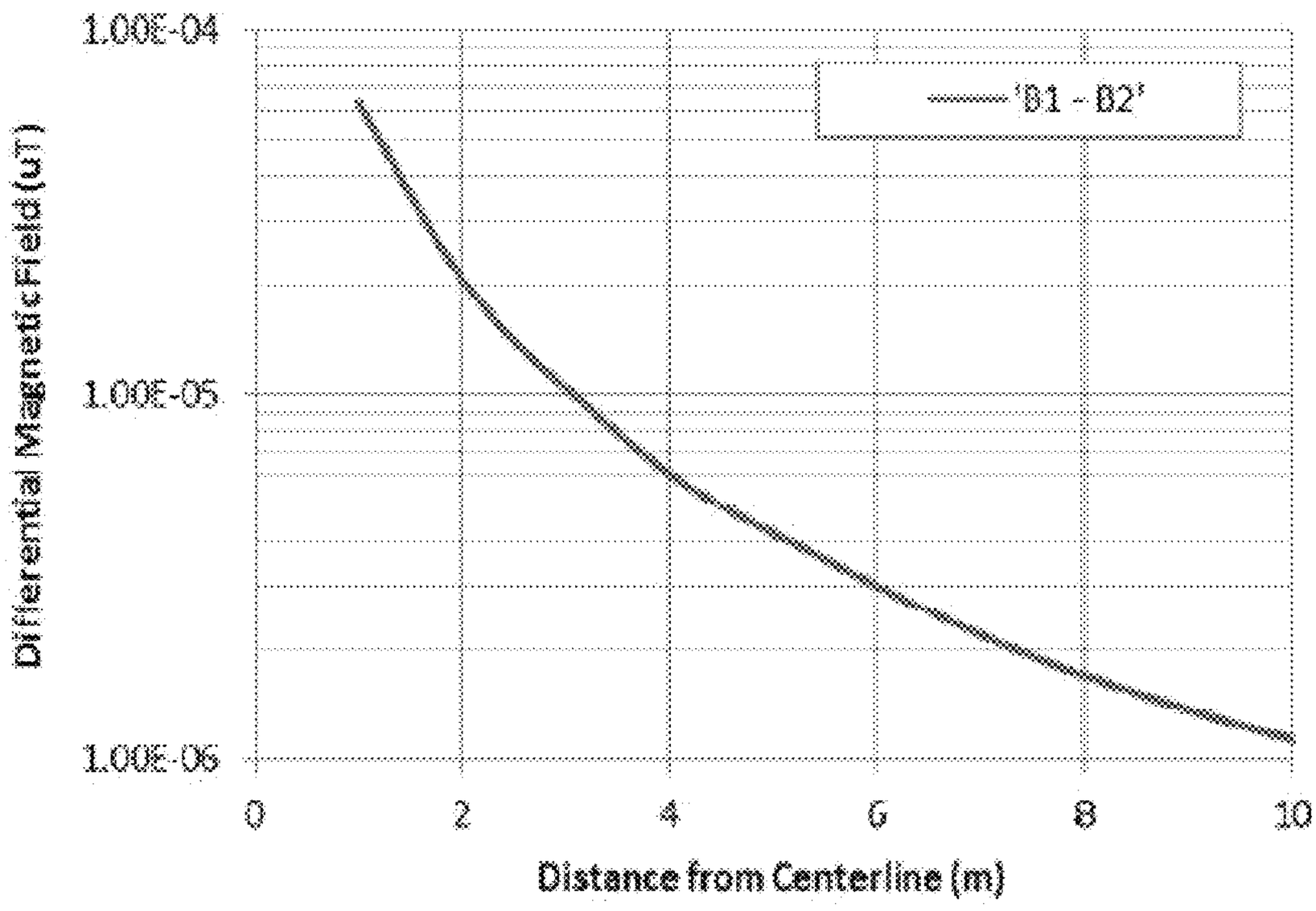
1.00E-04
1.00E-05
1.00E-06
'B1 - B2'
Differential Magnetic Field (uT)
0
2
4
6
8
10
Distance from Centerline (m)

FIG. 51

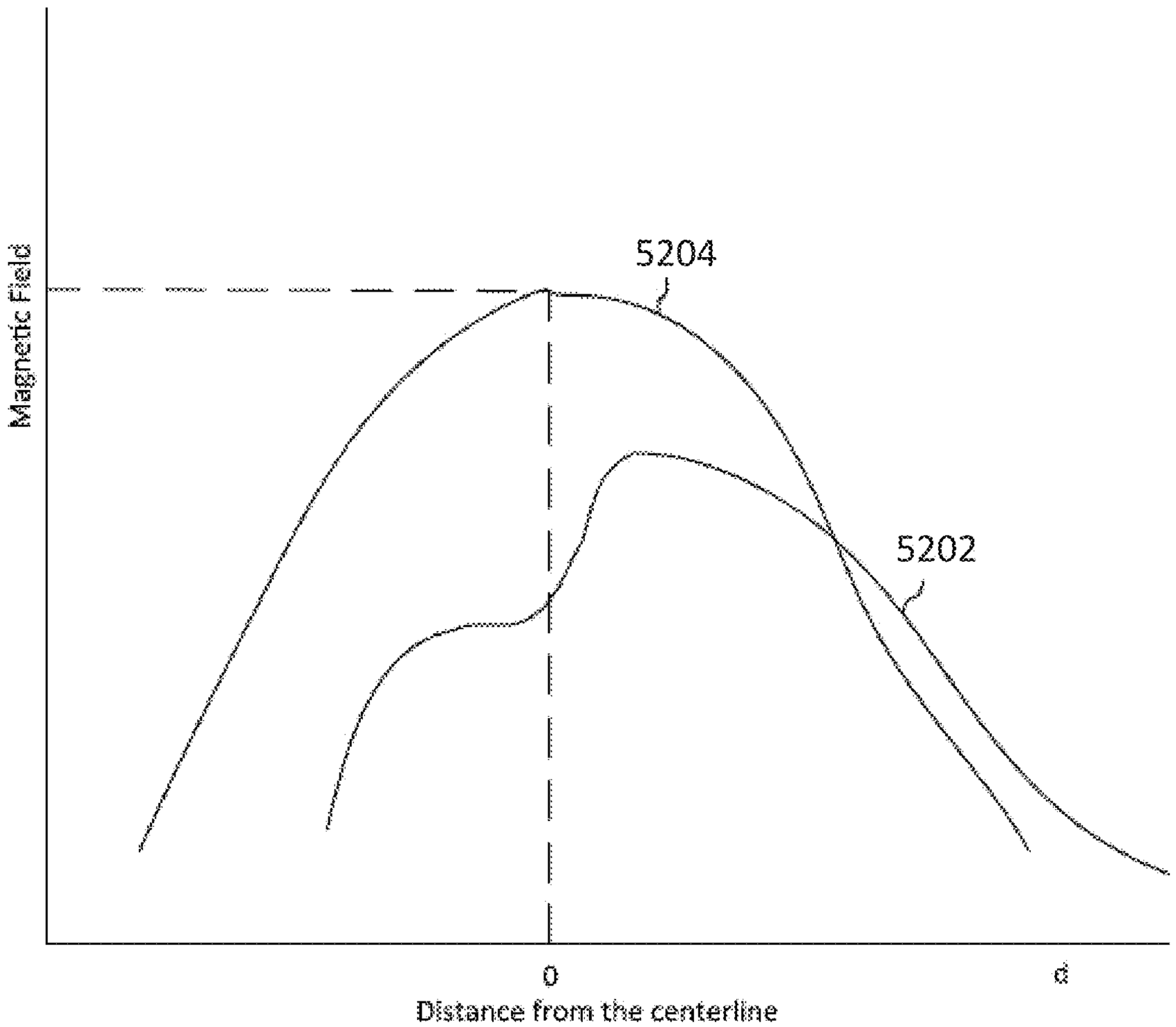

FIG. 52

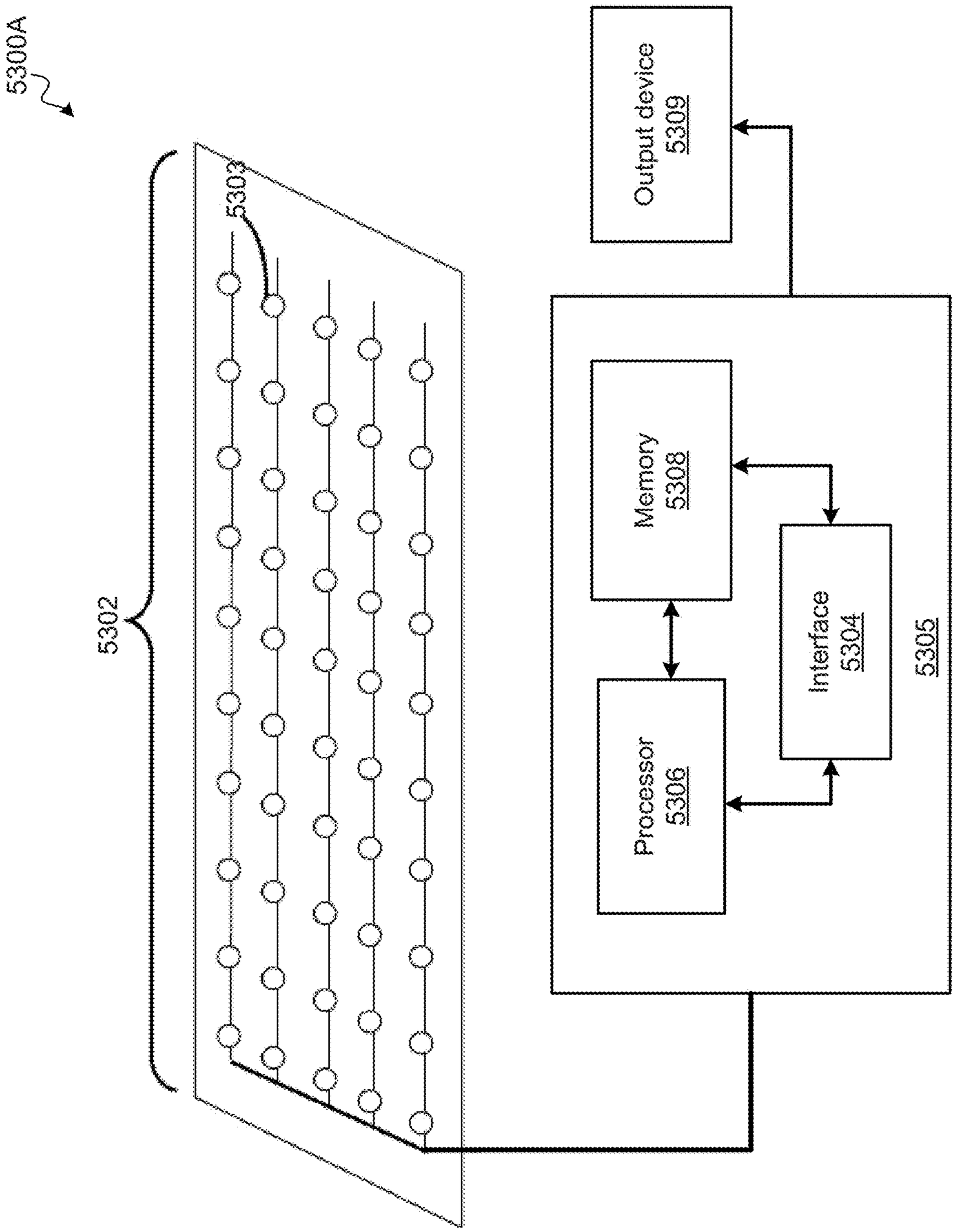
5300A
5303
5302
Output device
5309
Memory
5308
Processor
5306
Interface
5304
5305

FIG. 53A

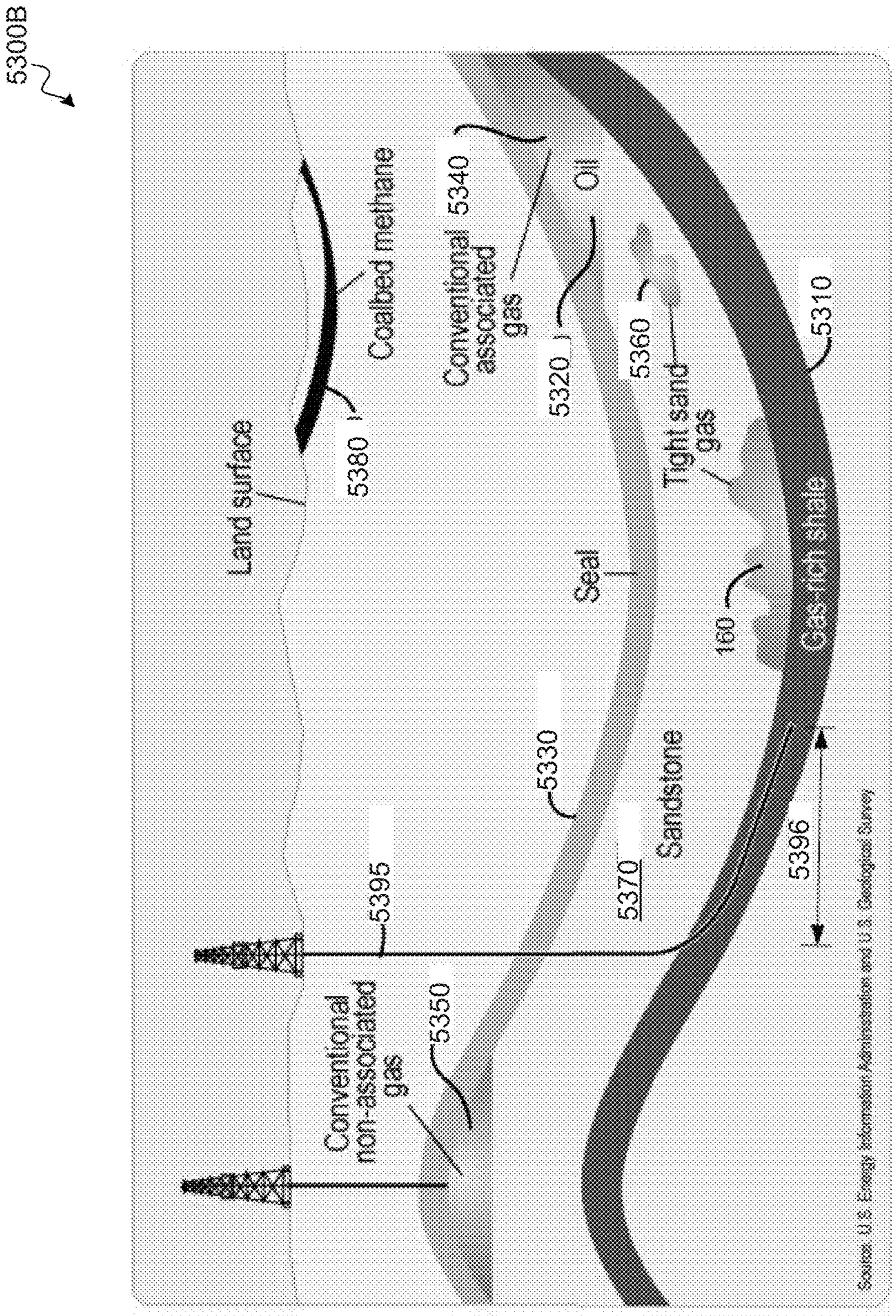
5300B
Land surface
5380
Coalbed methane
5340
Conventional associated gas
Oil
5320
5360
Tight sand gas
5310
Seal
5330
160
Carbonate
Sandstone
5370
5396
5395
Conventional non-associated gas
5350
Source: U.S. Energy Information Administration

FIG. 53B

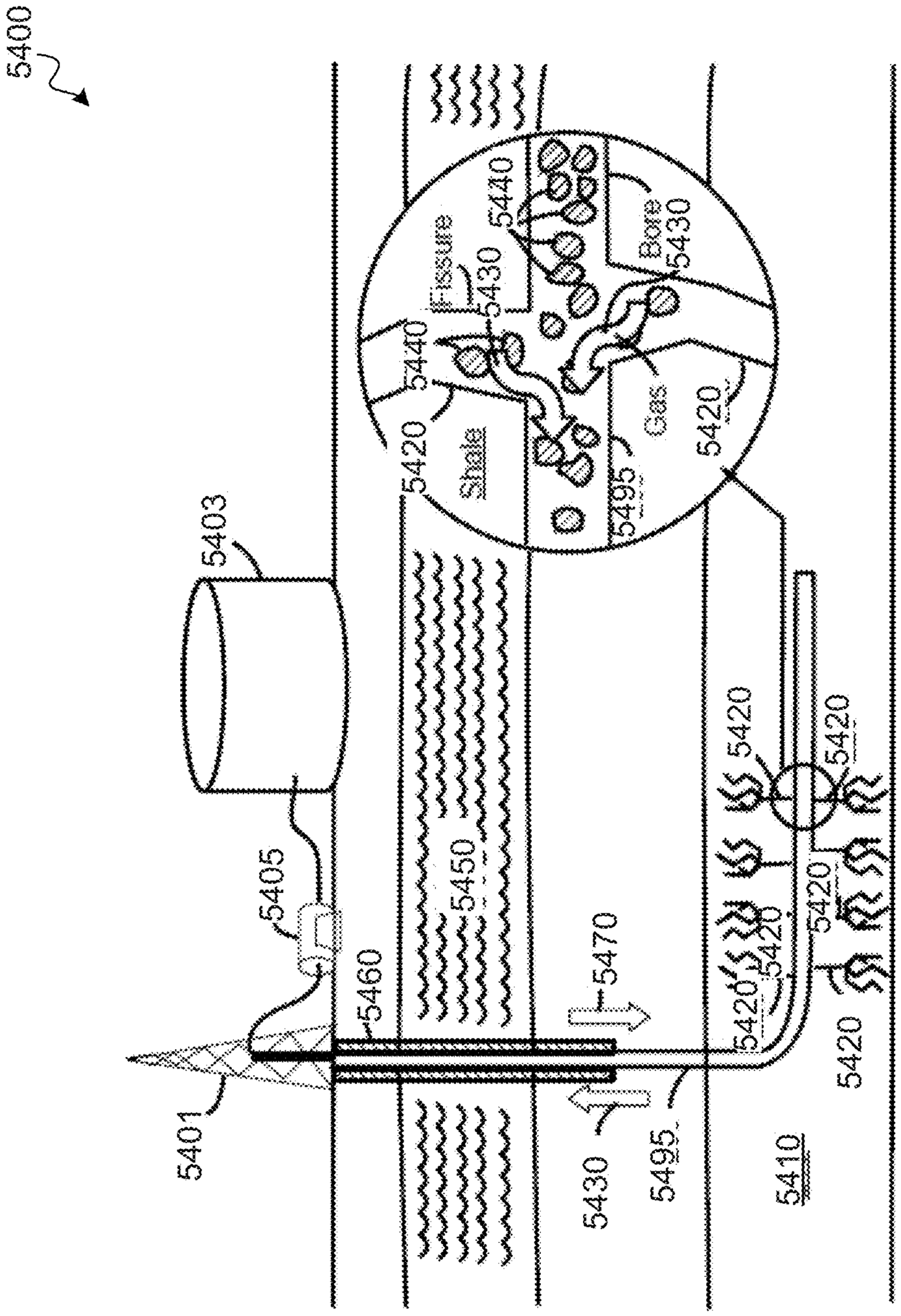
5400
5403
5405
5401
5460
5450
5470
5430
5495
5410
5420
5440
Fissure
Shale
Gas
Bore

FIG. 54

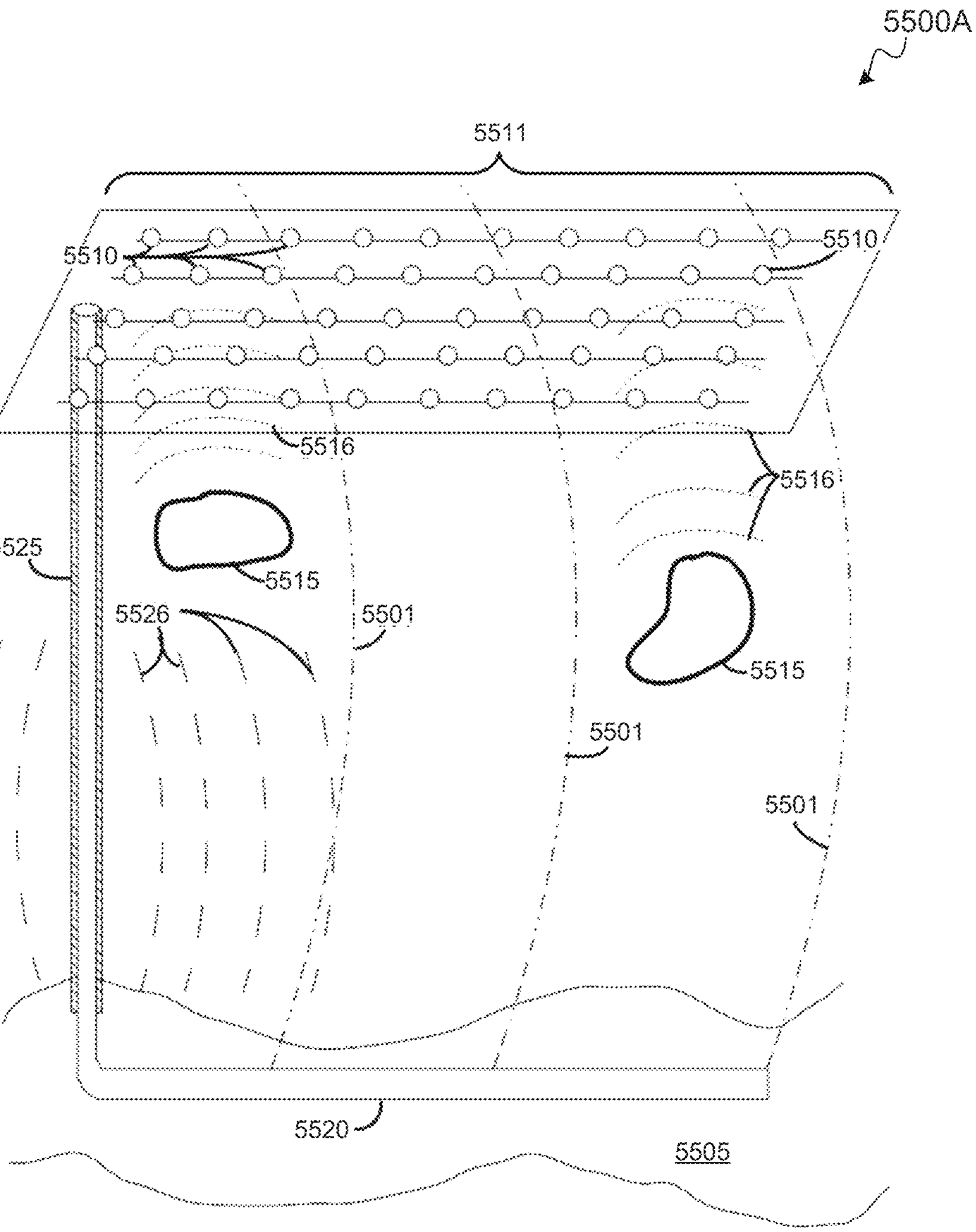
5500A
5511
5510
5510
5516
5516
5525
5515
5526
5501
5515
5501
5501
5520
5505

FIG. 55A

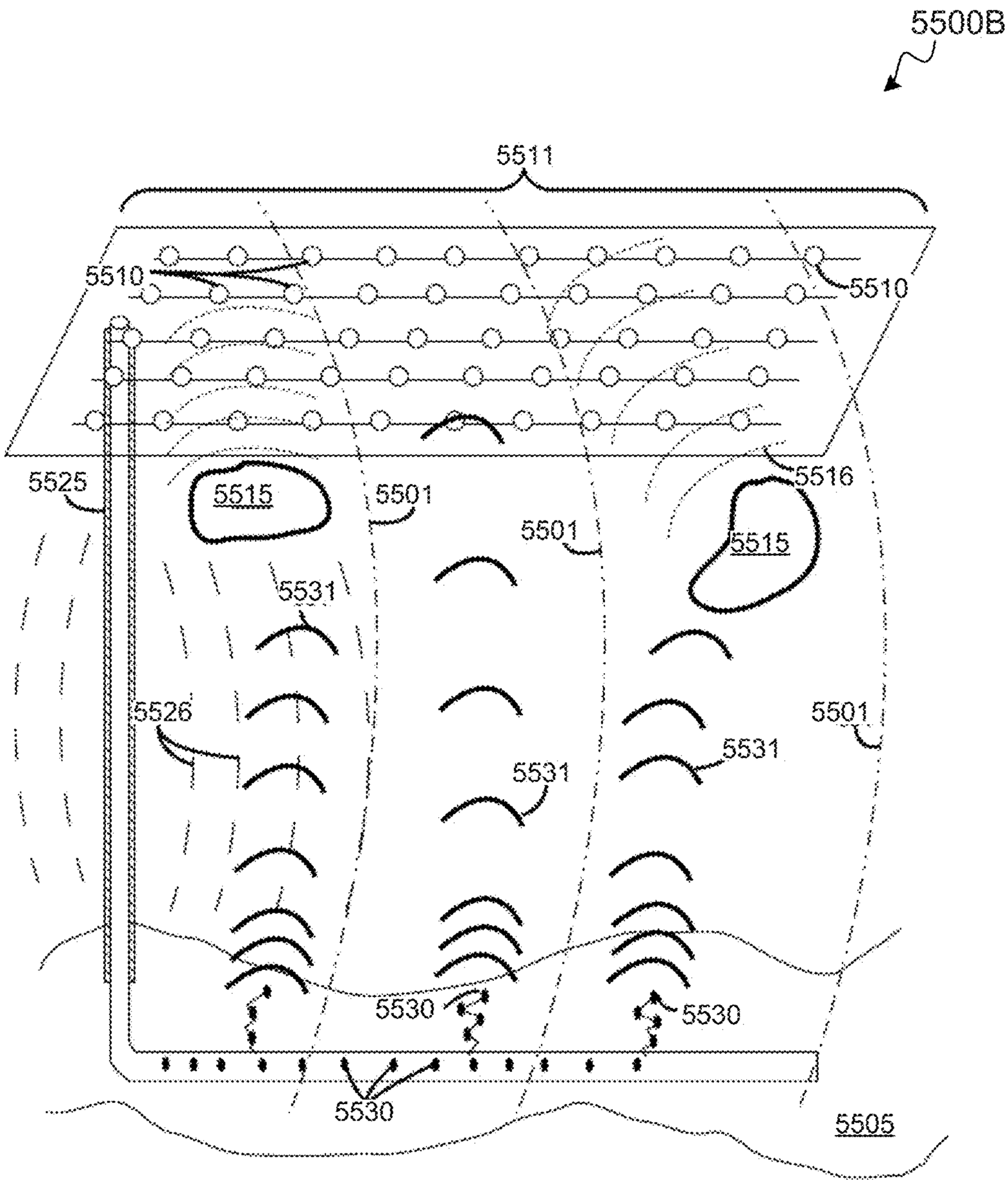
5500B
5511
5510
5510
5525
5515
5501
5501
5516
5515
5531
5526
5501
5531
5531
5530
5530
5530
5505

FIG. 55B

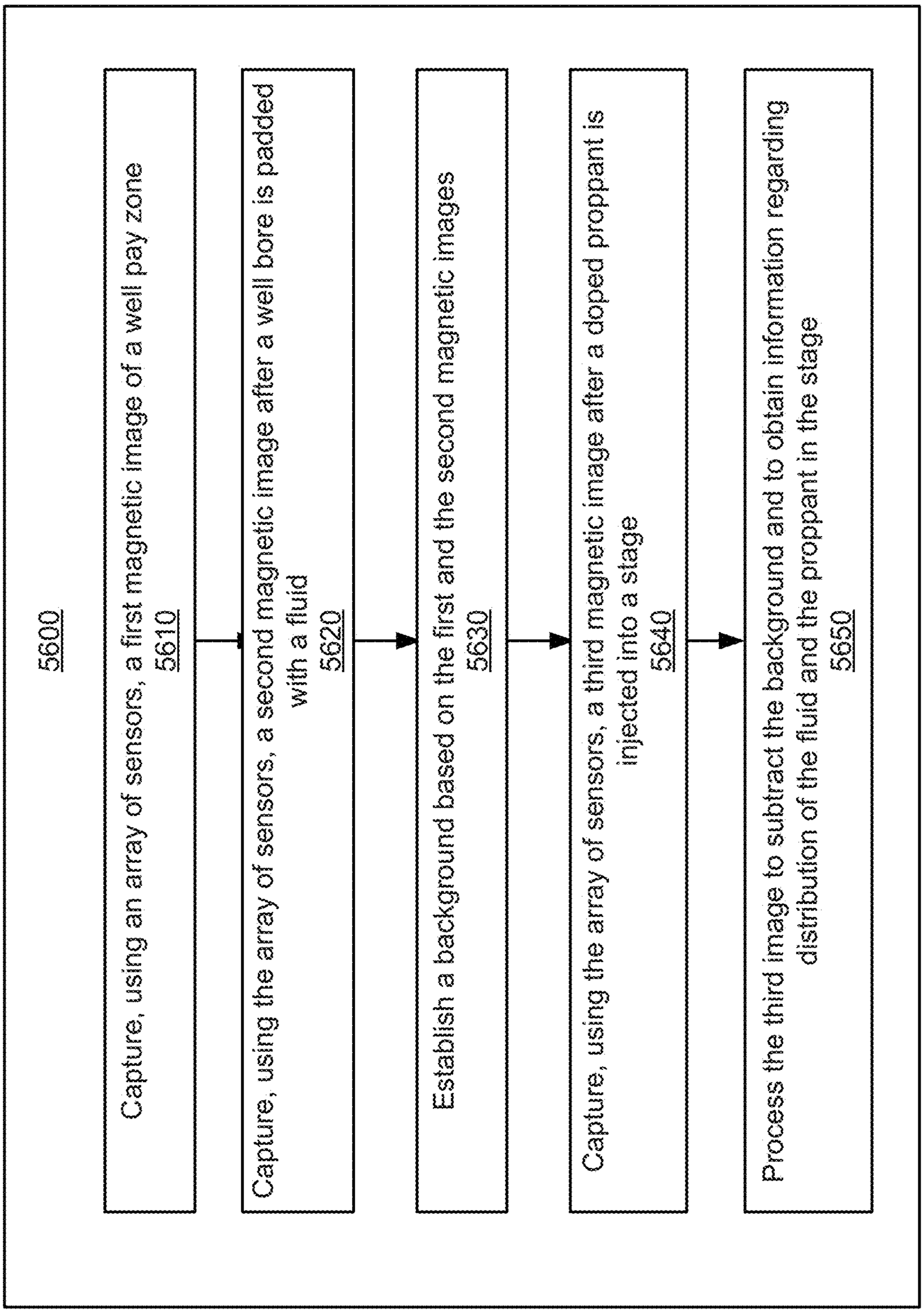
5600
Capture, using an array of sensors, a first magnetic image of a well pay zone
5610
Capture, using the array of sensors, a second magnetic image after a well bore is padded with a fluid
5620
Establish a background based on the first and the second magnetic images
5630
Capture, using the array of sensors, a third magnetic image after a doped proppant is injected into a stage
5640
Process the third image to subtract the background and to obtain information regarding distribution of the fluid and the proppant in the stage
5650

FIG. 56

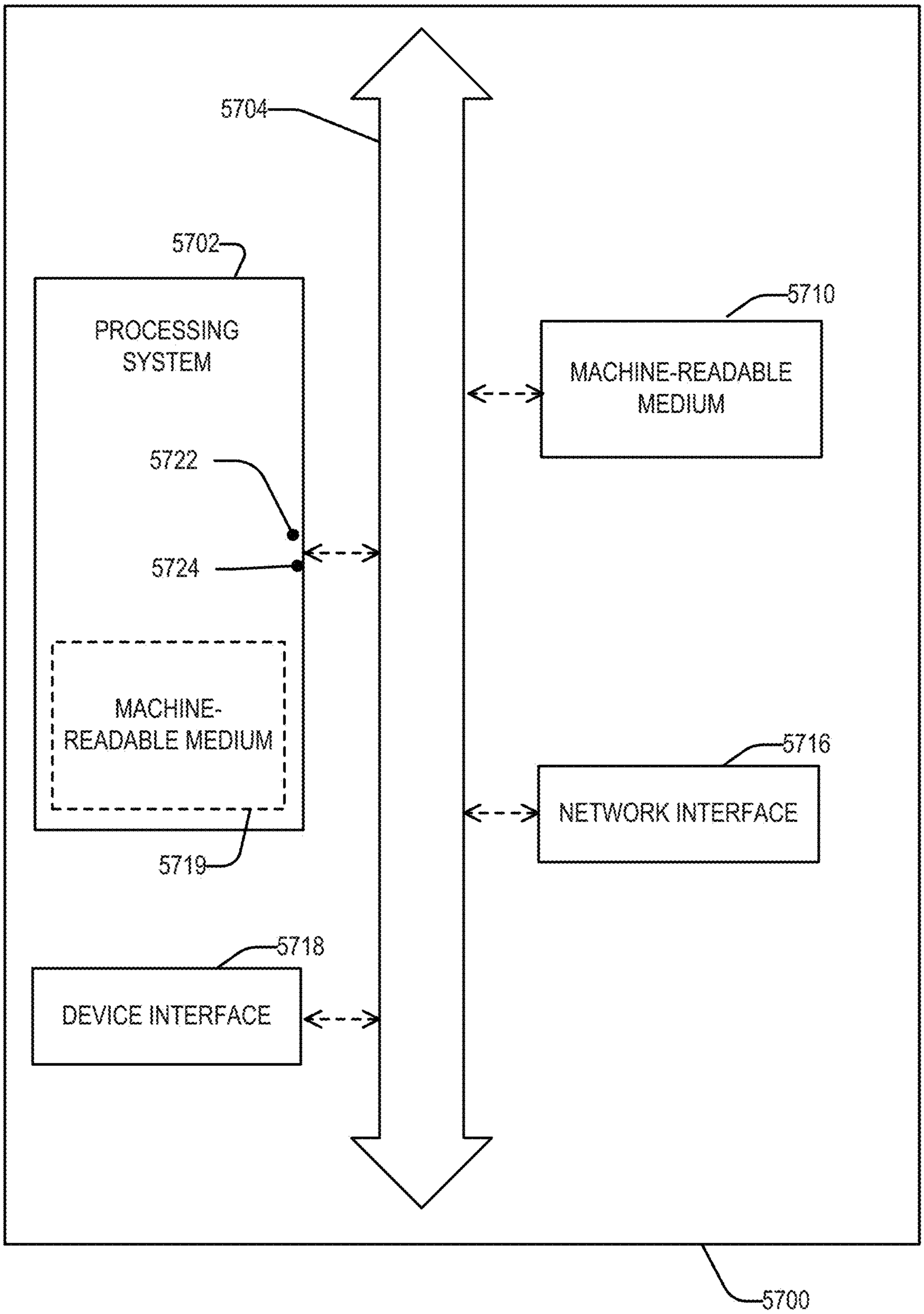
5704
5702
PROCESSING SYSTEM
5722
5724
MACHINE-READABLE MEDIUM
5719
5718
DEVICE INTERFACE
5710
MACHINE-READABLE MEDIUM
5716
NETWORK INTERFACE
5700

FIG. 57

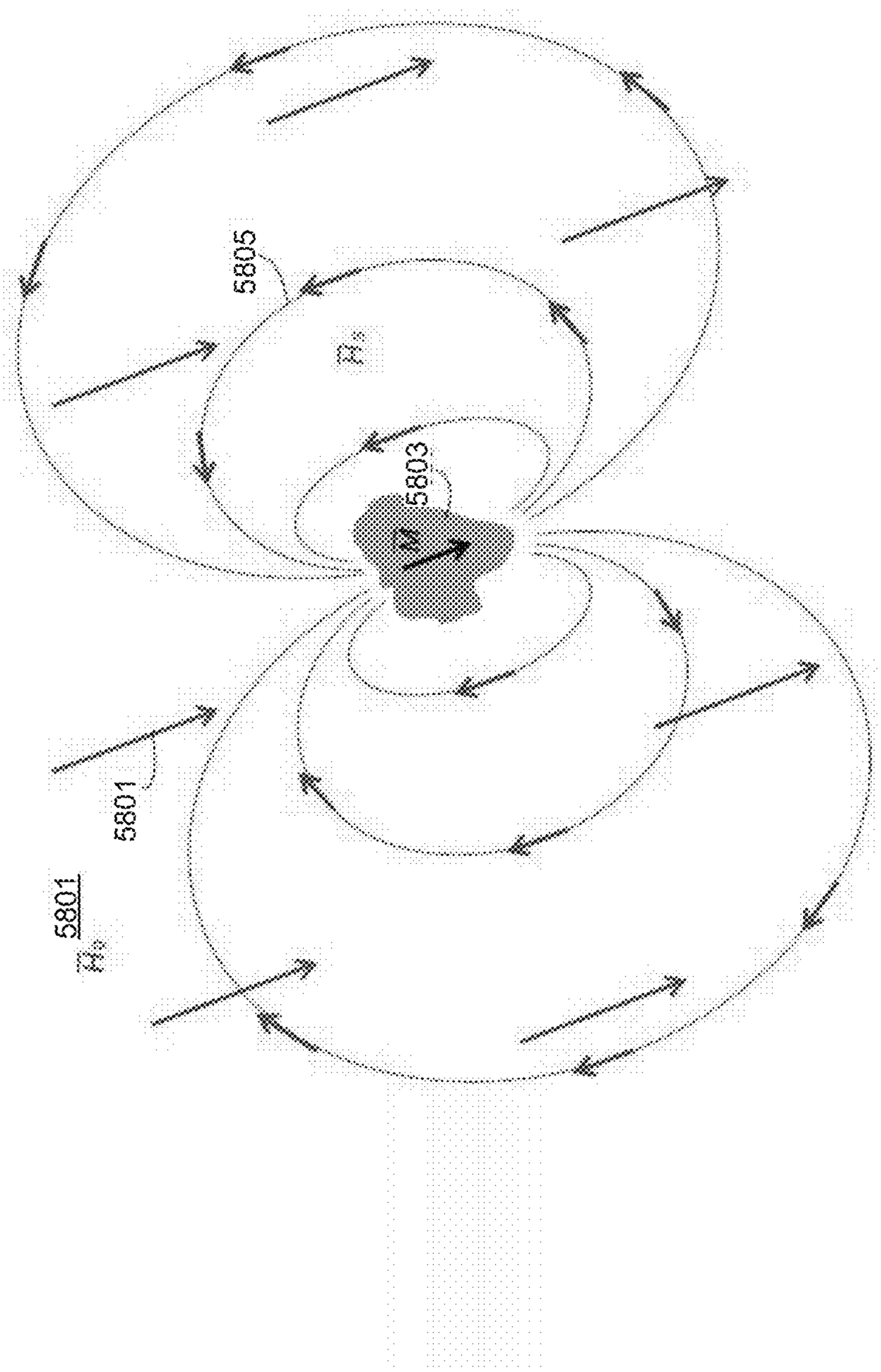

FIG. 58

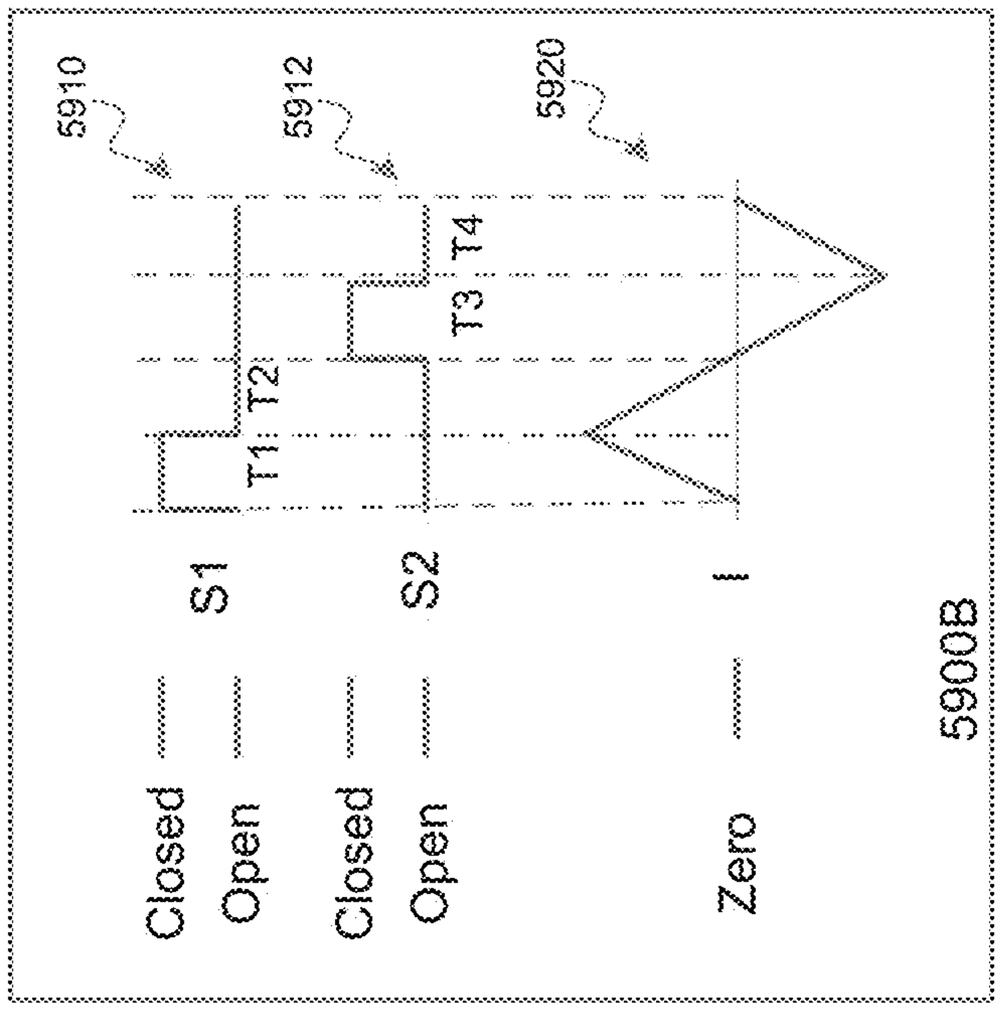

FIG. 59B

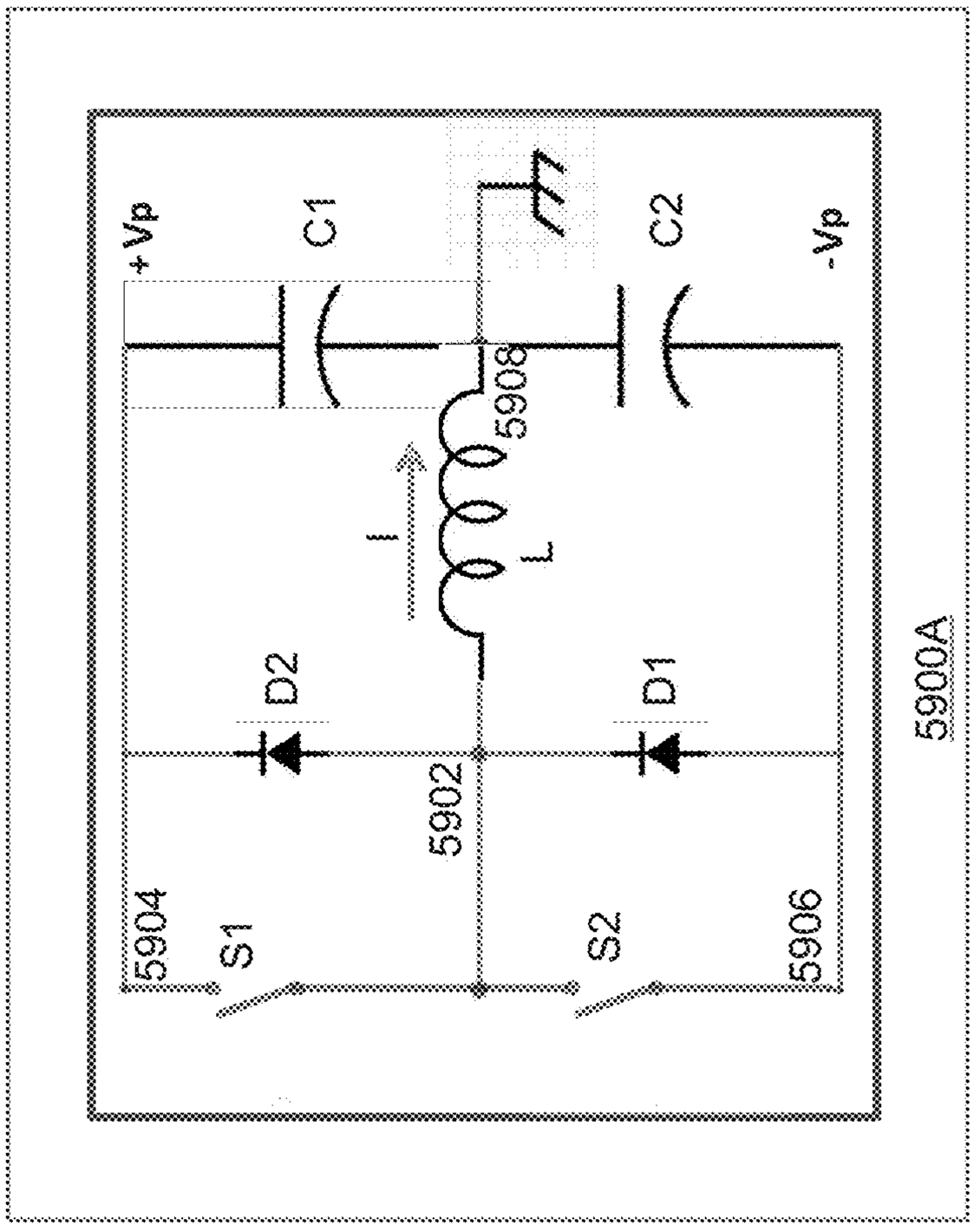

FIG. 59A

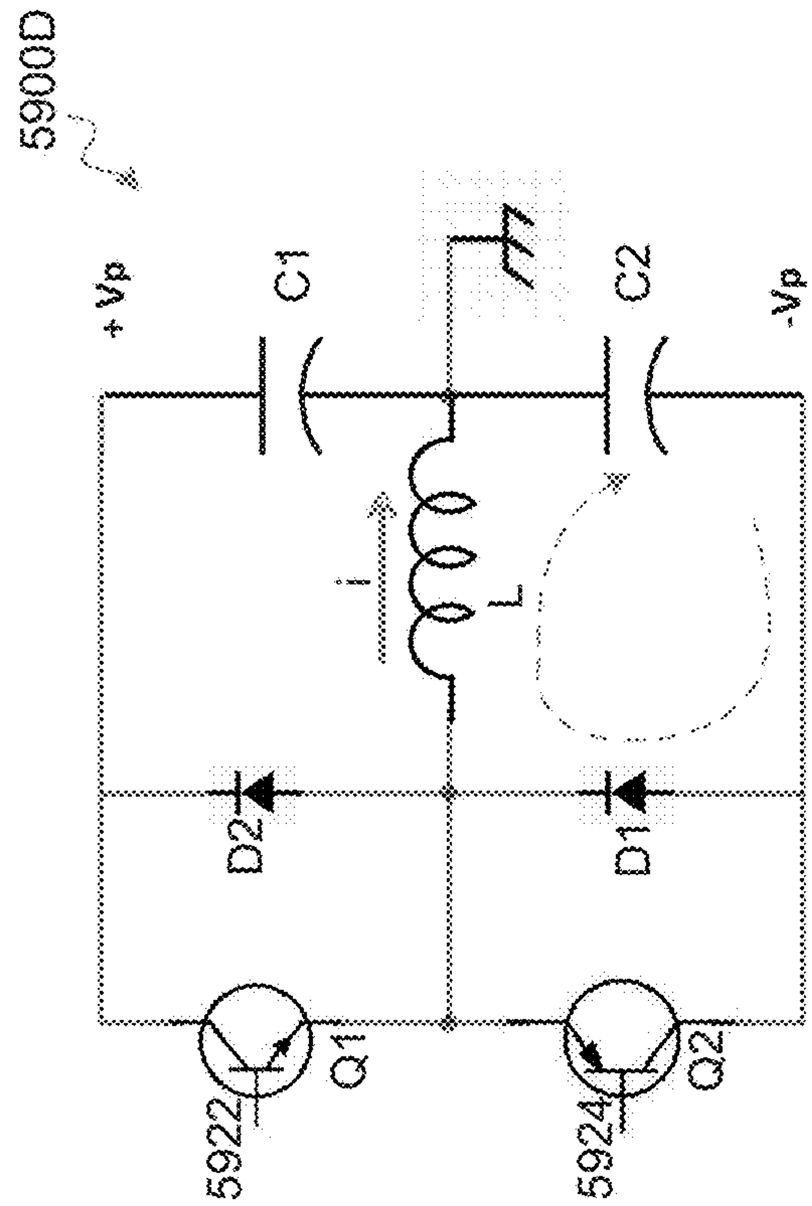

FIG. 59D

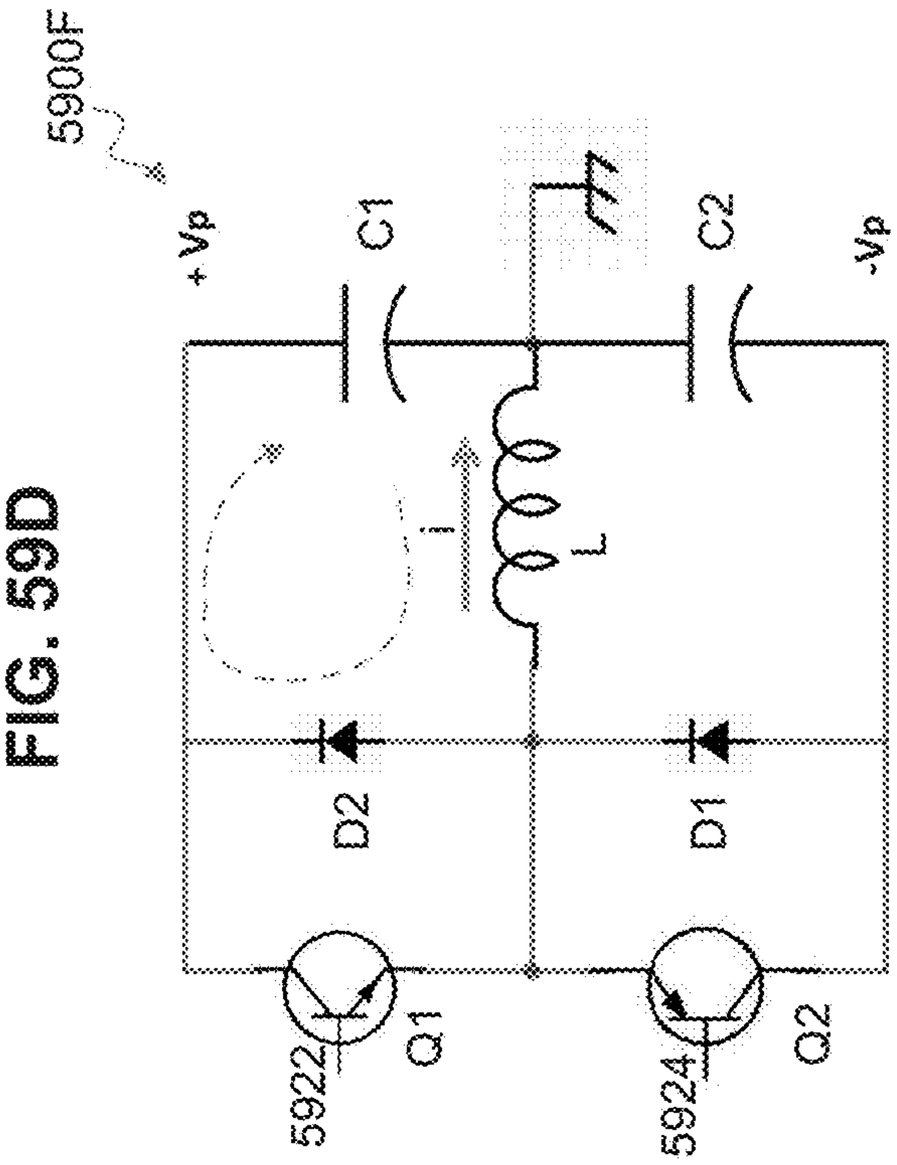

FIG. 59F

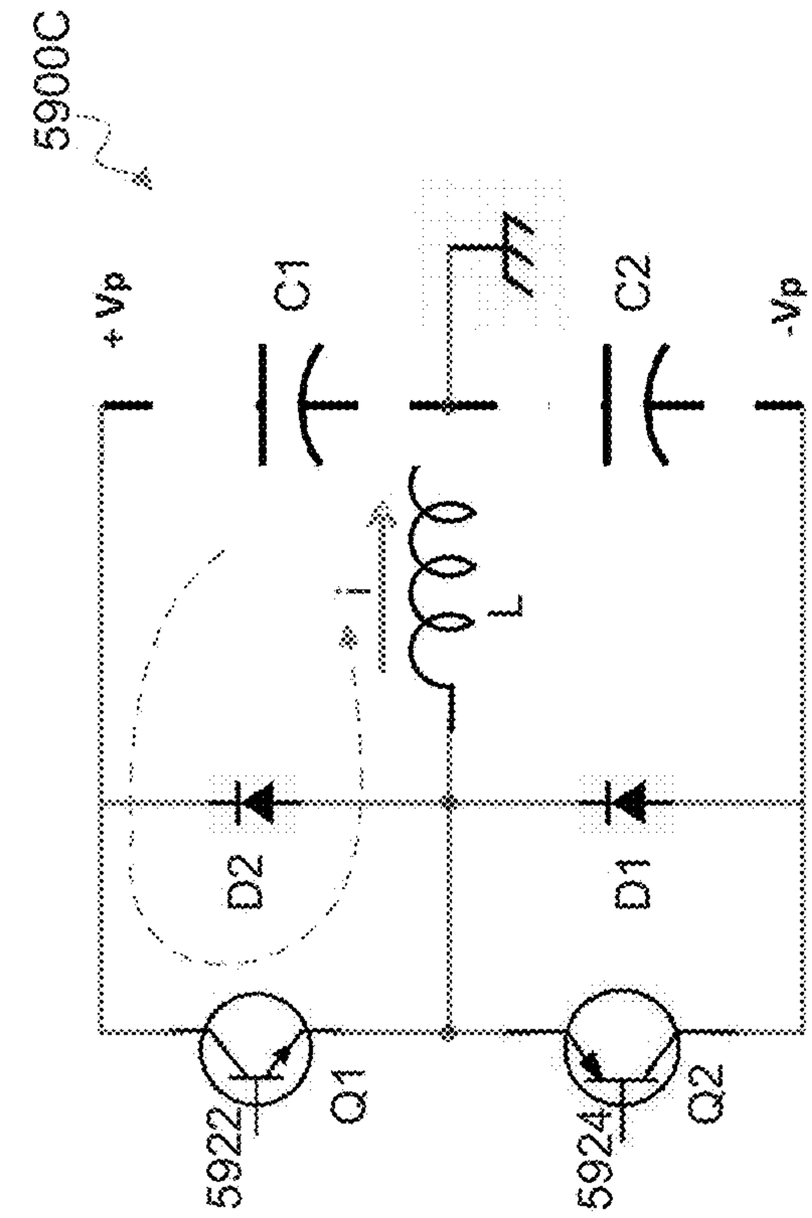

FIG. 59C

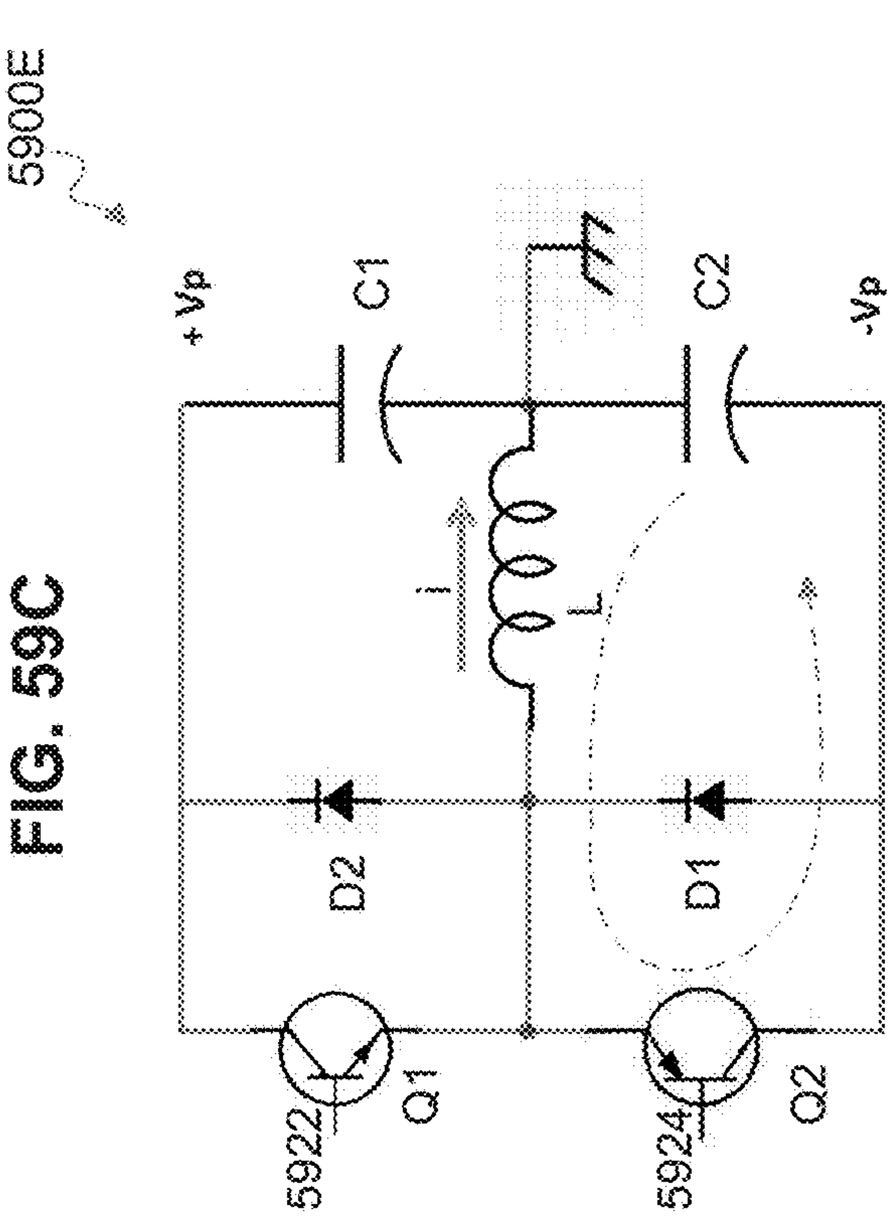

FIG. 59E

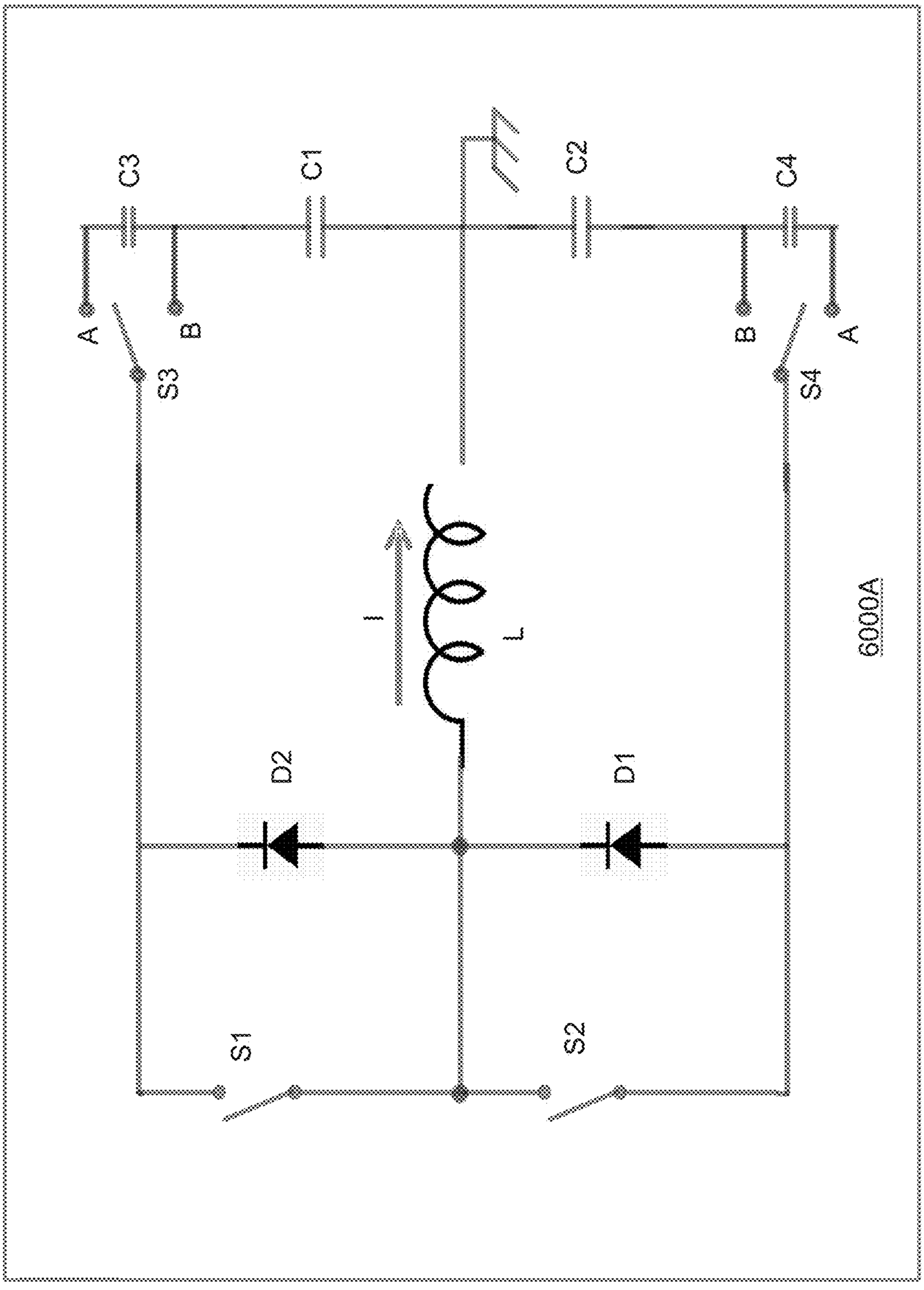

FIG. 60A

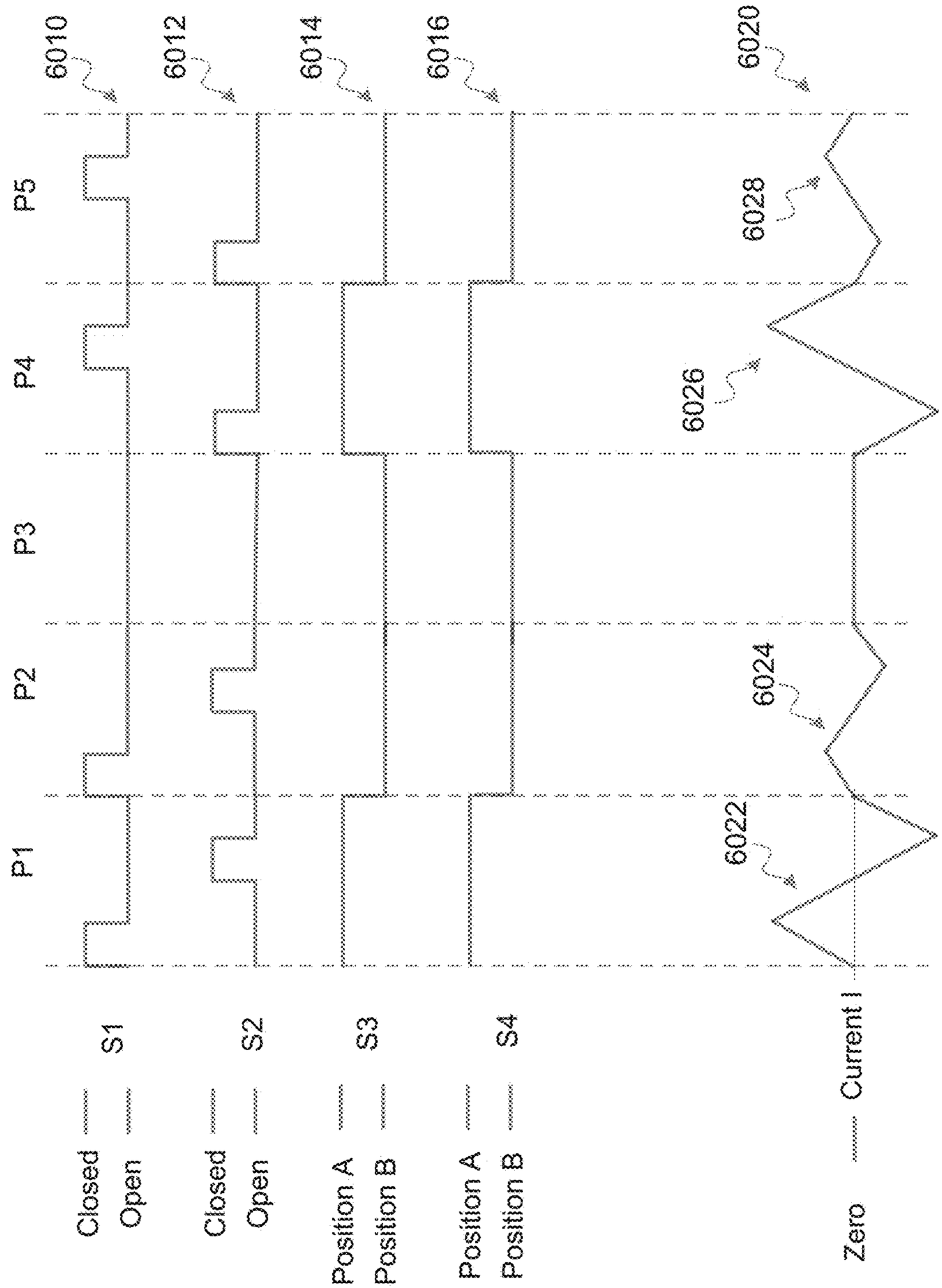
6010
6012
6014
6016
6020
6028
6026
6024
6022
P5
P4
P3
P2
P1
Closed
Open
S1
Closed
Open
S2
Position A
Position B
S3
Position A
Position B
S4
Zero
Current I

FIG. 60B

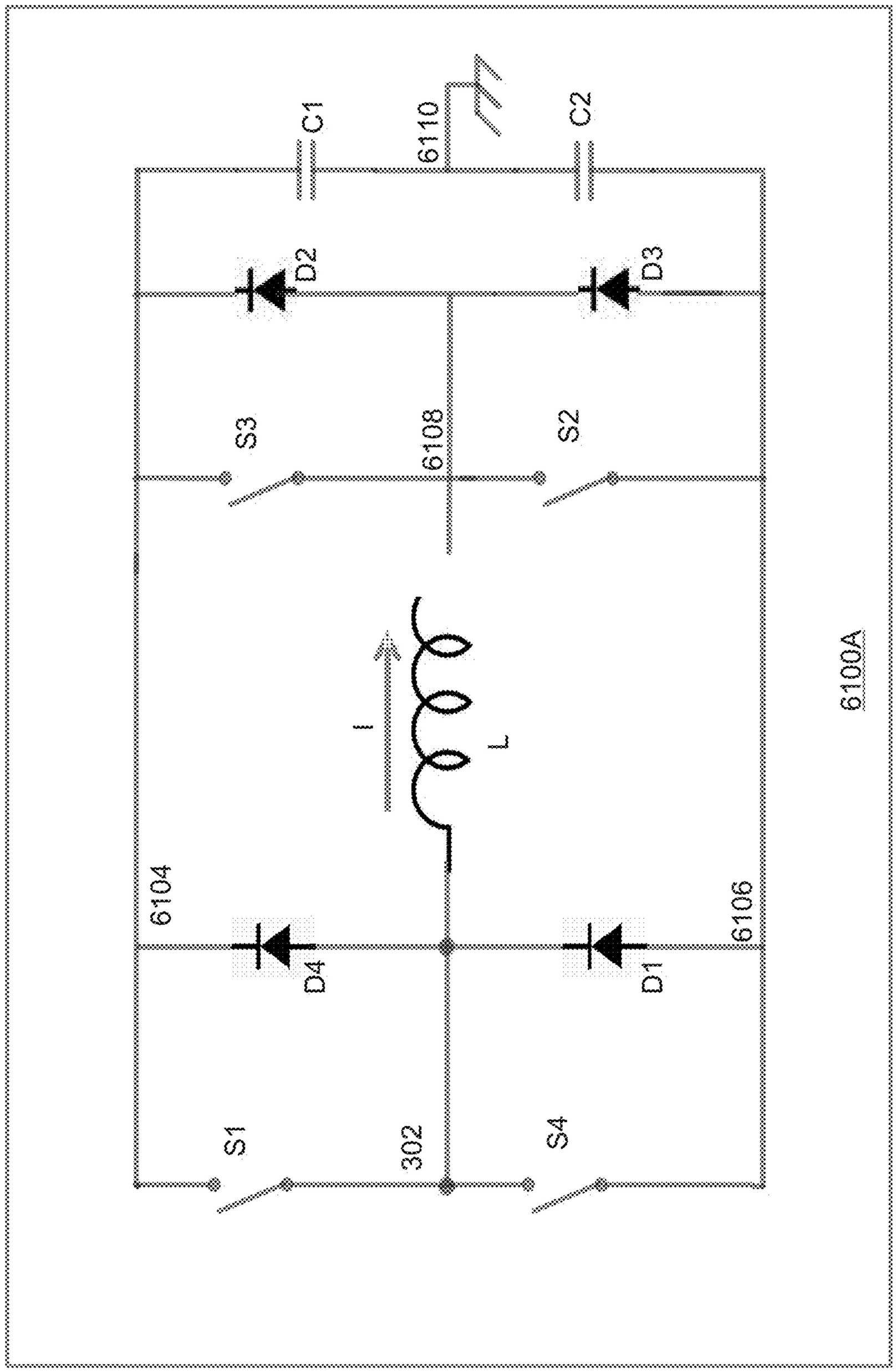

FIG. 61A

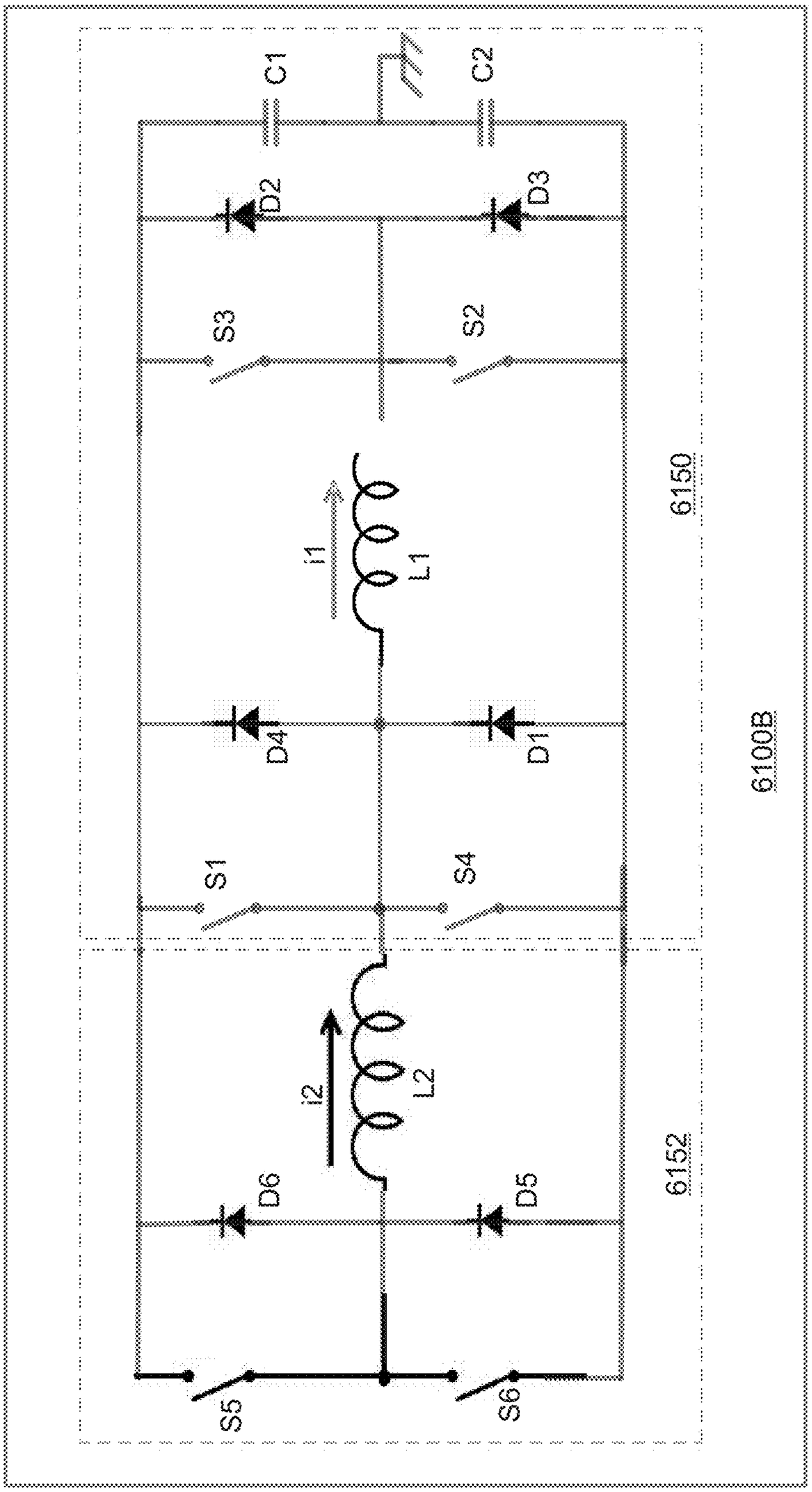

FIG. 61B

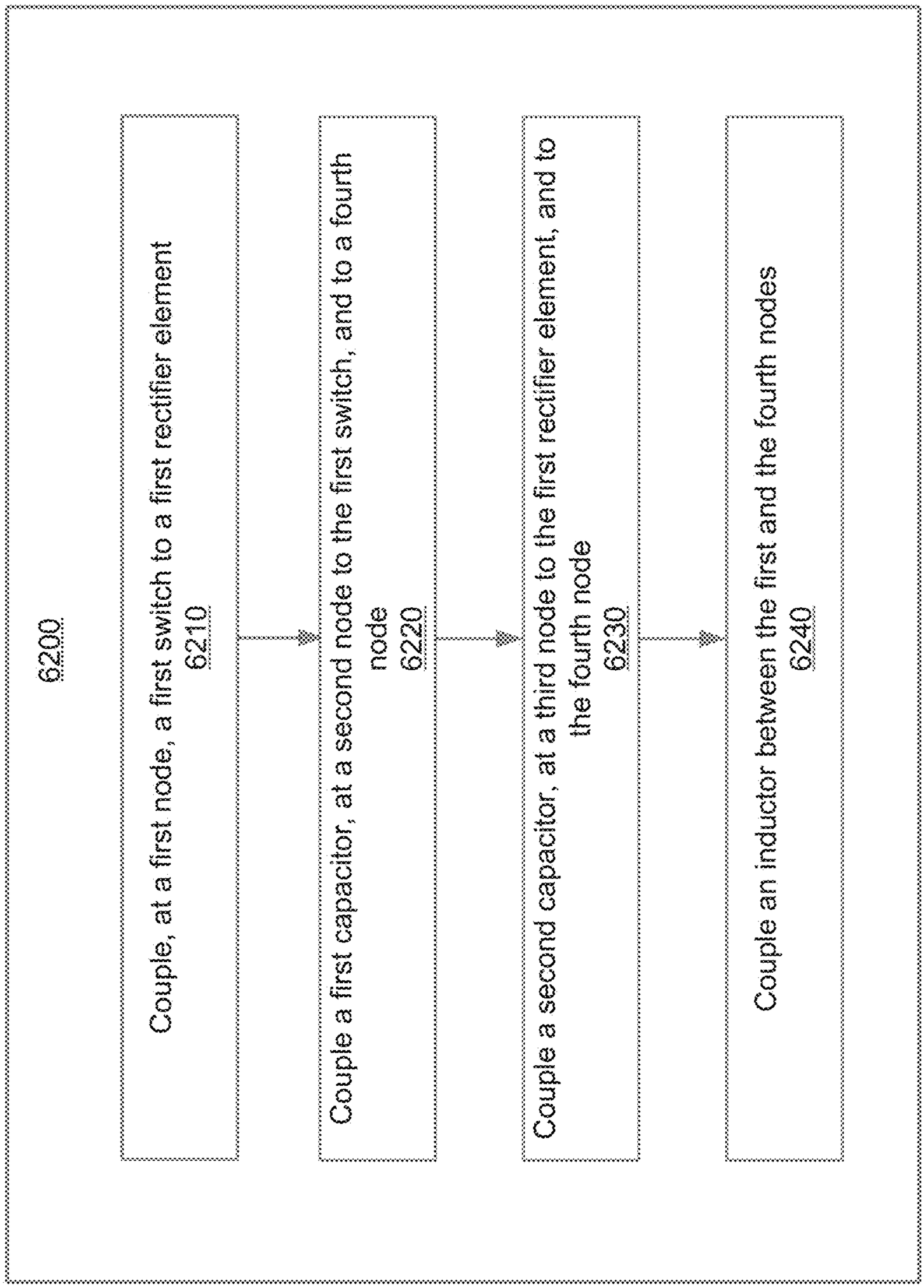
6200
Couple, at a first node, a first switch to a first rectifier element
6210
Couple a first capacitor, at a second node to the first switch, and to a fourth node
6220
Couple a second capacitor, at a third node to the first rectifier element, and to the fourth node
6230
Couple an inductor between the first and the fourth nodes
6240

FIG. 62

DNV MAGNETIC FIELD DETECTOR

CROSS-REFERENCE TO RELATED PATENT APPLICATIONS

This application is a continuation of co-pending U.S. patent application Ser. No. 15/179,957, filed Jun. 10, 2016, which is a continuation-in-part and claims the benefit of priority to co-pending U.S. patent application Ser. No. 15/003,797, filed Jan. 21, 2016, which made the following claims of the benefit of priority to and incorporation by reference in entirety:

"This application claims the benefit of priority from U.S. Provisional Patent Application No. 62/257,988, filed Nov. 20, 2015, which is incorporated herein by reference in its entirety. This application claims priority to U.S. Provisional Application No. 62/190,209, filed on Jul. 8, 2015, the entirety of which is incorporated herein by reference. The present application claims priority to U.S. Application No. 62/261,643, filed Dec. 1, 2015, which is incorporated by reference herein in its entirety. The present application claims the benefit of U.S. Provisional Application Nos. 62/109,006, filed Jan. 28, 2015, and 62/109,551, filed Jan. 29, 2015, each of which is incorporated by reference herein in its entirety. The present application claims the benefit of U.S. Provisional Application No. 62/214,792, filed Sep. 4, 2015, which is incorporated by reference herein in its entirety. This application claims the benefit of priority from U.S. Provisional Patent Application No. 62/258,003, filed Nov. 20, 2015, which is incorporated herein by reference in its entirety. This application claims the benefit of priority from U.S. Provisional Patent Application No. 62/190,218, filed Jul. 8, 2015, which is incorporated herein by reference in its entirety. This application claims the benefit of priority to U.S. Provisional Patent Application No. 62/107,289, filed Jan. 23, 2015, the entire contents of which are incorporated by reference herein in its entirety."

The present application is related to co-pending U.S. application Ser. No. 15/003,558, filed Jan. 21, 2016, titled "APPARATUS AND METHOD FOR HYPERSENSITIVITY DETECTION OF MAGNETIC FIELD," which is incorporated by reference herein in its entirety. The present application is related to co-pending U.S. application Ser. No. 15/003,062, filed Jan. 21, 2016, titled "IMPROVED LIGHT COLLECTION FROM DNV SENSORS," which is incorporated by reference herein in its entirety. The present application is related to co-pending U.S. application Ser. No. 15/003,652, filed Jan. 21, 2016, titled "PRECISION POSITION ENCODER/SENSOR USING NITROGEN VACANCY DIAMOND," which is incorporated by reference herein in its entirety. The present application is related to co-pending U.S. application Ser. No. 15/003,677, filed Jan. 21, 2016, titled "COMMUNICATION VIA A MAGNIO," which is incorporated by reference herein in its entirety. The present application is related to co-pending U.S. application Ser. No. 15/003,678, filed Jan. 21, 2016, titled "METHOD FOR RESOLVING NATURAL SENSOR AMBIGUITY FOR DNV DIRECTION FINDING APPLICATIONS," which is incorporated by reference herein in its entirety. The present application is related to co-pending U.S. application Ser. No. 15/003,177, filed Jan. 21, 2016, titled "HYDROPHONE," which is incorporated by reference herein in its entirety. The present application is related to co-pending U.S. application Ser. No. 15/003,206, filed Jan. 21, 2016, titled "MAGNETIC NAVIGATION METHODS AND SYSTEMS UTILIZING POWER GRID AND COMMUNICATION NETWORK," which is incorporated by reference herein in its entirety. The present application is related to co-pending U.S. application Ser. No. 15/003,193, filed Jan. 21, 2016, titled "RAPID HIGH-RESOLUTION MAGNETIC FIELD MEASUREMENTS FOR POWER LINE INSPECTION," which is incorporated by reference herein in its entirety. The present application is related to co-pending U.S. application Ser. No. 15/003,088, filed Jan. 21, 2016, titled "IN-SITU POWER CHARGING," which is incorporated by reference herein in its entirety. The present application is related to co-pending U.S. patent application Ser. No. 15/003,519, filed Jan. 21, 2016, titled "APPARATUS AND METHOD FOR CLOSED LOOP PROCESSING FOR A MAGNETIC DETECTION SYSTEM," which is incorporated by reference herein in its entirety. The present application is related to co-pending U.S. application Ser. No. 15/003,718, filed Jan. 21, 2016, titled "APPARATUS AND METHOD FOR RECOVERY OF THREE DIMENSIONAL MAGNETIC FIELD FROM A MAGNETIC DETECTION SYSTEM," which is incorporated by reference herein in its entirety. The present application is related to co-pending U.S. application Ser. No. 15/003,209, filed Jan. 21, 2016, titled "DIAMOND NITROGEN VACANCY SENSED FERRO-FLUID HYDROPHONE," which is incorporated by reference herein in its entirety. The present application is related to co-pending U.S. application Ser. No. 15/003,670, filed Jan. 21, 2016, titled "AC VECTOR MAGNETIC ANOMALY DETECTION WITH DIAMOND NITROGEN VACANCIES," which is incorporated by reference herein in its entirety. The present application is related to co-pending U.S. application Ser. No. 15/003,704, filed Jan. 21, 2016, titled "APPARATUS AND METHOD FOR ESTIMATING ABSOLUTE AXES' ORIENTATIONS FOR A MAGNETIC DETECTION SYSTEM," which is incorporated by reference herein in its entirety. The present application is related to co-pending U.S. application Ser. No. 15/003,590, filed Jan. 21, 2016, titled "APPARATUS AND METHOD FOR HIGH SENSITIVITY MAGNETOMETRY MEASUREMENT AND SIGNAL PROCESSING IN A MAGNETIC DETECTION SYSTEM," which is incorporated by reference herein in its entirety. The present application is related to co-pending U.S. application Ser. No. 15/003,176, filed Jan. 21, 2016, titled "MAGNETIC BAND-PASS FILTER," which is incorporated by reference herein in its entirety. The present application is related to co-pending U.S. application Ser. No. 15/003,145, filed Jan. 21, 2016, titled "DEFECT DETECTOR FOR CONDUCTIVE MATERIALS," which is incorporated by reference herein in its entirety. The present application is related to co-pending U.S. application Ser. No. 15/003,309, filed Jan. 21, 2016, titled "DIAMOND NITROGEN VACANCY SENSOR WITH DUAL RF SOURCES," which is incorporated by reference herein in its entirety. The present application is related to co-pending U.S. application Ser. No. 15/003,298, filed Jan. 21, 2016, titled "DIAMOND NITROGEN VACANCY SENSOR WITH COMMON RF AND MAGNETIC FIELDS GENERATOR," which is incorporated by reference herein in its entirety. The present application is related to co-pending U.S. application Ser. No. 15/003,292, filed Jan. 21, 2016, titled "MAGNETOMETER WITH A LIGHT EMITTING DIODE," which is incorporated by reference herein in its entirety. The present application is related to co-pending U.S. application Ser. No. 15/003,281, filed Jan. 21, 2016, titled "MAGNETOMETER WITH LIGHT PIPE," which is incorporated by reference herein in its entirety. The present application is related to co-pending

U.S. application Ser. No. 15/003,634, filed Jan. 21, 2016, titled "DIAMOND NITROGEN VACANCY SENSOR WITH CIRCUITRY ON DIAMOND," which is incorporated by reference herein in its entirety. The present application is related to co-pending U.S. application Ser. No. 15/003,577, filed Jan. 21, 2016, titled "MEASUREMENT PARAMETERS FOR QC METROLOGY OF SYNTHETICALLY GENERATED DIAMOND WITH NV CENTERS," which is incorporated by reference herein in its entirety. The present application is related to co-pending U.S. application Ser. No. 15/003,256, filed Jan. 21, 2016, titled "HIGHER MAGNETIC SENSITIVITY THROUGH FLUORESCENCE MANIPULATION BY PHONON SPECTRUM CONTROL," which is incorporated by reference herein in its entirety. The present application is related to co-pending U.S. application Ser. No. 15/003,396, filed Jan. 21, 2016, titled "MAGNETIC WAKE DETECTOR," which is incorporated by reference herein in its entirety. The present application is related to co-pending U.S. application Ser. No. 15/003,617, filed Jan. 21, 2016, titled "GENERAL PURPOSE REMOVAL OF GEOMAGNETIC NOISE," which is incorporated by reference herein in its entirety. The present application is related to co-pending U.S. application Ser. No. 15/003,336, filed Jan. 21, 2016, titled "REDUCED INSTRUCTION SET CONTROLLER FOR DIAMOND NITROGEN VACENCY SENSOR," which is incorporated by reference herein in its entirety. The present application is related to co-pending U.S. application Ser. No. 14/676,740, filed Apr. 1, 2015, titled "HIGH BIT-RATE MAGNETIC COMMUNICATION," which is incorporated by reference herein in its entirety."

This application additionally claims the benefit of priority to co-pending U.S. application Ser. No. 14/866,730, filed Sep. 25, 2015, which claims the benefit of priority to and incorporates by reference U.S. Provisional Patent Application No. 62/055,607, filed Sep. 25, 2014, both of which are incorporated by reference herein in their entirety. This application claims the benefit of priority to co-pending U.S. patent application Ser. No. 14/680,877, filed Apr. 7, 2015, which claims the benefit of priority to and incorporates by reference U.S. Provisional Patent Application No. 61/975,997, filed Apr. 7, 2014, both of which are incorporated by reference herein in their entirety. This application claims the benefit of priority to co-pending U.S. application Ser. No. 14/659,498, filed Mar. 16, 2015, which claims the benefit of priority to and incorporates by reference U.S. Provisional Patent Application No. 61/955,918, filed Mar. 20, 2014, both of which are incorporated by reference herein in their entirety. This application claims the benefit of priority to co-pending U.S. application Ser. No. 14/676,740, filed Apr. 1, 2015, which claims the benefit of priority to and incorporates by reference U.S. Provisional Patent Application No. 61/976,009, filed Apr. 7, 2014, both of which are incorporated by reference herein in their entirety.

The present application additionally claims the benefit of priority to co-pending U.S. application Ser. No. 15/003,558, filed Jan. 21, 2016, which claims the benefit of priority to and incorporates by reference U.S. Provisional Patent Application No. 62/257,988, filed Nov. 20, 2015, both of which are incorporated by reference herein in their entirety. The present application claims the benefit of priority to co-pending U.S. application Ser. No. 15/003,062, filed Jan. 21, 2016, which claims the benefit of priority to and incorporates by reference U.S. Provisional Patent Application No. 62/196,288, filed Jul. 23, 2015, both of which are incorporated by reference herein in their entirety. The present application claims the benefit of priority to co-pending U.S. application Ser. No. 15/003,652, filed Jan. 21, 2016, which claims the benefit of priority to and incorporates by reference U.S. Provisional Application No. 62/190,209, filed on Jul. 8, 2015, both of which are incorporated by reference herein in their entirety. The present application claims the benefit of priority to co-pending U.S. application Ser. No. 15/003,677, filed Jan. 21, 2016, which claims the benefit of priority to and incorporates by reference U.S. Provisional Application No. 62/261,643, filed Dec. 1, 2015, both of which are incorporated by reference herein in their entirety. The present application claims the benefit of priority to co-pending U.S. application Ser. No. 15/003,678, filed Jan. 21, 2016, which is incorporated by reference herein in its entirety. The present application claims the benefit of priority to co-pending U.S. application Ser. No. 15/003,177, filed Jan. 21, 2016, which is incorporated by reference herein in its entirety. The present application claims the benefit of priority to co-pending U.S. application Ser. No. 15/003,206, filed Jan. 21, 2016, which claims the benefit of priority to and incorporates by reference U.S. Provisional Application No. 62/109,006, filed Jan. 28, 2015, and U.S. Provisional Application No. 62/109,551, filed Jan. 29, 2015, all of which are incorporated by reference herein in their entirety. The present application claims the benefit of priority to co-pending U.S. application Ser. No. 15/003,193, filed Jan. 21, 2016, which claims the benefit of priority to and incorporates by reference U.S. Provisional Application No. 62/109,006, filed Jan. 28, 2015, and U.S. Provisional Application No. 62/109,551, filed Jan. 29, 2015, all of which are incorporated by reference herein in their entirety. The present application claims the benefit of priority to co-pending U.S. application Ser. No. 15/003,088, filed Jan. 21, 2016, which is incorporated by reference herein in its entirety. The present application claims the benefit of priority to co-pending U.S. patent application Ser. No. 15/003,519, filed Jan. 21, 2016, which claims the benefit of priority to and incorporates by reference U.S. Provisional Patent Application No. 62/258,003, filed Nov. 20, 2015, both of which are incorporated by reference herein in their entirety. The present application claims the benefit of priority to co-pending U.S. application Ser. No. 15/003,718, filed Jan. 21, 2016, which claims the benefit of priority to and incorporates by reference U.S. Provisional Patent Application No. 62/112,071, filed Feb. 4, 2015, both of which are incorporated by reference herein in their entirety. The present application claims the benefit of priority to co-pending U.S. application Ser. No. 15/003,209, filed Jan. 21, 2016, which is incorporated by reference herein in its entirety. The present application claims the benefit of priority to co-pending U.S. application Ser. No. 15/003,670, filed Jan. 21, 2016, which is incorporated by reference herein in its entirety. The present application claims the benefit of priority to co-pending U.S. application Ser. No. 15/003,704, filed Jan. 21, 2016, which claims the benefit of priority to and incorporates by reference U.S. Provisional Patent Application No. 62/112,079, filed Feb. 4, 2015, both of which are incorporated by reference herein in their entirety. The present application claims the benefit of priority to co-pending U.S. application Ser. No. 15/003,590, filed Jan. 21, 2016, which claims the benefit of priority to and incorporates by reference U.S. Provisional Patent Application No. 62/107,289, filed Jan. 23, 2015, both of which are incorporated by reference herein in their entirety. The present application claims the benefit of priority to co-pending U.S. application Ser. No. 15/003,176, filed Jan. 21, 2016, which claims the benefit of priority to and incorporates by reference U.S. Provisional Patent Application No. 62/250,874, filed Nov. 4,

2015, both of which are incorporated by reference herein in their entirety. The present application claims the benefit of priority to co-pending U.S. application Ser. No. 15/003,145, filed Jan. 21, 2016, which claims the benefit of priority to and incorporates by reference U.S. Provisional Patent Application No. 62/277,657, filed Jan. 12, 2016, both of which are incorporated by reference herein in their entirety. The present application claims the benefit of priority to co-pending U.S. application Ser. No. 15/003,309, filed Jan. 21, 2016, which is incorporated by reference herein in its entirety. The present application claims the benefit of priority to co-pending U.S. application Ser. No. 15/003,298, filed Jan. 21, 2016, which is incorporated by reference herein in its entirety. The present application claims the benefit of priority to co-pending U.S. application Ser. No. 15/003,292, filed Jan. 21, 2016, which is incorporated by reference herein in its entirety. The present application claims the benefit of priority to co-pending U.S. application Ser. No. 15/003,281, filed Jan. 21, 2016, which is incorporated by reference herein in its entirety. The present application claims the benefit of priority to co-pending U.S. application Ser. No. 15/003,634, filed Jan. 21, 2016, which is incorporated by reference herein in its entirety. The present application claims the benefit of priority to co-pending U.S. application Ser. No. 15/003,577, filed Jan. 21, 2016, which is incorporated by reference herein in its entirety. The present application claims the benefit of priority to co-pending U.S. application Ser. No. 15/003,256, filed Jan. 21, 2016, which is incorporated by reference herein in its entirety. The present application claims the benefit of priority to co-pending U.S. application Ser. No. 15/003,396, filed Jan. 21, 2016, which claims the benefit of priority to and incorporates by reference U.S. Provisional Application No. 62/214,792, filed Sep. 4, 2015, both of which are incorporated by reference herein in their entirety. The present application claims the benefit of priority to co-pending U.S. application Ser. No. 15/003,617, filed Jan. 21, 2016, which claims the benefit of priority to and incorporates by reference U.S. Provisional Patent Application No. 62/190,218, filed Jul. 8, 2015, both of which are incorporated by reference herein in their entirety. The present application claims the benefit of priority to co-pending U.S. application Ser. No. 15/003,336, filed Jan. 21, 2016, which is incorporated by reference herein in its entirety.

FIELD

The present disclosure generally relates to magnetometers.

BACKGROUND

Atomic-sized nitrogen-vacancy (NV) centers in diamond lattices have been shown to have excellent sensitivity for magnetic field measurement and enable fabrication of small magnetic sensors that can readily replace existing-technology (e.g., Hall-effect, SERF, SQUID, or the like) systems and devices. Nitrogen vacancy diamond (DNV) magnetometers are able to sense extremely small magnetic field variations by changes in the diamond's red photoluminescence that relate, through the gradient of the luminescent function, to frequency and thereafter to magnetic field through the Zeeman effect.

BRIEF DESCRIPTION OF THE DRAWINGS

FIG. **1** illustrates one orientation of an NV center in a diamond lattice.

FIG. **2** is an energy level diagram showing energy levels of spin states for the NV center.

FIG. **3** is a schematic illustrating an NV center magnetic sensor system.

FIG. **4** is a graph illustrating a fluorescence as a function of an applied RF frequency of an NV center along a given direction for a zero magnetic field.

FIG. **5** is a graph illustrating the fluorescence as a function of an applied RF frequency for four different NV center orientations for a non-zero magnetic field.

FIG. **6** is a schematic diagram illustrating a magnetic field detection system according to an embodiment of the present invention.

FIG. **7** is a graph illustrating a fluorescence as a function of an applied RF frequency for an NV center orientation in a non-zero magnetic field and a gradient of the fluorescence as a function of the applied RF frequency.

FIG. **8** is an energy level diagram showing a hyperfine structure of spin states for the NV center.

FIG. **9** is a graph illustrating a fluorescence as a function of an applied RF frequency for an NV center orientation in a non-zero magnetic field with hyperfine detection and a gradient of the fluorescence as a function of the applied RF frequency.

FIG. **10** is an overview of a reflector with a diamond having nitrogen vacancies.

FIG. **11** is a side view of an ellipsoidal reflector with a diamond having nitrogen vacancies and a photo detector.

FIG. **12** is a side view of an ellipsoidal diamond having nitrogen vacancies and a photo detector.

FIG. **13** is a side view of a parabolic reflector with a diamond having nitrogen vacancies and a photo detector.

FIG. **14** is a side view of a parabolic diamond having nitrogen vacancies and a photo detector.

FIG. **15** is a side view of a parabolic reflector with a flat diamond having nitrogen vacancies inserted parallel to a major axis of the parabolic reflector and a photo detector.

FIG. **16** is a side view of a parabolic reflector with a flat diamond having nitrogen vacancies inserted parallel to a minor axis of the parabolic reflector and a photo detector.

FIG. **17** is a side view of a sensor assembly with a parabolic diamond having nitrogen vacancies and a photo detector.

FIG. **18** is a side view of a sensor assembly with a waveguide provided within a parabolic reflector.

FIG. **19** is a process diagram for a method for constructing a DNV sensor.

FIG. **20** is another process diagram for a method for constructing a DNV sensor.

FIG. **21** is a block diagram depicting a general architecture for a computer system that may be employed to implement various elements of the systems and methods described and illustrated herein.

FIG. **22** is a schematic illustrating a position sensor system according to one embodiment.

FIG. **23** is a schematic illustrating a position sensor system including a rotary position encoder.

FIG. **24** is a schematic illustrating a top down view of a rotary position encoder.

FIG. **25** is a schematic illustrating a position sensor system including a linear position encoder.

FIG. **26** is a schematic illustrating a magnetic element arrangement of a position encoder according to one embodiment.

FIG. **27** is a schematic illustrating a magnetic element arrangement of a position encoder according to another embodiment.

FIG. **28** is a schematic illustrating a magnetic element arrangement of a position encoder according to another embodiment.

FIG. **29** is a schematic illustrating the relationship of a position sensor head and the magnetic elements of a position encoder.

FIG. **30** is a graph of measured magnetic field intensity attributable to magnetic elements of a position encoder for a first magnetic field sensor and a second magnetic field sensor of a position sensor head.

FIG. **31** is a flow chart illustrating the process of determining a position utilizing a position sensor system according to one embodiment.

FIGS. **32**A and **32**B are graphs illustrating the frequency response of a DNV sensor in accordance with an illustrative embodiment.

FIG. **33**A is a diagram of NV center spin states in accordance with an illustrative embodiment.

FIG. **33**B is a graph illustrating the frequency response of a DNV sensor in response to a changed magnetic field in accordance with an illustrative embodiment.

FIG. **34** is a block diagram of a magnetic communication system in accordance with an illustrative embodiment.

FIGS. **35**A and **35**B show the strength of a magnetic field versus frequency in accordance with an illustrative embodiment.

FIG. **36** is a block diagram of a computing device in accordance with an illustrative embodiment.

FIG. **37** is graphs illustrating the fluorescence as a function of applied RF frequency of four different NV center orientations for a magnetic field applied in opposite directions to the NV center diamond material.

FIG. **38** is a graph illustrating the fluorescence intensity as a function of time for a NV center diamond material with a pulsed RF excitation.

FIG. **39** is a graph illustrating the fluorescence as a function of applied RF frequency of four different NV center orientations for a magnetic field applied in opposite directions to the NV center diamond material, with a Lorentzian pair being identified in the graph.

FIG. **40** is a graph illustrating the fluorescence intensity as a function of time for a NV center diamond material for a pulse of RF excitation.

FIG. **41** is a graph illustrating the normalized fluorescence intensity as a function of time for a pair of Lorentzian peaks of a NV center diamond material.

FIG. **42** is a graph illustrating the time to 60% of the equilibrium fluorescence as a function of RF frequency for a negative and positive magnetic bias field applied to a NV center diamond material.

FIGS. **43**A and **43**B are diagrams illustrating hydrophone systems in accordance with illustrative embodiments.

FIG. **44** illustrates a low altitude flying object in accordance with some illustrative implementations.

FIG. **45**A illustrates a ratio of signal strength of two magnetic sensors, A and B, attached to wings of the UAS as a function of distance, x, from a center line of a power in accordance with some illustrative implementations.

FIG. **45**B illustrates a composite magnetic field (B-filed) in accordance with some illustrative implementations.

FIG. **46** illustrates a high-level block diagram of an example UAS navigation system in accordance with some illustrative implementations.

FIG. **47** illustrates an example of a power line infrastructure.

FIGS. **48**A and **48**B illustrate examples of magnetic field distribution for overhead power lines and underground power cables.

FIG. **49** illustrates examples of magnetic field strength of power lines as a function of distance from the centerline.

FIG. **50** illustrates an example of a UAS equipped with DNV sensors in accordance with some illustrative implementations.

FIG. **51** illustrates a plot of a measured differential magnetic field sensed by the DNV sensors when in close proximity of the power lines in accordance with some illustrative implementations.

FIG. **52** illustrates an example of a measured magnetic field distribution for normal power lines and power lines with anomalies according to some implementations.

FIGS. **53**A-**53**B are diagrams illustrating examples of a high-level architecture of a system for mapping and monitoring of hydraulic fracture and an environment where the system operates, according to certain embodiments;

FIG. **54** is a high-level diagram illustrating an example of implementation of hydraulic fracturing of a well to release gas reserves, according to certain embodiments;

FIG. **55**A is a diagram illustrating an example background magnetic signature of a well, according to certain embodiments;

FIG. **55**B is a diagram illustrating an example implementation of a mapping system for hydraulic fracturing of the well shown in FIG. **3**A, according to certain embodiments;

FIG. **56** is a diagram illustrating an example of a method for mapping and monitoring of hydraulic fracture, according to certain embodiments;

FIG. **57** is a diagram illustrating an example of a system for implementing some aspects of the subject technology; and

FIG. **58** is a diagram illustrating examples of primary and secondary magnetic fields in the presence of a doped proppant, according to certain embodiments.

FIGS. **59**A through **59**F are diagrams illustrating examples of a magnetic waveform generator circuit, a corresponding timing diagram, and various operational phases of the magnetic waveform generator circuit, according to certain embodiments;

FIGS. **60**A-**60**B are diagrams illustrating examples of a magnetic waveform generator circuit with amplitude modulation capability and corresponding timing diagrams, according to certain embodiments;

FIGS. **61**A-**61**B are diagrams illustrating examples of an H-bridge magnetic waveform generator circuit and an H-bridge magnetic waveform generator circuit with amplitude modulation capability, according to certain embodiments; and

FIG. **62** is a diagram illustrating an example of a method for providing a magnetic waveform generator circuit, according to certain embodiments.

DETAILED DESCRIPTION

Hypersensitivity Detection of Magnetic Field

Aspects of the disclosure relates to apparatuses and methods for elucidating hyperfine transition responses to determine an external magnetic field acting on a magnetic detection system. The hyperfine transition responses exhibit a steeper gradient than the gradient of aggregate Lorentzian responses measured in conventional systems, which can be up to three orders of magnitude larger. The steeper gradient exhibited by the hyperfine transition responses thus allow for a comparable increase in measurement sensitivity in a

magnetic detection system. By utilizing the largest gradient of the hyperfine responses for measuring purposes, external magnetic fields may be detected more accurately, especially low magnitude and/or rapidly changing fields.

The NV Center, its Electronic Structure, and Optical and RF Interaction

The NV center in a diamond comprises a substitutional nitrogen atom in a lattice site adjacent a carbon vacancy as shown in FIG. **1**. The NV center may have four orientations, each corresponding to a different crystallographic orientation of the diamond lattice.

The NV center may exist in a neutral charge state or a negative charge state. Conventionally, the neutral charge state uses the nomenclature NV^0, while the negative charge state uses the nomenclature NV, which is adopted in this description.

The NV center has a number of electrons, including three unpaired electrons, each one from the vacancy to a respective of the three carbon atoms adjacent to the vacancy, and a pair of electrons between the nitrogen and the vacancy. The NV center, which is in the negatively charged state, also includes an extra electron.

The NV center has rotational symmetry, and as shown in FIG. **2**, has a ground state, which is a spin triplet with $^3A_2$ symmetry with one spin state $m_s=0$, and two further spin states $m_s=+1$, and $m_s=-1$. In the absence of an external magnetic field, the $m_s=\pm1$ energy levels are offset from the $m_s=0$ due to spin-spin interactions, and the $m_s=\pm1$ energy levels are degenerate, i.e., they have the same energy. The $m_s=0$ spin state energy level is split from the $m_s=\pm1$ energy levels by an energy of 2.87 GHz for a zero external magnetic field.

Introducing an external magnetic field with a component along the NV axis lifts the degeneracy of the $m_s=\pm1$ energy levels, splitting the energy levels $m_s=\pm1$ by an amount $2g\mu_B Bz$, where g is the g-factor, μ_B is the Bohr magneton, and Bz is the component of the external magnetic field along the NV axis. This relationship is correct to a first order and inclusion of higher order corrections is straightforward matter and will not affect the computational and logic steps in the systems and methods described below.

The NV center electronic structure further includes an excited triplet state ^3E with corresponding $m_s=0$ and $m_s=\pm1$ spin states. The optical transitions between the ground state $^3A_2$ and the excited triplet ^3E are predominantly spin conserving, meaning that the optical transitions are between initial and final states that have the same spin. For a direct transition between the excited triplet ^3E and the ground state $^3A_2$, a photon of red light is emitted with a photon energy corresponding to the energy difference between the energy levels of the transitions.

There is, however, an alternative non-radiative decay route from the triplet ^3E to the ground state $^3A_2$ via intermediate electron states, which are thought to be intermediate singlet states A, E with intermediate energy levels. Significantly, the transition rate from the $m_s=\pm1$ spin states of the excited triplet ^3E to the intermediate energy levels is significantly greater than the transition rate from the $m_s=0$ spin state of the excited triplet ^3E to the intermediate energy levels. The transition from the singlet states A, E to the ground state triplet $^3A_2$ predominantly decays to the $m_s=0$ spin state over the $m_s=\pm1$ spins states. These features of the decay from the excited triplet ^3E state via the intermediate singlet states A, E to the ground state triplet $^3A_2$ allows that if optical excitation is provided to the system, the optical excitation will eventually pump the NV center into the $m_s=0$ spin state of the ground state $^3A_2$. In this way, the population of the $m_s=0$ spin state of the ground state $^3A_2$ may be "reset" to a maximum polarization determined by the decay rates from the triplet ^3E to the intermediate singlet states.

Another feature of the decay is that the fluorescence intensity due to optically stimulating the excited triplet ^3E state is less for the $m_s=\pm1$ states than for the $m_s=0$ spin state. This is so because the decay via the intermediate states does not result in a photon emitted in the fluorescence band, and because of the greater probability that the $m_s=\pm1$ states of the excited triplet ^3E state will decay via the non-radiative decay path. The lower fluorescence intensity for the $m_s=\pm1$ states than for the $m_s=0$ spin state allows the fluorescence intensity to be used to determine the spin state. As the population of the $m_s=\pm1$ states increases relative to the $m_s=0$ spin, the overall fluorescence intensity will be reduced.

The NV Center, or Magneto-Optical Defect Center, Magnetic Sensor System

FIG. **3** is a schematic diagram illustrating a conventional NV center magnetic sensor system **300** that uses fluorescence intensity to distinguish the $m_s=\pm1$ states, and to measure the magnetic field based on the energy difference between the $m_s=+1$ state and the $m_s=-1$ state. The system **300** includes an optical excitation source **310**, which directs optical excitation to an NV diamond material **320** with NV centers. The system further includes an RF excitation source **330**, which provides RF radiation to the NV diamond material **320**. Light from the NV diamond may be directed through an optical filter **350** to an optical detector **340**.

The RF excitation source **330** may be a microwave coil, for example. The RF excitation source **330**, when emitting RF radiation with a photon energy resonant with the transition energy between ground $m_s=0$ spin state and the $m_s=+1$ spin state, excites a transition between those spin states. For such a resonance, the spin state cycles between ground $m_s=0$ spin state and the $m_s=+1$ spin state, reducing the population in the $m_s=0$ spin state and reducing the overall fluorescence at resonances. Similarly, resonance occurs between the $m_s=0$ spin state and the $m_s=-1$ spin state of the ground state when the photon energy of the RF radiation emitted by the RF excitation source is the difference in energies of the $m_s=0$ spin state and the $m_s=-1$ spin state, or between the $m_s=0$ spin state and the $m_s=+1$ spin state, there is a decrease in the fluorescence intensity.

The optical excitation source **310** may be a laser or a light emitting diode, for example, which emits light in the green, for example. The optical excitation source **310** induces fluorescence in the red, which corresponds to an electronic transition from the excited state to the ground state. Light from the NV diamond material **320** is directed through the optical filter **350** to filter out light in the excitation band (in the green, for example), and to pass light in the red fluorescence band, which in turn is detected by the detector **340**. The optical excitation light source **310**, in addition to exciting fluorescence in the diamond material **320**, also serves to reset the population of the $m_s=0$ spin state of the ground state $^3A_2$ to a maximum polarization, or other desired polarization.

For continuous wave excitation, the optical excitation source **310** continuously pumps the NV centers, and the RF excitation source **330** sweeps across a frequency range that includes the zero splitting (when the $m_s=\pm1$ spin states have the same energy) energy of 2.87 GHz. The fluorescence for an RF sweep corresponding to a diamond material **320** with NV centers aligned along a single direction is shown in FIG. **4** for different magnetic field components Bz along the NV axis, where the energy splitting between the $m_s=-1$ spin state and the $m_s=+1$ spin state increases with Bz. Thus, the

component Bz may be determined. Optical excitation schemes other than continuous wave excitation are contemplated, such as excitation schemes involving pulsed optical excitation, and pulsed RF excitation. Examples of pulsed excitation schemes include Ramsey pulse sequence, and spin echo pulse sequence.

In general, the diamond material **320** will have NV centers aligned along directions of four different orientation classes. FIG. **5** illustrates fluorescence as a function of RF frequency for the case where the diamond material **320** has NV centers aligned along directions of four different orientation classes. In this case, the component Bz along each of the different orientations may be determined. These results, along with the known orientation of crystallographic planes of a diamond lattice, allow not only the magnitude of the external magnetic field to be determined, but also the direction of the magnetic field.

While FIG. **3** illustrates an NV center magnetic sensor system **300** with NV diamond material **320** with a plurality of NV centers, in general, the magnetic sensor system may instead employ a different magneto-optical defect center material, with a plurality of magneto-optical defect centers. The electronic spin state energies of the magneto-optical defect centers shift with magnetic field, and the optical response, such as fluorescence, for the different spin states is not the same for all of the different spin states. In this way, the magnetic field may be determined based on optical excitation, and possibly RF excitation, in a corresponding way to that described above with NV diamond material.

FIG. **6** is a schematic diagram of a system **600** for a magnetic field detection system according to an embodiment of the present invention. The system **600** includes an optical excitation source **610**, which directs optical excitation to an NV diamond material **620** with NV centers, or another magneto-optical defect center material with magneto-optical defect centers. An RF excitation source **630** provides RF radiation to the NV diamond material **620**.

As shown in FIG. **6**, a first magnetic field generator **670** generates a magnetic field, which is detected at the NV diamond material **620**. The first magnetic field generator **670** may be a permanent magnet positioned relative to the NV diamond material **620**, which generates a known, uniform magnetic field (e.g., a bias or control magnetic field) to produce a desired fluorescence intensity response from the NV diamond material **620**. In some embodiments, a second magnetic field generator **675** may be provided and positioned relative to the NV diamond material **620** to provide an additional bias or control magnetic field. The second magnetic field generator **675** may be configured to generate magnetic fields with orthogonal polarizations, for example. In this regard, the second magnetic field generator **675** may include one or more coils, such as a Helmholtz coils. The coils may be configured to provide relatively uniform magnetic fields at the NV diamond material **620** and each may generate a magnetic field having a direction that is orthogonal to the direction of the magnetic field generated by the other coils. For example, in a particular embodiment, the second magnetic field generator **675** may include three Helmholtz coils that are arranged to each generate a magnetic field having a direction orthogonal to the other direction of the magnetic field generated by the other two coils resulting in a three-axis magnetic field. In some embodiments, only the first magnetic field generator **670** may be provided to generate a bias or control magnetic field. Alternatively, only the second magnetic field generator **675** may be provided to generate the bias or control magnetic field. In yet other embodiments, the first and/or second magnetic field generators may be affixed to a pivot assembly (e.g., a gimbal assembly) that may be controlled to hold and position the first and/or second magnetic field generators to a predetermined and well-controlled set of orientations, thereby establishing the desired bias or control magnetic fields. In this case, the controller **680** may be configured to control the pivot assembly having the first and/or second magnetic field generators to position and hold the first and/or second magnetic field generators at the predetermined orientation.

The system **600** further includes a controller **680** arranged to receive a light detection or optical signal from the optical detector **640** and to control the optical excitation source **610**, the RF excitation source **630**, and the second magnetic field generator **675**. The controller may be a single controller, or multiple controllers. For a controller including multiple controllers, each of the controllers may perform different functions, such as controlling different components of the system **600**. The second magnetic field generator **675** may be controlled by the controller **680** via an amplifier **660**, for example.

The RF excitation source **630** may be a microwave coil, for example. The RF excitation source **630** is controlled to emit RF radiation with a photon energy resonant with the transition energy between the ground $m_s=0$ spin state and the $m_s=\pm 1$ spin states as discussed above with respect to FIG. **3**.

The optical excitation source **610** may be a laser or a light emitting diode, for example, which emits light in the green, for example. The optical excitation source **610** induces fluorescence in the red from the NV diamond material **620**, where the fluorescence corresponds to an electronic transition from the excited state to the ground state. Light from the NV diamond material **620** is directed through the optical filter **650** to filter out light in the excitation band (in the green, for example), and to pass light in the red fluorescence band, which in turn is detected by the optical detector **640**. The optical excitation light source **610**, in addition to exciting fluorescence in the NV diamond material **620**, also serves to reset the population of the $m_s=0$ spin state of the ground state $^3A_2$ to a maximum polarization, or other desired polarization.

The controller **680** is arranged to receive a light detection signal from the optical detector **640** and to control the optical excitation source **610**, the RF excitation source **630**, and the second magnetic field generator **675**. The controller may include a processor **682** and a memory **684**, in order to control the operation of the optical excitation source **610**, the RF excitation source **630**, and the second magnetic field generator **675**. The memory **684**, which may include a nontransitory computer readable medium, may store instructions to allow the operation of the optical excitation source **610**, the RF excitation source **630**, and the second magnetic field generator **675** to be controlled. That is, the controller **680** may be programmed to provide control.

Detection of Magnetic Field Changes

As discussed above, the interaction of the NV centers with an external magnetic field results in an energy splitting between the $m_s=-1$ spin state and the $m_s=+1$ spin state that increases with Bz as shown in FIG. **4**, for example. The pair of frequency responses (also known as Lorentzian responses, profiles, or dips) due to the component of the external magnetic field along the given NV axis manifest as dips in intensity of the emitted red light from the NV centers as a function of RF carrier frequency. Accordingly, a pair of frequency responses for each of the four axes of the NV center diamond lattice result in an energy splitting between the $m_s=-1$ spin state and the $m_s=+1$ spin state that corre-

sponds to the component of the external magnetic field along the axis for a total of eight Lorentzian profiles or dips, as shown in FIG. **5**. When a bias magnetic field is applied to the NV diamond material (such as by the first and/or second magnetic field generators **670**, **675** of FIG. **6**), in addition to an unknown external magnetic field existing outside the system, the total incident magnetic field may thus be expressed as $B_t(t)=B_{bias}(t)\ B_{ext}(t)$, where $B_{bias}(t)$ represents the bias magnetic field applied to the NV diamond material and $B_{ext}(t)$ represents the unknown external magnetic field. This total incident magnetic field creates equal and linearly proportional shifts in the Lorentzian frequency profiles for a given NV axis between the $m_s=-1$ spin state and the $m_s=+1$ spin state relative to the starting carrier frequency (e.g., about 2.87 GHz).

Because the applied bias magnetic field $B_{bias}(t)$ is already known and constant, a change or shift in the total incident magnetic field $B_t(t)$ will be due to a change in the external magnetic field $B_{ext}(t)$. To detect a change in the total incident magnetic field, the point of greatest sensitivity in measuring such a change will occur at the point where the frequency response is at its largest slope. For example, as shown in FIG. **7**, an intensity response $I(t)$ as a function of an RF applied frequency f (t) for a given NV axis due to a magnetic field is shown in the top graph. The change in intensity $\mathbf{1}(t)$ relative to the change in RF applied frequency,

$$\frac{dI(t)}{df},$$

is plotted against the RF applied frequency f (t) as shown in the bottom graph. Point **25** represents the point of the greatest gradient of the Lorentzian dip **20**. This point gives the greatest measurement sensitivity in detecting changes in the total incident magnetic field as it responds to the external magnetic field.

The Hyperfine Field

As discussed above and shown in the energy level diagram of FIG. **2**, the ground state is split by about 2.87 GHz between the $m_s=0$ and $m_s=\pm1$ spin states due to their spin-spin interactions. In addition, due to the presence of a magnetic field, the $m_s=\pm1$ spin states split in proportion to the magnetic field along the given axis of the NV center, which manifests as the four-pair Lorentzian frequency response shown in FIG. **5**. However, a hyperfine structure of the NV center exists due to the hyperfine coupling between the electronic spin states of the NV center and the nitrogen nucleus, which results in further energy splitting of the spin states. FIG. **8** shows the hyperfine structure of the ground state triplet $^3A_2$ of the NV center. Specifically, coupling to the nitrogen nucleus ^{14}N further splits the $m_s=\pm1$ spin states into three hyperfine transitions (labeled as m_1 spin states), each having different resonances. Accordingly, due to the hyperfine split for each of the $m_s=\pm1$ spin states, twenty-four different frequency responses may be produced (three level splits for each of the $m_s=\pm1$ spin states for each of the four NV center orientations).

Each of the three hyperfine transitions manifest within the width of one aggregate Lorentzian dip. With proper detection, the hyperfine transitions may be elucidated within a given Lorentzian response. To detect such hyperfine transitions, in particular embodiments, the NV diamond material **620** exhibits a high purity (e.g., low existence of lattice dislocations, broken bonds, or other elements beyond ^{14}N) and does not have an excess concentration of NV centers. In addition, during operation of the system **600** in some embodiments, the RF excitation source **630** is operated on a low power setting in order to further resolve the hyperfine responses. In other embodiments, additional optical contrast for the hyperfine responses may be accomplished by increasing the concentration of NV negative-charge type centers, increasing the optical power density (e.g., in a range from about 20 to about 1000 mW/mm^2), and decreasing the RF power to the lowest magnitude that permits a sufficient hyperfine readout (e.g., about 1 to about 10 W/mm^2).

FIG. **9** shows an example of fluorescence intensity as a function of an applied RF frequency for an NV center with hyperfine detection. In the top graph, the intensity response I(t) as a function of an applied RF frequency f (t) for a given spin state (e.g., $m_s=-1$) along a given axis of the NV center due to an external magnetic field is shown. In addition, in the bottom graph, the gradient

$$\frac{dI(t)}{df}$$

plotted against the applied RF frequency f (t) is shown. As seen in the figure, the three hyperfine transitions **200***a*-**200***c* constitute a complete Lorentzian response **20** (e.g., corresponding to the Lorenztian response **20** in FIG. **7**). The point of maximum slope may then be determined through the gradient of the fluorescence intensity as a function of the applied RF frequency, which occurs at the point **250** in FIG. **9**. This point of maximum slope may then be tracked during the applied RF sweep to detect movement of the point of maximum slope along the frequency sweep. Like the point of maximum slope **25** for the aggregate Lorentzian response, the corresponding movement of the point **250** corresponds to changes in the total incident magnetic field $B_t(t)$, which because of the known and constant bias field $B_{bias}(t)$, allows for the detection of changes in the external magnetic field $B_{ext}(t)$.

However, as compared to point **25**, point **250** exhibits a larger gradient than the aggregate Lorentzian gradient described above with regard to FIG. **7**. In some embodiments, the gradient of point **250** may be up to 1000 times larger than the aggregate Lorentzian gradient of point **25**. Due to this, the point **250** and its corresponding movement may be more easily detected by the measurement system resulting in improved sensitivity, especially in very low magnitude and/or very rapidly changing magnetic fields.

Improved Light Collection from DNV Sensors

In some aspects of the present technology, methods and configurations are disclosed for an efficient collection of fluorescence (e.g., red light) emitted by the nitrogen vacancies of a diamond of a DNV sensor. In some implementations, the subject technology can allow efficient collection of the emitted light of the diamond of the DNV sensor with a compact and low cost reflector. The reflector can focus the emitted light of the diamond of the DNV sensor to an optical or photo detector that can increase the amount of light detected from the diamond. In some implementations, such a configuration may detect virtually all light emitted by the diamond of the DNV sensor. In some aspects, the reflector may be shaped as a parabola, an ellipse, or other shapes that can convey the light emitted from a source to a focal point or focal area.

In some other implementations of the subject technology, the diamond of the DNV sensor may be machined or otherwise shaped to be a reflector itself. That is, the diamond

with nitrogen vacancies may be shaped to form a parabolic reflector, ellipsoidal reflector or other shapes that can convey the light emitted from the nitrogen vacancies to a focal point or focal area. For example, the reflector can be mostly parabolic or ellipsoidal such that the light hits the photo detector at a 90 degree angle with some margin of error, e.g., 2 to 10 degrees.

The nitrogen vacancies of the diamond will fluoresce in response to excitation with green light and will emit red light in random directions. Because the red light measurements are shot noise limited, collecting as much emitted light as possible is desirable. In some current collection approaches using large optics, the collection efficiencies were in the range of 20%. Some implementations use a large aperture lens mounted close to the diamond or DNV sensor, which limits light collection to a fraction of the light emitted by the diamond or DNV sensor. Other implementations use a flat diamond and a number of photo detectors (e.g., four) positioned at the edges of the flat diamond. This arrangement of photo detectors may be able to capture more of the emitted light conducted to edges of the flat diamond due to internal reflection, but increases the number of photo detectors required and may not capture light emitted from the faces of the flat diamond. The DNV sensors discussed herein provide an alternative to increase the collection efficiency.

FIG. **10** depicts an overview of an assembly **1000** with an example diamond **1002** having nitrogen vacancies and a reflector **1004** positioned about the diamond **1002** for a DNV light-collection apparatus. In the implementation shown, the reflector **1004** is positioned about the diamond **1002** to reflect a portion of the light emitted **1006** from the diamond **1002**. The reflector **1004** is an elliptical or ellipsoidal reflector with the diamond **1002** positioned within a portion of the reflector **1004**. In other implementations, as discussed in further detail herein, the reflector **1004** may be parabolic or any other geometric configuration to reflect light emitted from the diamond **1002**. In some implementations, the reflector **1004** may be a monolithic reflector, a hollow reflector, or any other type of reflector to reflect light emitted from the diamond **1002**. In the implementation shown, the diamond **1002** is positioned at a focus **1008** of the reflector **1004**. Thus, when light **1006** is emitted from the diamond **1002**, the light is reflected by the reflector **1004** toward another focus of the reflector **1004**. As will be discussed in further detail herein, a photo detector may be positioned at the second focus to collect the reflected light.

FIG. **11** depicts an assembly **1100** with an example diamond **1102** having nitrogen vacancies and an ellipsoidal reflector **1104** positioned about the diamond **1102** for a DNV light-collection apparatus. In some implementations, the ellipsoidal reflector **1104** can be a single monolithic component that can be considered to be divided into two portions, such as a reflector portion **1106** and a concentrator portion **1108**. In other implementations, the ellipsoidal reflector **1104** may be divided into two components, such as the reflector portion **1106** and the concentrator portion **1108** that are coupled and/or otherwise positioned relative to each other. For instance, the reflector portion **1106** and the concentrator portion **1108** may be separate parabolic components that can be combined to form the ellipsoidal reflector **1104**. In still further configurations, the ellipsoidal reflector **1104** may be composed of more than two components and can be coupled or otherwise positioned to form the ellipsoidal reflector **1104**.

The diamond **1102** is positioned at a first focus of the ellipsoidal reflector **1104** for the reflector portion **1106**. In some implementations, the diamond **1102** is positioned at the first focus using a mount for the diamond **1102**. In other implementations, the diamond **1102** is positioned at the first focus using a borehole through the ellipsoidal reflector **1104**. The borehole may be backfilled to seal the diamond **1102** in the ellipsoidal reflector **1104**.

The ellipsoidal reflector **1104** may also include an opening to allow an excitation laser beam to excite the diamond **1102**, such as a green excitation laser beam. The opening may be positioned at any location for the ellipsoidal reflector **1104**. When the diamond **1102** is excited (e.g., by applying green light to the diamond **1102**), then the reflector portion **1106** reflects the red light emitted **1110** from the diamond **1102** towards the concentrator portion **1108**.

The concentrator portion **1108** directs the emitted light **1110** toward a second focus of the ellipsoidal reflector **1104**. In the implementation shown, a photo detector **1120** is positioned to receive and measure the light from the concentrator portion **1108**. In some implementations, the photo detector **1120** is positioned at the second focus to receive the redirected emitted light. In some implementations the photo detector **1120** is coupled and/or sealed to a portion of the ellipsoidal reflector **1104**, such as to the concentrator portion **1108**. In some implementations, the opening may be adjacent or proximate to the photo detector **1120**, such as through the concentrator portion **1108**. In other implementations, the opening may be opposite the photo detector **1120**, such as through the reflector portion **1106**. In still further configurations, the opening may be at any other angle and/or orientation relative to the photo detector **1120**.

In some implementations, an optical filter, such as a red filter, may be applied to and/or positioned on the photo detector **1120** to filter out light except the relevant red light of interest. Thus, the ellipsoidal reflector **1104** is concatenated with a non-focusing concentrator that can capture the emitted light from a light source (e.g., from the nitrogen vacancies of the diamond of a DNV sensor) to a single photo detector. In some instances, the loss of emitted light can be limited to the light loss due to the mount for the diamond and/or the small entrance for the green stimulation laser beam.

The foregoing solution provides high light collection efficiency to collect the light emitted from the diamond **1102**, while utilizing a reflector **1104** that may not require high precision refinements. Such a reflector **1104** may be a low cost solution to increase the light collection efficiency, such as using a reflective mirror component. In addition, the shape of the ellipsoidal reflector **1104** may separate the electronics of the photo detector **1120** from the diamond **1102**, which may decrease the magnetic interaction between the electronics of the photo detector **1120** and the diamond **1102**.

The elliptical reflector **1104** may, in some implementations, include a substrate with a dielectric mirror film or coating applied to reflect the emitted light **1110**. The dielectric mirror film may be selected for the specific frequency of interest. In some implementations, the thickness of the dielectric mirror material may affect the specific frequency of interest. For instance, the substrate may possess a high clarity at a frequency of interest for the DNV sensor. The substrate may be made of a plastic, glass, diamond, quartz, and/or any other suitable material. The dielectric mirror film may be applied to the substrate such that the light emitted **1110** from the diamond **1102** is reflected within the ellipsoidal reflector **1104**. In some implementations, the dielectric mirror film may only reflect red light such that other colors or wavelengths of light pass through the ellipsoidal reflector **1104**. For instance, such a dielectric mirror film

may permit transmission of green wavelength light, such as from an excitation laser beam, through the ellipsoidal reflector **1104** to the diamond **1102** to excite the diamond **1102**.

In some aspects, such as for precision sensors, the separation between the diamond **1102** and the electronics of the photo detector **1120** can be extended, for example to several feet. In some implementations, the thin dielectric mirror film is used in the ellipsoidal reflector **1104** to allow an RF antenna to be located inside the ellipsoidal reflector **1104**. In some applications, the antenna may instead be outside of the ellipsoidal reflector **1104**.

FIG. **12** depicts an assembly **1200** with an example diamond **1202** having nitrogen vacancies that is formed or machined into a reflector configuration for a DNV light-collection apparatus. The diamond **1202** in the present configuration is formed or machined into an ellipsoidal reflector and is a monolithic component that can be considered to be divided into two portions, such as a reflector portion **1204** and a concentrator portion **1206**.

The diamond **1202** may have a dielectric mirror film coated on or applied to the diamond **1202**. The dielectric mirror film may be selected for the specific frequency of interest. In some implementations, the thickness of the dielectric mirror material may affect the specific frequency of interest. The dielectric mirror film may be applied such that the light emitted **1210** from the nitrogen vacancies within the diamond **1202** is reflected within the reflector portion **1204** and concentrator portion **1206** of the diamond **1202**. In some implementations, the dielectric mirror film may only reflect red light such that other colors or wavelengths of light pass through the diamond **1202**. For instance, such a dielectric mirror film may permit transmission of green wavelength light, such as from an excitation laser beam, through the dielectric mirror film to the nitrogen vacancies of the diamond **1202** to excite the nitrogen vacancies of the diamond **1202**.

The reflector portion **1204** of the diamond **1202** may internally reflect the emitted light **1210** via the dielectric mirror film applied to the diamond **1202**. Thus, the diamond **1202** internally reflects the red light emitted **1210** from the diamond **1202** towards the concentrator portion **1206**. The concentrator portion **1206** also redirects the light emitted **1210** by the nitrogen vacancies of the diamond **1202** toward a focus of the concentrator portion **1206** of the diamond **1202**. In the implementation shown, a photo detector **1220** is positioned to receive and measure the light from the concentrator portion **1206**. In some implementations, the photo detector **1220** is positioned at the focus to receive the redirected emitted light **1210**. In some implementations the photo detector **1220** is coupled and/or sealed to a portion of the diamond **1202**, such as to the concentrator portion **1206**.

In some implementations, an optical filter, such as a red filter, may be applied to and/or positioned on the photo detector **1220** to filter out light except the relevant red light of interest.

In some implementations, a portion of the diamond **1202** may be formed without nitrogen vacancies. That is, for instance, one or more layers for the diamond may be formed by chemical deposition without nitrogen vacancies. The one or more layers may be machined or formed for the concentrator portion such that the emitted light reflected by the reflector portion **1204** is not reabsorbed by nitrogen vacancies when travelling through the concentrator portion **1206** of the diamond **1202**.

FIG. **13** depicts an assembly **1300** with an example diamond **1302** having nitrogen vacancies and a parabolic reflector **1304** positioned about the diamond **1302** for a DNV light-collection apparatus. In some implementations, the parabolic reflector **1304** can be a single monolithic component. In some configurations, the parabolic reflector **1304** may be composed of more than two components and can be coupled or otherwise positioned to form the parabolic reflector **1304**.

The diamond **1302** is positioned at a focus of the parabolic reflector **1304**. In some implementations, the diamond **1302** is positioned at the focus using a mount for the diamond **1302**. In other implementations, the diamond **1302** is positioned at the focus using a borehole through the parabolic reflector **1304**. The borehole may be backfilled to seal the diamond **1302** in the parabolic reflector **1304**.

The parabolic reflector **1304** may also include an opening to allow an excitation laser beam to excite the diamond **1302**, such as a green excitation laser beam. The opening may be positioned at any location for the parabolic reflector **1304**. When the diamond **1302** is excited (e.g., by applying green light to the diamond **1302**), then the parabolic reflector **1304** reflects the red light emitted **1310** from the diamond **1302** towards a photo detector **1320**. In the implementation shown, a photo detector **1320** is positioned to receive and measure the light from the parabolic reflector **1304**. In some implementations the photo detector **1320** is coupled and/or sealed to a portion of the parabolic reflector **1304**. In some implementations, the opening may be adjacent or proximate to the photo detector **1320**. In other implementations, the opening may be opposite the photo detector **1320**. In still further configurations, the opening may be at any other angle and/or orientation relative to the photo detector **1320**.

In some implementations, an optical filter, such as a red filter, may be applied to and/or positioned on the photo detector **1320** to filter out light except the relevant red light of interest. Thus, the parabolic reflector **1304** is concatenated with a non-focusing concentrator that can capture the emitted light from a light source (e.g., from the nitrogen vacancies of the diamond of a DNV sensor) to a single photo detector. In some instances, the loss of emitted light can be limited to the light loss due to the mount for the diamond and/or the small entrance for the green stimulation laser beam.

The foregoing solution provides high light collection efficiency to collect the light emitted from the diamond **1302**, while utilizing a parabolic reflector **1304** that may not require high precision refinements. Such a parabolic reflector **1304** may be a low cost solution to increase the light collection efficiency, such as using a reflective mirror component. In addition, the shape of the parabolic reflector **1304** may separate the electronics of the photo detector **1320** from the diamond **1302**, which may decrease the magnetic interaction between the electronics of the photo detector **1320** and the diamond **1302**.

The parabolic reflector **1304** may, in some implementations, include a substrate with a dielectric mirror film or coating applied to reflect the emitted light **1310**. The dielectric mirror film may be selected for the specific frequency of interest. In some implementations, the thickness of the dielectric mirror material may affect the specific frequency of interest. For instance, the substrate may possess a high clarity at a frequency of interest for the DNV sensor. The substrate may be made of a plastic, glass, diamond, quartz, and/or any other suitable material. The dielectric mirror film may be applied to the substrate such that the light emitted **1310** from the diamond **1302** is reflected within the parabolic reflector **1304**. In some implementations, the dielectric mirror film may only reflect red light such that other colors or wavelengths of light pass through the parabolic reflector

1304. For instance, such a dielectric mirror film may permit transmission of green wavelength light, such as from an excitation laser beam, through the parabolic reflector **1304** to the diamond **1302** to excite the diamond **1302**.

In some aspects, such as for precision sensors, the separation between the diamond **1302** and the electronics of the photo detector **1320** can be extended, for example to several feet. In some implementations, the thin dielectric mirror film is used in the parabolic reflector **1304** to allow an RF antenna to be located inside the parabolic reflector **1304**. In some applications, the antenna may instead be outside of the parabolic reflector **1304**.

FIG. **14** depicts an assembly **1400** with an example diamond **1402** having nitrogen vacancies that is formed or machined into a reflector configuration for a DNV light-collection apparatus. The diamond **1402** in the present configuration is formed or machined into a parabolic reflector and is a monolithic component.

The diamond **1402** may have a dielectric mirror film coated on or applied to the diamond **1402**. The dielectric mirror film may be selected for the specific frequency of interest. In some implementations, the thickness of the dielectric mirror material may affect the specific frequency of interest. The dielectric mirror film may be applied such that the light emitted **1410** from the nitrogen vacancies within the diamond **1402** is reflected within the diamond **1402**. In some implementations, the dielectric mirror film may only reflect red light such that other colors or wavelengths of light pass through the diamond **1402**. For instance, such a dielectric mirror film may permit transmission of green wavelength light, such as from an excitation laser beam, through the dielectric mirror film to the nitrogen vacancies of the diamond **1402** to excite the nitrogen vacancies of the diamond **1402**.

The parabolic reflector configuration for the diamond **1402** may internally reflect the emitted light **1410** via the dielectric mirror film applied to the diamond **1402**. Thus, the diamond **1402** internally reflects the red light emitted **1410** from the diamond **1402** a photo detector **1420** that is positioned to receive and measure the light emitted. In some implementations the photo detector **1420** is coupled and/or sealed to a portion of the diamond **1402**.

In some implementations, an optical filter, such as a red filter, may be applied to and/or positioned on the photo detector **1420** to filter out light except the relevant red light of interest.

In some implementations, a portion of the diamond **1402** may be formed without nitrogen vacancies. That is, for instance, one or more layers for the diamond may be formed by chemical deposition without nitrogen vacancies. The one or more layers may be machined or formed near the junction for the photo detector **1420** such that the emitted light reflected by the parabolic reflector configuration of the diamond **1402** is not reabsorbed by nitrogen vacancies when travelling through the one or more layers of the diamond **1402**.

FIG. **15** depicts another implementation of a parabolic reflector configuration for an assembly **1500** for a DNV sensor. An example thin diamond **1502** having nitrogen vacancies may be inserted into a portion of a parabolic reflector **1504** positioned about the diamond **1502** for a DNV light-collection apparatus. In some implementations, the parabolic reflector **1504** can be a single monolithic component that is split into two portions to insert the thin diamond **1502**. In some other configurations, the parabolic reflector **1504** may be composed of more than two components and can be coupled or otherwise positioned to form the parabolic reflector **1504**. In the implementation shown, the thin diamond **1502** is inserted parallel to (and in some instances along) an axis of symmetry the parabolic reflector **1504**. In implementations utilizing an ellipsoidal reflector, the thin diamond **1502** may be inserted parallel to and/or along a major axis of the ellipsoidal reflector.

The parabolic reflector **1504** may also include an opening to allow an excitation laser beam to excite the diamond **1502**, such as a green excitation laser beam. The opening may be positioned at any location for the parabolic reflector **1504**. When the diamond **1502** is excited (e.g., by applying green light to the diamond **1502**), then the parabolic reflector **1504** reflects the red light emitted **1510** from the diamond **1502** towards a photo detector **1520**. In the implementation shown, a photo detector **1520** is positioned to receive and measure the light from the parabolic reflector **1504**. In some implementations the photo detector **1520** is coupled and/or sealed to a portion of the parabolic reflector **1504**. In some implementations, the opening may be adjacent or proximate to the photo detector **1520**. In other implementations, the opening may be opposite the photo detector **1520**. In still further configurations, the opening may be at any other angle and/or orientation relative to the photo detector **1520**.

In some implementations, an optical filter, such as a red filter, may be applied to and/or positioned on the photo detector **1520** to filter out light except the relevant red light of interest. Thus, the parabolic reflector **1504** is concatenated with a non-focusing concentrator that can capture the emitted light from a light source (e.g., from the nitrogen vacancies of the diamond of a DNV sensor) to a single photo detector. In some instances, the loss of emitted light can be limited to the light loss due to the mount for the diamond and/or the small entrance for the green stimulation laser beam.

The foregoing solution provides high light collection efficiency to collect the light emitted from the diamond **1502**, while utilizing a parabolic reflector **1504** that may not require high precision refinements. Such a parabolic reflector **1504** may be a low cost solution to increase the light collection efficiency, such as using a reflective mirror component. In addition, the shape of the parabolic reflector **1504** may separate the electronics of the photo detector **1520** from the diamond **1502**, which may decrease the magnetic interaction between the electronics of the photo detector **1520** and the diamond **1502**.

The parabolic reflector **1504** may, in some implementations, include a substrate with a dielectric mirror film or coating applied to reflect the emitted light **1510**. The dielectric mirror film may be selected for the specific frequency of interest. In some implementations, the thickness of the dielectric mirror material may affect the specific frequency of interest. For instance, the substrate may possess a high clarity at a frequency of interest for the DNV sensor. The substrate may be made of a plastic, glass, diamond, quartz, and/or any other suitable material. The dielectric mirror film may be applied to the substrate such that the light emitted **1510** from the diamond **1502** is reflected within the parabolic reflector **1504**. In some implementations, the dielectric mirror film may only reflect red light such that other colors or wavelengths of light pass through the parabolic reflector **1504**. For instance, such a dielectric mirror film may permit transmission of green wavelength light, such as from an excitation laser beam, through the parabolic reflector **1504** to the diamond **1502** to excite the diamond **1502**.

In some aspects, such as for precision sensors, the separation between the diamond **1502** and the electronics of the photo detector **1520** can be extended, for example to several

feet. In some implementations, the thin dielectric mirror film is used in the parabolic reflector **1504** to allow an RF antenna to be located inside the parabolic reflector **1504**. In some applications, the antenna may instead be outside of the parabolic reflector **1504**.

FIG. **16** depicts another implementation of a parabolic reflector configuration for an assembly **1600** for a DNV sensor. An example thin diamond **1602** having nitrogen vacancies may be inserted into a portion of a parabolic reflector **1604** positioned about the diamond **1602** for a DNV light-collection apparatus. In some implementations, the parabolic reflector **1604** can be a single monolithic component that is split into two portions to insert the thin diamond **1602**. In some other configurations, the parabolic reflector **1604** may be composed of more than two components and can be coupled or otherwise positioned to form the parabolic reflector **1604**. In the implementation shown, the thin diamond **1602** is inserted perpendicular to an axis of symmetry the parabolic reflector **1604**. In implementations utilizing an ellipsoidal reflector, the thin diamond **1602** may be inserted parallel to and/or along a minor axis of the ellipsoidal reflector. In some implementations, the thin diamond **1602** is positioned at a focus of the parabolic reflector **1604**.

The parabolic reflector **1604** may also include an opening to allow an excitation laser beam to excite the diamond **1602**, such as a green excitation laser beam. The opening may be positioned at any location for the parabolic reflector **1604**. When the diamond **1602** is excited (e.g., by applying green light to the diamond **1602**), then the parabolic reflector **1604** reflects the red light emitted **1610** from the diamond **1602** towards a photo detector **1620**. In the implementation shown, a photo detector **1620** is positioned to receive and measure the light from the parabolic reflector **1604**. In some implementations the photo detector **1620** is coupled and/or sealed to a portion of the parabolic reflector **1604**. In some implementations, the opening may be adjacent or proximate to the photo detector **1620**. In other implementations, the opening may be opposite the photo detector **1620**. In still further configurations, the opening may be at any other angle and/or orientation relative to the photo detector **1620**.

In some implementations, an optical filter, such as a red filter, may be applied to and/or positioned on the photo detector **1620** to filter out light except the relevant red light of interest. Thus, the parabolic reflector **1604** is concatenated with a non-focusing concentrator that can capture the emitted light from a light source (e.g., from the nitrogen vacancies of the diamond of a DNV sensor) to a single photo detector. In some instances, the loss of emitted light can be limited to the light loss due to the mount for the diamond and/or the small entrance for the green stimulation laser beam.

The foregoing solution provides high light collection efficiency to collect the light emitted from the diamond **1602**, while utilizing a parabolic reflector **1604** that may not require high precision refinements. Such a parabolic reflector **1604** may be a low cost solution to increase the light collection efficiency, such as using a reflective mirror component. In addition, the shape of the parabolic reflector **1604** may separate the electronics of the photo detector **1620** from the diamond **1602**, which may decrease the magnetic interaction between the electronics of the photo detector **1620** and the diamond **1602**.

The parabolic reflector **1604** may, in some implementations, include a substrate with a dielectric mirror film or coating applied to reflect the emitted light **1610**. The dielectric mirror film may be selected for the specific frequency of interest. In some implementations, the thickness of the dielectric mirror material may affect the specific frequency of interest. For instance, the substrate may possess a high clarity at a frequency of interest for the DNV sensor. The substrate may be made of a plastic, glass, diamond, quartz, and/or any other suitable material. The dielectric mirror film may be applied to the substrate such that the light emitted **1610** from the diamond **1602** is reflected within the parabolic reflector **1604**. In some implementations, the dielectric mirror film may only reflect red light such that other colors or wavelengths of light pass through the parabolic reflector **1604**. For instance, such a dielectric mirror film may permit transmission of green wavelength light, such as from an excitation laser beam, through the parabolic reflector **1604** to the diamond **1602** to excite the diamond **1602**.

In some aspects, such as for precision sensors, the separation between the diamond **1602** and the electronics of the photo detector **1620** can be extended, for example to several feet. In some implementations, the thin dielectric mirror film is used in the parabolic reflector **1604** to allow an RF antenna to be located inside the parabolic reflector **1604**. In some applications, the antenna may instead be outside of the parabolic reflector **1604**.

FIG. **17** depicts an assembly **1700** for a DNV sensor that incorporates the assembly **1400** of FIG. **15** where the diamond **1402** is formed or machined into a parabolic configuration. The assembly **1700** includes the photo detector **1420** coupled to and/or positioned to receive the emitted light **1410** from the diamond **1402**. The diamond **1402** includes the dielectric mirror film applied to the diamond **1402** to reflect the emitted red light **1410** within the diamond **1402**. In some implementations, the dielectric mirror film may only reflect red light such that other colors or wavelengths of light pass through the diamond **1402**. For instance, such a dielectric mirror film may permit transmission of green wavelength light **1710**, such as from an excitation laser beam, through the dielectric mirror film to the nitrogen vacancies of the diamond **1402** to excite the nitrogen vacancies of the diamond **1402**. The assembly **1700** includes microwave coils about the diamond **1402** such that, if the diamond **1402** is irradiated with microwaves at a certain frequency, then the diamond will cease and/or reduce the emission of red light. A microwave off is performed for the DNV sensor prior to illumination of the diamond **1402** to emit the red light **1410**. When the microwave frequency is moved to a different frequency, then the red light emitted is dimmed and the frequency is related to the strength of the magnetic field the DNV sensor is within.

In some implementations, the green light **1710** from the green laser may be applied through a fiber, rather than the free air, to the diamond **1402**. In some implementations, the entire apparatus of FIG. **17** may be as compact as ~2 mm. The assembly of the subject technology may be used in a number of applications, for example, in all areas of magnetometry, where DNV magnetometers are employed.

FIG. **18** depicts another implementation of a reflector configuration for an assembly **1800** for a DNV sensor that includes a waveguide **1830** positioned within the reflector to direct light to a diamond **1802** having nitrogen vacancies. An example diamond **1802** having nitrogen vacancies may be inserted into a portion of a reflector **1804** positioned about the diamond **1802** for a DNV light-collection apparatus. In some implementations, the reflector **1804** may be a parabolic reflector or an ellipsoidal reflector. The reflector **1804** can be a single monolithic component or can be a shell component with a fill, such as plastic or fiber optic material, or without a fill (e.g., empty). In the implementation shown,

a waveguide **1830** is formed or inserted along an axis of symmetry of the parabolic reflector **1804**. In other implementations, the waveguide **1830** is formed or inserted along a major axis of an ellipsoidal reflector **1804**. The waveguide **1830** may be a fiber optic component and/or may simply be a material having a differing refractive index than the reflector **1804** and/or the fill within the reflector **1804**.

The diamond **1802** is positioned at an end of the waveguide **1830** such that an excitation beam, such as green laser light, can be transmitted via the waveguide **1830** to the diamond **1802**. When the diamond **1802** is excited (e.g., by applying green light to the diamond **1802**), then the reflector **1804** reflects the red light emitted **1810** from the diamond **1802** towards a photo detector **1820**. In the implementation shown, a photo detector **1820** is positioned to receive and measure the light from the reflector **1804**. In some implementations the photo detector **1820** is coupled and/or sealed to a portion of the reflector **1804**. In some implementations, an opening for transmitting the excitation beam is through the photo detector **1820** such that the excitation beam can be transmitted via the waveguide **1830** to the diamond **1802**. In other implementations, an emitter to emit light to excite the nitrogen vacancy of the diamond **1802**, such as the excitation beam, may be provided at a first end of the waveguide **1830** with the diamond **1802** at a second end of the waveguide **1830**. In some implementations, the emitter may be formed and/or positioned within or at a center of the photo detector **1820** to generate and transmit the excitation beam along the waveguide **1830** to the diamond **1802**. The photo detector **1820** and emitter may be positioned on a single substrate. Thus, a single chip can include both the photo detector **1820** and the emitter for the excitation beam such that both the illumination and collection can be provided on the single chip.

In some implementations, an optical filter, such as a red filter, may be applied to and/or positioned on the photo detector **1820** to filter out light except the relevant red light of interest. Thus, the reflector **1804** is concatenated with a non-focusing concentrator that can capture the emitted light from a light source (e.g., from the nitrogen vacancies of the diamond of a DNV sensor) to a single photo detector. In some instances, the loss of emitted light can be limited to the light loss due to the mount for the diamond and/or any emitted light that travels back down the waveguide **1830**.

The foregoing solution provides high light collection efficiency to collect the light emitted from the diamond **1802**, while utilizing a reflector **1804** that may not require high precision refinements. Such a reflector **1804** may be a low cost solution to increase the light collection efficiency, such as using a reflective mirror component. In addition, the shape of the parabolic reflector **1804** may separate the electronics of the photo detector **1820** and/or emitter from the diamond **1802**, which may decrease the magnetic interaction between the electronics of the photo detector **1820** and/or emitter and the diamond **1802**.

The reflector **1804** may, in some implementations, include a substrate with a dielectric mirror film or coating applied to reflect the emitted light **1810**. The dielectric mirror film may be selected for the specific frequency of interest. In some implementations, the thickness of the dielectric mirror material may affect the specific frequency of interest. For instance, the substrate may possess a high clarity at a frequency of interest for the DNV sensor. The substrate may be made of a plastic, glass, diamond, quartz, and/or any other suitable material. The dielectric mirror film may be applied to the substrate such that the light emitted **1810** from the diamond **1802** is reflected within the reflector **1804**. In some implementations, the dielectric mirror film may only reflect red light such that other colors or wavelengths of light pass through the reflector **1804**.

In some aspects, such as for precision sensors, the separation between the diamond **1802** and the electronics of the photo detector **1820** can be extended, for example to several feet. In some implementations, the thin dielectric mirror film is used in the reflector **1804** to allow an RF antenna to be located inside the reflector **1804**. In some applications, the antenna may instead be outside of the reflector **1804**.

FIG. **19** depicts an implementation of a process **1900** to form a DNV sensor. The process **1900** includes providing a diamond having a nitrogen vacancy (block **1902**), machining a portion of the diamond to form a reflector (block **1904**), positioning a photo detector relative to the diamond to receive light emitted from the diamond (block **1906**), and/or applying a dielectric mirror film coat to a portion of the diamond (block **1908**). In some implementations, the process **1900** may include simple providing a diamond having a nitrogen vacancy (block **1902**) and applying a dielectric mirror film coat to a portion of the diamond (block **1908**).

In some implementations, the machining of the diamond to form a reflector (block **1904**) may machine a portion of the diamond to form a parabolic shape, an ellipsoidal shape, and/or any other suitable shape. In some implementations, a layer of the diamond may not have nitrogen vacancies.

FIG. **20** depicts another process **2000** to form a DNV sensor. The process **2000** includes providing a diamond having a nitrogen vacancy and a reflector (block **2002**), positioning the diamond within the reflector such that the reflector reflects a portion of the light from the diamond (block **2004**), and/or positioning a photo detector relative to the diamond to receive light emitted from the diamond (block **2006**).

In some implementations, the reflector is monolithic and the diamond is positioned within a borehole of the monolithic reflector. In some implementations, the borehole may be backfilled. In some implementations, the reflector may be formed from two or more pieces and positioning the diamond within the reflector includes inserting the diamond between the two or more pieces. In some instances, the diamond may be substantially flat, such as in the configuration shown in FIGS. **15-16**. The two or more pieces of the reflector may be parabolic in shape. The diamond may be positioned parallel to an axis of symmetry of the parabolic reflector or may be positioned perpendicular to the axis of symmetry. In other implementations, the two or more pieces of the reflector may be ellipsoidal in shape. The diamond may be positioned parallel to a major axis of the ellipsoidal reflector or may be positioned parallel to a minor axis of the ellipsoidal reflector. In some further implementations, positioning the diamond within the reflector may include casting the reflector about the diamond.

FIG. **21** is a diagram illustrating an example of a system **2100** for implementing some aspects of the subject technology. In some implementations, the system **2100** may be a processing system for processing the data output from a photo detector of the implementations describe in reference to FIGS. **11-19**. The system **2100** includes a processing system **2102**, which may include one or more processors or one or more processing systems. A processor can be one or more processors. The processing system **2102** may include a general-purpose processor or a specific-purpose processor for executing instructions and may further include a machine-readable medium **2119**, such as a volatile or non-volatile memory, for storing data and/or instructions for software programs. The instructions, which may be stored in

a machine-readable medium **2110** and/or **2119**, may be executed by the processing system **2102** to control and manage access to the various networks, as well as provide other communication and processing functions. The instructions may also include instructions executed by the processing system **2102** for various user interface devices, such as a display **2112** and a keypad **2114**. The processing system **2102** may include an input port **2122** and an output port **2124**. Each of the input port **2122** and the output port **2124** may include one or more ports. The input port **2122** and the output port **2124** may be the same port (e.g., a bi-directional port) or may be different ports.

The processing system **2102** may be implemented using software, hardware, or a combination of both. By way of example, the processing system **2102** may be implemented with one or more processors. A processor may be a general-purpose microprocessor, a microcontroller, a Digital Signal Processor (DSP), an Application Specific Integrated Circuit (ASIC), a Field Programmable Gate Array (FPGA), a Programmable Logic Device (PLD), a controller, a state machine, gated logic, discrete hardware components, or any other suitable device that can perform calculations or other manipulations of information.

A machine-readable medium can be one or more machine-readable media. Software shall be construed broadly to mean instructions, data, or any combination thereof, whether referred to as software, firmware, middleware, microcode, hardware description language, or otherwise. Instructions may include code (e.g., in source code format, binary code format, executable code format, or any other suitable format of code).

Machine-readable media (e.g., **2119**) may include storage integrated into a processing system such as might be the case with an ASIC. Machine-readable media (e.g., **2110**) may also include storage external to a processing system, such as a Random Access Memory (RAM), a flash memory, a Read Only Memory (ROM), a Programmable Read-Only Memory (PROM), an Erasable PROM (EPROM), registers, a hard disk, a removable disk, a CD-ROM, a DVD, or any other suitable storage device. Those skilled in the art will recognize how best to implement the described functionality for the processing system **2102**. According to one aspect of the disclosure, a machine-readable medium is a computer-readable medium encoded or stored with instructions and is a computing element, which defines structural and functional interrelationships between the instructions and the rest of the system, which permit the instructions' functionality to be realized. Instructions may be executable, for example, by the processing system **2102** or one or more processors. Instructions can be, for example, a computer program including code for performing methods of the subject technology.

A network interface **2116** may be any type of interface to a network (e.g., an Internet network interface), and may reside between any of the components shown in FIG. **21** and coupled to the processor via the bus **2104**.

A device interface **2118** may be any type of interface to a device and may reside between any of the components shown in FIG. **21**. A device interface **2118** may, for example, be an interface to an external device (e.g., USB device) that plugs into a port (e.g., USB port) of the system **2100**. In some implementations, the device interface **2118** may be an interface to the apparatus of FIGS. **10-18**, where some or all of the analysis of the detected red light by the photo detector electronics is handled by the processing system **2102**.

The foregoing description is provided to enable a person skilled in the art to practice the various configurations described herein. While the subject technology has been particularly described with reference to the various figures and configurations, it should be understood that these are for illustration purposes only and should not be taken as limiting the scope of the subject technology.

One or more of the above-described features and applications may be implemented as software processes that are specified as a set of instructions recorded on a computer readable storage medium (alternatively referred to as computer-readable media, machine-readable media, or machine-readable storage media). When these instructions are executed by one or more processing unit(s) (e.g., one or more processors, cores of processors, or other processing units), they cause the processing unit(s) to perform the actions indicated in the instructions. In one or more implementations, the computer readable media does not include carrier waves and electronic signals passing wirelessly or over wired connections, or any other ephemeral signals. For example, the computer readable media may be entirely restricted to tangible, physical objects that store information in a form that is readable by a computer. In one or more implementations, the computer readable media is non-transitory computer readable media, computer readable storage media, or non-transitory computer readable storage media.

In one or more implementations, a computer program product (also known as a program, software, software application, script, or code) can be written in any form of programming language, including compiled or interpreted languages, declarative or procedural languages, and it can be deployed in any form, including as a stand-alone program or as a module, component, subroutine, object, or other unit suitable for use in a computing environment. A computer program may, but need not, correspond to a file in a file system. A program can be stored in a portion of a file that holds other programs or data (e.g., one or more scripts stored in a markup language document), in a single file dedicated to the program in question, or in multiple coordinated files (e.g., files that store one or more modules, sub programs, or portions of code). A computer program can be deployed to be executed on one computer or on multiple computers that are located at one site or distributed across multiple sites and interconnected by a communication network.

While the above discussion primarily refers to microprocessor or multi-core processors that execute software, one or more implementations are performed by one or more integrated circuits, such as application specific integrated circuits (ASICs) or field programmable gate arrays (FPGAs). In one or more implementations, such integrated circuits execute instructions that are stored on the circuit itself.

In one or more implementations, the subject technology is directed to method and systems for an efficient collection of fluorescence (e.g., red light) emitted by the NV centers of a DNV sensor. In some aspects, the subject technology may be used in various markets, including for example and without limitation, advanced sensors and materials and structures.

Precision Position Encoder/Sensor Using Nitrogen Vacancy Diamond

A position sensor system may include a position sensor that includes a magnetic field sensor. The magnetic field sensor may be a DNV magnetic field sensor capable of resolving a magnetic field vector of the type described above. The high sensitivity of the DNV magnetic field sensor combined with an appropriate position encoder component is capable of resolving both a discrete position and a proportionally determined position between discrete positions. The position sensor system has a small size, light weight, and low power requirement.

As shown in FIG. **22**, the position sensor **2220** may be part of a system that also includes an actuator **2210** and a sensor component **2230**. The actuator **2210** may be connected to the position sensor **2220** by any appropriate attachment means **2214**, such as a rod or shaft. The actuator may be any actuator that produces the desired motion, such as an electro-mechanical actuator. The position sensor **2220** may be connected to the sensor component **2230** by any appropriate attachment means **2224**, such as a rod or shaft. A controller **2240** may be included in the system and connected to the position sensor **2220** and optionally the actuator **2210** by electronic interconnects **2222** and **2212**, respectively. The controller may be configured to receive a measured position from the position sensor **2220** and activate or deactivate the actuator to position the sensor **2230** in a desired position. According to one embodiment the controller may be on the same substrate as the magnetic field sensor of the position sensor. The controller may include a processor and a memory.

The position sensor may be a rotary position sensor. FIG. **23** depicts a rotary position sensor system that includes a rotary actuator **2380** that is configured to produce a rotation of a sensor **2390**. A rotary position encoder **2310** is connected to the rotary actuator **2380** by a connection means **2382**, such as a rod or shaft. A connection means **2392** is also provided between the rotary position encoder **2310** and the sensor **2390**. A position sensor head **2320** is located to measure the magnetic field of magnetic elements located on the rotary position encoder **2310**. The position sensor head **2320** is aligned with magnetic elements located on the rotary position encoder **2310** at a distance, r, from the center of the rotary position encoder. A surface of the rotary position encoder **2310** that includes magnetic elements is shown in FIG. **24**. The center **2440** of the rotary position encoder **2310** may be configured to attach to a connection means **2392**, **2394** that connects the rotary position encoder **2310** to the actuator **2320** or the sensor **2390**. Magnetic elements, such as uniform coarse magnetic elements **2434** and tapered fine magnetic elements **2432**, may be disposed on the surface of the rotary position encoder **2310** along an arc **2436** at a distance, r, from the center of the rotary position encoder. The magnetic elements on the rotary position encoder **2310** may be located on only a portion of the arc, as shown in FIG. **24**, or around an entirety of the arc forming a circle of magnetic elements.

The spacing between the magnetic elements on the rotary position encoder **2310** correlates to a discrete angular rotation, θ. The distance between magnetic elements associated with the discrete angular rotation, θ, increases as r increases. The sensitivity of the magnetic field sensors employed in the position sensor allows r to be reduced while maintaining a high degree of precision for the angular position of the rotary position encoder. The rotary position encoder may have an r on the order of mm, such as an r of 1 mm to about 30 mm, or about 5 mm to about 20 mm. The rotary position encoder allows for the measurement of a rotary position with a precision of 0.5 micro-radians.

The position sensor may be a linear position sensor. As shown in FIG. **25**, the linear position sensor system includes a linear actuator **2580** that is configured to produce linear motion of the linear position encoder **2510** and sensor **2590**. The linear position encoder **2510** may be connected to the linear actuator by a connecting means **2582**, such as a rod or shaft. The linear position encoder **2510** may be connected to the sensor **2590** by a connecting means **2592**, such as a rod or shaft. A position sensor head **2520** is located to measure the magnetic field produced by magnetic elements disposed on the linear position encoder. In some cases, a mechanical linkage, such as a lever arm, may be utilized to multiply the change in position of the linear position encoder for an associated movement of the sensor. The linear position sensor may have a sensitivity that allows a change in position on the order of hundreds of nanometers to be resolved, such as a position change of 500 nm.

The magnetic elements may be arranged on the linear or rotary position encoder in any appropriate configuration. As shown in FIG. **26**, the magnetic elements may include both uniform coarse magnetic elements **2634** and tapered fine magnetic elements **2632**. The uniform coarse magnetic elements **2634** may have an influence on the local magnetic field that is at least two orders of magnitude greater than the maximum influence of the tapered fine magnetic elements **2634**. The coarse magnetic elements **2634** may be formed on the position encoder by any suitable process. According to one embodiment, a polymer loaded with magnetic material may be utilized to form the uniform coarse magnetic elements. The amount of magnetic material that may be included in the coarse magnetic elements is limited by potential interference with other elements in the system.

The tapered fine magnetic elements may be formed by any suitable process on the position encoder. According to one embodiment, a polymer loaded with magnetic material may be utilized to form the tapered fine magnetic elements. The loading of the magnetic material in the polymer may be increased to produce a magnetic field gradient from a first end of the tapered fine magnetic element to a second end of the tapered fine magnetic element. Alternatively, the geometric size of the tapered fine magnetic element may be increased to create the desired magnetic field gradient. A magnetic field gradient of the tapered fine magnetic element may be about 10 nT/mm. The tapered fine magnetic elements **2632** as shown in FIG. **26** allow positions between the coarse magnetic elements **2634** to be accurately resolved. The position encoder on which the magnetic elements are disposed may be formed from any appropriate material, such as a ceramic, glass, polymer, or non-magnetic metal material.

The size of the magnetic elements is limited by manufacturing capabilities. The magnetic elements on the position encoder may have geometric features on the order of nanometers, such as about 5 nm.

FIG. **27** depicts an alternate magnetic element arrangement that may be employed when the additional precision provided by the tapered fine magnetic elements is not required. The magnetic element arrangement of FIG. **27** includes only coarse magnetic elements **2634**. FIG. **13** depicts a magnetic element arrangement that does not include coarse magnetic elements. A similar effect to the coarse magnetic elements **2634** may be achieved by utilizing the transitions between the maximum of the tapered fine magnetic elements **2632** and the minimum of the adjacent tapered fine magnetic elements as indicators in much the same way that the coarse magnetic elements shown in FIGS. **26** and **27** indicate a discrete change in position. While FIGS. **26-18** depict the magnetic element arrangements in linear form, similar magnetic element arrangements may be applied to a rotary position encoder.

According to an alternative embodiment, a single tapered magnetic element may be employed. Such an arrangement may be especially suitable for an application where only a small position range is required, as for a larger position range the increase in magnetic field with the increasing gradient of the magnetic element may interfere with other components of the position sensor system. The use of a

single tapered magnetic element may allow a position to be determined without first initializing the position sensor by setting the position encoder to a known position. The ability of the magnetic field sensor to resolve a magnetic field vector may allow a single magnetic field sensor to be employed in the position sensor head when a single tapered fine magnetic element is utilized on the position encoder.

The position sensor head **2620** may include a plurality of magnetic field sensors, as shown in FIG. **29**. For magnetic element arrangements including more than one element, at least two magnetic field sensors **2624** and **2622** may be utilized in the position head sensor. The magnetic field sensors may be separated by a distance, a. The distance, a, between the magnetic sensors **2622** and **2624** may be less than the distance, d, between the coarse magnetic elements **2634**. According to one embodiment, the relationship between the spacing of the magnetic field sensors and the spacing of the coarse magnetic elements may be 0.1 d<a<d. As shown in FIG. **29**, the position sensor head **2620** may include a third and fourth magnetic field sensor. The magnetic field sensors in the position sensor head may be DNV magnetic field sensors of the type described above.

The magnetic field sensor arrangement in the position sensor head **2620** depicted in FIG. **29** allows the direction of movement of the position encoder to be determined. As shown in FIG. **30**, the spacing between the magnetic field sensors **2624** and **2622** produces a delayed response to the magnetic field elements as the position encoder moves. The difference in measured magnetic field for each magnetic field sensor allows a direction of the movement of the position encoder to be determined, as for any given position of the position encoder a different output magnetic field will be measured by each magnetic field sensor. The increasing portion of the plots in FIG. **30** is produced by the tapered fine magnetic element and the square peak is produced by the coarse magnetic element. These measured magnetic fields may be utilized to determine the change in position of the position encoder, and thereby the sensor connected to the position encoder.

The controller of the position sensor system may be programmed to determine the position of position encoder, and thereby the sensor connected thereto, utilizing the output from the magnetic field sensors. As shown in FIG. **31**, the controller may include a line transection logic **402** function that determines when the coarse magnetic elements have passed the magnetic sensor. The output from two magnetic field sensors B**1** and B**2** may be utilized to determine the direction of the position change based on the order in which a coarse magnetic element is encountered by the magnetic field sensors, and to count the number of coarse magnetic elements measured by the magnetic field sensors. Each coarse magnetic element adds a known amount of position change due to the known spacing between the coarse magnetic elements on the position encoder. An element gradient logic processing function **400** is programmed in the controller to determine the position between coarse magnetic elements based on the magnetic field signal produced by the tapered fine magnetic elements located between the coarse magnetic elements. As shown in FIG. **31**, the element gradient logic processing **400** is utilized only when the line transection logic determines that the position is between coarse magnetic elements, or lines. In the case that the position is determined to be between coarse magnetic elements, a position correction, $\delta\theta$, is calculated based on the magnetic field associated with the tapered fine magnetic elements. The position correction is then added to the sum of the position change calculated from the number of coarse magnetic elements that were counted. A final position may be calculated by adding the calculated position change to a starting position of the position encoder. The logic processing in the controller may be conducted by analog or digital circuits.

The position sensor may be employed in a method for controlling the position of the position encoder. The method includes determining a movement direction required to reach a desired position, and activating the actuator to produce the desired movement. The position sensor is employed to monitor the change in position of the position encoder, and determine when to deactivate the actuator and stop the change in position. The change in position may be stopped once the desired position is reached. The method may additionally include initializing the position sensor system by moving the position encoder to a known starting point. The end position of the position encoder may be determined after the deactivation of the actuator, and the end position may be stored in a memory of the position sensor controller as a starting position for future movement.

The ability of the position sensor system to resolve positions between the coarse magnetic elements of the position encoder provides many practical benefits. For example, the position of the position encoder, and associated sensor, may be known with more precision while reducing the size, weight and power requirements of the position sensor system. Additionally, position control systems that offer resolution of discrete position movements can result in dithering when a desired position is between two discrete position values. Dithering can result in unwanted vibration and overheating of the actuator as the control system repeatedly tries to reach the desired position.

The characteristics of the position sensor system described above make it especially suitable for applications where precision, size, weight, and power requirements are important considerations. The position sensor system is well suited for astronautic applications, such as on space vehicles. The position sensor system is also applicable to robot arms, 3-d mills, machine tools, and X-Y tables.

The position sensor system may be employed to control the position of a variety of sensors and other devices. Non-limiting examples of sensors that could be controlled with the position sensor system are optical sensors.

Communication Via a Magnio

Radio waves can be used as a carrier for information. Thus, a transmitter can modulate radio waves at one location, and a receiver at another location can detect the modulated radio waves and demodulate the signals to receive the information. Many different methods can be used to transmit information via radio waves. However, all such methods use radio waves as a carrier for the information being transmitted.

However, radio waves are not well suited for all communication methods. For example, radio waves can be greatly attenuated by some materials. For example, radio waves do not generally travel well through water. Thus, communication through water can be difficult using radio waves. Similarly, radio waves can be greatly attenuated by the earth. Thus, wireless communication through the earth, for example for coal or other mines, can be difficult. It is often difficult to communicate wirelessly via radio waves from a metal enclosure. The strength of a radio wave signal can also be reduced as the radio wave passes through materials such as walls, trees, or other obstacles. Additionally, communication via radio waves is widely used and understood. Thus,

secret communication using radio waves requires complex methods and devices to maintain the secrecy of the information.

According to some embodiments described herein, wireless communication is achieved without using radio waves as a carrier for information. Rather, modulated magnetic fields can be used to transmit information. For example, a transmitter can include a coil or inductor. When current passes through the coil, a magnetic field is generated around the coil. The current that passes through the coil can be modulated, thereby modulating the magnetic field. Accordingly, information converted into a modulated electrical signal (e.g., the modulated current through the coil) can be used to transfer the information into a magnetic field. A magnetometer can be used to monitor the magnetic field. The modulated magnetic field can, therefore, be converted into traditional electrical systems (e.g., using current to transfer information). Thus, a communications signal can be converted into a magnetic field and a remote receiver (e.g., a magnetometer) can be used to retrieve the communication from the modulated magnetic field.

A diamond with a nitrogen vacancy (DNV) can be used to measure a magnetic field. DNV sensors generally have a quick response to magnetic fields, consume little power, and are accurate. Diamonds can be manufactured with nitrogen vacancy (NV) centers in the lattice structure of the diamond. When the NV centers are excited by light, for example green light, and microwave radiation, the NV centers emit light of a different frequency than the excitation light. For example, green light can be used to excite the NV centers, and red light can be emitted from the NV centers. When a magnetic field is applied to the NV centers, the frequency of the light emitted from the NV centers changes. Additionally, when the magnetic field is applied to the NV centers, the frequency of the microwaves at which the NV centers are excited changes. Thus, by shining a green light (or any other suitable color) through a DNV and monitoring the light emitted from the DNV and the frequencies of microwave radiation that excite the NV centers, a magnetic field can be monitored.

NV centers in a diamond are oriented in one of four spin states. Each spin state can be in a positive direction or a negative direction. The NV centers of one spin state do not respond the same to a magnetic field as the NV centers of another spin state. A magnetic field vector has a magnitude and a direction. Depending upon the direction of the magnetic field at the diamond (and the NV centers), some of the NV centers will be excited by the magnetic field more than others based on the spin state of the NV centers.

FIGS. **32**A and **32**B are graphs illustrating the frequency response of a DNV sensor in accordance with an illustrative embodiment. FIGS. **32**A and **32**B are meant to be illustrative only and not meant to be limiting. FIGS. **32**A and **32**B plot the frequency of the microwaves applied to a DNV sensor on the x-axis versus the amount of light of a particular frequency (e.g., red) emitted from the diamond. FIG. **32**A is the frequency response of the DNV sensor with no magnetic field applied to the diamond, and FIG. **32**B is the frequency response of the DNV sensor with a seventy gauss (G) magnetic field applied to the diamond.

As shown in FIG. **32**A, when no magnetic field is applied to the DNV sensor, there are two notches in the frequency response. With no magnetic field applied to the DNV sensor, the spin states are not resolvable. That is, with no magnetic field, the NV centers with various spin states are equally excited and emit light of the same frequency. The two notches shown in FIG. **32**A are the result of the positive and negative spin directions. The frequency of the two notches is the axial zero field splitting parameter.

When a magnetic field is applied to the DNV sensor, the spin states become resolvable in the frequency response. Depending upon the excitation by the magnetic field of NV centers of a particular spin state, the notches corresponding to the positive and negative directions separate on the frequency response graph. As shown in FIG. **32**B, when a magnetic field is applied to the DNV sensor, eight notches appear on the graph. The eight notches are four pairs of corresponding notches. For each pair of notches, one notch corresponds to a positive spin state and one notch corresponds to a negative spin state. Each pair of notches corresponds to one of the four spin states of the NV centers. The amount by which the pairs of notches deviate from the axial zero field splitting parameter is dependent upon how strongly the magnetic field excites the NV centers of the corresponding spin states.

As mentioned above, the magnetic field at a point can be characterized with a magnitude and a direction. By varying the magnitude of the magnetic field, all of the NV centers will be similarly affected. Using the graph of FIG. **32**A as an example, the ratio of the distance from 2.87 GHz of one pair to another will remain the same when the magnitude of the magnetic field is altered. As the magnitude is increased, each of the notch pairs will move away from 2.87 GHz at a constant rate, although each pair will move at a different rate than the other pairs.

When the direction of the magnetic field is altered, however, the pairs of notches do not move in a similar manner to one another. FIG. **33**A is a diagram of NV center spin states in accordance with an illustrative embodiment. FIG. **33**A conceptually illustrates the four spin states of the NV centers. The spin states are labeled NV A, NV B, NV C, and NV D. Vector **3301** is a representation of a first magnetic field vector with respect to the spin states, and Vector **3302** is a representation of a second magnetic field vector with respect to the spin states. Vector **3301** and vector **3302** have the same magnitude, but differ in direction. Accordingly, based on the change in direction, the various spin states will be affected differently depending upon the direction of the spin states.

FIG. **33**B is a graph illustrating the frequency response of a DNV sensor in response to a changed magnetic field in accordance with an illustrative embodiment. The frequency response graph illustrates the frequency response of the DNV sensor from the magnetic field corresponding to vector **3301** and to vector **3302**. As shown in FIG. **33**B, the notches corresponding to the NV A and NV D spin states moved closer to the axial zero field splitting parameter from vector **3301** to vector **3302**, the negative (e.g., lower frequency notch) notch of the NV C spin state moved away from the axial zero field splitting parameter, the positive (e.g., high frequency notch) of the NV C spin state stayed essentially the same, and the notches corresponding to the NV B spin state increased in frequency (e.g., moved to the right in the graph). Thus, by monitoring the changes in frequency response of the notches, the DNV sensor can determine the direction of the magnetic field.

Additionally, magnetic fields of different directions can be modulated simultaneously and each of the modulations can be differentiated or identified by the DNV sensor. For example, a magnetic field in the direction of NV A can be modulated with a first pattern, a magnetic field in the direction of NV B can be modulated with a second pattern, a magnetic field in the direction of NV C can be modulated with a third pattern, and a magnetic field in the direction of

NV D can be modulated with a fourth pattern. The movement of the notches in the frequency response corresponding to the various spin states can be monitored to determine each of the four patterns.

However, in some embodiments, the direction of the magnetic field corresponding to the various spin states of a DNV sensor of a receiver may not be known by the transmitter. In such embodiments, by monitoring at least three of the spin states, messages transmitted on two magnetic fields that are orthogonal to one another can be deciphered. Similarly, by monitoring the frequency response of the four spin states, messages transmitted on three magnetic fields that are orthogonal to one another can be deciphered. Thus, in some embodiments, two or three independent signals can be transmitted simultaneously to a receiver that receives and deciphers the two or three signals. Such embodiments can be a multiple-input multiple-output (MIMO) system. Diversity in the polarization of the magnetic field channels provides a full rank channel matrix even through traditionally keyhole channels. In an illustrative embodiment, a full rank channel matrix allows MIMO techniques to leverage all degrees of freedom (e.g., three degrees of polarization). Using a magnetic field to transmit information circumvents the keyhole effect that propagating a radio frequency field can have.

FIG. **34** is a block diagram of a magnetic communication system in accordance with an illustrative embodiment. An illustrative magnio system **3400** includes input data **3405**, a **3410**, a transmitter **3445**, a modulated magnetic field **3450**, a magnetometer **3455**, a magnio receiver **3460**, and output data **3495**. In alternative embodiments, additional, fewer, and/or different elements may be used.

In an illustrative embodiment, input data **3405** is input into the magnio system **3400**, transmitted wirelessly, and the output data **3495** is generated at a location remote from the generation of the input data **3405**. In an illustrative embodiment, the input data **3405** and the output data **3495** contain the same information.

In an illustrative embodiment, input data **3405** is sent to the magnio transmitter **3410**. The magnio transmitter **3410** can prepare the information received in the input data **3405** for transmission. For example, the magnio transmitter **3410** can encode or encrypt the information in the input data **3405**. The magnio transmitter **3410** can send the information to the transmitter **3445**.

The transmitter **3445** is configured to transmit the information received from the magnio transmitter **3410** via one or more magnetic fields. The transmitter **3445** can be configured to transmit the information on one, two, three, or four magnetic fields. That is, the transmitter **3445** can transmit information via a magnetic field oriented in a first direction, transmit information via a magnetic field oriented in a second direction, transmit information via a magnetic field oriented in a third direction, and/or transmit information via a magnetic field oriented in a fourth direction. In some embodiments in which the transmitter **3445** transmits information via two or three magnetic fields, the magnetic fields can be orthogonal to one another. In alternative embodiments, the magnetic fields are not orthogonal to one another.

The transmitter **3445** can be any suitable device configured to create a modulated magnetic field. For example, the transmitter **3445** can include one or more coils. Each coil can be a conductor wound around a central axis. For example, in embodiments in which the information is transmitted via three magnetic fields, the transmitter **3445** can include three coils. The central axis of each coil can be orthogonal to the central axis of the other coils.

The transmitter **3445** generates the modulated magnetic field **3450**. The magnetometer **3455** can detect the modulated magnetic field **3450**. The magnetometer **3455** can be located remotely from the transmitter **3445**. For example, with a current of about ten Amperes through a coil (e.g., the transmitter) and with a magnetometer magnetometer **3455** with a sensitivity of about one hundred nano-Tesla, a message can be sent, received, and recovered in full with several meters between the transmitter and receiver and with the magnetometer magnetometer **3455** inside of a Faraday cage. The magnetometer **3455** can be configured to measure the modulated magnetic field **3450** along three or four directions. As discussed above, a magnetometer **3455** using a DNV sensor can measure the magnetic field along four directions associated with four spin states. The magnetometer **3455** can transmit information, such as frequency response information, to the magnio receiver **3460**.

The magnio receiver **3460** can analyze the information received from the magnetometer **3455** and decipher the information in the signals. The magnio receiver **3460** can reconstitute the information contained in the input data **3405** to produce the output data **3495**.

In an illustrative embodiment, the magnio transmitter **3410** includes a data packet generator **3415**, an outer encoder **3420**, an interleaver **3425**, an inner encoder **34340**, an interleaver **34345**, and an output packet generator **3440**. In alternative embodiments, additional, fewer, and/or different elements may be used. The various components of the magnio transmitter **310** are illustrated in FIG. **34** as individual components and are meant to be illustrative only. However, in alternative embodiments, the various components may be combined. Additionally, the use of arrows is not meant to be limiting with respect to the order or flow of operations or information. Any of the components of the magnio transmitter **3410** can be implemented using hardware and/or software.

The input data **3405** can be sent to the data packet generator **3415**. In an illustrative embodiment, the input data **3405** is a series or stream of bits. The data packet generator **3415** can break up the stream of bits into packets of information. The packets can be any suitable size. In an illustrative embodiment, the data packet generator **3415** includes appending a header to the packets that includes transmission management information. In an illustrative embodiment the header can include information used for error detection, such as a checksum. Any suitable header may be used. In some embodiments, the input data **3405** is not broken into packets.

The stream of data generated by the data packet generator **3415** can be sent to the outer encoder **3420**. The outer encoder **3420** can encrypt or encode the stream using any suitable cypher or code. Any suitable type of encryption can be used such as symmetric key encryption. In an illustrative embodiment, the encryption key is stored on memory associated with the magnio transmitter **3410**. In an illustrative embodiment, the magnio transmitter **3410** may not include the outer encoder **3420**. For example, the messages may not be encrypted. In an illustrative embodiment, the outer encoder **3420** separates the stream into multiple channels. In an illustrative embodiment, the outer encoder outer encoder **3420** performs forward error correction (FEC). In some embodiments, the forward error correction dramatically increases the reliability of transmissions for a given power level.

In an illustrative embodiment, the encoded stream from the outer encoder **3420** is sent to the interleaver **3425**. In an illustrative embodiment, the interleaver **3425** interleaves bits

within each packet of the stream of data. In such an embodiment, each packet has the same bits, but the bits are shuffled according to a predetermined pattern. Any suitable interleaving method can be used. In an alternative embodiment, the packets are interleaved. In such an embodiment, the packets are shuffled according to a predetermined pattern. In some embodiments, the magnio transmitter **3410** may not include the interleaver **3425**.

In some embodiments, interleaving data can be used to prevent loss of a sequence of data. For example, if a stream of bits are in sequential order and there is a communication loss during a portion of the stream, there is a relatively large gap in the information corresponding to the lost bits. However, if the bits were interleaved (e.g., shuffled), once the stream is de-interleaved (e.g., unshuffled) at the receiver, the lost bits are not grouped together but are spread across the sequential bits. In some instances, if the lost bits are spread across the message, error correction can be more successful in determining what the lost bits were supposed to be.

In an illustrative embodiment, the interleaved stream from the interleaver **3425** is sent to the inner encoder **3430**. The inner encoder **3430** can encrypt or encode the stream using any suitable cypher or code. Any suitable type of encryption can be used such as symmetric key encryption. In an illustrative embodiment, the encryption key is stored on memory associated with the magnio transmitter **3410**. In an illustrative embodiment, the magnio transmitter **3410** may not include the inner encoder **3430**. In an illustrative embodiment, the inner encoder **3430** and the outer encoder **3420** perform different functions. For example, the inner encoder **3430** can use a deep convolutional code and can perform most of the forward error correction, and the outer encoder can be used to correct residual errors and can use a different coding technique from the inner encoder **3430** (e.g., a block-parity based encoding technique).

In an illustrative embodiment, the encoded stream from the inner encoder **3430** is sent to the interleaver **3435**. In an illustrative embodiment, the interleaver **3435** interleaves bits within each packet of the stream of data. In such an embodiment, each packet has the same bits, but the bits are shuffled according to a predetermined pattern. Any suitable interleaving method can be used. In an alternative embodiment, the packets are interleaved. In such an embodiments, the packets are shuffled according to a predetermined pattern. In an illustrative embodiment, interleaving the data spreads out burst-like errors across the signal, thereby facilitating the decoding of the message. In some embodiment, the magnio transmitter **3410** may not include the interleaver **3435**.

In an illustrative embodiment, the interleaved stream from the interleaver **3435** is sent to the output packet generator **3440**. The output packet generator **3440** can generate the packets that will be transmitted. For example, the output packet generator **3440** may append a header to the packets that includes transmission management information. In an illustrative embodiment the header can include information used for error detection, such as a checksum. Any suitable header may be used.

In an illustrative embodiment, the output packet generator **3440** appends a synchronization sequence to each of the packets. For example, a synchronization sequence can be added to the beginning of each packet. The packets can be transmitted on multiple channels. In such an embodiment, each channel is associated with a unique synchronization sequence. The synchronization sequence can be used to decipher the channels from one another, as is discussed in greater detail below with regard to the magnio receiver **3460**.

In an illustrative embodiment, the output packet generator **3440** modulates the waveform to be transmitted. Any suitable modulation can be used. In an illustrative embodiment, the waveform is modulated digitally. In some embodiments, minimum shift keying can be used to modulate the waveform. For example, non-differential minimum shift key can be used. In an illustrative embodiment, the waveform has a continuous phase. That is, the waveform does not have phase discontinuities. In an illustrative embodiment, the waveform is sinusoidal in nature.

In an illustrative embodiment, the modulated waveform is sent to the transmitter **3445**. In an illustrative embodiment, multiple modulated waveforms are sent to the transmitter **3445**. As mentioned above, two, three, or four signals can be transmitted simultaneously via magnetic fields with different directions. In an illustrative embodiment, three modulated waveforms are sent to the transmitter **3445**. Each of the waveforms can be used to modulate a magnetic field, and each of the magnetic fields can be orthogonal to one another.

The transmitter **3445** can use the received waveforms to produce the modulated magnetic field **3450**. The modulated magnetic field **3450** can be a combination of multiple magnetic fields of different directions. The frequency used to modulate the modulated magnetic field **3450** can be any suitable frequency. In an illustrative embodiment, the carrier frequency of the modulated magnetic field **3450** can be 10 kHz. In alternative embodiments, the carrier frequency of the modulated magnetic field **3450** can be less than or greater than 10 kHz. In some embodiments, the carrier frequency can be modulated to plus or minus the carrier frequency. That is, using the example in which the carrier frequency is 10 kHz, the carrier frequency can be modulated down to 0 Hz and up to 20 kHz. In alternative embodiments, any suitable frequency band can be used.

FIGS. **35**A and **35**B show the strength of a magnetic field versus frequency in accordance with an illustrative embodiment. FIGS. **35**A and **35**B are meant to be illustrative only and not meant to be limiting. In some instances, the magnetic spectrum is relatively noisy. As shown in FIG. **35**A, the noise over a large band (e.g., 0-200 kHz) is relatively high. Thus, communicating over such a large band may be difficult. FIG. **35**B illustrates the noise over a smaller band (e.g., 1-3 kHz). As shown in FIG. **35**B, the noise over a smaller band is relatively low. Thus, modulating the magnetic field across a smaller band of frequencies can be less noisy and more effective. In an illustrative embodiment, the magnio transmitter **3410** can monitor the magnetic field and determine a suitable frequency to modulate the magnetic fields to reduce noise. That is, the magnio transmitter **3410** can find a frequency that has a high signal to noise ratio. In an illustrative embodiment, the magnio transmitter **3410** determines a frequency band that has noise that is below a predetermined threshold.

In an illustrative embodiment, the magnio receiver **3460** includes the demodulator **3465**, the de-interleaver **3470**, the soft inner decoder **3475**, the de-interleaver **3480**, the outer decoder **3485**, and the output data generator **3490**. In alternative embodiments, additional, fewer, and/or different elements may be used. For example, the magnio receiver **3460** can include the magnetometer **3455** in some embodiments. The various components of the magnio receiver **3460** are illustrated in FIG. **34** as individual components and are meant to be illustrative only. However, in alternative embodiments, the various components may be combined.

Additionally, the use of arrows is not meant to be limiting with respect to the order or flow of operations or information. Any of the components of the magnio receiver **3460** can be implemented using hardware and/or software.

The magnetometer **3455** is configured to measure the modulated magnetic field **3450**. In an illustrative embodiment, the magnetometer **3455** includes a DNV sensor. The magnetometer **3455** can monitor the modulated magnetic field **3450** in up to four directions. As illustrated in FIG. **2**A, the magnetometer **3455** can be configured to measure the magnetometer **3455** in one or more of four directions that are tetrahedronally arranged. As mentioned above, the magnetometer **3455** can monitor n+1 directions where n is the number of channels that the transmitter **3445** transmits on. For example, the transmitter **3445** can transmit on three channels, and the magnetometer **3455** can monitor four directions. In an alternative embodiment, the transmitter **3445** can transmit via the same number of channels (e.g., four) as directions that the magnetometer **3455** monitors.

The magnetometer **3455** can send information regarding the modulated magnetic field **3450** to the demodulator **3465**. The demodulator **3465** can analyze the received information and determine the direction of the magnetic fields that were used to create the modulated magnetic field **3450**. That is, the demodulator **3465** can determine the directions of the channels that the transmitter **3445** transmitted on. As mentioned above, the transmitter **3445** can transmit multiple streams of data, and each stream of data is transmitted on one channel. Each of the streams of data can be preceded by a unique synchronization sequence. In an illustrative embodiment, the synchronization sequence includes 1023 bits. In alternative embodiments, the synchronization sequence includes more than or fewer than 1023 bits. Each of the streams can be transmitted simultaneously such that each of the channels are time-aligned with one another. The demodulator **3465** can monitor the magnetic field in multiple directions simultaneously. Based on the synchronization sequence, which is known to the magnio receiver **3460**, the demodulator **3465** can determine the directions corresponding to the channels of the transmitter **3445**. When the streams of synchronization sequences are time-aligned, the demodulator **3465** can monitor the modulated magnetic field **3450** to determine how the multiple channels mixed. Once the demodulator **3465** determines how the various channels are mixed, the channels can be demodulated.

For example, the transmitter **3445** transmits on three channels, with each channel corresponding to an orthogonal direction. Each channel is used to transmit a stream of information. For purposes of the example, the channels are named "channel A," "channel B," and "channel C." The magnetometer **3455** monitors the modulated magnetic field **3450** in four directions. The demodulator **3465** can monitor for three signals in orthogonal directions. For purposes of the example, the signals can be named "signal 1," "signal 2," and "signal 3." Each of the signals can contain a unique, predetermined synchronization sequence. The demodulator **3465** can monitor the modulated magnetic field **3450** for the signals to be transmitted on the channels. There is a finite number of possible combinations that the signals can be received at the magnetometer **3455**. For example, signal 1 can be transmitted in a direction corresponding to channel A, signal 2 can be transmitted in a direction corresponding to channel B, and signal 3 can be transmitted in a direction corresponding to channel C. In another example, signal 2 can be transmitted in a direction corresponding to channel A, signal 3 can be transmitted in a direction corresponding to channel B, and signal 1 can be transmitted in a direction corresponding to channel C, etc. The modulated magnetic field **3450** of the synchronization sequence for each of the possible combinations that the signals can be received at the magnetometer **3455** can be known by the demodulator **3465**. The demodulator **3465** can monitor the output of the magnetometer **3455** for each of the possible combinations. Thus, when one of the possible combinations is recognized by the demodulator **3465**, the demodulator **3465** can monitor for additional data in directions associated with the recognized combination. In another example, the transmitter **3445** transmits on two channels, and the magnetometer **3455** monitors the modulated magnetic field **3450** in three directions.

The demodulated signals (e.g., the received streams of data from each of the channels) is sent to the de-interleaver **3470**. The de-interleaver **3470** can undo the interleaving of the interleaver **3435**. The de-interleaved streams of data can be sent to the soft inner decoder **3475**, which can undo the encoding of the inner encoder **3430**. Any suitable decoding method can be used. For example, in an illustrative embodiment the inner encoder **3430** uses a three-way, soft-decision turbo decoding function. In an alternative embodiment, a two-way, soft-decision turbo decoding function may be used. For example, the expected cluster positions for signal levels are learned by the magnio receiver **3460** during the synchronization portion of the transmission. When the payload/data portion of the transmission is processed by the magnio receiver **3460**, distances from all possible signal clusters to the observed signal value are computed for every bit position. The bits in each bit position are determined by combining the distances with state transition probabilities to find the best path through a "trellis." The path through the trellis can be used to determine the most likely bits that were communicated.

The decoded stream can be transmitted to the de-interleaver **3480**. The de-interleaver **3480** can undo the interleaving of the interleaver **3425**. The de-interleaved stream can be sent to the outer decoder **3485**. In an illustrative embodiment, the outer decoder **3485** undoes the encoding of the outer encoder **3420**. The unencoded stream of information can be sent to the output data generator **3490**. In an illustrative embodiment, the output data generator **3490** undoes the packet generation of data packet generator **3415** to produce the output data **3495**.

FIG. **36** is a block diagram of a computing device in accordance with an illustrative embodiment. An illustrative computing device **3600** includes a memory **3610**, a processor **3605**, a transceiver **3615**, a user interface **3620**, and a power source **3625**. In alternative embodiments, additional, fewer, and/or different elements may be used. The computing device **3600** can be any suitable device described herein. For example, the computing device **3600** can be a desktop computer, a laptop computer, a smartphone, a specialized computing device, etc. The computing device **3600** can be used to implement one or more of the methods described herein.

In an illustrative embodiment, the memory **3610** is an electronic holding place or storage for information so that the information can be accessed by the processor **3605**. The memory **3610** can include, but is not limited to, any type of random access memory (RAM), any type of read only memory (ROM), any type of flash memory, etc. such as magnetic storage devices (e.g., hard disk, floppy disk, magnetic strips, etc.), optical disks (e.g., compact disk (CD), digital versatile disk (DVD), etc.), smart cards, flash memory devices, etc. The computing device **3600** may have one or more computer-readable media that use the same or a different memory media technology. The computing

device **3600** may have one or more drives that support the loading of a memory medium such as a CD, a DVD, a flash memory card, etc.

In an illustrative embodiment, the processor **3605** executes instructions. The instructions may be carried out by a special purpose computer, logic circuits, or hardware circuits. The processor **3605** may be implemented in hardware, firmware, software, or any combination thereof. The term "execution" is, for example, the process of running an application or the carrying out of the operation called for by an instruction. The instructions may be written using one or more programming language, scripting language, assembly language, etc. The processor **3605** executes an instruction, meaning that it performs the operations called for by that instruction. The processor **3605** operably couples with the user interface **3620**, the transceiver **3615**, the memory **3610**, etc. to receive, to send, and to process information and to control the operations of the computing device **3600**. The processor **3605** may retrieve a set of instructions from a permanent memory device such as a ROM device and copy the instructions in an executable form to a temporary memory device that is generally some form of RAM. An illustrative computing device **3600** may include a plurality of processors that use the same or a different processing technology. In an illustrative embodiment, the instructions may be stored in memory **3610**.

In an illustrative embodiment, the transceiver **3615** is configured to receive and/or transmit information. In some embodiments, the transceiver **3615** communicates information via a wired connection, such as an Ethernet connection, one or more twisted pair wires, coaxial cables, fiber optic cables, etc. In some embodiments, the transceiver **3615** communicates information via a wireless connection using microwaves, infrared waves, radio waves, spread spectrum technologies, satellites, etc. The transceiver **3615** can be configured to communicate with another device using cellular networks, local area networks, wide area networks, the Internet, etc. In some embodiments, one or more of the elements of the computing device **3600** communicate via wired or wireless communications. In some embodiments, the transceiver **3615** provides an interface for presenting information from the computing device **3600** to external systems, users, or memory. For example, the transceiver **3615** may include an interface to a display, a printer, a speaker, etc. In an illustrative embodiment, the transceiver **3615** may also include alarm/indicator lights, a network interface, a disk drive, a computer memory device, etc. In an illustrative embodiment, the transceiver **3615** can receive information from external systems, users, memory, etc.

In an illustrative embodiment, the user interface **3620** is configured to receive and/or provide information from/to a user. The user interface **3620** can be any suitable user interface. The user interface **3620** can be an interface for receiving user input and/or machine instructions for entry into the computing device **3600**. The user interface **3620** may use various input technologies including, but not limited to, a keyboard, a stylus and/or touch screen, a mouse, a track ball, a keypad, a microphone, voice recognition, motion recognition, disk drives, remote controllers, input ports, one or more buttons, dials, joysticks, etc. to allow an external source, such as a user, to enter information into the computing device **3600**. The user interface **3620** can be used to navigate menus, adjust options, adjust settings, adjust display, etc.

The user interface **3620** can be configured to provide an interface for presenting information from the computing device **3600** to external systems, users, memory, etc. For example, the user interface **3620** can include an interface for a display, a printer, a speaker, alarm/indicator lights, a network interface, a disk drive, a computer memory device, etc. The user interface **3620** can include a color display, a cathode-ray tube (CRT), a liquid crystal display (LCD), a plasma display, an organic light-emitting diode (OLED) display, etc.

In an illustrative embodiment, the power source **36236** is configured to provide electrical power to one or more elements of the computing device **3600**. In some embodiments, the power source **3625** includes an alternating power source, such as available line voltage (e.g., 120 Volts alternating current at 60 Hertz in the United States). The power source **3625** can include one or more transformers, rectifiers, etc. to convert electrical power into power useable by the one or more elements of the computing device **3600**, such as 1.5 Volts, 8 Volts, 12 Volts, 24 Volts, etc. The power source **3625** can include one or more batteries.

Method for Resolving Natural Sensor Ambiguity for DNV Direction Finding Applications

Natural Ambiguity of NV Center Magnetic Sensor System

The NV center magnetic sensor that operates as described above is capable of resolving a magnetic field to an unsigned vector. As shown in FIG. **37**, due to the symmetry of the peaks for the ms=−1 and the ms=+1 spin states around the zero splitting photon energy the structure of the DNV material produces a measured fluorescence spectrum as a function of RF frequency that is the same for a positive and a negative magnetic field acting on the DNV material. The symmetry of the fluorescence spectra makes the assignment of a sign to the calculated magnetic field vector unreliable. The natural ambiguity introduced to the magnetic field sensor is undesirable in some applications, such as magnetic field based direction sensing.

In some circumstances, real world conditions allow the intelligent assignment of a sign to the unsigned magnetic field vector determined from the fluorescence spectra described above. If a known bias field is used that is much larger than the signal of interest, the sign of the magnetic field vector may be determine by whether the total magnetic field, cumulative of the bias field and the signal of interest, increases or decreases. If the magnetic sensor is employed to detect submarines from a surface ship, assigning the calculated magnetic field vector a sign that would place a detected submarine above the surface ship would be nonsensical. Alternatively, where the sign of the vector is not important a sign can be arbitrarily assigned to the unsigned vector.

It is possible to unambiguously determine a magnetic field vector with a DNV magnetic field sensor. The method of determining the signed magnetic field vector may be performed with a DNV magnetic field sensor of the type shown in FIG. **6** and described above. In general, the recovery of the vector may be achieved as described in U.S. application Ser. No. 15/003,718, filed Jan. 21, 2016, titled "APPARATUS AND METHOD FOR RECOVERY OF THREE DIMENSIONAL MAGNETIC FIELD FROM A MAGNETIC DETECTION SYSTEM", which issued as U.S. Pat. No. 9,541,610 on Jan. 10, 2017, and is incorporated by reference herein in its entirety.

As shown in FIG. **2**, the energy levels of the ms=−1 and the ms=+1 spin states are different. For this reason, the relaxation times from the excited triplet states (3E) to the excited intermediate singlet state (A) for electrons with the ms=−1 and the ms=+1 spin states are not the same. The difference in relaxation times for electrons of ms=−1 and the ms=+1 spin states is on the order of picoseconds or nano-

seconds. It is possible to measure the difference in relaxation times for the electrons with the ms=−1 and the ms=+1 spin states by utilizing pulsed RF excitation such that the inequality in the relaxation times accumulates over a large number of electron cycles, producing a difference in observed relaxation times on the order of microseconds.

As described above, the application of RF excitation to the DNV material produces a decrease in fluorescence intensity at the resonant RF frequencies for the ms=−1 and the ms=+1 spin states. For this reason, at RF frequencies that excite electrons to the ms=−1 and the ms=+1 spin states, an equilibrium fluorescence intensity will be lower than the equilibrium fluorescence intensity in the absence of the applied RF excitation. The time it takes to transition from the equilibrium fluorescence intensity in the absence of RF excitation to the equilibrium fluorescence intensity with the application of RF excitation may be employed to calculate an "equilibration time."

An "equilibration time" as utilized herein refers to the time between the start of an RF excitation pulse and when a predetermined percentage of the equilibrium fluorescence intensity is achieved. The predetermined amount of the equilibrium fluorescence at which the equilibration time is calculated may be about 20% to about 80% of the equilibrium fluorescence, such as about 30%, 40%, 50%, 60%, or 70% of the equilibrium fluorescence. The equilibration time as shown in FIGS. **38**, **40** and **41** is actually a decay time, as the fluorescence intensity is actually decreasing in the presence of the RF excitation, but has been inverted for the sake of clarity.

A shown in FIG. **38**, the fluorescence intensity of the DNV material varies with the application of a pulsed RF excitation source. When the RF pulse is in the "on" state, the electrons decay through a non-fluorescent path and a relatively dark equilibrium fluorescence is achieved. The absence of the RF excitation, when the pulse is in the "off" state, results in a relatively bright equilibrium fluorescence. The transition between the two fluorescence equilibrium states is not instantaneous, and the measurement of the equilibration time at a predetermined value of fluorescence intensity provides a repeatable indication of the relaxation time for the electrons at the RF excitation frequency.

The difference in the relaxation time between the electrons of the ms=−1 and the ms=+1 spin states may be measured due to the different RF excitation resonant frequencies for each spin state. As shown in FIG. **39**, a fluorescence intensity spectra of the DNV material measured as a function of RF excitation frequency includes four Lorentzian pairs, one pair for each crystallographic plane of the DNV material. The peaks in a Lorentzian pair correspond to a ms=−1 and a ms=+1 spin state. By evaluating the equilibration time for each peak in a Lorentzian pair, the peak which corresponds to the higher energy state may be identified. The higher energy peak provides a reliable indication of the sign of the magnetic field vector.

The Lorentzian pair of the fluorescence spectra which are located furthest from the zero splitting energy may be selected to calculate the equilibration time. These peaks include the least signal interference and noise, allowing a more reliable measurement. The preferred Lorentzian pair is boxed in FIG. **39**.

A plot of the fluorescence intensity for a single RF pulse as a function of time is shown in FIG. **40**. The frequency of the pulsed RF excitation is selected to be the maximum value for each peak in the Lorentzian pair. The other conditions for the measurement of an equilibration time for each peak in the Lorentzian pair are held constant. As shown in FIG. **41**, the peaks of the Lorentzian pair have an equilibration time when calculated to 60% of the equilibrium intensity value that is distinguishable. The RF pulse duration may be set such that the desired percentage of the equilibrium fluorescence intensity is achieved for each "on" portion of the pulse, and the full "bright" equilibrium intensity is achieved during the "off" portion of the pulse.

The equilibrium fluorescence intensity under the application of the RF excitation may be set by any appropriate method. According to some embodiments, the RF excitation may be maintained until the intensity becomes constant, and the constant intensity may be considered the equilibrium intensity value utilized to calculate the equilibration time. Alternatively, the equilibrium intensity may be set to the intensity at the end of an RF excitation pulse. According to other embodiments, a decay constant may be calculated based on the measured fluorescence intensity and a theoretical data fit employed to determine the equilibrium intensity value.

The peak in the Lorentzian pair that exhibits the higher measured equilibration time is associated with the higher energy level electron spin state. For this reason, the peak of the Lorentzian pair with the longer equilibration time is assigned the ms=+1 spin state, and the other peak in the Lorentzian pair is assigned the ms=−1 spin state. The signs of the peaks in the other Lorentzian pairs in the fluorescence spectra of the DNV material as a function of RF frequency may then be assigned, and the signed magnetic field vector calculated.

To demonstrate that the equilibration time of each peak in a Lorentzian pair does indeed vary with magnetic field direction, the equilibration time for a single peak in a Lorentzian pair was measured under both a positive and a negative magnetic bias field which were otherwise equivalent. As shown in FIG. **42**, a real and measurable difference in equilibration time was observed between the opposite bias fields.

The method of determining a sign of a magnetic field vector with a DNV magnetic sensor described herein may be performed with the DNV magnetic field sensor shown in FIG. **6**. No additional hardware is required.

The controller of the magnetic field sensor may be programmed to determine the location of peaks in a fluorescence spectra of a DNV material as a function of RF frequency. The equilibration time for the peaks of a Lorentzian pair located the furthest from the zero field energy may then be calculated. The controller may be programmed to provide a pulsed RF excitation energy by controlling a RF excitation source and also control an optical excitation source to excite the DNV material with continuous wave optical excitation. The resulting optical signal received at the optical detector may be analyzed by the controller to determine the equilibration time associated with each peak in the manner described above. The controller may be programmed to assign a sign to each peak based on the measured equilibration time. The peak with the greater measured equilibration time may be assigned the ms=+1 spin state.

The method of assigning a sign to a magnetic field vector described above may also be applied to magnetic field sensors based on magneto-optical defect center materials other than DNV.

The DNV magnetic field sensor described herein that produces a signed magnetic field vector may be especially useful in applications in which the direction of a measured magnetic field is important. For example, the DNV magnetic

field sensor may be employed in magnetic field based navigation or positioning systems.

Hydrophone

FIGS. **43**A and **43**B are diagrams illustrating hydrophone systems in accordance with illustrative embodiments. An illustrative system **4300** includes a hull **4305** and a magnetometer **4310**. In alternative embodiments, additional, fewer, or different elements can be used. For example, an acoustic transmitter can be used to generate one or more acoustic signals. In the embodiments in which a transmitter is not used, the system **4300** can be used as a passive sonar system. For example, the system **4300** can be used to detect sounds created by something other than a transmitter (e.g., a ship, a boat, an engine, a mammal, ice movement, etc.).

In an illustrative embodiment, the hull **4305** is the hull of a vessel such as a ship or a boat. The hull **4305** can be any suitable material, such as steel or painted steel. In alternative embodiments, the magnetometer **4310** is installed in alternative structures such as a bulk head or a buoy.

As illustrated in FIG. **43**A, the magnetometer **4310** can be located within the **4305**. In the embodiment, the magnetometer **4310** is located at the outer surface of the hull **4305**. In alternative embodiments, the magnetometer **4310** can be located at any suitable location. For example, magnetometer **4310** can be located near the middle of the hull **4305**, at an inner surface of the hull **4305**, or on an inner or outer surface of the hull **4305**.

In an illustrative embodiment, the magnetometer **4310** is a magnetometer with a diamond with NV centers. In an illustrative embodiment, the magnetometer **4310** has a sensitivity of about 0.1 micro Tesla. In alternative embodiments, the magnetometer **4310** has a sensitivity of greater than or less than 0.1 micro Tesla.

In the embodiment illustrated in FIG. **43**A, sound waves **4315** propagate through a fluid with dissolved ions, such as sea water. As the sound waves **4315** move the ions in the fluid, the ions create a magnetic field. For example, as the ions move within the magnetic field of the Earth, the ions create a magnetic field that is detectable by the magnetometer **4310**. In another embodiment, a magnetic field source such as a permanent magnet or an electromagnet can be used. The movement of the ions with respect to the source of the magnetic field (e.g., the Earth) creates the magnetic field detectable by the magnetometer **4310**.

In an illustrative embodiment, the sound waves **4315** travel through sea water. The density of dissolved ions in the fluid near the magnetometer **4310** depends on the location in the sea that the magnetometer **4310** is. For example, some locations have a lower density of dissolved ions than others. The higher the density of the dissolved ions, the greater the combined magnetic field created by the movement of the ions. In an illustrative embodiment, the strength of the combined magnetic field can be used to determine the density of the dissolved ions (e.g., the salinity of the sea water).

In an illustrative embodiment, the hull **4305** is the hull of a ship that travels through the sea water. As noted above, the movement of the ions relative to the source magnetic field can be measured by the magnetometer **4310**. Thus, the magnetometer **4310** can be used to detect and measure the sound waves **4315** as the magnetometer **4310** moves through the sea water and as the magnetometer **4310** is stationary in the sea water.

In an illustrative embodiment, the magnetometer **4310** can measure the magnetic field caused by the moving ions in any suitable direction. For example, the magnetometer **4310** can measure the magnetic field caused by the movement of the ions when the sound waves **4315** is perpendicular to the hull **4305** or any other suitable angle. In some embodiments, the magnetometer **4310** measures the magnetic field caused by the movement of ions caused by sound waves **4315** that are parallel to the surface of the hull **4305**.

An illustrative system **4350** includes the hull **4305** and an array of magnetometers **4355**. In alternative embodiments, additional, fewer, and/or different elements can be used. For example, although FIG. **43**B illustrates four magnetometers **4355** are used. In alternative embodiments, the system **4350** can include fewer than four magnetometers **4355** or more than magnetometers **4355**. The array of the magnetometers **4355** can be used to increase the sensitivity of the hydrophone. For example, by using multiple magnetometers **4355**, the hydrophone has multiple measurement points.

The array of magnetometers **4355** can be arranged in any suitable manner. For example, the magnetometers **4355** can be arranged in a line. In another example, the magnetometers **4355** can be arranged in a circle, in concentric circles, in a grid, etc. The array of magnetometers **4355** can be uniformly arranged (e.g., the same distance from one another) or non-uniformly arranged. The array of magnetometers **4355** can be used to determine the direction from which the sound waves **4315** travel. For example, the sound waves **4315** can cause ions near one the bottom magnetometer of the magnetometers **4355** of the embodiment illustrated in the system **4350** to create a magnetic field before the sound waves **4315** cause ions near the top magnetometer of the magnetometers **4355**. Thus, it can be determined that the sound waves **4315** travels from the bottom to the top of FIG. **43**B.

In an illustrative embodiment, the magnetometer **4310** or the magnetometers **4355** can determine the angle that the sound waves **4315** travel relative to the magnetometer **4310** based on the direction of the magnetic field caused by the movement of the ions. For example, individual magnetometers of the magnetometers **4355** can each be configured to measure the magnetic field of the ions in a different direction. Principles of beamforming can be used to determine the direction of the magnetic field. In alternative embodiments, any suitable magnetometer **4310** or magnetometers **4355** can be used to determine the direction of the magnetic field and/or the direction of the acoustic signal.

Magnetic Navigation Methods and Systems Utilizing Power Grid and Communication Network

In some embodiments, methods and configurations are disclosed for diamond nitrogen-vacancy (DNV) magnetic navigation via power transmission and distribution lines. The characteristic magnetic signature of human infrastructure provides context for navigation. For example, power lines, which have characteristic magnetic signatures, can serve as roads and highways for mobile platforms (e.g., UASs). Travel in relatively close proximity to power lines may allow stealthy transit, may provide the potential for powering the mobile platform itself, and may permit point-to-point navigation both over long distances and local routes.

Some implementations can include one or more magnetic sensors, a magnetic navigation database, and a feedback loop that controls the UAS position and orientation. DNV magnetic sensors and related systems and methods may provide high sensitivity magnetic field measurements. The DNV magnetic systems and methods can also be low cost, space, weight, and power (C-SWAP) and benefit from a fast settling time. The DNV magnetic field measurements may allow UAS systems to align themselves with the power lines, and to rapidly move along the power-line infrastruc-

ture routes. The subject solution can enable navigation in poor visibility conditions and/or in GPS-denied environments. Such magnetic navigation allows for UAS operation in close proximity to power lines facilitating stealthy transit. DNV-based magnetic systems and methods can be approximately 100 times smaller than conventional systems and can have a reaction time that that is approximately 100,000 times faster than other systems.

FIG. **44** is a diagram illustrating an example of UAS **4402** navigation along power lines **4404**, **4406**, and **4408**, according to some implementations of the subject technology. The UAS **4402** can exploit the distinct magnetic signatures of power lines for navigation such that the power lines can serve as roads and highways for the UAS **4402** without the need for detailed a priori knowledge of the route magnetic characteristics. As shown in FIG. **45**A, a ratio of signal strength of two magnetic sensors, A and B (**4410** and **4412** in FIG. **44**), attached to wings of the UAS **4402**, varies as a function of distance, x, from a center line of an example three-line power transmission line structure **4404**, **4406**, and **4408**. When the ratio is near 1, point **4522**, the UAS **4402** is centered over the power transmission line structure, x=0 at point **4520**.

A composite magnetic field (B-field) **4506** from all (3) wires shown in FIG. **45**B. This field is an illustration of the strength of the magnetic field measured by one or more magnetic sensors in the UAS. In this example, the peak of the field **4508** corresponds to the UAS **4402** being above the location of the middle line **4406**. When the UAS **4402** has two magnetic sensors, the sensors would read strengths corresponding to points **4502** and **4504**. A computing system on the UAS or remote from the UAS, can calculate combined readings. Not all of the depicted components may be required, however, and one or more implementations may include additional components not shown in the figure. Variations in the arrangement and type of the components may be made, and additional components, different components, or fewer components may be provided.

As an example of some implementations, a vehicle, such as a UAS, can include one or more navigation sensors, such as DNV sensors. The vehicle's mission could be to travel to an initial destination and possibly return to a final destination. Known navigation systems can be used to navigate the vehicle to an intermediate location. For example, a UAS can fly using GPS and/or human controlled navigation to the intermediate location. The UAS can then begin looking for the magnetic signature of a power source, such as power lines. To find a power line, the UAS can continually take measurements using the DNV sensors. The UAS can fly in a circle, straight line, curved pattern, etc. and monitor the recorded magnetic field. The magnetic field can be compared to known characteristics of power lines to identify if a power line is in the vicinity of the UAS. For example, the measured magnetic field can be compared with known magnetic field characteristics of power lines to identify the power line that is generating the measured magnetic field. In addition, information regarding the electrical infrastructure can be used in combination with the measured magnetic field to identify the current source. For example, a database regarding magnetic measurements from the area that were previously taken and recorded can be used to compare the current readings to help determine the UAS's location.

In some implementations, once the UAS identifies a power line the UAS positions itself at a known elevation and position relative to the power line. For example, as the UAS flies over a power line, the magnetic field will reach a maximum value and then begin to decrease as the UAS moves away from the power line. After one sweep of a known distance, the UAS can return to where the magnetic field was the strongest. Based upon known characteristics of power lines and the magnetic readings, the UAS can determine the type of power line.

Once the current source has been identified, the UAS can change its elevation until the magnetic field is a known value that corresponds with an elevation above the identified power line. For example, as shown in FIG. **6**, a magnetic field strength can be used to determine an elevation above the current source. The UAS can also use the measured magnetic field to position itself offset from directly above the power line. For example, once the UAS is positioned above the current source, the UAS can move laterally to an offset position from the current source. For example, the UAS can move to be 10 kilometers to the left or right of the current source.

The UAS can be programmed, via a computer **306**, with a flight path. In some implementations, once the UAS establishes its position, the UAS can use a flight path to reach its destination. In some implementations, the magnetic field generated by the transmission line is perpendicular to the transmission line. In some implementations, the vehicle will fly perpendicular to the detected magnetic field. In one example, the UAS can follow the detected power line to its destination. In this example, the UAS will attempt to keep the detected magnetic field to be close to the original magnetic field value. To do this, the UAS can change elevation or move laterally to stay in its position relative to the power line. For example, a power line that is rising in elevation would cause the detected magnetic field to increase in strength as the distance between the UAS and power line decreased. The navigation system of the UAS can detect this increased magnetic strength and increase the elevation of the UAS. In addition, on board instruments can provide an indication of the elevation of the UAS. The navigation system can also move the UAS laterally to the keep the UAS in the proper position relative to the power lines.

The magnetic field can become weaker or stronger, as the UAS drifts from its position of the transmission line. As the change in the magnetic field is detected, the navigation system can make the appropriate correction. For a UAS that only has a single DNV sensor, when the magnetic field had decreased by more than a predetermined amount the navigation system can make corrections. For example, the UAS can have an error budget such that the UAS will attempt to correct its course if the measured error is greater than the error budget. If the magnetic field has decreased, the navigation system can instruct the UAS to move to the left. The navigation system can continually monitor the magnetic field to see if moving to the left corrected the error. If the magnetic field further decreased, the navigation system can instruct the UAS to fly to the right to its original position relative to the current source and then move further to the right. If the magnetic field decreased in strength, the navigation system can deduce that the UAS needs to decrease its altitude to increase the magnetic field. In this example, the UAS would originally be flying directly over the current source, but the distance between the current source and the UAS has increased due to the current source being at a lower elevation. Using this feedback loop of the magnetic field, the navigation system can keep the UAS centered or at an offset of the current source. The same analysis can be done when the magnetic field increases in strength. The navigation can maneuver until the measured magnetic field is within the proper range such that the UAS in within the flight path.

The UAS can also use the vector measurements from one or more DNV sensors to determine course corrections. The readings from the DNV sensor are vectors that indicate the direction of the sensed magnetic field. Once the UAS knows the location of the power line, as the magnitude of the sensed magnetic field decreases, the vector can provide an indication of the direction the UAS should move to correct its course. For example, the strength of the magnetic field can be reduced by a threshold amount from its ideal location. The magnetic vector of this field can be used to indicate the direction the UAS should correct to increase the strength of the magnetic field. In other words, the magnetic field indicates the direction of the field and the UAS can use this direction to determine the correct direction needed to increase the strength of the magnetic field, which could correct the UAS flight path to be back over the transmission wire.

Using multiple sensors on a single vehicle can reduce the amount of maneuvering that is needed or eliminate the maneuvering all together. Using the measured magnetic field from each of the multiple sensors, the navigation system can determine if the UAS needs to correct its course by moving left, right, up, or down. For example, if both DNV sensors are reading a stronger field, the navigation system can direct the UAS to increase its altitude. As another example if the left sensor is stronger than expected but the right sensor is weaker than expected, the navigation system can move the UAS to the left.

In addition to the current readings from the one or more sensors, a recent history of readings can also be used by the navigation system to identify how to correct the UAS course. For example, if the right sensor had a brief increase in strength and then a decrease, while the left sensor had a decrease, the navigation system can determine that the UAS has moved to far to the left of the flight path and could correct the position of the UAS accordingly.

FIG. **46** illustrates a high-level block diagram of an example UAS navigation system **4600**, according to some implementations of the subject technology. In some implementations, the UAS navigation system of the subject technology includes a number of DNV sensors **4602***a*, **4602***b*, and **4602***c*, a navigation database **4604**, and a feedback loop that controls the UAS position and orientation. In other implementations, a vehicle can contain a navigation control that is used to navigate the vehicle. For example, the navigation control can change the vehicle's direction, elevation, speed, etc. The DNV magnetic sensors **4602***a*-**4602***c* have high sensitivity to magnetic fields, low C-SWAP and a fast settling time. The DNV magnetic field measurements allow the UAS to align itself with the power lines, via its characteristic magnetic field signature, and to rapidly move along power-line routes. Not all of the depicted components may be required, however, and one or more implementations may include additional components not shown in the figure. Variations in the arrangement and type of the components may be made, and additional components, different components, or fewer components may be provided.

FIG. **47** illustrates an example of a power line infrastructure. It is known that widespread power line infrastructures, such as shown in FIG. **47**, connect cities, critical power system elements, homes and businesses. The infrastructure may include overhead and buried power distribution lines, transmission lines, railway catenary and 3rd rail power lines and underwater cables. Each element has a unique electromagnetic and spatial signature. It is understood that, unlike electric fields, the magnetic signature is minimally impacted by man-made structures and electrical shielding. It is understood that specific elements of the infrastructure will have distinct magnetic and spatial signatures and that discontinuities, cable droop, power consumption and other factors will create variations in magnetic signatures that can also be leveraged for navigation.

FIGS. **48**A and **48**B illustrate examples of magnetic field distribution for overhead power lines and underground power cables. Both above-ground and buried power cables emit magnetic fields, which unlike electrical fields are not easily blocked or shielded. Natural Earth and other man-made magnetic field sources can provide rough values of absolute location. However, the sensitive magnetic sensors described here can locate strong man-made magnetic sources, such as power lines, at substantial distances. As the UAS moves, the measurements can be used to reveal the spatial structure of the magnetic source (point source, line source, etc.) and thus identify the power line as such. In addition, once detected the UAS can guide itself to the power line via its magnetic strength. Once the power line is located its structure is determined, and the power line route is followed and its characteristics are compared to magnetic way points to determine absolute location. Fixed power lines can provide precision location reference as the location and relative position of poles and towers are known. A compact on-board database can provide reference signatures and location data for waypoints. Not all of the depicted components may be required, however, and one or more implementations may include additional components not shown in the figure. Variations in the arrangement and type of the components may be made, and additional components, different components, or fewer components may be provided.

FIG. **49** illustrates examples of magnetic field strength of power lines as a function of distance from the centerline showing that even low current distribution lines can be detected to distances in excess of 10 km. Here it is understood that DNV sensors provide 0.01 uT sensitivity (1e-10 T), and modeling results indicates that high current transmission line (e.g. with 1000 A-4000 A) can be detected over many tens of km. These strong magnetic sources allow the UAS to guide itself to the power lines where it can then align itself using localized relative field strength and the characteristic patterns of the power-line configuration as described below.

FIG. **50** illustrates an example of a UAS **5002** equipped with DNV sensors **5004** and **5006**. FIG. **51** is a plot of a measured differential magnetic field sensed by the DNV sensors when in close proximity of the power lines. While power line detection can be performed with only a single DNV sensor precision alignment for complex wire configurations can be achieved using multiple arrayed sensors. For example, the differential signal can eliminate the influence of diurnal and seasonal variations in field strength. Not all of the depicted components may be required, however, and one or more implementations may include additional components not shown in the figure. Variations in the arrangement and type of the components may be made, and additional components, different components, or fewer components may be provided.

In various other implementations, a vehicle can also be used to inspect power transmission lines, power lines, and power utility equipment. For example, a vehicle can include one or more magnetic sensors, a magnetic waypoint database, and an interface to UAS flight control. The subject technology may leverage high sensitivity to magnetic fields of DNV magnetic sensors for magnetic field measurements. The DNV magnetic sensor can also be low cost, space,

weight, and power (C-SWAP) and benefit from a fast settling time. The DNV magnetic field measurements allow UASs to align themselves with the power lines, and to rapidly move along power-line routes and navigate in poor visibility conditions and/or in GPS-denied environments. It is understood that DNV-based magnetic sensors are approximately 100 times smaller than conventional magnetic sensors and have a reaction time that that is approximately 100,000 times faster than sensors with similar sensitivity such as the EMDEX LLC Snap handheld magnetic field survey meter.

The fast settling time and low C-SWAP of the DNV sensor enables rapid measurement of detailed power line characteristics from low-C-SWAP UAS systems. In one or more implementations, power lines can be efficiently surveyed via small unmanned aerial vehicles (UAVs) on a routine basis over long distance, which can identify emerging problems and issues through automated field anomaly identification. In other implementations, a land based vehicle or submersible can be used to inspect power lines. Human inspectors are not required to perform the initial inspections. The inspections of the subject technology are quantitative, and thus are not subject to human interpretation as remote video solutions may be.

FIG. **52** illustrates an example of a measured magnetic field distribution for power lines **904** and power lines with anomalies **902** according to some implementations. The peak value of the measured magnetic field distribution, for the normal power lines, is in the vicinity of the centerline (e.g., d=0). The inspection method of the subject technology is a high-speed anomaly mapping technique that can be employed for single and multi-wire transmission systems. The subject solution can take advantage of existing software modeling tools for analyzing the inspection data. In one or more implementations, the data form a normal set of power lines may be used as a comparison reference for data resulting from inspection of other power lines (e.g., with anomalies or defects). Damage to wires and support structure alters the nominal magnetic field characteristics and is detected by comparison with nominal magnetic field characteristics of the normal set of power lines. It is understood that the magnetic field measurement is minimally impacted by other structures such as buildings, trees, and the like. Accordingly, the measured magnetic field can be compared to the data from the normal set of power lines and the measured magnetic field's magnitude and if different by a predetermined threshold the existence of the anomaly can be indicated. In addition, the vector reading between the difference data can also be compared and used to determine the existence of anomaly.

Mapping and Monitoring of Hydraulic Fracture Using Vector Magnetometers

The present disclosure is directed, in part, to mapping and monitoring of hydraulic fractures using vector magnetometers. Magnetic images are capture at various phases of the hydraulic fracturing operation (also referred to as "fracking"), which include padding and injection of fracking (frac) fluid and proppant, as described in more detail herein. The subject technology allows monitoring and adjustment of the fracking operation by providing a map of the distribution of the frac fluid and proppant in various stages.

The disclosed solution can be used in conjunction with micro-seismic monitoring. Micro-seismic monitoring is very challenging due to the fact that initial times for the shear fracture events are unknown, which results in large uncertainty in the depth migration problem of seismic processing. Other limiting factors include observation of only shear fractures, and the fact that fracture events themselves don't indicate whether or not the induced fracture was effectively propped open subsequent to removal of pressurized frac fluid.

The subject solution provides indication of proppant penetration into the fracture network during and subsequent to the frac process, which is the key to better controlling the overall fracking process. Fracking is typically a multiple stage or zonal process per each well. The disclosed solution also enables adapting initial frac plan to evolving conditions.

FIGS. **53**A-**53**B are diagrams illustrating examples of a high-level architecture of a system **5300**A for mapping and monitoring of hydraulic fracture and an environment **5300**B where the system operates, according to certain embodiments. The system **5300**A includes a sensor array **5302** including multiple sensors **5303**, an analyzer **5305**, and an output device **5309**. Each sensor **5303** includes at least a magnetometer communicatively coupled to the analyzer **5305**. The analyzer **5305** includes one or more processors **5306**, memory **5308** and an interface **5304**. Each sensor may communicate data signal to the analyzer **5305**. The communication between the sensors and the analyzer **5305** may be wired, optical, or wireless communication. The analyzer **5305** may communicate with the sensors **5303** individually or with the sensor array **5302** through the interface **5304** to receive sensor data. The analyzer **5305** may store the sensor data received from the sensors **5303** or the sensor array **5302** to the memory **5308**. The stored data may be accessed by processor(s) **5306** for processing the data subsequent to the sensors storing their respective data. The processor(s) **5306** may be configured to receive executable instructions for processing the data according to the constrained geophysical processing described herein. The signals produced by the sensor array **5302** may include magnetic imaging data for generation of a magnetic profile of a region defined by the well which is intended to be processed using hydraulic fracturing. Each magnetometer sensor **5303** may save its vector field measurement every few minutes throughout the entire fracking process. All saved data is time tagged by some simple means such as a common clock or a trigger for later processing of the data.

The memory **5308** is in communication with processor **5306** and the interface **5304**. Memory **5308** may store information, such as the sensor array **5302** signals received by the analyzer **5305**. Further, memory **5308** may store magnetic images or signals that have been received from sensor array **5302** and further processed by processor(s) **5306**. The interface **5304** communicates data from the analyzer **5305** to an output device **5309**. The output device **5309** may be any device or apparatus that can communicate information about the processed signals received from sensor array **5302**. For example, the output device **5309** may be a display configured to display a graphical depiction of a well site, including a mapping of an induced fracture network produced during hydraulic fracturing. In some aspects, the output **5717** may be a printing device providing information (e.g. reports) relating to a hydraulic fracturing operation.

In one or more implementations, the sensors **5303** are arranged in a sensor array **5302** and communicatively connected to analyzer **5305**. The sensors **5303** may include a magnetometer for measuring a magnetic field in the proximity of the sensor **5303**, which is communicated to the analyzer **5305**. The magnetic fields measured by sensor array **5302** may be related to a well being processed using hydraulic fracturing. The magnetic field measured by the sensors **5303** may include magnetic fluences relating to the Earth's magnetic field, as well as remnant magnetism in the

rock formation and magnetic properties of the well apparatus itself, such as the well casing. As the well is fractured by injecting fluid and proppants into the well bore at selected stages along the bore, the magnetic field in the region of the hydraulic fluids and proppants affect the surrounding magnetic fields that are subsequently measured by the sensors **5303**. As hydraulic fracturing proceeds in the well, subsequent magnetic images are captured by the sensor array **5302** and communicated to the analyzer **5305**. The received magnetic images are processed by processor(s) **5306** to determine changes in the magnetic profile between successive magnetic images captured by the sensor array **5302**. The changes are processed to map the distribution of frac fluid and proppant in the well, which are indicative of the induce fracture network into which the fluid and proppant has flowed during hydraulic fracturing.

FIG. **53**B shows the environment **5300**B, which is representation of the geology of natural gas resources. The growth of natural gas reserves and production from shale formations has sparked interest in the nation's natural gas resources. The diagram in FIG. **53**B shows the geologic nature of most major sources of natural gas in the United States in schematic form. Gas rich shale **110** is the source rock for many natural gas resources, but until recently, has not been a focus for production. Horizontal drilling and hydraulic fracturing have made shale gas an economically viable alternative to conventional gas resources. Conventional gas accumulations **5340**, **5350**, or plays, occur when gas migrates from gas-rich shale into an overlying sandstone formation, and then becomes trapped by an overlying impermeable formation, called the seal **5330**. Associated gas **5340** accumulates in conjunction with oil **5320**, while non-associated gas **5350** does not accumulate with oil. Tight sand gas accumulations **5360** occur when gas migrates from a source rock into a sandstone formation **5370**, but is limited in its ability to migrate upward due to reduced permeability in the sandstone. Finally, coal bed methane **5380** does not originate from shale, but is generated during the transformation of organic material to coal.

Conventional gas accumulations **5340**, **5350** may be accessed via horizontal drilling techniques in which the well bore is substantially vertical. To access non-conventional plays such as gas-rich shale formations **5310**, horizontal drilling techniques in which the well bore **5395** extends substantially horizontally **5396** may be needed. Generally, the permeability of unconventional reservoirs is too low for production, thus requiring directional drilling and well stimulation. For example, the permeability of a typical shale formation may be on the order of 10^{-9} Darcy. Tight sand formations may have permeability of about 10^{-6} Darcy. In contrast, a conventional play may have permeability of 10^{-2} Darcy.

FIG. **54** is a high-level diagram illustrating an example of implementation of hydraulic fracturing of a well to release gas reserves, according to certain embodiments. A well head **5401** is installed at ground level and attached to a water supply from a storage container **5402** via a pump **5402**. The pump provides a frac fluid at a sufficient pressure in the well bore **5480** to produce fracturing of the underlying shale layer **5410**. Natural gas trapped within the natural fissures **5420** in the shale layer **5410** are released as the newly formed fractures expand existing fissures while creating newly induced fractures and pathways through the remaining shale formation **5410**.

Shale is a finely grained sedimentary form of rock. Spaces between the grains are typically very small. As natural gas is formed, some of the gas becomes trapped within these small spaces. Using conventional mining and drilling techniques these trapped resources are difficult to access. Despite the resource richness of these sources, the production from wells in these types of formations has proven to be economically infeasible. Yet despite the inability to access the trapped gas due to the high impermeability of the shale, the shale contains a high volume of pore space that may contain substantial amounts of gas collected over long geological timeframes. Hydraulic fracturing provides access to this pore space, allowing the trapped gas **5430** migrate toward the well bore **5480** and be collected at the well head **5401**.

Frac fluid is stored near the well head **5401** in storage container **5402**. The frac fluid is provided to the well bore **5480** under pressure provided by the pump **5402**. The frac fluid is primarily water, but other additives or chemicals may be added to the frac fluid. For example, water pumped into the shale layer **5410** at pressure, creates new fractures in the grains of the shale formation. When the pressure is relieved, such as by turning off the pump **5402**, the newly formed cracks in the shale tend to reclose under the pressure caused by the mass of the overlying layers. To maintain the openings created by the hydraulic pressure, a substance called a proppant **5440** is added to the frac fluid. The proppant **5440** props open the newly formed cracks **5420** to allow the trapped natural gas **5430** to migrate toward the well bore **5480**. The proppant **5440** typically includes sand, which has a compressibility sufficient to maintain the openings in the shale, while providing enough permeability to allow the migration of the natural gas within the shale formation. While frac sand is a commonly used proppant, other materials, for example, aluminum beads, ceramic beads, sintered bauxite and other materials may be used, provided the material is crush-resistant and provides adequate permeability.

Other materials or chemicals may be added to frac fluid to provide additional functionality. For example, thickening agents may be added to the frac fluid to form a gel, which is effective at carrying the proppant particles deep into the rock formation. Other chemicals may be added to reduce friction, maintain rock debris from the fracking process in suspension for ease of removal, prevent corrosion of equipment, kill bacteria, control pH, as well as perform other functions.

The frac fluid is introduced to the well bore **5480** under pressure (as indicated by arrow **5470**) and enters the natural fissures **5420** located within the shale layer **5410**. Hydrostatic pressure builds in the shale until the pressure creates force which exceeds the tensile strength of the shale grains causing the grains to fracture and split. The entire well bore **5480** does not need to be pressurized. Plugs may be placed beyond the regions of shale being targeted for fracturing to produce the desired pressure within a targeted region or stage.

The well bore **5480** may extend from the surface for thousands of feet to reach the shale layer **5410** below. Overlying layers, include the aquifer **5450** which may provide the water supply for the area surrounding the well **5400**. To protect the water supply from contamination, the well bore **5480** is lined with a steel casing **5460**. The space between the outside of the steel casing **5460** and the walls of the well bore **5480** are then filled with concrete to a depth greater than the aquifer **5450**. As the well bore **5480** approaches the depth containing the gas-rich shale formation **5410**, the well bore **5480** is angled to a horizontal or nearly horizontal direction to run longitudinally through the shale formation **5410**. As the pressurized frac fluid is applied to the shale layer **5410** the existing fissures **5420** are expanded

and newly formed fractures are created. As shown in detail in the inset of FIG. **54**, the frac fluid and proppant **5440** enter the existing fissures **5420** and create new fissures. Proppant particles **5440** contained in the frac fluid hold the fissures open and provide permeability for gas **5430** located within the fissures to migrate through the frac fluid and proppant particles to the well bore **5480** and back to the surface.

During production of a non-conventional play, a horizontal pay zone extending about 4,000 feet through the pay zone may be established. Fracturing is performed along the horizontal pay zone in typically uniform stages extending about 400 feet. For a typical fractured well, 10-20 million square feet of additional surface area is created by the fractures. The fracking is performed beginning at the toe or end of the well, and processed stage by stage back toward the well opening. Fracking a typical well requires about 2.5 million pounds of proppant and about 4-6 million gallons of frac fluid. The fracturing process seeks to push proppant radially out from the well bore into the formation up to 1,000 feet. Ideally, fractures create sheet-like openings that extend orthogonally to the direction of the well bore. To this end, wells are typically drilled based on prior knowledge of the in situ stress state of the rock formation. Spacing for the fracturing stages are selected based, at least in part, on the anticipated induced fracture and empirically determined flow rates into the fracture network to ensure that production is commensurate with the intended 20-30 year life expectancy of a typical well installation. A production field may contain a number of wells configured as described above. The wells are spaced according to the corresponding designed pay zone of each well. The use of hydraulic fracturing is intended to maximize the stimulated rock volume (SRV) per dollar cost of production.

Experience has shown, however, that induced fractures define complicated networks of fractures rather than the ideal sheet-like openings. Accordingly, mapping the occurrence and location of actual fractures becomes valuable in determining the effectiveness of the current operations, and provides insight into future actions to maximize production efficiency of the well. Factors that create uncertainty in the hydraulic fracturing process include the loss of frac fluid and proppants to pre-existing or natural fractures which may open further during the fracking process. Injected fluid and proppant is accommodated, (e.g., space/volume become available) by the compliance of the surrounding rock which becomes compressed, and thereby alters the rock's stress state. This changes the stress field from one stage's fracture to the next. This results in added uncertainty as to the final placement of proppants to maintain openings formed by the fracking after the hydraulic pressure is removed.

Mapping induced fractures caused by hydraulic fracturing allows for greater production and maximized stimulated reservoir volume (SRV). In addition, concerns expressed over the process of fracking, including the proliferation of the fracking materials into the environment, may require accurate mapping of induced fractures and the introduction of frac fluids and proppants to those fractures to meet further regulatory requirements designed to control and regulate impact to the environment caused by hydraulic fracturing.

Presently, attempts at mapping fractures include passive micro-seismic monitoring. In micro-seismic monitoring, a passive array of seismic sensors is arranged at the surface overlying the fractured pay zone, or the sensors may be placed down hole in the fracked well or in a nearby observation well. The seismic sensors are configured to detect shear pops that occur when an induced tensile crack intersects with a natural fracture which emits a popping type of impulse. The impulses are converted to signals which are processed to determine the source of the impulse. Micro-seismic monitoring is passive. That is, no active seismic signal is generated and used to create returned signals. The sensors merely monitor the surroundings for seismic activity if and when such activity occurs. Since it not known when a fracture may be induced by the hydraulic pressure, or where such fractures may occur, there is considerable uncertainty in seismic monitoring. This uncertainty is compounded by the very low energy seismic signals which must be detected. Further, seismic monitoring does not provide insight as to the effective placement of proppants, as the impulses used to generate signals occur at the initiation of an induced fracture and do not indicate if the fractures were successfully propped open, or reclosed after the initial fracture. Therefore, it is difficult to verify that the mapping information generated is reliable. The subject solution may be used alone or in cooperation with existing techniques including micro-seismic monitoring.

According to one or more implementations, an array of sensors is placed on or near the surface of a well or active pay zone. The array of sensors includes at least a magnetometer sensor for measuring a magnetic field around the sensor. In an alternative embodiment, one or more of the magnetometer sensors may be placed down hole in the well, although this is not a requirement and a system may be embodied using solely surface arrays. The environment around the well has a magnetic signature that may be measured by the sensor array. For example, the Earth's magnetic field will influence the overall magnetic signature in the area of the well. Additionally, remnant sources of magnetic fields, such as the host rock or intrusions of magnetite further influence the magnetic field sensed by the array of magnetometer sensors. Further, as the well casing is driven down in the well bore, the well casing tends to become magnetized, thereby affecting the magnetic field measured at the magnetometer sensor array.

According to an embodiment, a process includes placing an array of sensors proximate to a well pay zone. Prior to introducing any frac fluid for hydraulic fracturing, a baseline magnetic profile is established by measuring the magnetic signature prior to any hydraulic fracturing being performed. The baseline magnetic signature includes the Earth's magnetic field, remnant sources of magnetism in the earth and the magnetic field which is associated with the well casing. The magnetometer sensor may be based on a diamond nitrogen vacancy (DNV) sensor. A DNV sensor includes a synthetic diamond substrate which is created having intentional impurities introduced into the carbon lattice structure of the diamond. Nitrogen atoms replace the carbon atoms at varying locations in the lattice, thereby creating vacancies which contain electrons. The electrons have various spin states which may be measured. The spin states are sensitive to the surrounding magnetic environment. As the magnetic environment changes, the spin states of the electrons change and the difference in spin may be correlated to the corresponding change in the magnetic environment. Magnetometers based on DNV technologies are very sensitive and can detect small changes in magnetic fields in a sensor which is considerably smaller than other technologies. For example, a typical conventional magnetometer capable of detecting small changes in the magnetic profile of a well's pay zone may require a sensor which is the size of a small van. In contrast, a DNV based magnetometer may be embodied in a sensor the size of a cellular telephone or smaller. Thus, a number of small, very sensitive magnetometers can be

carried on site and arranged in an array about the surface in the area defining the well pay zone.

FIG. **55**A is a diagram illustrating an example background magnetic signature **5500**A of a well, according to certain embodiments. A well may include a bore **320** that is drilled vertically from the surface to a desired depth, at which point the bore **320** is extended horizontally along the pay zone. A well casing **5525** is inserted into the bore to insulate the well bore **320** from the surrounding rock formation and to prevent introduction of mining materials into the surrounding rock near the surface. As the well casing **5525** is driven into the rock formation, the casing tends to become magnetized and form the magnetic field **5526**. The surrounding rock formation contains naturally occurring remnant magnetism **5516** which may be in the host rock or intrusions of other materials such as magnetite **5515**. In addition, the Earth has its own global magnetic field **5501** that extends through the area defined by the well and its pay zone.

FIG. **55**B is a diagram illustrating an example implementation of a mapping system **5500**B for hydraulic fracturing of the well shown in FIG. **55**A, according to certain embodiments. The mapping system **5500**B includes the sensor array **5511** including magnetometer sensors **5510** arranged on the surface in an area defining the pay zone of the well. According to some aspects, a one-to-one placement of magnetometers with geophones (e.g., for concurrent micro-seismic mapping) at the surface may be used. This configuration provides a wide aperture and allows for triangulating locations. The addition of magnetometer data requires minimal modification to procedures already established for micro-seismic techniques. Where the well is cased, monitoring the opened holes may involve introducing sensors at a subsurface level. Downhole placements of sensors may also be used to provide much stronger signals.

The sum of the magnetic fields created by the Earth's magnetic field **5501**, the remnant magnetism in the host rock **5515**, and additional magnetic influence of the mining materials, such as the well casing **5526**, define a baseline magnetic field of the well region which is measured by the array of magnetometers at the surface before any introduction of fracking material into the well bore **5520**. Frac fluid is introduced at high pressure to the well bore opening and the well bore **5520** is filled with the fluid through the bore **5520** to the toe of the well which initiates fractures in the rock. The fluid introduced prior to introducing proppant and other additives to the fluid is called padding. A typical well may receive millions of gallons of frac fluid in addition to millions of pounds of proppant **5530**. This large additional mass is received by the surrounding formation and may affect the surrounding magnetic signature. For this reason, the sensor array **5511** may be configured to measure the baseline magnetic signature of the well adjusted for the additional mass provided by the padding fluid and proppant **5530**.

After the baseline magnetic signature has been measured, introduction of additional frac fluid and proppant **5530** to the well may begin. The fluid is provided to the well in stages. A typical 4,000 foot horizontal pay zone may be hydraulically fractured in stages of about 400 feet at a time. In some aspects, the first stage is the length of the well bore **5520** closest to the toe. Subsequent stages are processed sequentially, working from the toe back to the well opening. As the frac fluid is introduced to a new stage, the sensor array **5511** measures the magnetic signature of the well pay zone region. The addition of the fluid causes hydraulic fracturing of the rock **5505** surrounding the horizontal well bore in the area of the stage presently being processed. Changes from the baseline measured magnetic signature indicate the presence of the additional fluid and proppant **5530** as it extends into the new induced fractures caused by the pressurized fluid. The changes may be monitored as subsequent stages are processed, with incremental changes in the measured magnetic signature being analyzed to provide insight into the progress and location of the newly formed fracture network.

To augment the information received at the sensor array as each stage is processed, the frac fluid and/or the proppant **5530** may be treated or infused with a magnetically susceptible material. For example, small ferrite particles may be added to the proppant particles **5530**. The ferrite particles have a greater effect on the overall magnetic signature of the area to which they are introduced due to their magnetic susceptibility. According to some implementations, the proppant **5530** is mixed with a magnetically susceptible material. In other implementations, the frac fluid may be mixed with the magnetically susceptible material, or both the fluid and the proppant **5530** may be treated with the magnetically susceptible material. The differential magnetic signature is determined based on measuring the magnetic signature with the magnetometer sensor array after the magnetically susceptible proppant or fluid is added to a processing stage, and compared with the previous measured magnetic signatures measured prior to the addition of the proppant or fluid.

When adding a magnetic susceptible material to the frac fluid or the proppant **5530**, the material is selected such that the addition of the material does not substantially increase the weight of the proppant of fluid. Along the horizontal pay zone, fractures in the rock extend in varying directions in a web-like manner radially from the horizontal well bore. Therefore, as the well is hydraulically fractured, the frac fluid and proppant **5530** must flow from the well bore in all radial directions, including upward against the force of gravity. If the added magnetically susceptible material adds too much weight to the fluid or the proppant **5530**, the heavier material will tend to settle due to gravity and not flow into the upward regions of the surrounding rock formation.

A sequence of changes in the passive magnetic images captured by the magnetometer sensors during the fracking process are used to determine the proppant placement. The frac fluid and/or the synthetic proppant may be doped with a magnetically susceptible material. Monitoring of the hydraulic fracturing process continues as multiple magnetic images are captured throughout the proppant injection phase. The background or baseline magnetic profile is removed from the images formed throughout the propping phase. Constrained geophysical processing of the resulting group of magnetic images provides information about the distributions of fluid and proppant.

FIG. **56** is a diagram illustrating an example of a method **5600** for mapping and monitoring of hydraulic fracture, according to certain embodiments. According to the method **5600**, using an array of sensors (e.g., **5302** of FIG. **53**A or **5511** of FIG. **55**A), a first magnetic image of a well pay zone (e.g., **5400** of FIG. **54**) is captured (**5610**). Using the array of sensors, a second magnetic image is captured after a well bore (e.g., **5480** of FIG. **54**) is padded with a fluid (**5620**). A background is established based on the first and the second magnetic images (**5630**). Using the array of sensors, a third magnetic image is captured after a doped proppant (e.g., **5440** of FIG. **54**) is injected into a stage (e.g., **5420** of FIG. **54**) (**5640**). The third image is processed to subtract the background and to obtain information regarding distribution of the fluid and the proppant in the stage (**5650**).

FIG. **57** is a diagram illustrating an example of a system **5700** for implementing some aspects of the subject technology. The system **5700**, for example, may be a system that the analyzer **5305** of FIG. **53**A is implemented on or may perform the functionalities of the analyzer **5305** of FIG. **53**A. In some implementations, the system **5700** may perform simulations described herein. The system **5700** includes a processing system **5702**, which may include one or more processors or one or more processing systems. A processor can be one or more processors. The processing system **5702** may include a general-purpose processor or a specific-purpose processor for executing instructions and may further include a machine-readable medium **5719**, such as a volatile or non-volatile memory, for storing data and/or instructions for software programs. The instructions, which may be stored in a machine-readable medium **5710** and/or **5719**, may be executed by the processing system **5702** to control and manage access to the various networks, as well as provide other communication and processing functions. The instructions may also include instructions executed by the processing system **5702** for various user interface devices, such as a display **5712** and a keypad **5714**. The processing system **5702** may include an input port **5722** and an output port **5724**. Each of the input port **5722** and the output port **5724** may include one or more ports. The input port **5722** and the output port **5724** may be the same port (e.g., a bi-directional port) or may be different ports.

The processing system **5702** may be implemented using software, hardware, or a combination of both. By way of example, the processing system **5702** may be implemented with one or more processors. A processor may be a general-purpose microprocessor, a microcontroller, a Digital Signal Processor (DSP), an Application Specific Integrated Circuit (ASIC), a Field Programmable Gate Array (FPGA), a Programmable Logic Device (PLD), a controller, a state machine, gated logic, discrete hardware components, or any other suitable device that can perform calculations or other manipulations of information.

In one or more implementations, the transformation means (e.g., algorithms) and the signal processing of the subject technology may be performed by the processing system **5702**. For example, the processing system **5702** may perform the functionality of the processor **5306** of FIG. **53**A or other or computational functions or simulations described herein.

A machine-readable medium can be one or more machine-readable media. Software shall be construed broadly to mean instructions, data, or any combination thereof, whether referred to as software, firmware, middleware, microcode, hardware description language, or otherwise. Instructions may include code (e.g., in source code format, binary code format, executable code format, or any other suitable format of code).

Machine-readable media (e.g., **5719**) may include storage integrated into a processing system such as might be the case with an ASIC. Machine-readable media (e.g., **5710**) may also include storage external to a processing system, such as a Random Access Memory (RAM), a flash memory, a Read Only Memory (ROM), a Programmable Read-Only Memory (PROM), an Erasable PROM (EPROM), registers, a hard disk, a removable disk, a CD-ROM, a DVD, or any other suitable storage device. Those skilled in the art recognizes how best to implement the described functionality for the processing system **5702**. According to one aspect of the disclosure, a machine-readable medium is a computer-readable medium encoded or stored with instructions and is a computing element, which defines structural and functional interrelationships between the instructions and the rest of the system, which permit the instructions' functionality to be realized. Instructions may be executable, for example, by the processing system **5702** or one or more processors. Instructions can be, for example, a computer program including code for performing methods of the subject technology.

A network interface **5716** may be any type of interface to a network (e.g., an Internet network interface), and may reside between any of the components shown in FIG. **57** and coupled to the processor via the bus **5704**.

A device interface **5718** may be any type of interface to a device and may reside between any of the components shown in FIG. **57**. A device interface **5718** may, for example, be an interface to an external device that plugs into a port (e.g., USB port) of the system **5700**.

FIG. **58** is a diagram illustrating examples of primary and secondary magnetic fields in the presence of a doped proppant, according to certain embodiments. According to an aspect of the disclosure, FIG. **58** depicts a scenario wherein proppant doped with magnetically susceptible matter **5803** (e.g. the dopant) becomes magnetized and aligns with an external magnetic field, $\overline{H}_0$ **5801**. Such external magnetic field may consist of the Earth's natural (geomagnetic) field, as well as possibly that of the surrounding rocks having remnant magnetization, and a magnetized well casing. The external field **5801** is commonly/synonymously referred to as the primary, background, or inducing field, which may be represented as a vector quantity having strength or magnitude, and direction.

Magnetization is also represented as a vector quantity, and the magnetization of the volume of doped proppant **5803** depicted below is labeled $\overline{M}$. Upon becoming magnetized, the susceptible proppant **5803** gives rise to an induced or secondary field **5805**, $\overline{H}_s$. The induced field **5805** is distinct from, but caused, by the primary field **5801**. The total magnetic field is then determined as the superposition of the primary field **5801** and secondary field **5805**. In the simplest case (e.g. isotropic), magnetization relates to the total field by a scalar-valued susceptibility χ, according to:

$$\overline{M}=\chi\overline{H}=\chi(\overline{H}_0+\overline{H}_s) \qquad \text{Eq. (1)}$$

In a non-limiting embodiment, a standard approximation may be made which assumes the primary field **5801** is significantly greater than the secondary field **5805**. Thus, the system's calculation may be made according to $\overline{M}\approx\chi_0$ and wherein the magnetization is parallel to the primary field **5801** and is linearly proportional to it through the susceptibility at any given location.

Generally, the vector field at an observation or measurement point P due to a distribution of magnetized matter (e.g. doped proppant) within a source region Ω is given by:

$$\begin{aligned}\vec{H}(P) &= \vec{H}_0(P)+\vec{H}_S(P) \qquad \text{Eq. (2)}\\ &= \vec{H}_0(P)+\frac{1}{4\pi}\int\int_{\Omega}\int \vec{M}(\xi)\cdot\nabla\nabla\frac{1}{\rho(P,\xi)}d\Omega\end{aligned}$$

Given the quantities as previously defined, and ξ taking on all locations within the relevant source magnetic region. However, using the standard approximation this reduces to a model for the secondary field **8505** depending on the susceptibility distributed throughout the relevant (i.e., non-negligible magnetic source) domain:

$$\vec{H}_S(P) = \frac{1}{4\pi}\int_{\Omega}\int\int \chi(\xi)\vec{H}_0(\xi)\cdot\nabla\nabla\frac{1}{\rho(P,\xi)}d\Omega \quad \text{Eq. (3)}$$

The magnetic source domain for an embodiment of the disclosure comprises the subsurface region surrounding the well that is being fracked, and extending outward from the well to a distance greater than the proppant would reasonably be expected to reach.

If the primary field **5801** existing prior to injecting any doped proppant or frac fluid is complicated by unknown but significant remnants, then Eq. (2) may be used and the magnetization vector may be solved. Alternatively, Eq. (3) may be used to solve for the scalar susceptibility distribution assuming the primary field vector is known throughout the domain of interest, which is taken to be Earth's geomagnetic background, and is well characterized. This approach may represent a simpler implementation.

Consistent with the assumptions stated above, the difference between DNV-based vector magnetic field measurements taken before and during the injection of doped proppant comprises a measure of the secondary field **5805** modeled by Eq. (3) above, induced throughout the fracking process.

According to an aspect of the subject solution, the subsurface domain Ω surrounding the well is subdivided into many model "cells" that are right rectangular prisms of uniform size (other geometric shapes can be used but it is much less common). The unknown susceptibility of the material region associated with each model cell is taken to be constant. Cell sizes are chosen so that this approximation is reasonable, while also being large enough to keep the overall problem tractable (e.g. not too many cells), yet small enough to offer useful resolution (e.g. smooth variation) of the susceptibility being solved for.

After this discretization of the domain into many smaller discrete, uniform subdomain "cells," the susceptibilities for each cell being held constant can be removed from the volume integral and the integrals evaluated and arranged in a coefficient matrix (G) which multiplies the unknown susceptibilities (m) of each cell to compute secondary field values (d) that are expected to match the measured values. This forward model comprises a simple matrix-vector multiplication stated as:

$$d=Gm \quad \text{Eq. (4)}$$

The influence coefficient (G) maps the susceptibility values of all cells in the modeled domain to magnetic field values at each measurement point. As there are many more cells in the model than there are measurement locations, this problem is severely underdetermined and has no unique solution (e.g. it has an infinite number of solutions). This is typical of geophysical inversion problems.

Regularized inversion provides a solution to this dilemma and is a mainstay of geophysics, wherein additional constraints are introduced to yield uniqueness and enable solving for the many unknowns. Types of constraints vary widely, ranging from totally artificial and mathematically contrived, to constraints that are very much physics-based and well applied to certain problems.

A general formulation that encapsulates most of these approaches comprises the simultaneous minimization of data misfit and constraint violation. Data misfit is the difference between measured data and modeled data reconstructed by the forward model of Equation (4) for a specified set of cell susceptibilities. This can be written as a scalar, two-term performance index or cost function:

$$\phi(m)=\phi_d(m)+\gamma\phi_m(m) \quad \text{Eq. (5)}$$

where φ_d represents the data misfit term that takes on large values when a specified set of susceptibilities poorly reconstructs (via the forward model of Eq. (4)) the measured magnetic field values, and small values when the data is well matched. A quadratic form is common:

$$\phi_d(m)=(\tilde{d}-d)^T R^{-1}(\tilde{d}-d) \quad \text{Eq. (6)}$$

where the tilde (~) annotation indicates actual measured data and square matrix (R) is the measurement error covariance matrix associated with the data. Accordingly, individual data entries known to be very accurate may require being very closely matched by the reconstruction. Otherwise their mismatch produces large penalties.

The term φ_m is a model adjustment term that embodies problem constraints that give uniqueness to the problem while also providing physical insight to the problem being solved. A simple example for this term is one that takes on large values for specified susceptibilities that differ greatly from a-priori values (note the a-priori values are often zero, which for a hydraulic fracturing application implies no proppant is pushed into the geologic subdomain corresponding to a cell of the forward model). A simple quadratic form for this term is:

$$\phi_m(m)=(m_0-m)^T W(m_0-m) \quad \text{Eq. (7)}$$

where m_0 comprises the a-priori susceptibilities of the cells one intends to keep the solution near, and the square matrix (W) reflects the possibly differential importance or preference of keeping certain cell values closer to their a-priori values than others. The non-diagonal entries of W may be represented as zero entries, wherein W is diagonal and hence symmetric. Diagonal entries of W are all positive-valued.

Returning to the overall performance index of Eq. (5), the second (model adjustment) term is weighted by a scalar (γ) to achieve a balance between the two terms. For example, (γ) is typically heuristically adjusted so the overall performance index is evenly apportioned between the data misfit and model adjustment terms.

Susceptibilities are then solved for the quadratic case as:

$$m=(G^T R^{-1}G+\gamma W)^{-1}(G^T R^{-1}\tilde{d}+\gamma W m_0) \quad \text{Eq. (8)}$$

The above described solutions provide the benefit of being easy to solve. The model adjustment term may encapsulate the following constraints, which may be particularly useful for embodiments according to this specification: (1) The well geometry is known a-priori, so model cells outside the fracked stage and potentially its neighboring stages are unlikely to have significant changes in their susceptibility; (2) the total amount of susceptible matter pumped down the well is known and must be matched by the recovered model; (3) alternatively to the quadratic adjustment term of Eq. (7) allowing small adjustment of all susceptibilities, a so-called focused inversion may be implemented wherein only susceptibilities of a subset (e.g. minimum) number of model cells are allowed to change during the solution.

The geophysical inversion calculations may be implemented in hardware, software or a combination of hardware and software, for example by the processing system **5702** of FIG. **57**. A general purpose computer processor (e.g., **5702** or processor **5306** of FIG. **53**A) for receiving magnetic and/or micro-seismic signals may be configured to receive and execute computer readable instructions. The instructions

may be stored on a computer readable medium in communication with the processor. One or more processors may be used for calculation some or all of the magnetic and/or micro-seismic signals according to a non-limiting embodiment of the present disclosure.

Energy Efficient Controlled Magnetic Field Generator Circuit

The present disclosure is directed, in part, to an energy efficient controlled magnetic field generator circuit. The subject technology uses a coil electromagnet to establish a variable magnetic field that reaches out a significant distance. This subject solution transfers energy between energy storage devices (e.g., inductors and capacitors) using a switching scheme that enables the control of the ramp rate and duration of each cycle of the magnetic field waveform. The ramp rate is the rate of change of the magnetic field, and by varying the ramp rate, among other things, a triangle wave of selectable amplitude, can be created. The subject technology provides a family of circuits that can accomplish the energy transfer with substantially low energy consumption. Ideally, the disclosed circuits use no energy if lossless devices such as switches, capacitors, and inductors were used. In practice, no device is perfectly lossless, so the circuits do draw energy. However, the energy consumption of the disclosed circuits is substantially low compared to the generated magnetic field strength.

Traditionally, an efficient approach to generate a magnetic field is using a series LC resonators circuit that generates a sinusoidal waveform. There are techniques for varying the average amplitude and/or frequency of the resonance. These techniques are not single-cycle control techniques. It is understood that resonant LC circuits that work with many cycles of the waveform to deliver information have a lower rate of information delivery. By being able to modulate each cycle of the waveform, more bits per second can be delivered. In addition, by achieving the control through ramp rate control, the waveform can have a triangle shape which can have higher amplitude, and more importantly, a higher L2-norm than a sine wave with the same peak slope. The peak slope corresponds to the maximum voltage that the circuit can tolerate. The triangular waveform can achieve a higher signal-to-noise ratio (SNR) for a given maximum voltage in the drive circuit. For sensing applications (e.g., magnetic ping), single cycle control can perform identification with a shorter signal duration, requiring higher sophistication and cost on the part of the adversary to cancel, and also allowing a shorter duty cycle and thus more stealth and energy efficiency.

FIGS. **59**A through **59**F are diagrams illustrating examples of a magnetic waveform generator circuit **5900**A, a corresponding timing diagram **5900**B, and various operational phases **5900**C through **5900**F of the magnetic waveform generator circuit, according to certain embodiments. The magnetic waveform generator circuit **5900**A (hereinafter "circuit **5900**A") includes a first switch S**1** coupled between a first node **5902** (hereinafter "node**5902**") and a second node **5904** (hereinafter "node**5904**"), a second switch S**2** coupled between node **5902** and a third node **5906** (hereinafter "node**5906**"), a first rectifier element D**1** coupled in parallel to the switch S**2**, and a second rectifier element D**2** coupled in parallel to the switch S**1**. The circuit **5900**A further includes an inductor L coupled between node **5902** and a fourth node **5908** (hereinafter "node**5908**"), a first capacitors C**1** coupled between nodes **5904** and **5908**, and a second capacitors C**2** coupled between nodes **5908** and **5906**. Node **5908** is coupled to ground potential and capacitors C**1** and C**2** are precharged to +Vp (e.g., 100V) and −Vp (e.g., −100V).

In one or more implementations, the switches S**1** and S**2** can be implemented with semiconductor switches such as transistors (e.g., bipolar junction transistor (BJT), field-effect transistor (FET)) or other types of switches). The rectifier elements D**1** and D**2** can be semiconductor diodes (e.g., silicon diodes) or other rectifier elements. The inductor L is a magnetic coil of the magnetic waveform generator and can have an inductance value of the order of hundreds of micro-Henry (μH), for example, 300 μH, and capacitance values of the capacitors C**1** and C**2** can be of the order of hundreds of micro-farad (μF). The circuit **5900**A can generate a current i in the in inductor L that has an optimized waveform, for example, a triangular waveform, by controlling the switches S**1** and S**2**, as shown in the timing diagram **5900**B of FIG. **59**B.

The timing diagram **5900**B includes control pulses **5910** and **5912** applied to the switches S**1** and S**2**, and a triangular waveform **5920** for the current i of the inductor L of FIG. **59**A. During a time period T**1**, switch S**1** is closed and switch S**2** is open. During a time period T**2**, both switches S**1** and S**2** are open, and during a time period T**3**, switch S**1** is open and switch S**2** is closed, and during a time period T**4**, both switches S**1** and S**2** are open again. The four phases of switches S**1** and S**2** can cause the current i of the inductor L run through the ramp-up and ramp-down cycles to create a full cycle of the triangular waveform **5920**. More detailed operational descriptions of the circuit **5900**A are provided below with respect to FIGS. **59**C through **59**F.

The operational phase **5900**C shown in FIG. **59**C depicts the operation of the circuit **5900**A of FIG. **59**A during the time period T**1** of FIG. **59**B. Transistors Q**1** (e.g., an NPN transistor) and Q**2** (e.g., a PNP transistor) are example implementations of the switches S**1** and S**2** of FIG. **59**A. During the operational phase **5900**C, the transistor Q**1** is on and the transistor Q**2** is off, and diodes D**1** and D**2** are both reverse biased by the initial voltage (e.g., 5900V) of the capacitors C**1** and C**2**. The capacitor C**1** discharges through the transistor Q**1** and the inductor L, thereby passing a positive up-ramping (increasing) current i in the inductor L, which forms the first quarter cycle, corresponding to the time period T**1**, of the triangular waveform **5920** of FIG. **59**B. In practice, the current i ramps up in a manner which can be closely approximated with a linear ramp when the capacitor sizing and switch closure interval are such that the capacitor voltage remains nearly constant during discharging or recharging intervals.

The operational phase **5900**D shown in FIG. **59**D depicts the operation of the circuit **5900**A of FIG. **59**A during the time period T**2** of FIG. **59**B. During the operational phase **5900**D, both transistors Q**1** and Q**2** and diode D**2** are off. The stored energy in the inductor L during the phase **5900**C, is delivered to capacitor C**2** and charges this capacitor through the diode D**1** and the inductor L, thereby passing a positive down-ramping (decreasing) current i in the inductor L, which forms the second quarter cycle, corresponding to the time period T**2**, of the triangular waveform **5920** of FIG. **59**B.

The operational phase **5900**E shown in FIG. **59**E depicts the operation of the circuit **5900**A of FIG. **59**A during the time period T**3** of FIG. **59**B. During the operational phase **5900**E, the transistors Q**2** is on and the transistor Q**1** and both diodes D**1** and D**2** are off. During this phase, capacitor C**2** discharges through the transistor Q**2** and the inductor L and induces a negative increasing current in the inductor L,

which continues the down-ramping leg of the triangular waveform **5920** until the end of period T**3**.

The operational phase **5900**F shown in FIG. **59**F depicts the operation of the circuit **5900**A of FIG. **59**A during the time period T**4** of FIG. **59**B. During the operational phase **5900**F, both transistors Q**1** and Q**2** and diode D**1** are off, and the capacitor C**1** is charged through diode D**2** and the inductor L. The current i of the inductor L is negative and decreasing and reaches zero as the capacitor C**1** is charged nearly to its initial voltage. In the circuits **5900**A and **5900**C through **5900**F, the drive circuitry, protection circuitry, power supplies, and internal resistors (e.g., for the inductor L) are not shown for simplicity. With ideal lossless circuit elements, at the completion of the four switching periods (T**1** through T**4**), the capacitors would have exactly the same voltage as they had at the beginning of the four periods. However, because of internal resistors and non-ideal switches and rectifiers, there is some energy loss, with the result that the capacitors do not have exactly their original voltage after the sequence of four switching periods. To compensate for this energy loss, some means of recharging (e.g., a trickle charge or a rapid charge with the inductor disengaged) the capacitors can be employed to prevent any operation failure due to the non-idealities. The effect of this deviation from the ideal straight line in the triangular waveform may be compensated for by using, in the receiver, a demodulator that is matched with the non-ideal waveform.

FIGS. **60**A-**60**B are diagrams illustrating examples of a magnetic waveform generator circuit **6000**A with amplitude modulation capability and corresponding timing diagrams **6010**, **6012**, **6014**, **6016**, and **6020**, according to certain embodiments. The magnetic waveform generator circuit **6000**A is similar to the circuit **5900**A of FIG. **59**A, except for the additional switches S**3** and S**4** and capacitors C**3** and C**4**. The addition of the switches S**3** and S**4** and capacitors C**3** and C**4** enable circuit **6000**A to generate a current i in the inductor L with a triangular waveform that can be amplitude modulated. The switches S**3** and S**4** are dipole switches that can be set to be connecting at either of two positions A or B. When set to be at position A, the switches S**3** and S**4**, allow the capacitors C**3** and C**4** to be connected in series with the capacitors C**1** and C**2**, respectively. When switches S**3** and S**4** are set to be connecting at position B, the circuit **6000** becomes similar and operates similarly to the circuit **5900**A. The switches S**3** and S**4** can be implemented as semiconductor dipole switches using known transistor or diode switch circuitry.

When the switches S**3** and S**4** are set to be connecting at position A, as mentioned above, capacitors C**3** and C**4** are connected in series with capacitors C**1** and C**2** to provide a higher voltage for driving the current i through the inductor L, which can form the high current amplitude of the amplitude modulated waveform, as shown in the timing diagram **6020** of FIG. **60**B. In the circuit **6000**A, the drive circuitry, protection circuitry, power supplies, and internal resistors (e.g., for the inductor L) are not shown for simplicity.

The timing diagrams **6010**, **6012**, **6014**, **6016** shown in FIG. **60**B are control pulses applied to switches S**1** through S**4**. The timing diagrams are shown for five consecutive cycles (e.g., periods) P**1** P**2** . . . P**5**. During the first cycle P**1**, switches S**1** and S**2** are toggled as explained with respect to phases **5900**C through **5900**F of FIGS. **59**C through **1**F, and the switches S**3** and S**4** are set at position A, to allow capacitors C**3** and C**4** be connected in series with the capacitors C**1** and C**2**, thereby providing the high amplitude triangular waveform, as shown by waveform **6022**. The amplitude of the triangular waveform may be reduced by removing the capacitors C**3** and C**4** from the circuit **6000**A, thereby providing smaller voltage to drive the inductor current through the inductor L. This is done at cycle P**2**, where the switches S**3** and S**4** are both set to position B and switches S**1** and S**2** go through the phases to generate a triangular waveform as explained above. The ratio of amplitudes of the waveforms **6022** and **6024** depend on the capacitance values of the capacitors C**1**, C**2**, C**3**, and C**4**. For example, if the capacitance values of the capacitors C**1**, C**2**, C**3**, and C**4** are the same, the amplitude of the waveform **6024** would be half of the amplitude of the waveform **6022**. Other amplitude ratios can be achieved by suitably selecting the capacitance values of the capacitors C**1**, C**2**, C**3**, and C**4**.

During the third cycle P**3**, switches S**1** and S**2** are open and switches S**3** and S**4** are set at position B, and the charged capacitors C**1** have no path for driving current into the inductor L. Therefore, during cycle –P**3**, zero current passes through the inductor L. During this cycle, a recharge circuit (not shown for simplicity) can return the voltages of capacitors C**1** and C**2** to their desired level, correcting for resistive losses, without generating a current in the inductor L and therefore without affecting the magnetic field. During the cycles P**4** and P**5**, the setting of switches S**3** and S**4** are the same as cycles P**1** and P**2**, but the status of switches S**1** and S**2** in cycles P**4** and P**5** are reversed relative to cycles P**1** and P**2**, respectively. As a consequence, the direction of currents in the inductor L are also reversed, resulting in waveforms **6026** and **6028**, which have the same amplitudes as their respective waveforms **6022** and **6024**, but with opposite polarities.

The waveforms **6022**, **6024**, **6026**, and **6028** can be used to represent, for example, binary symbols 11, 10, 01, and 00 by a magnetic communications transmitter using the circuit **6000**A as the magnetic field generator. The cycle P**3**, which has no signal, can be used as the OFF symbol to allow for calibration, synchronization, and background cancellation in the receiver side.

FIGS. **61**A-**61**B are diagrams illustrating examples of an H-bridge magnetic waveform generator circuit **6100**A and an H-bridge magnetic waveform generator circuit **6100**B with amplitude modulation capability, according to certain embodiments. The bridge magnetic waveform generator circuit **6100**A (hereinafter "circuit **6100**A") is similar to circuit **5900**A of FIG. **59**A, except for the additional switches S**3** and S**2** and diodes D**2** and D**3** and the fact that node **6108** of the inductor L is not connected to the ground potential. The switch S**3** is coupled between nodes **6104** and **6108**, and switch S**2** is coupled between nodes **6108** and **6106**. Diodes D**2** and D**3** are coupled in parallel with switches S**3** and S**2**, respectively. The capacitors C**1** and C**2** join at node **6110** that is coupled to ground potential. In the circuit **6100**A, the drive circuitry, protection circuitry, power supplies, and internal resistors (e.g., for the inductor L) are not shown for simplicity. Switches S**2** and S**3** and diodes D**2** and D**3** can be implemented in the same semiconductor chip using transistor switches and semiconductor (e.g., silicon) diodes.

The configuration of circuit **6100**A has the advantageous feature that allows using lower supply voltage values. For example, the capacitors C**1** and C**2** can each be precharged to 50V (instead of 100V for circuit **100**A) and the circuit **6100**A still provides the same amplitude triangular waveform for the current in the inductor L. The operation of the circuit **6100**A includes four phases, during which status of switches S**1**, S**2**, S**3**, and S**4** are controlled to be different to allow suitable paths for flow of current from or to the capacitors C**1** and C**2** through the inductor L.

During a first phase, switches S1 and S2 are closed and switches S3 and S4 are open, and diodes D1 and D2 are reverse biased. During the first phase, the capacitors C1 and C2 discharge to drive a positive increasing (up-ramping) current through the switches S1 and S2 and the inductor L. This current provides the first quarter-cycle of a triangular current waveform (e.g., **5920** of FIG. **59**B). During a second phase, switches S1, S2, S3, and S4 are open, and diodes D1 and D2 are forward biased and conduct current. During this phase, the capacitors C1 and C2 recharge, which causes driving a positive decreasing (down-ramping) current through the diodes D1 and D2 into the inductor L. This current provides the second quarter-cycle of the triangular current waveform.

During a third phase, switches S3 and S4 are closed and switches S1 and S2 are open, and diodes D1 and D2 are reverse biased. During this phase, the capacitors C1 and C2 discharge to drive a negative (e.g., with revered direction) increasing amplitude current through the switches S3 and S4 and the inductor L. This current provides the third quarter-cycle of the triangular current waveform. During a fourth phase, switches S1, S2, S3, and S4 are open, and diodes D3 and D4 are forward biased and conduct current. During this phase, the capacitors C1 and C2 recharge and cause driving a negative decreasing current into the inductor L through diodes D3 and D4. This current provides the fourth quarter-cycle of the triangular current waveform. The circuit **6100**A can be modified to provide amplitude modulation as discussed herein.

The H-bridge magnetic waveform generator circuit **6100**B (hereinafter "circuit **6100**B") shown in FIG. **61**B has amplitude modulation capability. The circuit **6100**B has a portion **6150** that is similar to the circuit **6100**A and an additional portion **6152** including an inductor L2, diodes D5 and D6, and switches S5 and S6. Here, the inductor L2 does not create an external magnetic field at long distances as, for example, a toroidal inductor. Whereas the inductor L1 creates an external magnetic waveform as, for example, a magnetic coil. The operation of portion **6150** is also similar to the operation of circuit **6100**A, as discussed above. The portion **6150** is used to generate a high (e.g., maximum)-amplitude triangular current waveform (e.g., **6022** of FIG. **60**B), during the four phased as discussed above with respect to FIG. **61**A. During these phases switches S5 and S6 are open. When generating a low-amplitude triangular current waveform (e.g., **6024** of FIG. **60**B), the portion **6152** comes into the play and switches S5 and S6 are suitably opened or closed (while S1 and S4 are kept open) to allow driving currents in two different directions, as explained above, into series connected inductors L1 and L2. The series connection of inductors L1 and L2 increases the impedance in the path of the current and thereby decrease the amplitude of the current passing through the inductors L1 and L2. The ratio of amplitudes of the low-amplitude and high-amplitude waveforms depend on the inductance values of the inductors L1 and L2. For example, if the inductance values of the inductors L1 and L2 are the same, the amplitude of the low-amplitude waveform would be half of the amplitude of the high-amplitude waveform. Other amplitude ratios can be achieved by suitably selecting the inductance values of the inductors L1 and L2.

FIG. **62** is a diagram illustrating an example of a method **6200** for providing a magnetic waveform generator circuit, according to certain embodiments. According to the method **6200**, a first switch (e.g., S1 of FIG. **59**A) is coupled, at a first node (e.g., **5902** of FIG. **59**A), to a first rectifier element (e.g., D1 of FIG. **59**A) (**6210**). A first capacitor (e.g., C1 of FIG. **59**A) is coupled, at a second node (e.g., **5904** of FIG. **59**A) to the first switch, and to a fourth node (e.g., **5908** of FIG. **59**A) (**6220**). A second capacitor may be coupled, at a third node (e.g., **5906** of FIG. **59**A) to the first rectifier element, and to the forth node (**6230**). An inductor (e.g., L of FIG. **59**A) may be coupled between the first and the fourth nodes (**6240**). The first switch is operable to be in an ON state during a first time period (e.g., T1 of FIG. **59**B) and in an off state during a second time period (e.g., T2 of FIG. **59**B). The first switch and the first rectifier element are configured to enable the inductor to generate, during the first and the second time periods, a magnetic field having a waveform resembling a positive half-cycle of a triangular waveform (e.g., **5920** of FIG. **59**B).

In some implementations, a vehicle may need to avoid objects that are in their navigation path. For example, a ground vehicle may need to maneuver around people or objects, or a flying vehicle may need to avoid a building or power line equipment. In these implementations, the vehicle can be equipment with sensors that are used to locate the obstacles that are to be avoided. Systems such as a camera system, focal point array, radar, acoustic sensors, etc., can be used to identify obstacles in the vehicles path. The navigation system can then identify a course correction to avoid the identified obstacles.

The herein described subject matter sometimes illustrates different components contained within, or connected with, different other components. It is to be understood that such depicted architectures are merely exemplary, and that in fact many other architectures can be implemented which achieve the same functionality. In a conceptual sense, any arrangement of components to achieve the same functionality is effectively "associated" such that the desired functionality is achieved. Hence, any two components herein combined to achieve a particular functionality can be seen as "associated with" each other such that the desired functionality is achieved, irrespective of architectures or intermedial components. Likewise, any two components so associated can also be viewed as being "operably connected," or "operably coupled," to each other to achieve the desired functionality, and any two components capable of being so associated can also be viewed as being "operably couplable," to each other to achieve the desired functionality. Specific examples of operably couplable include but are not limited to physically mateable and/or physically interacting components and/or wirelessly interactable and/or wirelessly interacting components and/or logically interacting and/or logically interactable components.

With respect to the use of substantially any plural and/or singular terms herein, those having skill in the art can translate from the plural to the singular and/or from the singular to the plural as is appropriate to the context and/or application. The various singular/plural permutations may be expressly set forth herein for sake of clarity.

It will be understood by those within the art that, in general, terms used herein, and especially in the appended claims (e.g., bodies of the appended claims) are generally intended as "open" terms (e.g., the term "including" should be interpreted as "including but not limited to," the term "having" should be interpreted as "having at least," the term "includes" should be interpreted as "includes but is not limited to," etc.). It will be further understood by those within the art that if a specific number of an introduced claim recitation is intended, such an intent will be explicitly recited in the claim, and in the absence of such recitation no such intent is present. For example, as an aid to understanding, the following appended claims may contain usage of the

introductory phrases "at least one" and "one or more" to introduce claim recitations. However, the use of such phrases should not be construed to imply that the introduction of a claim recitation by the indefinite articles "a" or "an" limits any particular claim containing such introduced claim recitation to inventions containing only one such recitation, even when the same claim includes the introductory phrases "one or more" or "at least one" and indefinite articles such as "a" or "an" (e.g., "a" and/or "an" should typically be interpreted to mean "at least one" or "one or more"); the same holds true for the use of definite articles used to introduce claim recitations. In addition, even if a specific number of an introduced claim recitation is explicitly recited, those skilled in the art will recognize that such recitation should typically be interpreted to mean at least the recited number (e.g., the bare recitation of "two recitations," without other modifiers, typically means at least two recitations, or two or more recitations). Furthermore, in those instances where a convention analogous to "at least one of A, B, and C, etc." is used, in general such a construction is intended in the sense one having skill in the art would understand the convention (e.g., "a system having at least one of A, B, and C" would include but not be limited to systems that have A alone, B alone, C alone, A and B together, A and C together, B and C together, and/or A, B, and C together, etc.). In those instances where a convention analogous to "at least one of A, B, or C, etc." is used, in general such a construction is intended in the sense one having skill in the art would understand the convention (e.g., "a system having at least one of A, B, or C" would include but not be limited to systems that have A alone, B alone, C alone, A and B together, A and C together, B and C together, and/or A, B, and C together, etc.). It will be further understood by those within the art that virtually any disjunctive word and/or phrase presenting two or more alternative terms, whether in the description, claims, or drawings, should be understood to contemplate the possibilities of including one of the terms, either of the terms, or both terms. For example, the phrase "A or B" will be understood to include the possibilities of "A" or "B" or "A and B." Further, unless otherwise noted, the use of the words "approximate," "about," "around," "substantially," etc., mean plus or minus ten percent.

The foregoing description of illustrative embodiments has been presented for purposes of illustration and of description. It is not intended to be exhaustive or limiting with respect to the precise form disclosed, and modifications and variations are possible in light of the above teachings or may be acquired from practice of the disclosed embodiments. It is intended that the scope of the invention be defined by the claims appended hereto and their equivalents.

What is claimed is:

1. A system for magnetic detection, comprising:

a magneto-optical defect center sensor comprising:

a magneto-optical defect center material comprising at least one magneto-optical defect center;

a radio frequency (RF) excitation source configured to provide RF excitations at various frequencies to the magneto-optical defect material;

an optical excitation source configured to provide optical excitation to the magneto-optical defect material;

an optical detector configured to receive the emitted optical signal from the magneto-optical defect center material, wherein the emitted optical signal varies in intensity based responsiveness of the magneto-optical defect center material to the optical excitation with RF excitations at various frequencies;

a controller configured to control the RF excitation source and the optical excitation source to provide a sequence of pulses to the magneto-optical defect center material at RF excitations at various frequencies;

wherein the controller is further configured to detect variations in the emitted optical signal based on responsiveness of the magneto-optical defect center material to the optical excitation at an RF excitation; and

wherein the controller is further configured to utilize RF excitations at various frequencies to detect vector variations in responsiveness of the magneto-optical defect center material.

2. The system of claim **1**, wherein the magneto-optical defect center sensor is configured to detect the magnetic field as a vector.

3. The system of claim **1**, wherein the magneto-optical defect center sensor is configured to detect the magnetic field in individual directions.

4. The system of claim **1**, wherein the magneto-optical defect center sensor further comprises:

a magnetic field generator comprising at least two magnetic field generators including a first magnetic field generator configured to generate a first magnetic field and a second magnetic field generator configured to generate a second magnetic field;

wherein the controller is further configured to:

modulate a first code packet and control the first magnetic field generator to apply a first time varying magnetic field at the magneto-optical defect center material based on the modulated first code packet, and

modulate a second code packet and control the second magnetic field generator to apply a second time varying magnetic field at the magneto-optical defect center material based on the modulated second code packet, wherein the first code packet and the second code packet are binary sequences which have a low cross correlation with each other, and each of the binary sequences has a good autocorrelation.

5. The system of claim **4**, wherein a direction of the first time varying magnetic field at the magneto-optical defect center material is different from a direction of the second time varying magnetic field at the magneto-optical defect center material.

6. The system of claim **5**, wherein the magneto-optical defect center sensor further comprises a reflector positioned about the magneto-optical defect center material to reflect a portion of light emitted from the magneto-optical defect center material.

7. The system of claim **1**, further comprising:

a first magnetic field sensor that includes the magneto-optical defect center sensor,

a second magnetic field sensor that includes a second magneto-optical defect center sensor, and

a position encoder component comprising a magnetic region configured to produce a magnetic field gradient from a first end of the magnetic region to the second end of the magnetic region.

8. The system of claim **7**, wherein the magnetic region comprises a ferromagnetic component.

9. The system of claim **7**, wherein the magnetic region comprises a magnetic polymer.

10. The system of claim **7**, further comprising a third magnetic field sensor and a fourth magnetic field sensor.

11. The system of claim 1, further comprising:
a vehicle that includes the magneto-optical defect center sensor, wherein the magneto-optical defect center sensor is configured to detect a magnetic vector or a magnetic field;
one or more electronic processors configured to:
receive the magnetic vector of the magnetic field from the magneto-optical defect center sensor; and
a navigation control configured to navigate the vehicle based upon the presence of the magnetic vector.

12. The system of claim 1, wherein the magneto-optical defect center material comprises a nitrogen vacancy (NV) diamond material comprising a plurality of NV centers.

13. A system for magnetic detection, comprising:
a magneto-optical defect center sensor comprising:
a magneto-optical defect center material comprising a plurality of magneto-optical defect centers;
a radio frequency (RF) excitation source configured to provide RF excitation at various frequencies to the magneto-optical defect center material;
an optical excitation source configured to provide optical excitation to the magneto-optical defect center material;
an optical detector configured to receive an optical signal emitted by the magneto-optical defect center material, wherein the optical signal varies in intensity based on responsiveness of the magneto-optical defect center material to the optical excitation with RF excitation at various frequencies;
a controller configured to detect the optical signal emitted by the magneto-optical defect center material, wherein the controller is further configured to utilize the multiple RF excitations at various frequencies to detect vector variations in responsiveness of the magneto-optical defect center material; and
an array of sensors comprising the magneto-optical defect center sensor, wherein the array is configured to capture a first magnetic image and a second magnetic image; and
a processor communicatively coupled to the array, wherein the processor is configured to:
determine a background image based on the first magnetic image and identify discrepancies to the second magnetic image.

14. The system of claim 13, wherein some sensors of the array are arranged on a surface area of a well pay zone, wherein some sensors of the array are positioned in locations within or near the well bore.

15. The system of claim 13, wherein the processor is further configured to determine the background by subtracting the first magnetic image from the second magnetic image, such background being used with further magnetic images.

16. The system of claim 13, wherein the discrepancies identify a ferromagnetic material.

17. The system of claim 13, wherein the magneto-optical defect center material comprises a nitrogen vacancy (NV) diamond material comprising a plurality of NV centers.

18. A system for magnetic detection, comprising:
a magneto-optical defect center sensor comprising:
a magneto-optical defect center means for generating an emitted optical signal comprising a plurality of magneto-optical defect centers;
a radio frequency (RF) excitation source configured to provide RF excitation at multiple frequencies to the magneto-optical defect center material;
an optical excitation source configured to provide optical excitation to the magneto-optical defect center material;
an optical detector configured to receive an optical signal emitted by the magneto-optical defect center means, wherein the optical signal is based on responsiveness of the magneto-optical defect center material to optical excitation and RF excitation at multiple frequencies; and,
a controller configured to detect the optical signal emitted by the magneto-optical defect center material, wherein the controller is further configured to utilize the RF excitation at multiple frequencies to detect vector variations in responsiveness of the magneto-optical defect center means.

19. The system of claim 18, further comprising a magnetic waveform generator circuit that comprising:
a first switch coupled to a first rectifier element at a first node;
a first capacitor coupled, at a second node to the first switch, and to a fourth node;
a second capacitor coupled, at a third node to the first rectifier element, and to the fourth node; and
an inductor coupled between the first and the fourth nodes,
wherein the magnetic waveform generator circuit is configured to enable the inductor to generate a first magnetic field having a waveform resembling a positive half-cycle of a triangular waveform; and
wherein the magneto-optical defect center sensor is configured to detect the first magnetic field.

20. The system of claim 18, wherein the magneto-optical defect center material comprises a nitrogen vacancy (NV) diamond material comprising a plurality of NV centers.

* * * * *